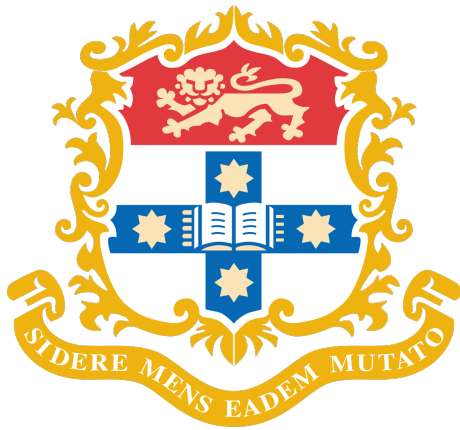


UNIVERSITY OF SYDNEY



TAILPLANE Box DESIGN, BUILD & TEST GROUP 4 FINAL REPORT

05-11-23

<i>K. AlMeheiri</i>	500028951
<i>T. Bullock</i>	530754154
<i>K. Ganya</i>	530706142
<i>C. Legge-Wilkinson</i>	460495765
<i>K. Leung</i>	500490181
<i>J. Serrano</i>	530706050
<i>J. Vorenkamp</i>	440554828

Executive Summary

To comply with the desired specification, the tailplane box had to meet the requirements set out in the design brief. The specification can be broken down into dimensional, structural, weight and cost design requirements. Each individual requirement and its respective compliance is given in tables 1, 2 and 3 below. Note that the figures referenced in table 1 relate to those in the design brief.

Table 1: Dimensional requirements.

Requirement	Compliance
Figure 2 - Tailplane Box Layout	Compliant
Figure 3 - Tailplane Box Interface Control Drawing	Compliant
Figure 4 - Tailplane Box View A, Section B-B	Compliant
Figure 5 - Tailplane Box Envelope	Non-Compliant (Width Exceeded)

Table 2: Structural requirements.

Requirement	Compliance
Supports Ultimate Load	Non-Compliant (Failed at Limit Load)
Maximum Ultimate Shear Buckling Ratios	Compliant
All Margins of Safety > 0	Compliant

Table 3: Weight and cost requirements.

Requirement	Compliance
Weight Target per Ship-Set of 2.2kg	Non-Compliant (2.760 kg)
Cost Target per Ship-Set of \$4200	Non-Compliant (\$5530)

Total Mass of Tailplane Box Ship-Set: 2.760 kg

Total Cost of Tailplane Box Ship-Set: \$5530

Contents

Executive Summary	i
List of Figures	vi
List of Tables	viii
1 Weight & Cost Report	1
1.1 Centre of Mass Calculation	2
2 Stress Report	4
2.1 Introduction	4
2.2 Margin of Safety Summary	4
2.3 Material Data	5
2.4 External Loads and Reactions	7
2.4.1 Load Case 1	8
2.4.2 Load Case 2	10
2.4.3 Load Case 3	11
2.4.4 Load Case 4	12
2.5 Calculation of Internal Loads	14
2.5.1 Calculation of Spar Cap Loads & Method 1 Shear Flows	14
2.5.2 Calculation of Method 2 Shear Flows	17
2.6 FEM Re-Calculation of Internal Loads	18
2.7 Spar Cap Geometry	20
2.7.1 Spar Cap Geometry Summary	20
2.7.2 Spar Cap Component Geometry Calculations	25
2.7.2.1 Spar Flange & Web	25
2.7.2.2 Spar Cap Reinforcement 4	27
2.7.3 Spar Cap Configuration 2 Geometry Calculations	29
2.8 Stress Analysis	31
2.8.1 Spar Web & Skin Shear Buckling Ratios	31
2.8.1.1 Calculation of Spar Web & Skin Shear Buckling Ratios	32
2.8.2 Spar Cap Stress Analysis	33
2.8.2.1 Spar Cap Stress Analysis Summary	33
2.8.2.2 Spar Cap Configuration 2 Stress Analysis	35
2.8.2.2.1 Tension Failure	35
2.8.2.2.2 Compression Yield Failure	35
2.8.2.2.3 Crippling Failure	36
2.8.2.2.4 Crippling Failure with Diagonal Tension	37
2.8.2.2.5 Shear Failure	38
2.8.2.2.6 Rivet Shear Failure	38
2.8.3 Rib Stress Analysis	39
2.8.3.1 Flange Compression Yield Failure	39

2.8.3.2	Shear Failure	40
2.8.3.3	Rivet Shear Failure	40
2.8.4	Fitting Stress Analysis	41
2.8.4.1	Fitting Stress Analysis Summary	41
2.8.4.2	Lug P Stress Analysis	42
2.8.4.2.1	Rivet Shear Failure	42
2.8.4.2.2	Tension Failure	43
2.8.4.2.3	Bearing Shear Out Failure	44
2.8.4.2.4	Transverse Shear Out Failure	45
3	Test Plan	47
4	Test Report	51
4.1	Background	51
4.2	Method	51
4.3	Results & Discussion	52
4.4	Conclusion	54
5	Drawing List & Bill of Material	56
6	Drawings	59
7	Preliminary Design Review	85
8	Critical Design Review	91
A	Detailed Geometry Calculations	105
A.1	Spar Cap Component Geometry Calculations	105
A.1.1	Spar Cap Reinforcement 1	105
A.1.2	Spar Cap Reinforcement 2	107
A.1.3	Spar Cap Reinforcement 3	109
A.1.4	Spar Cap Reinforcement 5	111
A.1.5	Spar Cap Reinforcement 6	114
A.1.6	Spar Cap Reinforcement 7	116
A.2	Spar Cap Configuration Geometry Calculations	118
A.2.1	Spar Cap Configuration 1	118
A.2.2	Spar Cap Configuration 3	119
A.2.3	Spar Cap Configuration 4	120
A.2.4	Spar Cap Configuration 5	122
A.2.5	Spar Cap Configuration 6	123
A.2.6	Spar Cap Configuration 7	125
A.2.7	Spar Cap Configuration 8	126
A.2.8	Spar Cap Configuration 9	128
A.2.9	Spar Cap Configuration 10	129
A.2.10	Spar Cap Configuration 11	130

B Spar Cap Stress Analysis Calculations	133
B.1 Spar Cap Configuration 1 Stress Analysis	133
B.1.1 Tension Failure	133
B.1.2 Compression Yield Failure	133
B.1.3 Crippling Failure	133
B.1.4 Crippling Failure with Diagonal Tension	134
B.1.5 Shear Failure	135
B.2 Spar Cap Configuration 3 Stress Analysis	136
B.2.1 Tension Failure	136
B.2.2 Compression Yield Failure	136
B.2.3 Crippling Failure	137
B.2.4 Crippling Failure with Diagonal Tension	138
B.2.5 Shear Failure	139
B.2.6 Rivet Shear Failure	139
B.3 Spar Cap Configuration 4 Stress Analysis	140
B.3.1 Tension Failure	140
B.3.2 Crippling Failure	140
B.3.3 Crippling Failure with Diagonal Tension	142
B.3.4 Shear Failure	143
B.3.5 Rivet Shear Failure	143
B.4 Spar Cap Configuration 5 Stress Analysis	144
B.4.1 Tension Failure	144
B.4.2 Compression Yield Failure	144
B.4.3 Crippling Failure	145
B.4.4 Crippling Failure with Diagonal Tension	146
B.4.5 Shear Failure	147
B.4.6 Rivet Shear Failure	147
B.5 Spar Cap Configuration 6 Stress Analysis	148
B.5.1 Tension Failure	148
B.5.2 Compression Yield Failure	148
B.5.3 Crippling Failure	148
B.5.4 Crippling Failure with Diagonal Tension	150
B.5.5 Shear Failure	151
B.5.6 Rivet Shear Failure	151
B.6 Spar Cap Configuration 7 Stress Analysis	152
B.6.1 Tension Failure	152
B.6.2 Compression Yield Failure	152
B.6.3 Crippling Failure	152
B.6.4 Crippling Failure with Diagonal Tension	154
B.6.5 Shear Failure	155
B.6.6 Rivet Shear Failure	155
B.7 Spar Cap Configuration 8 Stress Analysis	156
B.7.1 Tension Failure	156
B.7.2 Compression Yield Failure	156
B.7.3 Crippling Failure	156

B.7.4	Crippling Failure with Diagonal Tension	158
B.7.5	Shear Failure	159
B.7.6	Rivet Shear Failure	159
B.8	Spar Cap Configuration 9 Stress Analysis	159
B.8.1	Tension Failure	159
B.8.2	Compression Yield Failure	160
B.8.3	Crippling Failure	160
B.8.4	Crippling Failure with Diagonal Tension	161
B.8.5	Shear Failure	162
B.8.6	Rivet Shear Failure	162
B.9	Spar Cap Configuration 10 Stress Analysis	162
B.9.1	Tension Failure	162
B.9.2	Compression Yield Failure	163
B.9.3	Crippling Failure	163
B.9.4	Crippling Failure with Diagonal Tension	165
B.9.5	Shear Failure	165
B.9.6	Rivet Shear Failure	166
B.10	Spar Cap Configuration 11 Stress Analysis	166
B.10.1	Tension Failure	166
B.10.2	Compression Yield Failure	166
B.10.3	Crippling Failure	167
B.10.4	Crippling Failure with Diagonal Tension	168
B.10.5	Shear Failure	169
C	Fitting Stress Analysis Calculations	170
C.1	Lug A & Lug B Stress Analysis	170
C.1.1	Rivet Shear Failure	170
C.1.2	Tension Failure	171
C.1.3	Bearing Shear Out Failure	171
C.1.4	Transverse Shear Out Failure	172
C.2	Lug C Stress Analysis	173
C.2.1	Rivet Shear Failure	173
C.2.2	Tension & Bearing Shear Out Failure	174
C.2.3	Transverse Shear Out Failure	174
D	Figures	176

List of Figures

1	Material properties for 2024-T3 clad sheet; excerpt taken from page 3-74 of MIL-HDBK-5H.	5
2	Allowables for CR3213-4 1/8" blind rivets; excerpt take from page 8-56 in MIL-HDBK-5H.	6
3	Allowables for 1/8" pop rivets.	6
4	Diagram of the tailplane box denoting load application (lug P) and reaction (lugs A, B and C) points.	8
5	Load case 1 free body diagram.	8
6	Load case 2 free body diagram.	10
7	Load case 3 free body diagram.	11
8	Load case 4 free body diagram.	12
9	Free body diagram of a cut section of the tailplane box subject to shear load V_t	15
10	From left to right, top to bottom, graphs of load split parameters, spar shear forces, spar moments, spar cap loads and mid-bay skin and spar shear flows using method 1 (section 2.5.1) and method 2 (section 2.5.2), computed for load case 1, at limit load.	16
11	Graphs of rib shear flows computed as the difference of top skin mid-bay shear flows using method 1 (section 2.5.1) and method 2 (section 2.5.2), computed for load case 1, at limit load.	17
12	Free body diagram of a cut section of the tailplane box subject to direct load P ; note that the depiction of shear flows q_3 and q_4 has been simplified for clarity.	18
13	From left to right, top to bottom, graphs of mid-bay spar cap loads, average bay shear flows, average rib shear flows and spar cap total deflections computed for load case 1, at limit load, using the provided HughFEM finite element code.	19
14	Spar cap component section geometry diagrams.	22
15	Spar cap configurations 1 to 8 section geometry diagrams.	24
16	Spar cap configurations 9 to 11 section geometry diagrams.	25
17	Free body diagram of lug P rivet shear subject to load case 1.	42
18	Free body diagram of lug P tension subject to load case 3.	43
19	Free body diagram of lug P bearing shear out subject to load case 3.	44
20	Free body diagram of lug P transverse shear out subject to load case 1.	45
21	Photos of the testing station setup showing (left) the tailplane box mounted in the test jig and (right) the connection between the tailplane box and test jig.	51
22	Photo of the full testing station setup, with jack, rulers for measuring deflections and digital scales for measuring the applied load.	52
23	Tailplane box front and rear spar deflections with respect to loading at lug P.	53
24	Photos of (left) shanking of lug P prior to testing and (right) the tailplane box post lug P failure.	55
25	Photo of the outboard tip rib showing the lug P failure as a result of shanking.	55
26	Free body diagram of lug A rivet shear subject to load case 1.	170
27	Free body diagram of lug A tension subject to load case 1.	171

28	Free body diagram of lug A bearing shear out subject to load case 1.	171
29	Free body diagram of lug A transverse shear out subject to load case 1.	172
30	Free body diagram of lug C rivet shear subject to load case 1.	173
31	Free body diagram of lug C transverse shear out subject to load case 1.	174
32	Inter-rivet buckling stress for riveted 2024-T3 clad plate; excerpt taken from Bruhn.	177
33	Diagonal tension factor for diagonal tension calculations; excerpt taken from Bruhn.	178
34	Tension and shear-bearing efficiency factors for aluminium and steel alloy lugs; excerpt taken from Bruhn.	179
35	Transverse shear out efficiency factor for aluminium alloy lugs; excerpt taken from Bruhn.	180

List of Tables

1	Dimensional requirements.	i
2	Structural requirements.	i
3	Weight and cost requirements.	i
4	Left tailplane box manufacturing costs, based on the requirements set out in the design brief.	1
5	Left tailplane box centre of mass summary. Note that local coordinates are relative to the inboard bottom rear corner of the tailplane box.	2
6	Left tailplane box detailed centre of mass calculations. Note that local coordinates are relative to the inboard bottom rear corner of the tailplane box.	3
7	Margin of safety summary table.	4
8	Reaction forces obtained from the analyses of section 2.4.	7
9	Summary of spar cap component geometric properties; see figure 14 for section diagrams. Note that $c = b'/t$ and A_m are the average side length divided by thickness and the mid-line area, respectively, of the spar cap component for crippling calculations.	21
10	Summary of spar cap configuration geometric properties; see figures 15 and 16 for section diagrams	23
11	Shear buckling ratios for load case 1; note that bay 1 is the most inboard bay.	32
12	Shear buckling ratios for load case 2; note that bay 1 is the most inboard bay.	32
13	Top-front and top-rear spar cap configuration margin of safety summary table.	33
14	Outboard and bottom-front spar cap configuration margin of safety summary table.	34
15	Bottom-rear spar cap configuration margin of safety summary table.	35
16	Derived data used to compute the allowable crippling stress at BL388 for spar cap configuration 2 (section 2.7.3).	36
17	Rib margin of safety summary table.	39
18	Fitting margin of safety summary table.	41
19	Derived data used to compute the maximum rivet shear load in lug P.	43
20	Left tailplane box bill of material (assembly 6011-001).	57
21	Right tailplane box bill of material (assembly 6011-002).	58
22	Derived data used to compute the allowable crippling stress at BL268 for spar cap configuration 3 (appendix A.2.2).	137
23	Derived data used to compute the allowable crippling stress at BL196 for spar cap configuration 4 (appendix A.2.3).	141
24	Derived data used to compute the allowable crippling stress at BL148 for spar cap configuration 5 (appendix A.2.4).	145
25	Derived data used to compute the allowable crippling stress at BL364 for spar cap configuration 6 (appendix A.2.5).	149
26	Derived data used to compute the allowable crippling stress at BL316 for spar cap configuration 7 (appendix A.2.6).	153
27	Derived data used to compute the allowable crippling stress at BL268 for spar cap configuration 8 (appendix A.2.7).	157

28	Derived data used to compute the allowable crippling stress at BL172 for spar cap configuration 9 (appendix A.2.8).	160
29	Derived data used to compute the allowable crippling stress at BL148 for spar cap configuration 10 (appendix A.2.9).	163
30	Derived data used to compute the allowable crippling stress at BL364 for spar cap configuration 11 (appendix A.2.10).	167
31	Derived data used to compute the maximum rivet shear load in lug C.	174

1 Weight & Cost Report

The weight analysis is based on a comparison of the theoretical and measured weight of the tailplane box. The estimated weight without rivets is 1198 g, given in table 6, with an actual measured weight of 1380 g. The weight was calculated from the bill of material (BOM) using a spreadsheet. Given 431 pop rivets and 44 CherryMax rivets were used, and assuming a rivet weight of 0.3 g, the total estimated weight of the tailplane box is 1341 g. With respect to the financial cost analysis, costing is given in table 4 for the production of the tailplane box and is based on the requirements set out in the design brief. The costs associated with this design have been assessed against the BOM using the time and labour costs stipulated in the design brief.

Table 4: Left tailplane box manufacturing costs, based on the requirements set out in the design brief.

Component	Task	Quantity	Time [hrs]	Cost [\$ AUD]
Fasteners	Riveting	475	15.83	1108
	Routing	4	1	70
	Assembly	4	1	70
Fittings	Cutting	28	0.9333	65.33
	Folding	28	2.333	163.3
	Assembly	12	3	210
Ribs	Cutting	10	0.3333	23.33
	Folding	6	0.5	35
	Assembly	Inclusive in Rib Assembly		
Spars	Cutting	8	0.2667	18.67
	Folding	1	0.08333	5.833
	Assembly	2	0.5	35
Skins	Cutting	40	1.333	93.33
	Folding	14	1.167	81.67
	Assembly	10	2.5	175
Reinforcement	Cutting	168	5.6	392
	Assembly	Inclusive in Rib Assembly		
	Drawings	6	-	180
Material (2024-T3)		1.264 kg	-	37.92
		Total	36.38	2765
		Total per Ship-Set	72.76	5530

1.1 Centre of Mass Calculation

A summary of the centre of mass calculation is provided in table 5, with a detailed centre of mass calculation provided in table 6, and was found by computing the moment arm in the x , y and z direction for each individual component which was then divided by the combined mass to determine the local x , y and z coordinates, which in turn are converted into global coordinates for the aircraft. The centre of mass calculations have excluded the mass and locations of the rivets as their mass distribution has been assumed to be negligible. The material used for the tailplane box is aviation grade aluminium sheet, 2024-T3 in 0.41 mm and 0.41 mm thicknesses.

Table 5: Left tailplane box centre of mass summary. Note that local coordinates are relative to the inboard bottom rear corner of the tailplane box.

x [cm]	Global X	y [cm]	Global Y	z [cm]	Global Z
10.98	FS5611	29.36	BL393.5	3.102	WL1492

Table 6: Left tailplane box detailed centre of mass calculations. Note that local coordinates are relative to the inboard bottom rear corner of the tailplane box.

Part/Description	Part No.	Mass [g]	x [cm]	M_x [kg·cm]	y [cm]	M_y [kg·cm]	z [cm]	M_z [kg·cm]
Front Spar	6112-101	86.91	20	1.74	37.0	3.219	3.5	0.304
Rear Spar	6112-103	86.91	0	0	37.0	3.219	3.5	0.304
Inbrd. End Cap	6112-105	28.14	10	0.28	0	0	4	0.112
Outbrd. End Cap	6112-107	19.15	10	0.19	74.5	1.416	2	0.038
Rib BL250	6112-109	28.25	10	0.28	25.0	0.7	2.3	0.064
Rib BL350	6112-111	27.12	10	0.27	35.0	0.945	3.2	0.086
Rib BL542	6112-113	24.45	10	0.25	54.2	1.355	4	0.1
Rib BL710	6112-115	21.3	10	0.21	71.0	1.491	4	0.084
Lower Skin	6113-117	203.6	10	2.03	37.5	7.61	0	0
Upper Skin	6113-119	201.3	10	2.03	37.0	7.51	6	1.218
Lug P	6111-121	32.15	20	0.64	75.3	2.410	2	0.064
Lugs A/B	6111-123	101.64	20.3	2.063	3.0	0.3	4	0.4
Lug C	6111-125	23.65	-0.3	-0.0084	1.5	0.042	4	0.112
FT Stiff 1	6114-127	19.36	20	0.392	13.0	0.255	7.7	0.151
FT Stiff 2	6114-129	9.17	20	0.18	7.0	0.063	7.9	0.071
FT Stiff 3	6114-131	5.69	20	0.12	5.0	0.03	8	0.048
RT Stiff	6114-133	17.47	0	0	12	0.216	7.8	0.140
RB Stiff 1	6114-135	49.84	0	0	28	1.396	0	0
RB Stiff 2	6114-137	22.14	0	0	14	0.310	0	0
FB Stiff 1	6114-139	15.25	20	0.310	11	0.168	0	0
FB Stiff 2	6114-141	25.21	20	0.504	20	0.504	0	0
FB Stiff 3	6114-143	15.95	20	0.319	11	0.176	0	0
FB Stiff 4	6114-145	10.52	20	0.210	8	0.084	0	0
3× E Cap Spc.	6115-147	6.33	10	0.0633	1	0.006	4	0.025
6× E Cap Spc.	6115-149	9.54	10	0.095	1	0.010	4	0.038
3× R BL250 Spc.	6115-151	4.77	10	0.048	25	0.119	4	0.019
2× R Long BL350 Spc.	6115-153	3.86	10	0.038	35	0.135	4	0.015
2× R Short BL350 Spc.	6115-155	2.86	10	0.029	35	0.135	4	0.015
2× R BL542 Spc.	6115-157	3.04	10	0.030	54.2	0.165	3	0.009
2× R BL710 Spc.	6115-159	2.28	10	0.023	71	0.162	2.1	0.005
3× R U-Long Spc.	6115-161	11.55	10	0.116	1	0.012	7.8	0.090
3× R U-Short Spc.	6115-163	10.95	10	0.110	1	0.011	7.8	0.085
4× R L-Long Spc.	6115-165	24.04	10	0.240	1	0.024	0.2	0.005
4× R L-Short Spc.	6115-167	20.64	10	0.207	1	0.021	0.2	0.0041
2× U-Spar Strap	6115-169	9.28	10	0.093	15	0.139	7	0.065
3× U-Stiff Strap	6115-171	8.94	10	0.089	15	0.134	7	0.065
Disp. Lug	6111-173	0.84	0.5	0.000	75	0.063	2	0.002
Total		1198	10.976	13.153	29.365	35.191	3.102	3.717

2 Stress Report

2.1 Introduction

The stress report outlines the detailed stress analyses of the tailplane box, presenting configuration specific margin of safety calculations and the technical engineering justification for the proposed design. Section 2.2 provides an overall margin of safety summary for the entire tailplane box, giving the absolute minimum margins of safety of all the components and failure modes analysed; following this, material data is given in section 2.3. Section 2.4 provides detailed calculations of the reaction forces at lugs A, B and C for all four load cases, after which section 2.5 details the methods used to compute the predicted internal direct and shear loads in the tailplane box for the critical load cases 1 and 2 at limit load. These loads are then compared to the results of a finite element simulation of load case 1 at limit load, performed using the provided HughFEM MATLAB code, in section 2.6. Detailed calculations of the spar cap geometry are then provided in section 2.7, which was kept separate from the spar cap stress analysis in order to reduce repetitive calculations in that section. Finally, the stress analysis is given, starting with the calculation of skin shear buckling ratios in section 2.8.1, followed by the spar cap stress analysis in section 2.8.2, the rib stress analysis in section 2.8.3 and the fitting stress analysis in section 2.8.4.

2.2 Margin of Safety Summary

Table 7: Margin of safety summary table.

Component	Drawing/Part	Failure Mode	Load Case	Material	Allowable	Limit	MS	Section
Fittings								
Lug P	6111-121	Rivet Shear	1	CR3213-4 Rivets	1246	711.5	0.01521	2.8.4.2.1
Lug A	6111-123	Tension		2024-T3	29775 N	11293 N	0.5285	C.1.2
		Bearing Shear Out			20118 N		0.03273	C.1.3
Lug C	6111-125	Transverse Shear Out			15021 N	1012 N	High	C.2.3
Spar Caps								
Config 1	6011, SH13, F2	Tension	1	2024-T3	8763 N	2633 N	High	B.1.1
Config 5	6011, SH3, A3	Compression Yield			34333 N	7626 N	High	B.4.2
Config 4	Figure 15(d)	Crippling			10505 N	5896 N	0.1878	B.3.2
Config 5	6011, SH3, A3	Crippling w/DT			100.3 N/mm ²	65.01 N/mm ²	0.02856	B.4.4
Config 1	6011, SH13, F3	Spar Cap Shear			4348 N	377.8 N	High	B.1.5
Config 6	6011, SH11, E3	Rivet Shear		Pop Rivets	600 N	379.4 N	0.05430	B.5.6
Ribs								
BL350	6112-111	Flange Compression Yield	1	2024-T3	3963	636.5	High	2.8.3.1
BL100	6112-105	Rib Shear			4348	300.7	High	2.8.3.2
		Rivet Shear		CR3213-4 Rivets	600	300.7	0.3301	2.8.3.3

2.3 Material Data

All parts were manufactured from 2024-T3 clad sheet. Material properties are given in figure 1 (excerpt taken from page 3-74 of MIL-HDBK-5H). Fittings were fastened to the tailplane box using CR3213-4 1/8" blind rivets and all other riveted connections were made using 1/8" pop rivets. Rivet allowables are given in figure 2 for CR3213-4 1/8" blind rivets (excerpt take from page 8-56 in MIL-HDBK-5H) and figure 3 for 1/8" pop rivets.

AMS-QQ-A-250/5												
Flat sheet and plate												
T351												
T3												
0.008- 0.009												
Specification	Form	Temper	Thickness, in.	A	B	C	D	E	F	G	H	
Mechanical Properties:				0.010- 0.009	0.010- 0.009	0.063- 0.128	0.129- 0.249	0.250- 0.499	1.000- 1.500 ^a	1.000- 1.500 ^a	1.501- 2.000 ^a	
F_{ut} , ksi:	L	59	60	60	59	61	62	63	64	61	63	60
	LT	58	58	59	60	61	62	63	64	61	63	60
	ST
F_y , ksi:	L	44	45	44	45	45	47	45	48	45	48	47
	LT	39	40	39	40	40	42	40	42	40	42	40
	ST
F_{yp} , ksi:	L	36	37	36	37	37	39	37	39	37	39	37
	LT	42	43	42	43	43	45	43	45	42	44	42
	ST
$F_{y0.2}$, ksi:	L	37	37	37	38	38	39	39	40	37	38	37
	LT	42	43	42	43	43	45	43	45	42	44	42
	ST
F_{by} , ksi: (e/D = 1.5)	...	96	97	99	101	102	102	104	94	97	95	91
(e/D = 2.0)	...	119	121	121	123	125	127	127	119	113	117	111
F_{by} , ksi: (e/D = 1.5)	...	68	70	68	70	70	73	70	69	72	69	72
(e/D = 2.0)	...	82	84	82	84	84	88	84	82	86	82	86
e , percent (S-basis):	LT	10	...	d	...	15	...	15	...	12	...	8
E , 10^3 ksi:	Primary
	Secondary	9.5	10.5	10.5	10.5	10.5	10.5	10.5	10.5	10.5	10.5	10.5
E_c , 10^3 ksi: Primary	...	10.7	10.7	10.7	10.7	10.7	10.7	10.7	10.7	10.7	10.7	10.7
Secondary	9.7	10.2	10.2	10.2	10.2	10.2	10.2	10.2	10.2	10.2	10.2	10.2
G , 10^3 ksi
μ
Physical Properties:	ω , lb/in ³	0.100	0.100	0.100	0.100	0.100	0.100	0.100	0.100	0.100	0.100	0.100
	C , K , and α

^a These values, except in the ST direction, have been adjusted to represent the average properties across the whole section, including the 2 1/2 percent nominal cladding thickness.
^b Caution: This specific alloy, temper, and product form exhibits poor stress-corrosion cracking resistance in this grain direction. It corresponds to an SCC resistance rating of D, as indicated in Table 3.1.2.3.1(a).

^c Bearing values are "dry pin" values per Section 1.4.7.1. See Table 3.1.2.1.1.

^d See Table 3.2.3.0(f).

Figure 1: Material properties for 2024-T3 clad sheet; excerpt taken from page 3-74 of MIL-HDBK-5H.

Table 8.1.3.1.2(p). Static Joint Strength of Protruding Head Locked Spindle Aluminum Alloy Blind Rivets in Aluminum Alloy Sheet

Rivet Type	HC6253 ^a ($F_u = 50$ ksi)			
Sheet Material	Clad 2024-T3			
Rivet Diameter, in. (Nominal Hole Diameter, in.)	1/8 (0.144)	5/32 (0.178)	3/16 (0.207)	
Sheet thickness, in.:		Ultimate Strength, lbs		
0.016	
0.020	
0.025	
0.032	344	419	...	
0.040	436	532	613	
0.050	513	674	777	
0.063	559	789	992	
0.071	588	824	1055	
0.080	620	864	1101	
0.090	656	908	1152	
0.100	691	952	1204	
0.125	781	1063	1332	
0.160	814	1217	1512	
0.190	1245	1666	
0.250	1685	
Rivet shear strength ^b	814	1245	1685	
Sheet thickness, in.:		Yield Strength ^c , lbs		
0.016	
0.020	
0.025	
0.032	344 ^d	419 ^d	...	
0.040	403	532 ^d	613 ^d	
0.050	462	619	731	
0.063	523	715	879	
0.071	541	774	948	
0.080	560	805	1025	
0.090	583	832	1079	
0.100	605	859	1110	
0.125	660	928	1190	
0.160	738	1024	1302	
0.190	1270	1397	
0.250	1588	

^a Data supplied by Huck International, Inc.^b Rivet shear strength is documented in MIL-R-7885D.^c Permanent set at yield load: 4% of nominal hole diameter (see 9.4.1.3.3).^d Yield reduced to match ultimate strength.

Figure 2: Allowables for CR3213-4 1/8" blind rivets; excerpt take from page 8-56 in MIL-HDBK-5H.

Sheet Thickness (mm)	Rivet Material	
	Aluminium (N)	Steel (N)
0.016	600	600
0.020	676	783
0.025	676	1228
0.032	676	1606

Figure 3: Allowables for 1/8" pop rivets.

2.4 External Loads and Reactions

A summary of the reaction forces computed for each limit load case is provided in table 8 and a general diagram of the tailplane box denoting the load application and reaction points is given in figure 4. Values obtained for each limit load case were computed by hand and validated using MATLAB. For the purpose of this exercise, it was assumed that,

$$A_x = B_x = C_x \quad \text{and} \quad A_z = B_z \quad (1)$$

Table 8: Reaction forces obtained from the analyses of section 2.4.

Lug	P_x [N]	P_y [N]	P_z [N]
Load Case 1			
A	0	11293	-66.00
B	0	-11293	-66.00
C	0	0	1012
P	0	0	-880
Load Case 2			
A	0	-5133	30.00
B	0	5133	30.00
C	0	0	-460.0
P	0	0	400
Load Case 3			
A	-33.33	192.5	5.000
B	-33.33	192.5	5.000
C	-33.33	-385.0	-10.00
P	100	0	0
Load Case 4			
A	0	40.83	0
B	0	-25.83	0
C	0	-115.0	0
P	0	100	0

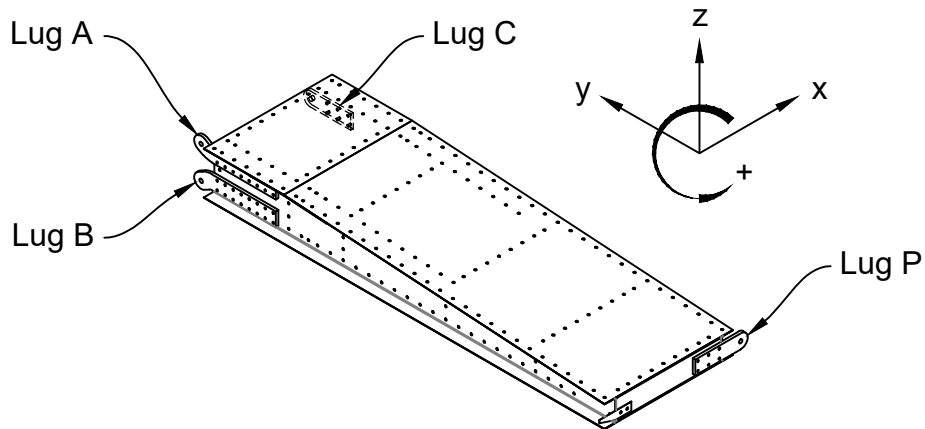


Figure 4: Diagram of the tailplane box denoting load application (lug P) and reaction (lugs A, B and C) points.

2.4.1 Load Case 1

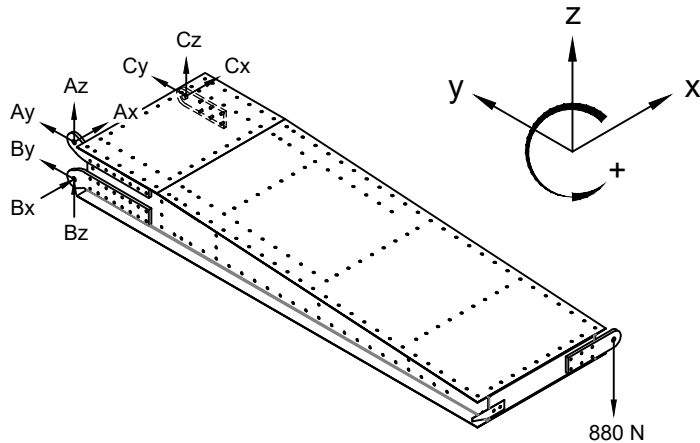


Figure 5: Load case 1 free body diagram.

A free body diagram (FBD) is given for load case 1 in figure 5. Summing forces,

$$\Sigma F_x = 0 = A_x + B_x + C_x \quad (2)$$

$$\Sigma F_y = 0 = A_y + B_y + C_y \quad (3)$$

$$\Sigma F_z = 0 = A_z + B_z + C_z - 880 \quad (4)$$

Summing moments about lug C,

$$\Sigma M_{xc} = 0 = -30A_y + 30B_y + 770 \times 880 \quad (5)$$

$$\Sigma M_{yc} = 0 = 200A_z + 200B_z + 30 \times 880 \quad (6)$$

$$\Sigma M_{zc} = 0 = -200A_y - 200B_y \quad (7)$$

As (2) is a free equation,

$$A_x = B_x = C_x = 0 \text{ N} \quad (8)$$

From (7),

$$A_y = -B_y \quad (9)$$

Hence substituting (9) into (3),

$$C_y = 0 \quad (10)$$

From (6),

$$A_z + B_z = -\frac{30 \times 880}{200} \longrightarrow A_z = B_z = -\frac{30 \times 880}{2 \times 200} = -66 \text{ N} \quad (11)$$

Substituting (11) into (4),

$$C_z = 880 + \frac{30 \times 880}{200} = 1012 \text{ N} \quad (12)$$

Substituting (9) into (5),

$$60B_y = -770 \times 880 \longrightarrow B_y = -\frac{770 \times 880}{60} = -11.29 \text{ kN} \quad (13)$$

$$\longrightarrow A_y = -B_y = 11.29 \text{ kN} \quad (14)$$

2.4.2 Load Case 2

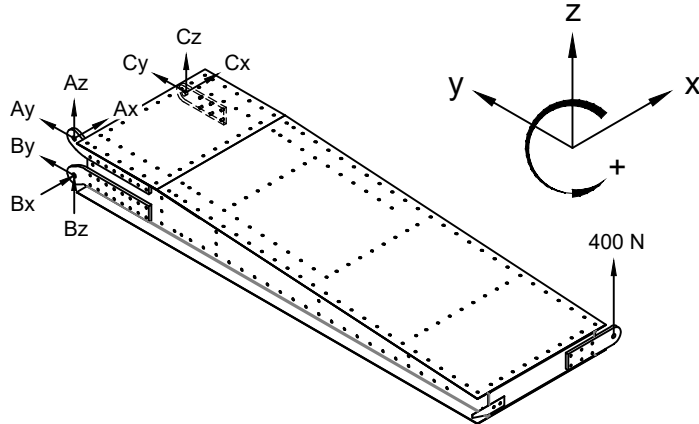


Figure 6: Load case 2 free body diagram.

A FBD is given for load case 2 in figure 6. As load case 2 is a scalar multiple of load case 1, the reaction forces were obtained by substitution of -880 N with +400 N in (11), (12) and (13), giving,

$$A_z = B_z = \frac{30 \times 400}{2 \times 200} = 30 \text{ N} \quad (15)$$

$$C_z = -400 - \frac{30 \times 400}{200} = -460 \text{ N} \quad (16)$$

$$B_y = \frac{770 \times 400}{60} = 5.133 \text{ kN} \quad (17)$$

$$\rightarrow A_y = -B_y = -5.133 \text{ kN} \quad (18)$$

and,

$$C_y = 0 \text{ N} \quad (19)$$

$$A_x = B_x = C_x = 0 \text{ N} \quad (20)$$

as before.

2.4.3 Load Case 3

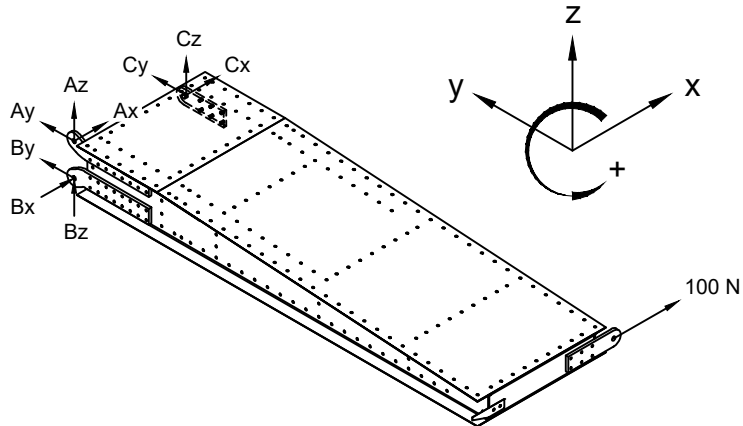


Figure 7: Load case 3 free body diagram.

A FBD is given for load case 3 in figure 7. Summing forces,

$$\Sigma F_x = 0 = A_x + B_x + C_x + 100 \quad (21)$$

$$\Sigma F_y = 0 = A_y + B_y + C_y \quad (22)$$

$$\Sigma F_z = 0 = A_z + B_z + C_z \quad (23)$$

Summing moments about lug C,

$$\Sigma M_{xc} = 0 = -30A_y + 30B_y \quad (24)$$

$$\Sigma M_{yc} = 0 = 30A_x - 30B_x + 200A_z + 200B_z - 20 \times 100 \quad (25)$$

$$\Sigma M_{zc} = 0 = -200A_y - 200B_y + 770 \times 100 \quad (26)$$

From (21),

$$A_x = B_x = C_x = -33.33 \text{ N} \quad (27)$$

From (24),

$$B_y = A_y \quad (28)$$

Hence substituting (28) into (26),

$$400A_y = 770 \times 100 \rightarrow A_y = B_y = \frac{770 \times 100}{400} = 192.5 \text{ N} \quad (29)$$

Substituting (29) into (22),

$$C_y = -385.0 \text{ N} \quad (30)$$

From (25),

$$A_z + B_z = \frac{20 \times 100}{200} \rightarrow A_z = B_z = \frac{20 \times 100}{400} = 5.000 \text{ N} \quad (31)$$

Hence substituting (31) into (23),

$$C_z = -10.00 \text{ N} \quad (32)$$

2.4.4 Load Case 4

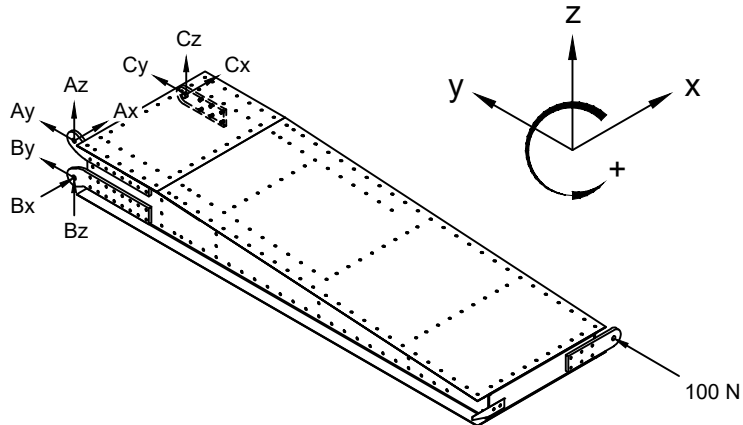


Figure 8: Load case 4 free body diagram.

A FBD is given for load case 4 in figure 8. Summing forces,

$$\Sigma F_x = 0 = A_x + B_x + C_x \quad (33)$$

$$\Sigma F_y = 0 = A_y + B_y + C_y + 100 \quad (34)$$

$$\Sigma F_z = 0 = A_z + B_z + C_z \quad (35)$$

Summing moments about lug C,

$$\Sigma M_{xc} = 0 = -30A_y + 30B_y + 20 \times 100 \quad (36)$$

$$\Sigma M_{yc} = 0 = 30A_x - 30B_x + 200A_z + 200B_z \quad (37)$$

$$\Sigma M_{zc} = 0 = -200A_y - 200B_y + 30 \times 100 \quad (38)$$

From (37) and (35),

$$A_z = B_z = C_z = 0 \text{ N} \quad (39)$$

Hence from (37), (33) and (39),

$$A_x = B_x = C_x = 0 \text{ N} \quad (40)$$

From (36) and (38),

$$A_y - B_y = \frac{20 \times 100}{30} \quad (41)$$

$$A_y + B_y = \frac{30 \times 100}{200} \quad (42)$$

Adding (41) and (42),

$$2A_y = \frac{20 \times 100}{30} + \frac{30 \times 100}{200} \rightarrow A_y = \frac{20 \times 100}{2 \times 30} + \frac{30 \times 100}{2 \times 200} = 40.83 \text{ N} \quad (43)$$

Hence substituting (43) into (36),

$$B_y = A_y - \frac{20 \times 100}{30} = 40.83 - \frac{20 \times 100}{30} = -25.84 \text{ N} \quad (44)$$

Hence substituting (43) and (44) into (34),

$$C_y = -A_y - B_y - 100 = -40.83 + 25.84 - 100 = -115.0 \text{ N} \quad (45)$$

2.5 Calculation of Internal Loads

Spar cap loads, mid-bay shear flows and rib shear flows were computed in MATLAB using the methods presented in the following sections. Graphs of load split parameters, spar shear forces and moments, and spar cap loads computed using a semi-empirical approach, along with the resultant mid-bay skin and spar shear flows validated using two separate methods, are given in figure 10. The corresponding resultant rib shear flows are given in figure 11. Further validation of these results is provided in section 2.6, where a FEM analysis of the tailplane box using HughFEM is given.

2.5.1 Calculation of Spar Cap Loads & Method 1 Shear Flows

A semi-empirical approach was employed in the calculation of the spar cap loads and shear flows. This approach is based on two empirical parameters, known as the cap load split and shear load split parameters. In the context of the tailplane box, the cap load split parameter is defined as,

$$\lambda = \frac{P_r}{P_t} \quad (46)$$

where P_r is the direct load acting on the rear spar cap and P_t is the total direct load acting on the front and rear spar caps. An explicit expression for λ was hence derived, based on FEM analysis of a generic tailplane box design, and is given as,

$$\lambda(\xi) = \begin{cases} 0.47 - 0.47 \left(\frac{\xi - 500}{250} \right), & 500 \leq \xi \leq 750 \\ 0.57 - 0.1 \left(\frac{\xi}{500} \right), & 0 \leq \xi < 500 \end{cases} \quad (47)$$

where $\xi = 750 - y$ is the tip coordinate, measured relative the tailplane box tip rib, and y is the root coordinate, measured relative to the tailplane box root rib. Hence the rear spar cap moment was computed as,

$$M_r = \lambda(\xi) V_t \xi \quad (48)$$

where V_t is the total shear force acting on the tailplane box. Hence the rear spar cap shear force,

$$V_r = \frac{dM_r}{d\xi} = \frac{d\lambda}{d\xi} V_t \xi + \lambda V_t = \eta V_t \quad (49)$$

Hence by inspection, the shear load split parameter,

$$\eta = \frac{d\lambda}{d\xi} \xi + \lambda = \frac{V_r}{V_t} \quad (50)$$

With λ and η , and with reference to the situation depicted in figure 9, the spar cap loads were thus be computed as,

$$P_{h_f} = \frac{V_t \xi}{h} (1 - \lambda) \quad P_{h_r} = \frac{V_t \xi}{h} \lambda \quad (51)$$

$$P_{t_*} = \frac{P_{h_*}}{\cos \theta}$$

$$P_{v_*} = P_{h_*} \tan \theta$$

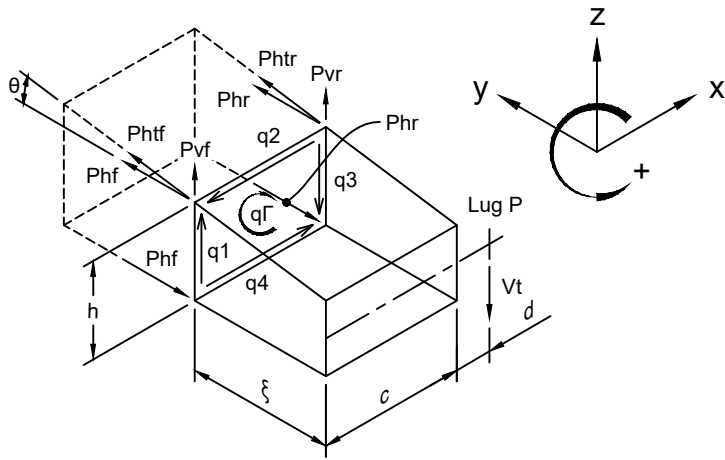


Figure 9: Free body diagram of a cut section of the tailplane box subject to shear load V_t .

where subscripts h , v , f , r and t denote horizontal, vertical, front, rear and total quantities respectively, and subscript $*$ denotes either a front or rear quantity, with h and θ being the instantaneous height and taper angle of the tailplane box at tip coordinate ξ . Hence the total shear flow before torsion balance at tip coordinate ξ was computed as,

$$q_1 = \frac{V_t(1 - \eta) - P_{v_f}}{h} \quad q_3 = \frac{V_t \eta - P_{v_r}}{h} \quad (52)$$

$$q_2 = q_4 = 0$$

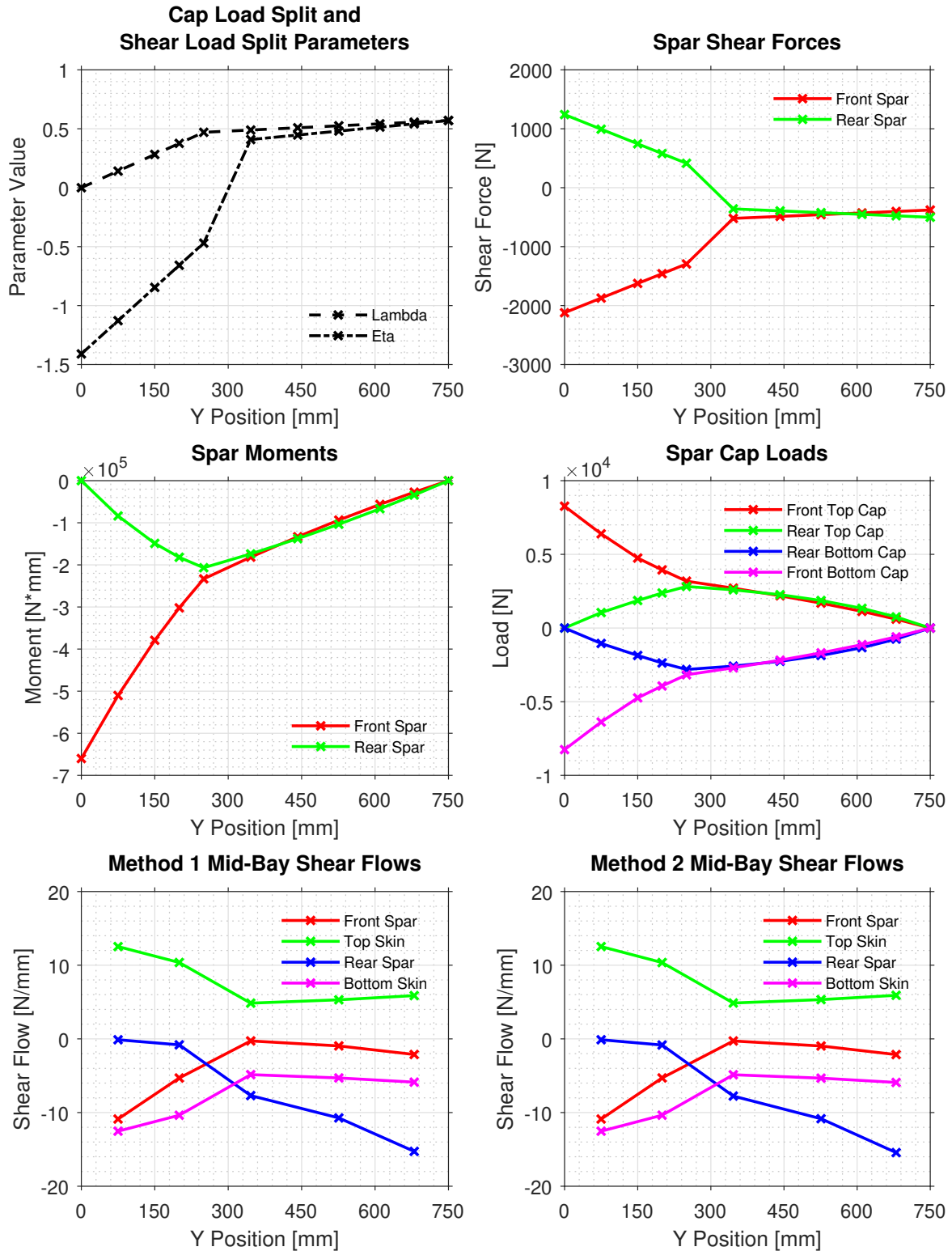


Figure 10: From left to right, top to bottom, graphs of load split parameters, spar shear forces, spar moments, spar cap loads and mid-bay skin and spar shear flows using method 1 (section 2.5.1) and method 2 (section 2.5.2), computed for load case 1, at limit load.

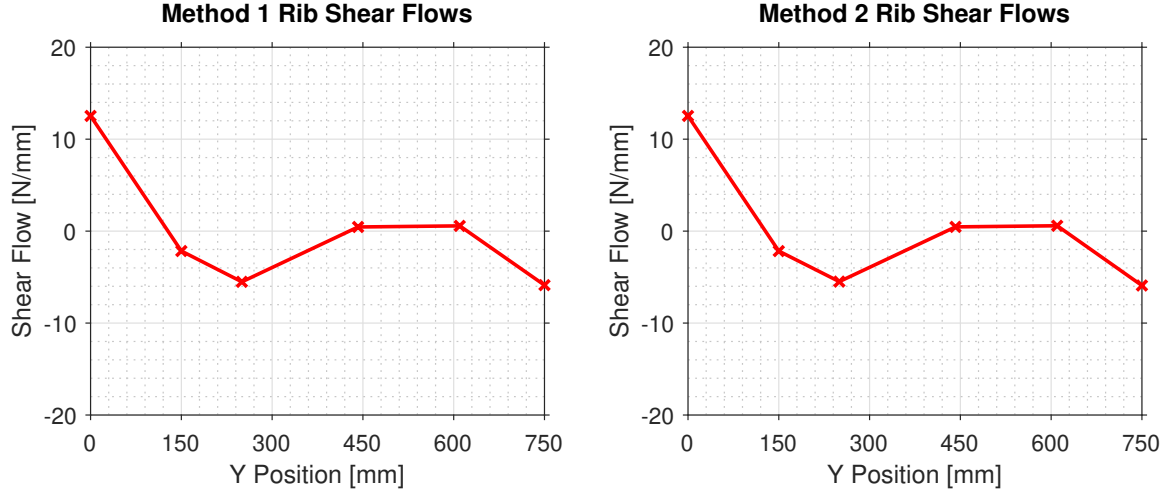


Figure 11: Graphs of rib shear flows computed as the difference of top skin mid-bay shear flows using method 1 (section 2.5.1) and method 2 (section 2.5.2), computed for load case 1, at limit load.

Hence balancing moments, the cross sectional torsion reaction was computed as,

$$q_{\Gamma} = -\frac{(q_1 h + P_{v_f})(c + d) + (q_3 h + P_{v_r})d}{2ch} \quad (53)$$

Adding and subtracting q_{Γ} to q_1 through q_4 as necessary yielded the instantaneous shear flow at tip coordinate ξ .

2.5.2 Calculation of Method 2 Shear Flows

From the spar cap loads computed using (51), a second method for computing the resultant instantaneous shear flow at tip coordinate ξ was employed in addition to the method described above. Four independent linear equations were derived and solved simultaneously in MATLAB. With reference to figure 12, three equations were derived from balancing forces at three spar caps,

$$\begin{aligned} (q_1 - q_2) \frac{L}{\cos \theta} &= P_{tf(1)} - P_{tf(2)} \\ (q_2 - q_3) \frac{L}{\cos \theta} &= P_{tr(1)} - P_{tr(2)} \\ (q_3 - q_4) L &= P_{hr(1)} - P_{hr(2)} \end{aligned} \quad (54)$$

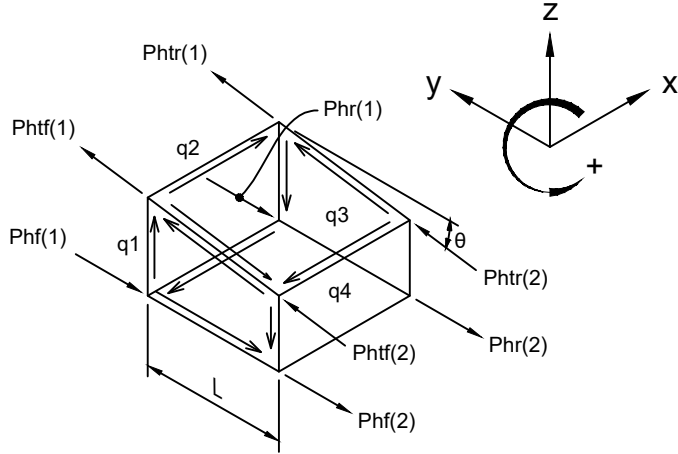


Figure 12: Free body diagram of a cut section of the tailplane box subject to direct load P ; note that the depiction of shear flows q_3 and q_4 has been simplified for clarity.

with the fourth being derived from balancing moments,

$$q_1 h (c + d) + q_3 h d + (q_2 + q_4) \frac{ch}{2} = -P_{v_f}(c + d) - P_{v_r} d \quad (55)$$

Recasting (54) and (55) as a system of linear equations,

$$\begin{bmatrix} \frac{L}{\cos \theta} & -\frac{L}{\cos \theta} & 0 & 0 \\ 0 & \frac{L}{\cos \theta} & -\frac{L}{\cos \theta} & 0 \\ 0 & 0 & L & -L \\ h(c+d) & \frac{ch}{2} & hd & \frac{ch}{2} \end{bmatrix} \begin{bmatrix} q_1 \\ q_2 \\ q_3 \\ q_4 \end{bmatrix} = \begin{bmatrix} P_{t_f(1)} - P_{t_f(2)} \\ P_{t_r(1)} - P_{t_r(2)} \\ P_{h_r(1)} - P_{h_r(2)} \\ -P_{v_f}(c+d) - P_{v_r} d \end{bmatrix} \quad (56)$$

Hence solving (56) in MATLAB yielded the instantaneous shear flow at tip coordinate ξ .

2.6 FEM Re-Calculation of Internal Loads

A FEM analysis of the tailplane box was performed using the provided HughFEM MATLAB code, the results of which are given in figure 13. Comparing figure 13 to figures 10 and 11 it can be seen that the computed spar cap loads and shear flows are identical, within some margin, except at BL250 where the taper begins. The reason for this is the semi-empirical nature of the method used to compute the spar cap loads in section 2.5. As the cap load split parameter, λ , used to compute the spar cap loads is characterised by a piece-wise function whose gradient changes suddenly at BL250, there is a slight but noticeable change in the gradient of the spar cap loads at this point as shown in figure 10. This is carried through to the calculation of shear flows where, again, a slight but noticeable kink in the computed

mid-bay shear flows can be seen in figure 10 at BL250, which is exacerbated by the piece-wise nature of the shear load split parameter, η , a function of λ . Ultimately, this discrepancy does not significantly impact the stress analysis, and hence use of the results obtained in section 2.5 was deemed acceptable for the final design.

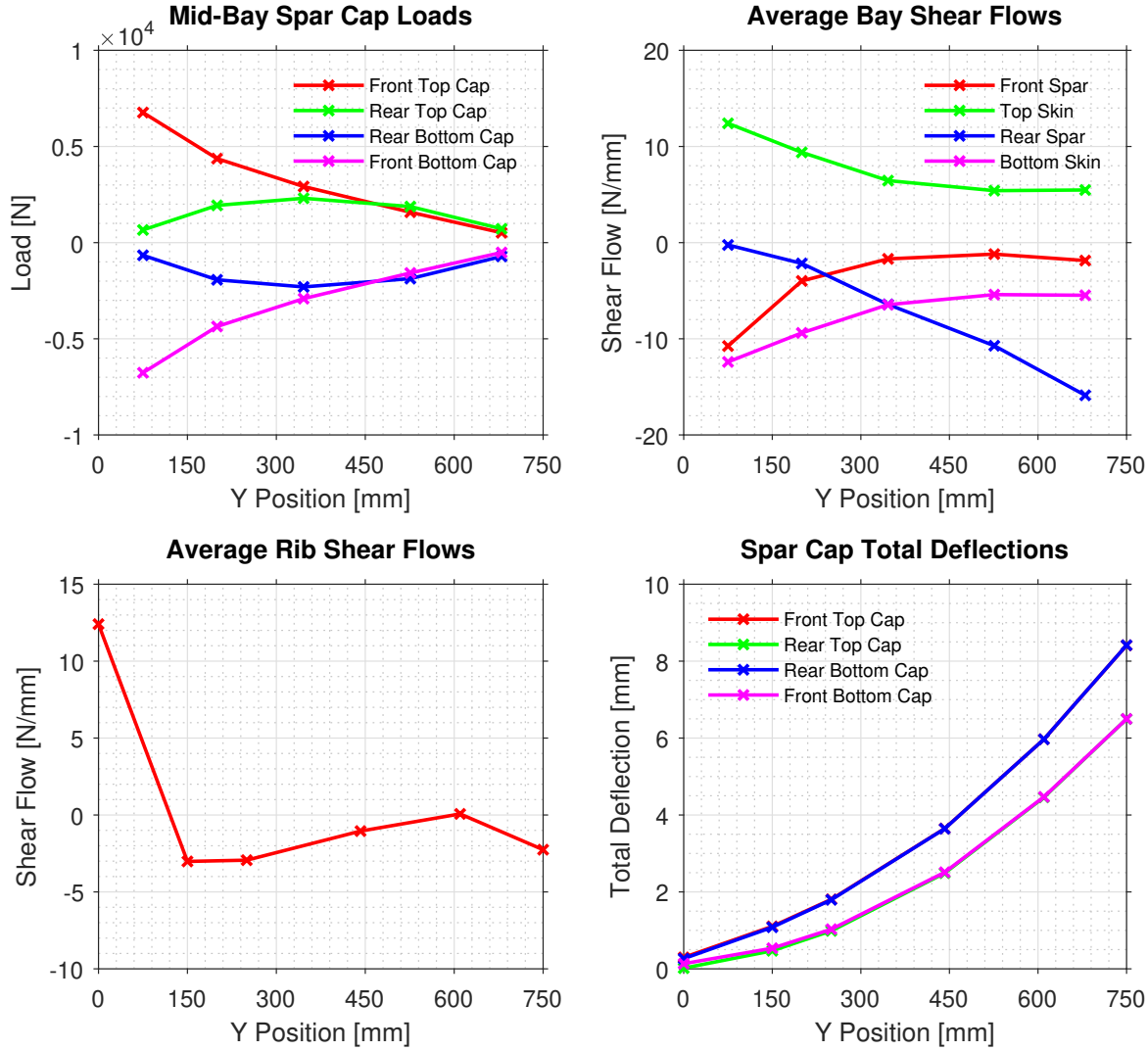


Figure 13: From left to right, top to bottom, graphs of mid-bay spar cap loads, average bay shear flows, average rib shear flows and spar cap total deflections computed for load case 1, at limit load, using the provided HughFEM finite element code.

2.7 Spar Cap Geometry

2.7.1 Spar Cap Geometry Summary

See section 6 for general details of the tailplane box assembly and part geometry. This section outlines the geometry used in the spar cap stress analysis and was added in order to reduce repetitive calculations in the following sections. The spar cap geometry was standardised for ease of analysis and construction, with the lower spar cap reinforcements being made from 0.64 mm 2024-T3 angled clad plate whilst the upper spar cap reinforcements were made from 0.41 mm 2024-T3 angled clad plate. A standard reinforcing angle size of 15×25 mm was adopted and is shown diagrammatically in figures 14(b) and 14(f) below for both thicknesses. Figure 14(a) also shows the standard spar flange width of 20 mm along with rivet line dimensions in figure 16(l).

In certain sections, no reinforcement was required, and this will be demonstrated in the spar cap stress analysis. For other sections, greater reinforcement was necessary. In this case, the spar cap reinforcement consists of a series of nested angles, with the geometry shown in figures 14(b) and 14(f) being the geometry of the inner-most nested reinforcing angle, and the width and height of all other angles increased in order to remain flush with the edges of the inner-most angle, thus allowing the rivet line of the inner-most angle to be maintained. An example of this is shown in figure 15(e) for spar cap configuration 5. Summaries of the geometric properties of each spar cap component and of each spar cap configuration are given in tables 9 and 10 respectively. Detailed sample calculations are given for spar cap configuration 2 in the following sections in order to demonstrate the method used to compute the spar cap geometry, with detailed calculations for the remaining 10 spar cap configurations given in appendix A.

Table 9: Summary of spar cap component geometric properties; see figure 14 for section diagrams. Note that $c = b'/t$ and A_m are the average side length divided by thickness and the mid-line area, respectively, of the spar cap component for crippling calculations.

Component	w [mm]	h [mm]	t [mm]	c	A_t [mm 2]	A_m [mm 2]	\bar{x} [mm]	\bar{y} [mm]	I_{xx} [mm 4]	I_{yy} [mm 4]
Spar Flange & Web	20	20	0.41	30.75	15.98	16.23	5.213	5.213	660.0	660.0
Spar Cap Reinforcement 1	25	15	0.64	30.75	24.57	25.19	8.206	3.081	491.7	1683
Spar Cap Reinforcement 2	25.64	15.64	0.64	31.75	25.39	26.01	8.355	3.234	555.6	1828
Spar Cap Reinforcement 3	26.28	16.28	0.64	32.75	26.21	26.83	8.504	3.387	624.8	1981
Spar Cap Reinforcement 4	26.92	16.92	0.64	33.75	27.03	27.65	8.654	3.541	699.6	2142
Spar Cap Reinforcement 5	25	15	0.41	48.28	15.98	16.23	8.074	2.995	319.0	1095
Spar Cap Reinforcement 6	25.41	15.41	0.41	49.28	16.32	16.57	8.168	3.091	345.2	1155
Spar Cap Reinforcement 7	25.82	15.82	0.41	50.28	16.66	16.90	8.262	3.188	372.8	1217

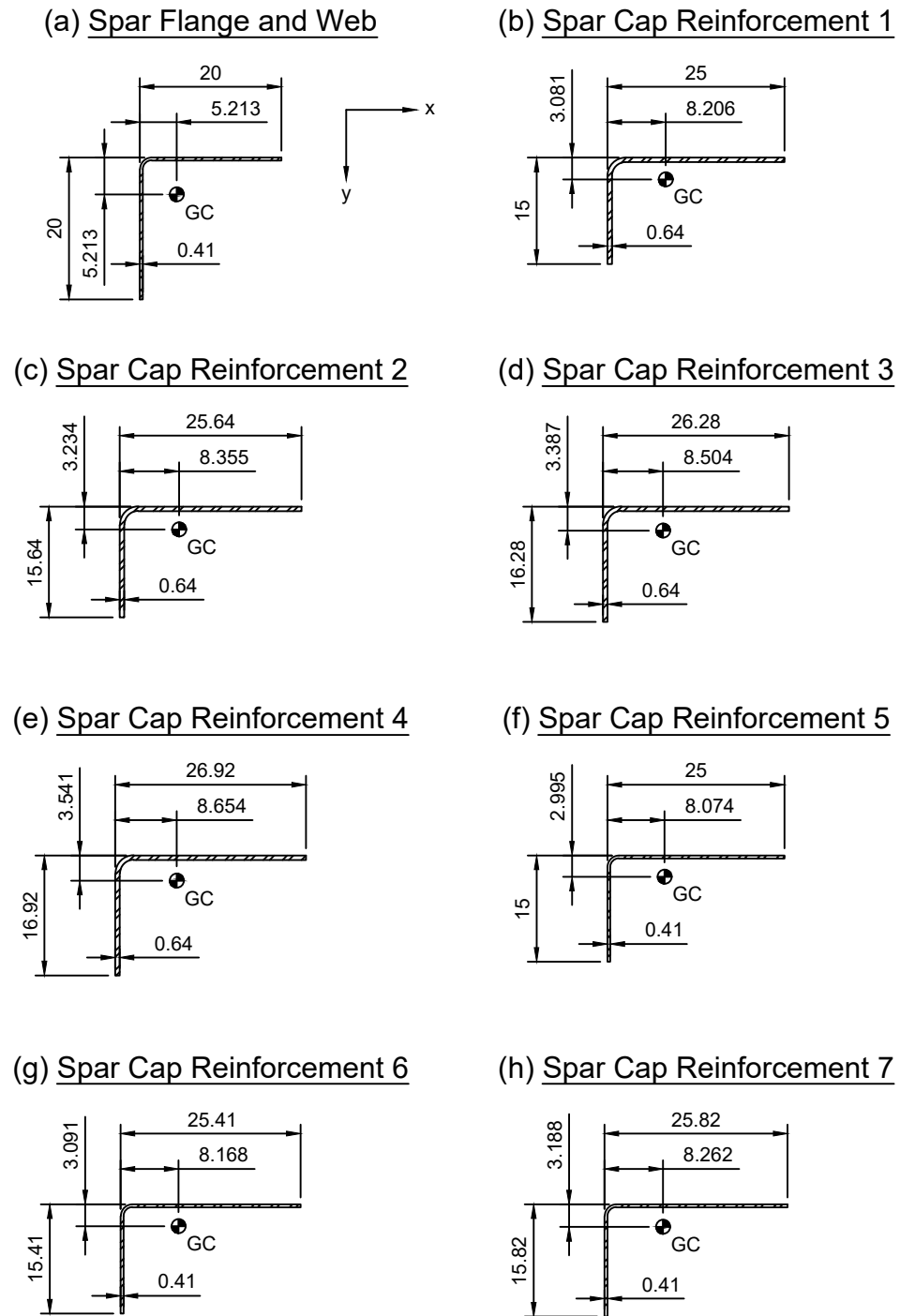
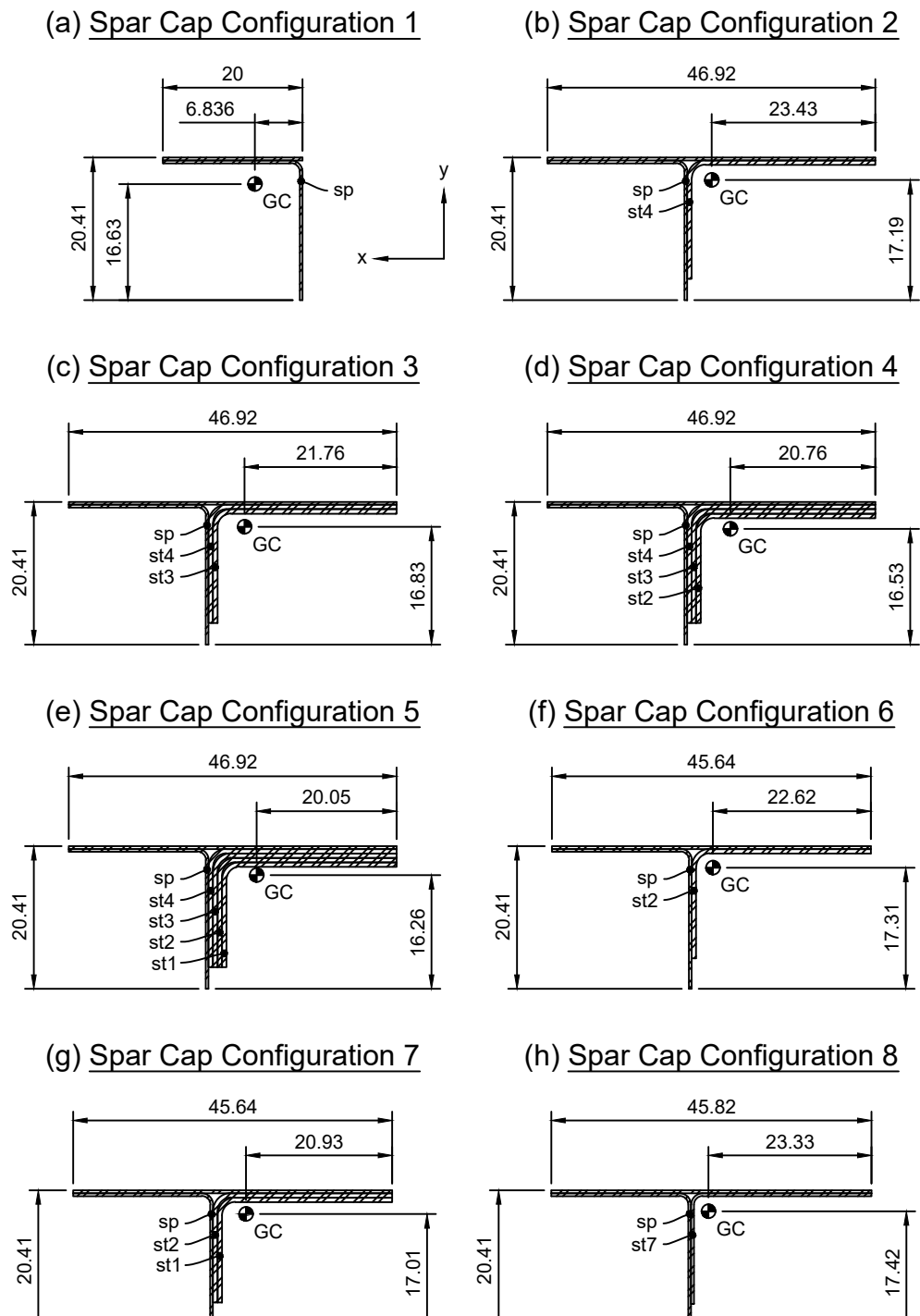


Figure 14: Spar cap component section geometry diagrams.

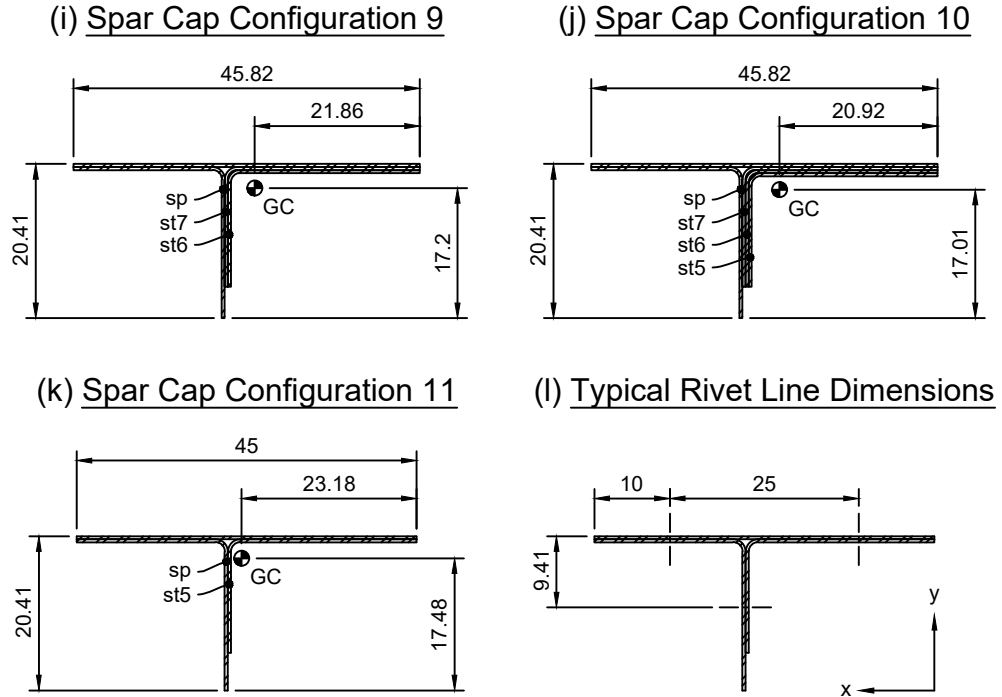
Table 10: Summary of spar cap configuration geometric properties; see figures 15 and 16 for section diagrams

Configuration	W_c [mm]	H_c [mm]	A_t [mm 2]	A_{sk} [mm 2]	\bar{X}_c [mm]	\bar{Y}_c [mm]	I_{cxx} [mm 4]	I_{cyy} [mm 4]
Spar Cap Configuration 1	20	20.41	15.98	8.200	6.836	16.63	819.3	1058
Spar Cap Configuration 2	46.92	20.41	43.01	19.24	23.43	17.19	1642	8260
Spar Cap Configuration 3	46.92	20.41	69.22	19.24	21.76	16.83	2294	10830
Spar Cap Configuration 4	46.92	20.41	94.61	19.24	20.76	16.53	2885	13052
Spar Cap Configuration 5	46.92	20.41	119.2	19.24	20.05	16.26	3424	15054
Spar Cap Configuration 6	45.64	20.41	41.37	18.71	22.62	17.31	1482	7541
Spar Cap Configuration 7	45.64	20.41	65.94	18.71	20.93	17.01	1992	9817
Spar Cap Configuration 8	45.82	20.41	32.64	18.79	23.33	17.42	1295	6474
Spar Cap Configuration 9	45.82	20.41	48.96	18.79	21.86	17.20	1651	8089
Spar Cap Configuration 10	45.82	20.41	64.94	18.79	20.92	17.01	1983	9498
Spar Cap Configuration 11	45	20.41	31.96	18.45	23.18	17.48	1236	6291



Key: sp = spar flange and web, st = spar cap reinforcement

Figure 15: Spar cap configurations 1 to 8 section geometry diagrams.



Key: sp = spar flange and web, st = spar cap reinforcement

Figure 16: Spar cap configurations 9 to 11 section geometry diagrams.

2.7.2 Spar Cap Component Geometry Calculations

2.7.2.1 Spar Flange & Web

A diagram of the cross sectional area of the spar web and flange is given in figure 14(a). For a bend radius of $3t$, the bend areas for 0.41 mm clad sheet was computed as,

$$A_{r(0.41)} = \frac{\pi}{4}(16t_{sp}^2 - 9t_{sp}^2) = \frac{7}{4}\pi \times (0.41)^2 = 0.9242 \text{ mm}^2 \quad (57)$$

The straight area of the spar flange and web was computed as,

$$A_{w_{sp}} = t_{sp}(w_{sp} - 4t_{sp}) = 0.41 \times (20 - 4 \times 0.41) = 7.528 \text{ mm}^2 \quad (58)$$

The total spar flange and web area was thus computed as,

$$\begin{aligned} A_{sp} &= 2A_{w_{sp}} + A_{r(0.41)} \\ &= 2 \times 7.528 + 0.9242 = 15.98 \text{ mm}^2 \end{aligned} \quad (59)$$

The mid-line spar flange and web area was computed as,

$$\begin{aligned} A_{spm} &= (2w_{sp} - t_{sp})t_{sp} \\ &= (2 \times 20 - 0.41) \times 0.41 = 16.23 \text{ mm}^2 \end{aligned} \quad (60)$$

The average side length divided by thickness of the spar flange and web for crippling calculations was computed as,

$$c_{sp} = \frac{2w_{sp} - t}{2t} = \frac{2 \times 20 - 0.64}{2 \times 0.64} = 30.75 \quad (61)$$

Taking the x and y ordinate directions to be those shown in figure 14(a), the centroid was computed relative to the edges of the angle as shown in figure 14(a). For a bend radius of $3t$, the bend centroid for 0.41 mm clad sheet was computed as,

$$\begin{aligned} \bar{x}_{r(0.41)} &= \bar{y}_{r(0.41)} = 4t_{sp} - \frac{8}{3\pi} \sin\left(\frac{\pi}{4}\right) \frac{64t_{sp}^3 - 27t_{sp}^3}{16t_{sp}^2 - 9t_{sp}^2} \\ &= 4 \times 0.41 - \frac{8 \times 37 \times (0.41)^3}{\sqrt{18}\pi \times 7 \times (0.41)^2} \\ &= 0.3393 \text{ mm} \end{aligned} \quad (62)$$

The centroid of the spar flange was computed as,

$$\bar{x}_{w_{sp}} = \frac{w_{sp} - 4t}{2} + 4t_{sp} = \frac{20 - 4 \times 0.41}{2} + 4 \times 0.41 = 10.82 \text{ mm} \quad (63)$$

$$\bar{y}_{w_{sp}} = \frac{t}{2} = \frac{0.41}{2} = 0.2050 \text{ mm} \quad (64)$$

The total spar flange and web centroid was thus computed as,

$$\begin{aligned} \bar{x}_{sp} &= \bar{y}_{sp} = \frac{\sum \bar{x}_{sp(i)} A_{sp(i)}}{\sum A_{sp(i)}} \\ &= \frac{(\bar{x}_{w_{sp}} + \bar{y}_{w_{sp}}) A_{w_{sp}} + \bar{x}_{r(0.41)} A_{r(0.41)}}{A_{sp}} \\ &= \frac{(10.82 + 0.2050) \times 7.528 + 0.3393 \times 0.9242}{15.98} \\ &= 5.213 \text{ mm} \end{aligned} \quad (65)$$

For a bend radius of $3t$, the bend second moment of area for 0.41 mm clad sheet was computed as,

$$I_{rxx(0.41)} = I_{ryy(0.41)} = \frac{\pi}{16}(256t_{sp}^4 - 81t_{sp}^4) = \frac{175\pi \times (0.41)^4}{16} = 0.9710 \text{ mm}^4 \quad (66)$$

The straight second moments of area of the spar flange were computed as,

$$I_{w_{sp}xx} = \frac{(w_{sp} - 4t_{sp})t_{sp}^3}{12} = \frac{(20 - 4 \times 0.41)(0.41)^3}{12} = 0.1054 \text{ mm}^4 \quad (67)$$

$$I_{w_{sp}yy} = \frac{t(w_{sp} - 4t_{sp})^3}{12} = \frac{0.41 \times (20 - 4 \times 0.41)^3}{12} = 211.5 \text{ mm}^4 \quad (68)$$

Hence the total second moments of area of the spar flange were computed as,

$$\begin{aligned} I_{spxx} = I_{spyy} &= I_{w_{sp}xx} + I_{w_{sp}yy} + I_{rxx(0.41)} + [(\bar{y}_{sp} - \bar{y}_{w_{sp}})^2 + (\bar{y}_{sp} - \bar{x}_{w_{sp}})^2] A_{w_{sp}} \\ &\quad + (\bar{y}_{sp} - \bar{y}_{r(0.41)})^2 A_{r(0.41)} \\ &= 0.1054 + 211.5 + 0.9710 + [(5.213 - 0.2050)^2 + (5.213 - 10.82)^2] \times 7.528 \\ &\quad + (5.213 - 0.3393)^2 \times 0.9242 \\ &= 660.0 \text{ mm}^4 \end{aligned} \quad (69)$$

2.7.2.2 Spar Cap Reinforcement 4

A diagram of the cross sectional area of the spar cap reinforcement is given in figure 14(e). Detailed calculations of all quantities relating to the spar cap reinforcement 3 geometry (denoted by a subscript 3) that are referenced in the calculation of the spar cap reinforcement 4 geometry can be found in appendix A.1.3. The total spar cap reinforcement area was computed as,

$$A_{st4} = A_{st3} + 2t_{st1}^2 = 26.21 + 2 \times (0.64)^2 = 27.03 \text{ mm}^2 \quad (70)$$

The width and height of the spar cap reinforcement were computed as,

$$\begin{aligned} w_{st4} &= w_{st3} + t_{st1} = 26.28 + 0.64 = 26.92 \text{ mm} \\ h_{st4} &= h_{st3} + t_{st1} = 16.28 + 0.64 = 16.92 \text{ mm} \end{aligned} \quad (71)$$

The mid-line area of the spar cap reinforcement was thus computed as,

$$\begin{aligned} A_{st4m} &= (w_{st4} + h_{st4} - t_{st1})t_{st1} \\ &= (26.92 + 16.92 - 0.64) \times 0.64 = 27.65 \text{ mm}^2 \end{aligned} \quad (72)$$

The average side length divided by thickness of the spar cap reinforcement for crippling calculations was computed as,

$$c_{st4} = \frac{w_{st4} + h_{st4} - t}{2t} = \frac{26.92 + 16.92 - 0.64}{2 \times 0.64} = 33.75 \quad (73)$$

The centroid of the additional horizontal area of the spar cap reinforcement was computed as,

$$\bar{x}_{w_{st4}} = \bar{x}_{w_{st3}} + t_{st1} = 25.96 + 0.64 = 26.60 \text{ mm} \quad (74)$$

$$\bar{y}_{w_{st4}} = \bar{y}_{w1_{st}} = 0.3200 \text{ mm} \quad (75)$$

The centroid of the additional vertical area of the spar cap reinforcement was computed as,

$$\bar{x}_{h_{st4}} = \bar{x}_{h1_{st}} = 0.3200 \text{ mm} \quad (76)$$

$$\bar{y}_{h_{st4}} = \bar{y}_{h_{st3}} + t_{st1} = 15.96 + 0.64 = 16.60 \text{ mm} \quad (77)$$

The total spar cap reinforcement centroid was thus computed as,

$$\begin{aligned} \bar{x}_{st4} &= \frac{\sum \bar{x}_{st4(i)} A_{st4(i)}}{\sum A_{st4(i)}} \\ &= \frac{\bar{x}_{st3} A_{st3} + (\bar{x}_{w_{st4}} + \bar{x}_{h_{st4}}) t_{st1}^2}{A_{st4}} \\ &= \frac{8.504 \times 26.21 + (26.60 + 0.3200)(0.64)^2}{27.03} \\ &= 8.654 \text{ mm} \end{aligned} \quad (78)$$

$$\begin{aligned} \bar{y}_{st4} &= \frac{\sum \bar{y}_{st4(i)} A_{st4(i)}}{\sum A_{st4(i)}} \\ &= \frac{\bar{y}_{st3} A_{st3} + (\bar{y}_{w_{st4}} + \bar{y}_{h_{st4}}) t_{st1}^2}{A_{st4}} \\ &= \frac{3.387 \times 26.21 + (0.3200 + 16.60)(0.64)^2}{27.03} \\ &= 3.541 \text{ mm} \end{aligned} \quad (79)$$

Hence the total second moments of area of the spar cap reinforcement were computed as,

$$\begin{aligned}
I_{st4xx} &= I_{st3xx} + \frac{1}{6}t_{st1}^4 + (\bar{y}_{st4} - \bar{y}_{st3})^2 A_{st3} \\
&\quad + [(\bar{y}_{st4} - \bar{y}_{w_{st4}})^2 + (\bar{y}_{st4} - \bar{y}_{h_{st4}})^2] t_{st1}^2 \\
&= 624.8 + \frac{1}{6}(0.64)^4 + (3.541 - 3.387)^2 \times 26.21 \\
&\quad + [(3.541 - 0.3200)^2 + (3.541 - 16.60)^2] (0.64)^2 \\
&= 699.6 \text{ mm}^4
\end{aligned} \tag{80}$$

$$\begin{aligned}
I_{st4yy} &= I_{st3yy} + \frac{1}{6}t_{st1}^4 + (\bar{x}_{st4} - \bar{x}_{st3})^2 A_{st3} \\
&\quad + [(\bar{x}_{st4} - \bar{x}_{w_{st4}})^2 + (\bar{x}_{st4} - \bar{x}_{h_{st4}})^2] t_{st1}^2 \\
&= 1981 + \frac{1}{6}(0.64)^4 + (8.654 - 8.504)^2 \times 26.21 \\
&\quad + [(8.654 - 26.60)^2 + (8.654 - 0.3200)^2] (0.64)^2 \\
&= 2142 \text{ mm}^4
\end{aligned} \tag{81}$$

2.7.3 Spar Cap Configuration 2 Geometry Calculations

A diagram of the cross sectional area of the spar cap configuration is given in figure 15(b). The true area of the configuration, excluding the skin, was computed as,

$$A_{t2} = A_{sp} + A_{st4} = 15.98 + 27.03 = 43.01 \text{ mm}^2 \tag{82}$$

The total width and height of the configuration were computed as,

$$\begin{aligned}
W_{c2} &= W_{c1} + w_{st4} = 20 + 26.92 = 46.92 \text{ mm} \\
H_{c2} &= H_{c1} = 20.41 \text{ mm}
\end{aligned} \tag{83}$$

The true skin area was computed as,

$$A_{sk2} = W_{c2}t_{sk} = 46.92 \times 0.41 = 19.24 \text{ mm}^2 \tag{84}$$

The centroids of the skin, spar flange and web and spar cap reinforcement, relative to the global configuration coordinates shown in figure 15(b), were computed, respectively, as,

$$\begin{aligned}\bar{X}_{sk2} &= \frac{W_{c2}}{2} = \frac{46.92}{2} = 23.46 \text{ mm} \\ \bar{Y}_{sk2} &= \bar{Y}_{sk1} = 20.21 \text{ mm} \\ \bar{X}_{sp2} &= \bar{x}_{sp} + w_{st4} = 5.213 + 26.92 = 32.13 \text{ mm} \\ \bar{Y}_{sp2} &= \bar{Y}_{sp1} = 14.79 \text{ mm}\end{aligned}\tag{85}$$

$$\begin{aligned}\bar{X}_{st2} &= W_{c2} - (w_{sp} + \bar{x}_{st4}) = 46.92 - (20 + 8.654) = 18.27 \text{ mm} \\ \bar{Y}_{st2} &= H_{c2} - (\bar{y}_{st4} + t_{sk}) = 20.41 - (3.541 + 0.41) = 16.46 \text{ mm}\end{aligned}$$

The total centroid of the configuration, relative to the global configuration coordinates shown in figure 15(b), was thus computed as,

$$\begin{aligned}\bar{X}_{c2} &= \frac{\sum \bar{X}_{c2(i)} A_{c2(i)}}{\sum A_{c2(i)}} \\ &= \frac{\bar{X}_{sk2} A_{sk2} + \bar{X}_{sp2} A_{sp} + \bar{X}_{st2} A_{st4}}{A_{sk2} + A_{sp} + A_{st4}} \\ &= \frac{23.46 \times 19.24 + 32.13 \times 15.98 + 18.27 \times 27.03}{19.24 + 15.98 + 27.03} \\ &= 23.43 \text{ mm}\end{aligned}\tag{86}$$

$$\begin{aligned}\bar{Y}_{c2} &= \frac{\sum \bar{Y}_{c2(i)} A_{c2(i)}}{\sum A_{c2(i)}} \\ &= \frac{\bar{Y}_{sk2} A_{sk2} + \bar{Y}_{sp2} A_{sp} + \bar{Y}_{st2} A_{st4}}{A_{sk2} + A_{sp} + A_{st4}} \\ &= \frac{20.21 \times 19.24 + 14.79 \times 15.98 + 16.46 \times 27.03}{19.24 + 15.98 + 27.03} \\ &= 17.19 \text{ mm}\end{aligned}\tag{87}$$

Hence the total second moments of area of the configuration were computed as,

$$\begin{aligned}
 I_{c2xx} &= I_{spxx} + I_{st4xx} + \frac{W_{c2}t_{sk}^3}{12} + (\bar{Y}_{c2} - \bar{Y}_{sp2})^2 A_{sp} \\
 &\quad + (\bar{Y}_{c2} - \bar{Y}_{st2})^2 A_{st4} + (\bar{Y}_{c2} - \bar{Y}_{sk2})^2 A_{sk2} \\
 &= 660.0 + 699.6 + \frac{46.92 \times (0.41)^3}{12} + (17.19 - 14.79)^2 \times 15.98 \\
 &\quad + (17.19 - 16.46)^2 \times 27.03 + (17.19 - 20.21)^2 \times 19.24 \\
 &= 1642 \text{ mm}^4
 \end{aligned} \tag{88}$$

$$\begin{aligned}
 I_{c2yy} &= I_{spyy} + I_{st4yy} + \frac{t_{sk}W_{c2}^3}{12} + (\bar{X}_{c2} - \bar{X}_{sp2})^2 A_{sp} \\
 &\quad + (\bar{X}_{c2} - \bar{X}_{st2})^2 A_{st4} + (\bar{X}_{c2} - \bar{X}_{sk2})^2 A_{sk2} \\
 &= 660.0 + 2142 + \frac{0.41 \times (46.92)^3}{12} + (23.43 - 32.13)^2 \times 15.98 \\
 &\quad + (23.43 - 18.27)^2 \times 27.03 + (23.43 - 23.46)^2 \times 19.24 \\
 &= 8260 \text{ mm}^4
 \end{aligned} \tag{89}$$

2.8 Stress Analysis

2.8.1 Spar Web & Skin Shear Buckling Ratios

The following section outlines the spar web and skin shear buckling analysis of the tailplane box. With six ribs in place, the design consists of a total of five bays where it is necessary to analyse four panels in each bay. Shear buckling ratios were computed for each panel and compared to the limit given in the design specification, $BR \leq 5$. Summaries of the shear buckling ratios computed for load cases 1 and 2 are given in tables 11 and 12 respectively. It is clear from both tables that the design specification is met for all panels except for top and bottom skin panels in bay 1 for load case 1. As shear buckling is not a critical failure mode, it was decided that no further modification to the design was necessary in order to reduce said buckling ratios, as any such modification would involve the addition of a rib or stiffener between the ribs at BL100 and BL250, thus increasing the mass of the final design, a more significant priority.

Table 11: Shear buckling ratios for load case 1; note that bay 1 is the most inboard bay.

Panel	Bay 5	Bay 4	Bay 3	Bay 2	Bay 1
Front Spar	0.1675	0.1120	0.04791	0.8646	2.135
Top Skin	3.794	4.284	4.682	3.406	5.455
Rear Spar	1.213	1.259	1.310	0.1361	0.02375
Bottom Skin	3.794	4.284	4.682	3.406	5.455

Table 12: Shear buckling ratios for load case 2; note that bay 1 is the most inboard bay.

Panel	Bay 5	Bay 4	Bay 3	Bay 2	Bay 1
Front Spar	0.07615	0.05093	0.02178	0.3930	0.9705
Top Skin	1.725	1.947	2.128	1.548	2.480
Rear Spar	0.5514	0.5724	0.5953	0.06185	0.01080
Bottom Skin	1.725	1.947	2.128	1.548	2.480

2.8.1.1 Calculation of Spar Web & Skin Shear Buckling Ratios

For each panel of the tailplane box, the buckling constant was computed as,

$$k_b = 4.84 + 3.55 \frac{b^2}{a^2} \quad (90)$$

where a is the length of the longest panel edge and b is the length of the shortest panel edge. Where a panel is tapered, as in the case of the front and rear spar webs, the lengths of the non-tapered edges are approximated as the average length of both edges. Hence the crippling stress was computed as,

$$\sigma_{cr} = k_b E_c \frac{t^2}{b^2} \quad (91)$$

where E_c is the compressive modulus and t the panel thickness. Hence the shear buckling ratio was computed for each panel as,

$$BR = \frac{q}{\sigma_{cr} t} \quad (92)$$

where q is the panel shear flow computed in section 2.5.

2.8.2 Spar Cap Stress Analysis

2.8.2.1 Spar Cap Stress Analysis Summary

The following section outlines the spar cap stress analysis, a summary of which is given in tables 13, 14 and 15. Detailed sample calculations are given in this section for spar cap configuration 2 in order to demonstrate the method used for the stress analysis, with detailed calculations for the remaining 10 spar cap configurations given in appendix B. The following analysis is given for only the most critical loads encountered by each spar cap configuration in the context of each of the six failure modes analysed and, as such, only the minimum margins of safety are provided.

Table 13: Top-front and top-rear spar cap configuration margin of safety summary table.

Configuration	Drawing/Part	Failure Mode	Load Case	Material	Allowable	Limit	MS	Section	
8	6011 Sheet 7 Detail C2 See Figure 15(h)	Tension	1	2024-T3	17706 N	4872 N	High	B.7.1	
		Compression	2		12755 N	2214 N	High	B.7.2	
		Crippling			4014 N	2025 N	0.3215	B.7.3	
		Crippling w/DT	1		87.20 N/mm ²	47.98 N/mm ²	0.2116	B.7.4	
		Spar Cap Shear			4348 N	248.6 N	High	B.7.5	
		Rivet Shear	Pop Rivets	600 N	248.6 N	0.6088	B.7.6		
9	6011 Sheet 5 Detail B2 See Figure 16(i)	Tension	1	2024-T3	23274 N	6462 N	High	B.8.1	
		Compression	2		16802 N	2937 N	High	B.8.2	
		Crippling			5233 N	2937 N	0.1878	B.8.3	
		Crippling w/DT	N/A		N/A	N/A	N/A	B.8.4	
		Spar Cap Shear	1		6521 N	300.7 N	High	B.8.5	
		Rivet Shear	Pop Rivets	600 N	300.7 N	0.3301	B.8.6		
10	6011 Sheet 2 Detail A1 See Figure 16(j)	Tension	1	2024-T3	28703 N	7642 N	High	B.9.1	
		Compression	2		20765 N	3474 N	High	B.9.2	
		Crippling			6427 N	3200 N	0.3390	B.9.3	
		Crippling w/DT	1		80.24 N/mm ²	44.50 N/mm ²	0.2021	B.9.4	
		Spar Cap Shear			8695 N	300.7 N	High	B.9.5	
		Rivet Shear	Pop Rivets	600 N	300.7 N	0.3301	B.9.6		
11	6011 Sheet 6 Detail C1 See Figure 16(k)	Tension	1	2024-T3	17292 N	2792 N	High	B.10.1	
		Compression	2		12502 N	1269 N	High	B.10.2	
		Crippling			3990 N	1269 N	High	B.10.3	
		Crippling w/DT	1		88.63 N/mm ²	28.53 N/mm ²	High	B.10.4	
		Spar Cap Shear			4348 N	248.6 N	High	B.10.5	
		Rivet Shear	Pop Rivets	600 N	248.6 N	0.6088	B.10.5		

Table 14: Outboard and bottom-front spar cap configuration margin of safety summary table.

Configuration	Drawing/Part	Failure Mode	Load Case	Material	Allowable	Limit	MS	Section	
1	6011 Sheets 12 & 13 Details F1 to F4 See Figure 15(a)	Tension	1	2024-T3	8763 N	2633 N	High	B.1.1	
		Compression	2		5997 N	1197 N	High	B.1.2	
		Crippling			2147 N	1197 N	0.1958	B.1.3	
		Crippling w/DT			103.5 N/mm ²	50.52 N/mm ²	0.3658	B.1.4	
		Spar Cap Shear	1		4348 N	377.8 N	High	B.1.5	
		Rivet Shear	Pop Rivets	600 N	377.8 N	0.05876	B.1.5		
2	6011 Sheet 11 Detail E4 See Figure 15(b)	Tension	2	2024-T3	21506 N	1359 N	High	2.8.2.2.1	
		Compression	1		15438 N	2990 N	High	2.8.2.2.2	
		Crippling			5357 N	2990 N	0.1944	2.8.2.2.3	
		Crippling w/DT			99.09 N/mm ²	50.85 N/mm ²	0.2991	2.8.2.2.4	
		Spar Cap Shear	1		5567 N	127.9 N	High	2.8.2.2.5	
		Rivet Shear	Pop Rivets	600 N	127.9 N	High	2.8.2.2.6		
3	6011 Sheet 7 Detail C4 See Figure 15(c)	Tension	2	2024-T3	30496 N	2021 N	High	B.2.1	
		Compression	1		21938 N	4445 N	High	B.2.2	
		Crippling			7944 N	4445 N	0.1915	B.2.3	
		Crippling w/DT			98.94 N/mm ²	58.02 N/mm ²	0.1368	B.2.4	
		Spar Cap Shear	1		8960 N	300.7 N	High	B.2.5	
		Rivet Shear	Pop Rivets	600 N	300.7 N	0.3301	B.2.6		
4	See Figure 15(d)	Tension	2	2024-T3	39152 N	2680 N	High	B.3.1	
		Compression	1		28235 N	5896 N	High	B.3.1	
		Crippling			10505 N	5896 N	0.1878	B.3.2	
		Crippling w/DT			99.49 N/mm ²	54.67 N/mm ²	0.2132	B.3.3	
		Spar Cap Shear	1		12353 N	349.4 N	High	B.3.4	
		Rivet Shear	Pop Rivets	600 N	349.4 N	0.1448	B.3.5		
5	6011 Sheet 5 Detail B4 See Figure 15(e)	Tension	2	2024-T3	47482 N	3466 N	High	B.4.1	
		Compression	1		34333 N	7626 N	High	B.4.2	
		Crippling			13044 N	7025 N	0.2379	B.4.3	
		Crippling w/DT			100.3 N/mm ²	65.01 N/mm ²	0.02856	B.4.4	
		Spar Cap Shear	1		15747 N	349.4 N	High	B.4.5	
		Rivet Shear	Pop Rivets	600 N	349.4	0.1448	B.4.6		

Table 15: Bottom-rear spar cap configuration margin of safety summary table.

Configuration	Drawing/Part	Failure Mode	Load Case	Material	Allowable	Limit	MS	Section	
6	6011 Sheet 11 Detail E3 See Figure 15(f)	Tension	2	2024-T3	20624 N	1266 N	High	B.5.1	
		Compression	1		14900 N	2786 N	High	B.5.2	
		Crippling			5299 N	2786 N	0.2680	B.5.3	
		Crippling w/DT			102.0 N/mm ²	57.70 N/mm ²	0.1785	B.5.4	
		Spar Cap Shear			5567 N	379.4 N	High	B.5.5	
		Rivet Shear			Pop Rivets	600 N	379.4 N	0.05430	B.5.6
7	6011 Sheet 7 Detail C3 See Figure 15(g)	Tension	2	2024-T3	28947 N	1241 N	High	B.6.1	
		Compression	1		20993 N	2731 N	High	B.6.2	
		Crippling			7835 N	2521 N	High	B.6.3	
		Crippling w/DT			102.5 N/mm ²	54.65 N/mm ²	0.2504	B.6.4	
		Spar Cap Shear			8960 N	349.4 N	High	B.6.5	
		Rivet Shear			Pop Rivets	600 N	349.4 N	0.1448	B.6.6

2.8.2.2 Spar Cap Configuration 2 Stress Analysis

2.8.2.2.1 Tension Failure

Spar cap configuration 2 is located in the bottom-front corner of the tailplane box and, as such, experiences the most critical tensile loading as a result of load case 2. The critical failure point is at BL388, where, according to the analysis of section 2.5, the direct limit load, $P_{load} = 1359$ N. From the area computed for spar cap configuration 2 in section 2.7.3, the allowable load, given a rivet hole diameter, $d_r = 3.2$ mm,

$$\begin{aligned}
 P_{allow} &= A_{nett} F_{tu} = [A_{t2} + A_{sk2} - 2d_r(t_{st1} + t_{sp} + t_{sk})] F_{tu} \\
 &= [43.01 + 19.24 - 2 \times 3.2 \times (0.64 + 0.41 + 0.41)] \times 406.5 \\
 &= 21506 \text{ N}
 \end{aligned} \tag{93}$$

Hence the margin of safety,

$$MS = \frac{P_{allow}}{F_{uf} P_{load}} - 1 = \frac{21506}{1.5 \times 1359} - 1 = 9.550 \tag{94}$$

2.8.2.2.2 Compression Yield Failure

Spar cap configuration 2 is located in the bottom-front corner of the tailplane box and, as such, experiences the most critical compressive loading as a result of load case 1. The critical failure point is at BL388, where, according to the analysis of section 2.5, the direct limit load, $P_{load} = 2990$ N. From the area computed for spar cap configuration 2 in section 2.7.3, the allowable load,

$$P_{allow} = A_{gross}F_{cy} = (A_{t2} + A_{sk2})F_{cy} = (43.01 + 19.24) \times 248.0 = 15438 \text{ N} \quad (95)$$

Hence the margin of safety,

$$MS = \frac{P_{allow}}{F_{uf}P_{load}} - 1 = \frac{15438}{1.5 \times 2990} - 1 = 2.442 \quad (96)$$

2.8.2.2.3 Crippling Failure

Spar cap configuration 2 is located in the bottom-front corner of the tailplane box and, as such, experiences the most critical crippling load without diagonal tension as a result of load case 1. The critical failure point is at BL388, where, according to the analysis of section 2.5, the direct limit load, $P_{load} = 2990 \text{ N}$. Needham's method was first used to compute the allowable stress. Derived data used to compute the allowable crippling stress at BL388 for spar cap configuration 2 is given in table 16.

Table 16: Derived data used to compute the allowable crippling stress at BL388 for spar cap configuration 2 (section 2.7.3).

Component	c	$t [\text{mm}]$	C_e	$A_m [\text{mm}^2]$	$A_t [\text{mm}^2]$	$E_c [\text{N/mm}^2]$	$F_{cy} [\text{N/mm}^2]$	$F_{cs} [\text{N/mm}^2]$	$A_m F_{cs} [\text{N}]$
Spar Flange and Web	30.75	0.41	0.316	16.23	15.98	7.372×10^4	248.0	103.5	1680
Spar Cap Reinforcement 4	33.75	0.64	0.316	27.65	27.03	7.372×10^4	248.0	96.49	2668
			Σ	43.88	43.01			Σ	4348

Dividing the spar cap into individual angled components, the crippling stress for each angled element was computed as,

$$F_{cs} = C_e \frac{\sqrt{E_c F_{cy}}}{c^{0.75}} \quad (97)$$

where $C_e = 0.316$ for angled elements with two free edges, E_c is the compressive modulus, F_{cy} is the compressive yield strength, and c is the average side length divided by thickness of the angled element, as computed in section 2.7.2. The allowable stress was then computed as,

$$F_{allow} = \frac{\sum A_{m(i)} F_{cs(i)}}{\sum A_{m(i)}} = \frac{4348}{43.88} = 99.09 \text{ N/mm}^2 \quad (98)$$

where $A_{m(i)}$ and $F_{cs(i)}$ are the mid-line areas, as computed in section 2.7.2, and crippling stresses respectively of each angled element. From the allowable stress, the effective inter-rivet and edge skin widths were computed, respectively, as,

$$w_{eff_{ir}} = 1.7 t_{sk} \sqrt{\frac{E_c}{F_{allow}}} = 1.7 \times 0.41 \times \sqrt{\frac{7.372 \times 10^4}{99.09}} = 19.01 \text{ mm}$$

$$(99)$$

$$w_{eff_{edge}} = 0.6 t_{sk} \sqrt{\frac{E_c}{F_{allow}}} = \frac{0.6}{1.7} \times 19.01 = 6.709 \text{ mm}$$

From these, the total effective skin width was obtained as the sum of the non-overlapping portions of effective skin width, from which the effective skin area, A_{eff} , was obtained. Given the inter-rivet distance between the spar flange and spar cap reinforcement rivet lines is 25 mm, the total effective skin width was computed as,

$$w_{eff} = w_{eff_{edge}} + \frac{3}{2} w_{eff_{ir}} = 6.709 + \frac{3}{2} \times 19.01 = 35.22 \text{ mm} \quad (100)$$

Accounting for longitudinal inter-rivet buckling, for an inter-rivet distance to thickness ratio of $R_{ir} = d_{ir}/t = 24/0.41 \approx 59$, from figure 32 in appendix D, the inter-rivet buckling stress for a universal head rivet, $F_{ir} \approx 11 \text{ ksi} = 75.79 \text{ N/mm}^2$. Hence the total effective skin width was corrected to be,

$$w_{corrected} = \min \left(\frac{F_{ir}}{F_{allow}} w_{eff}, w_{eff} \right) = \frac{75.79}{99.09} \times 35.22 = 26.94 \text{ mm} \quad (101)$$

Hence the effective skin area,

$$A_{eff} = w_{corrected} t_{sk} = 26.94 \times 0.41 = 11.05 \text{ mm}^2 \quad (102)$$

Hence the allowable crippling load was computed, for spar cap configuration 2, as,

$$P_{allow} = (A_{t2} + A_{eff}) F_{allow} = (43.01 + 11.05) \times 99.09 = 5357 \text{ N} \quad (103)$$

Hence the margin of safety,

$$MS = \frac{P_{allow}}{F_{uf} P_{load}} - 1 = \frac{5357}{1.5 \times 2990} - 1 = 0.1944 \quad (104)$$

2.8.2.2.4 Crippling Failure with Diagonal Tension

Spar cap configuration 2 is located in the bottom-front corner of the tailplane box and, as such, experiences the most critical crippling load with diagonal tension as a result of load case 1. The critical failure point is at BL532, where, according to the analysis of section 2.5, the direct limit load, $P_{load} = 2240 \text{ N}$. The allowable crippling stress is given in (98) for spar cap configuration 2 and the largest contribution resulting from diagonal tension at BL532 originates from the lower skin of the tailplane box. The skin shear buckling ratio at this point was taken to be the maximum skin shear buckling ratio either side of the corresponding rib, $BR = 4.682$, as given in table 11. Likewise, the skin shear flow and inter-rib distance

were taken to be the maximum either side of the rib at BL532, $q_{sk} = 5.330 \text{ N/mm}$ and $b = 192 \text{ mm}$ respectively. Hence the diagonal tension factor was found from figure 33 in appendix D to be $k \approx 0.32$, and thus the maximum bending moment experienced by the spar cap was computed as,

$$M_{max} = \frac{kq_{sk}b^2}{12} = \frac{0.32 \times 5.330 \times (192)^2}{12} = 5240 \text{ N} \cdot \text{mm} \quad (105)$$

Hence the total applied stress at the critical point was computed as,

$$\begin{aligned} F_{total} &= \frac{P_{load}}{(A_{t2} + A_{sk2})} + M_{max} \frac{\bar{X}_{c2}}{I_{c2yy}} \\ &= \frac{2240}{43.01 + 19.24} + 5240 \times \frac{23.43}{8260} \\ &= 50.85 \text{ N/mm}^2 \end{aligned} \quad (106)$$

Hence the margin of safety,

$$MS = \frac{F_{allow}}{F_{uf}F_{total}} - 1 = \frac{99.09}{1.5 \times 50.85} - 1 = 0.2991 \quad (107)$$

2.8.2.2.5 Shear Failure

Spar cap configuration 2 is located in the bottom-front corner of the tailplane box and experiences the most critical shear flow as a result of load case 1. The critical failure point is at BL508, where, according to the analysis of section 2.5, the bottom skin shear flow, $q_{sk} = 5.330 \text{ N/mm}$. For a shear ultimate strength, $F_{su} = 254.9 \text{ N/mm}^2$ and inter-rivet distance, $d_{ir} = 24 \text{ mm}$, the margin of safety was computed as,

$$\begin{aligned} MS &= \frac{F_{su}(d_{ir} - d_r)(t_{sk} + t_{st1})}{F_{uf}q_{sk}d_{ir}} - 1 \\ &= \frac{254.9 \times (24 - 3.2)(0.41 + 0.64)}{1.5 \times 5.330 \times 24} - 1 \\ &= 28.01 \end{aligned} \quad (108)$$

2.8.2.2.6 Rivet Shear Failure

Spar cap configuration 2 is located in the bottom-front corner of the tailplane box and experiences the most critical shear flow as a result of load case 1. The critical failure point is at BL508, where, according to the analysis of section 2.5, the bottom skin shear flow, $q_{sk} = 5.330 \text{ N/mm}$. For a pop rivet ultimate load, $P_{ru} = 600 \text{ N}$, taken from figure 3, the margin of safety was computed as,

$$MS = \frac{P_{ru}}{F_{uf}q_{sk}d_{ir}} - 1 = \frac{600}{1.5 \times 5.330 \times 24} - 1 = 2.127 \quad (109)$$

2.8.3 Rib Stress Analysis

The following section outlines the rib stress analysis, a summary of which is given in table 17. As the rib flange and web geometry across all ribs are identical to the spar flange and web geometry computed in section 2.7.2.1, analyses of only the most critical loads encountered by any one rib are given in the context of the three failure modes analysed, and, as such, only the minimum margins of safety are provided.

Table 17: Rib margin of safety summary table.

Rib	Drawing/Part	Failure Mode	Load Case	Material	Allowable [N]	Limit [N]	MS	Section
BL350	6112-111	Flange Compression Yield	1	2024-T3	3963	636.5	High	2.8.3.1
BL100	6112-105	Rib Shear			4348	300.7	High	2.8.3.2
		Rivet Shear		CR3213-4 Rivets	600	300.7	0.3301	2.8.3.3

2.8.3.1 Flange Compression Yield Failure

Flange compression yield failure is most critical in the bottom flange of rib BL350 at BL340 as a result of load case 1. The largest contribution resulting from diagonal tension at BL340 originates from the bottom skin of the tailplane box. The skin shear buckling ratio at this point was taken to be the maximum skin shear buckling ratio either side of the corresponding rib, $BR = 4.682$, as given in table 11. Likewise, the skin shear flow and inter-rib distance were taken to be the maximum either side of rib BL350, $q_{sk} = 10.36 \text{ N/mm}$ and $b = 192 \text{ mm}$ respectively. Hence the diagonal tension factor was found from figure 33 in appendix D to be $k \approx 0.32$, and thus the stiffener load was computed as,

$$P_{stiff} = -kq_{sk}b = -0.32 \times 10.36 \times 192 = -636.5 \text{ N} \quad (110)$$

Hence given the rib flange geometry is identical to that of the spar flange and web geometry computed in section 2.7.2.1, the allowable load,

$$P_{allow} = A_{sp}F_{cy} = 15.98 \times 248.0 = 3963 \text{ N} \quad (111)$$

Hence the margin of safety,

$$MS = \frac{P_{allow}}{F_{uf}P_{stiff}} - 1 = \frac{3963}{1.5 \times 636.5} - 1 = 3.151 \quad (112)$$

2.8.3.2 Shear Failure

Shear failure is most critical in the bottom flange of rib BL100 at BL124 as a result of load case 1. According to the analysis of section 2.5, rib BL100 will experience a shear flow of $q_{rib} \approx 12.53 \text{ N/mm}$. Hence neglecting spacers between the skin and rib flange, for a shear ultimate strength, $F_{su} = 254.9 \text{ N/mm}^2$ and inter-rivet distance, $d_{ir} = 24 \text{ mm}$, the margin of safety was computed as,

$$\begin{aligned} MS &= \frac{F_{su}(d_{ir} - d_r)(t_{sk} + t_{rib})}{F_{uf}q_{rib}d_{ir}} - 1 \\ &= \frac{254.9 \times (24 - 3.2)(0.41 + 0.41)}{1.5 \times 12.53 \times 24} - 1 \\ &= 8.638 \end{aligned} \quad (113)$$

2.8.3.3 Rivet Shear Failure

Rivet shear failure is most critical in the bottom flange of rib BL100 at BL124 as a result of load case 1. According to the analysis of section 2.5, rib BL100 will experience a shear flow of $q_{rib} \approx 12.53 \text{ N/mm}$. Hence for a pop rivet ultimate load, $P_{ru} = 600 \text{ N}$, taken from figure 3, the margin of safety was computed as,

$$MS = \frac{P_{ru}}{F_{uf}q_{rib}d_{ir}} - 1 = \frac{600}{1.5 \times 12.53 \times 24} - 1 = 0.3301 \quad (114)$$

2.8.4 Fitting Stress Analysis

2.8.4.1 Fitting Stress Analysis Summary

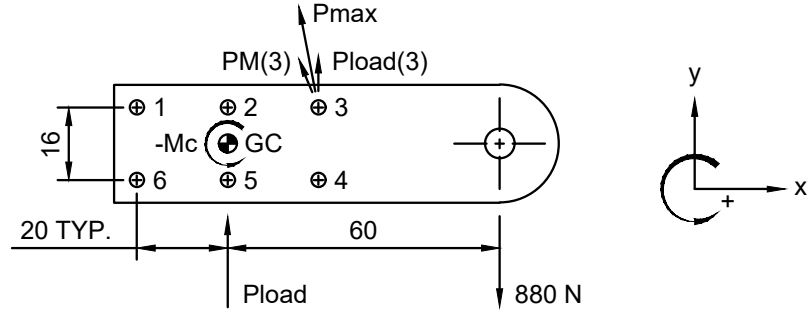
The following section outlines the fitting stress analysis, a summary of which is given in table 18. Detailed sample calculations are given in this section for lug P in order to demonstrate the method used for the stress analysis, with detailed calculations for the remaining 3 fittings given in appendix C. The following analysis is given for only the most critical loads encountered by each lug in the context of each of the four failure modes analysed and, as such, only the minimum margins of safety are provided.

Table 18: Fitting margin of safety summary table.

Lug	Drawing/Part	Failure Mode	Load Case	Material	Allowable [N]	Limit [N]	MS	Section	
A	6111-123	Rivet Shear	1	CR3213-4 Rivets 2024-T3	1246	705.8	0.02340	C.1.1	
		Tension			29775	11293	0.5285	C.1.2	
		Bearing Shear Out			20118	11293	0.03273	C.1.3	
		Transverse Shear Out			15021	66	High	C.1.4	
B	6111-123	Rivet Shear	1	CR3213-4 Rivets 2024-T3	1246	705.8	0.02340	C.1.1	
		Tension	2		29775	5133	High	C.1.2	
		Bearing Shear Out			20118	5133	High	C.1.3	
		Transverse Shear Out	1		15021	66	High	C.1.4	
C	6111-125	Rivet Shear	1	CR3213-4 Rivets 2024-T3	1246	708.8	0.01907	C.2.1	
		Tension	N/A		N/A	N/A	N/A	C.2.2	
		Bearing Shear Out			N/A	N/A	N/A	C.2.2	
		Transverse Shear Out	1		15021	1012	High	C.2.3	
P	6111-121	Rivet Shear	1	CR3213-4 Rivets 2024-T3	1246	711.5	0.01521	2.8.4.2.1	
		Tension	3		29775	100	High	2.8.4.2.2	
		Bearing Shear Out			20118	100	High	2.8.4.2.3	
		Transverse Shear Out	1		15021	880	High	2.8.4.2.4	

2.8.4.2 Lug P Stress Analysis

2.8.4.2.1 Rivet Shear Failure



Lug P Rivet Shear (Load Case 1)

Figure 17: Free body diagram of lug P rivet shear subject to load case 1.

The critical load case for rivet shear failure in lug P is load case 1, with an applied load, $P_z = -P_{load} = -880 \text{ N}$; a free body diagram of the situation is given in figure 17. From the geometry given in figure 17, the moment at the centroid of the rivet pattern was computed as,

$$M_c = P_{load}L_c = -880 \times 60 = -52800 \text{ N} \cdot \text{mm} \quad (115)$$

Hence derived data used to compute the maximum rivet shear load is given in table 19, where the moment and direct shear loads of the i th rivet were computed, respectively, as,

$$P_{M(i)} = \frac{|M_c| d_i}{\sum d_i^2} \quad P_{load(i)} = \frac{P_{load}}{N} \quad (116)$$

where N is the total number of rivets. Hence, accounting for the direction of the applied moment at the centroid, the total rivet shear load of the i th rivet was computed as,

$$P_{tot(i)} = \sqrt{(P_{M(i)x} + P_{load(i)x})^2 + (P_{M(i)y} + P_{load(i)y})^2} \quad (117)$$

Table 19: Derived data used to compute the maximum rivet shear load in lug P.

Rivet	d_i [mm]	d_i^2 [mm ²]	$P_{M(i)}$ [N]	$\cos \theta$	$\sin \theta$	$P_{M(i)x}$ [N]	$P_{M(i)y}$ [N]	$P_{load(i)}$ [N]	$P_{load(i)x}$ [N]	$P_{load(i)y}$ [N]	$P_{tot(i)}$ [N]
1	21.54	464.0	573.2	0.9285	0.3714	-212.9	-532.2	146.7	0	146.7	440.4
2	8	64	212.9	0	1	-212.9	0	146.7	0	146.7	258.5
3	21.54	464.0	573.2	0.9285	0.3714	-212.9	532.2	146.7	0	146.7	711.5
4	21.54	464.0	573.2	0.9285	0.3714	212.9	532.2	146.7	0	146.7	711.5
5	8	64	212.9	0	1	212.9	0	146.7	0	146.7	258.5
6	21.54	464.0	573.2	0.9285	0.3714	212.9	-532.2	146.7	0	146.7	440.4
Σ		1984									

From table 19, the maximum rivet shear load is $P_{max} = 711.5$ N. Hence for a CR3213-4 1/8" blind rivet ultimate load, $P_{ru} = 1246$ N, taken from figure 2, the margin of safety was computed as,

$$MS = \frac{P_{ru}}{F_{uf}F_{fit}P_{max}} - 1 = \frac{1246}{1.5 \times 1.15 \times 711.5} - 1 = 0.01521 \quad (118)$$

2.8.4.2.2 Tension Failure

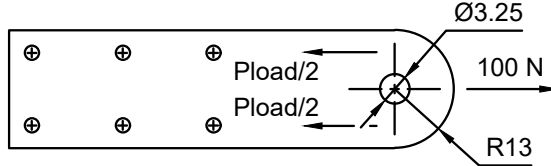
Lug P Tension (Load Case 3)

Figure 18: Free body diagram of lug P tension subject to load case 3.

The critical load case for tension failure in lug P is load case 3, with an applied load, $P_x = P_{load} = 100$ N; a free body diagram of the situation is given in figure 18. From the geometry given in figure 18, the ratio of the lug width to hole diameter, $w_{lug}/d_{lug} = 26/6.5 = 4$, hence the nett tension efficiency factor was found from figure 34 in appendix D to be $k_t \approx 0.74$. Hence the allowable load was computed as,

$$\begin{aligned} P_{allow} &= k_t F_{tu} A_{nett} = k_t F_{tu} (w_{lug} - d_{lug}) t_{lug} \\ &= 0.74 \times 427.2 \times (26 - 6.5) \times 4.83 \\ &= 29775 \text{ N} \end{aligned} \quad (119)$$

Hence the margin of safety,

$$MS = \frac{P_{allow}}{F_{uf} F_{fit} P_{load}} - 1 = \frac{29775}{1.5 \times 1.15 \times 100} - 1 = 171.6 \quad (120)$$

2.8.4.2.3 Bearing Shear Out Failure

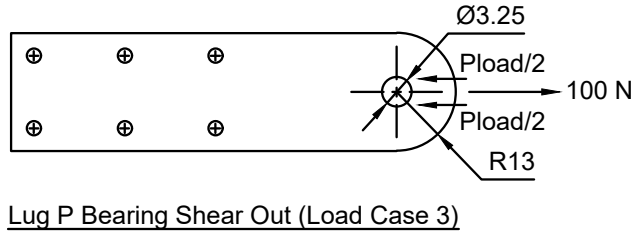


Figure 19: Free body diagram of lug P bearing shear out subject to load case 3.

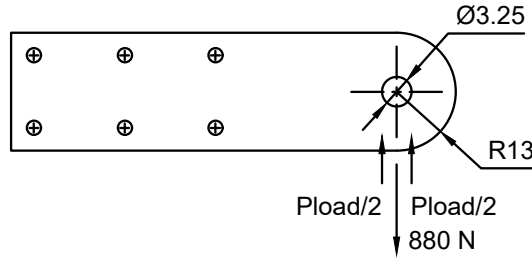
The critical load case for bearing shear out failure in lug P is load case 3, with an applied load, $P_x = P_{load} = 100$ N; a free body diagram of the situation is given in figure 19. From the geometry given in figure 19, the ratio of the edge distance to hole diameter, $w_{lug}/(2 d_{lug}) = 13/6.5 = 2$, hence the shear-bearing efficiency factor was found from figure 34 in appendix D to be $k_{br} \approx 1.5$. Hence the allowable load was computed as,

$$\begin{aligned} P_{allow} &= k_{br} F_{tu} A_{br} = k_{br} F_{tu} d_{lug} t_{lug} \\ &= 1.5 \times 427.2 \times 6.5 \times 4.83 \\ &= 20118 \text{ N} \end{aligned} \quad (121)$$

Hence the margin of safety,

$$MS = \frac{P_{allow}}{F_{uf} F_{fit} P_{load}} - 1 = \frac{20118}{1.5 \times 1.15 \times 100} - 1 = 115.6 \quad (122)$$

2.8.4.2.4 Transverse Shear Out Failure



Lug P Transverse Shear Out (Load Case 3)

Figure 20: Free body diagram of lug P transverse shear out subject to load case 1.

The critical load case for transverse shear out failure in lug P is load case 1, with an applied load, $P_z = -P_{load} = -880 \text{ N}$; a free body diagram of the situation is given in figure 20. From the geometry given in figure 20, the lug is symmetric about its longitudinal axis and the lug hole is concentric with the lug radius, hence the areas A_2 and A_3 denoted in figure 35, appendix D, were computed as,

$$A_2 = A_3 = \frac{(w_{lug} - d_{lug})t_{lug}}{2} = \frac{(26 - 6.5) \times 4.83}{2} = 47.09 \text{ mm}^2 \quad (123)$$

and the areas A_1 and A_4 were computed as,

$$A_1 = A_4 = \left(\frac{w_{lug}}{2} - \frac{d_{lug}}{\sqrt{2}} \right) t_{lug} = \left(\frac{26}{2} - \frac{6.5}{\sqrt{2}} \right) \times 4.83 = 40.59 \text{ mm}^2 \quad (124)$$

Hence the average bearing area, based on a type I lug as shown in figure 35 in appendix D, was computed as,

$$\begin{aligned} A_{av} &= \frac{6}{\frac{3}{A_1} + \frac{1}{A_2} + \frac{1}{A_3} + \frac{1}{A_4}} = \frac{6}{\frac{4}{A_1} + \frac{2}{A_2}} \\ &= \frac{6}{\frac{4}{40.59} + \frac{2}{47.09}} \\ &= 42.55 \text{ mm}^2 \end{aligned} \quad (125)$$

The ratio of the bearing area to the average bearing area, $A_{br}/A_{av} = 6.5 \times 4.83/42.55 = 0.7378$, hence the transverse shear out efficiency factor was found from figure 35 in appendix D to be $k_{tru} \approx 1.12$. Hence the allowable load was computed as,

$$\begin{aligned} P_{allow} &= k_{tru} F_{tu} A_{br} = k_{tru} F_{tu} d_{lug} t_{lug} \\ &= 1.12 \times 427.2 \times 6.5 \times 4.83 \\ &= 15021 \text{ N} \end{aligned} \quad (126)$$

Hence the margin of safety,

$$MS = \frac{P_{allow}}{F_{uf} F_{fit} P_{load}} - 1 = \frac{15021}{1.5 \times 1.15 \times 880} - 1 = 8.895 \quad (127)$$

3 Test Plan

AERO3465 team – Design, Build & Test	
<i>Group number:</i>	4
<i>Group members:</i>	James, Chris, Tom, Jorge, Kelly, Khalid, Kyam

Test Plan																	
<i>Testing aim:</i>	The right side of a tapered tailplane box will be evaluated through the testing under 4 different load cases. Experimental results will be compared to theoretical findings (literature), verifying the accuracy and reliability.																
<i>Description of test rig, with supports and load application method:</i>	The tailplane box will be mounted upside down in the testing rig, attached to it using NAS bolts, with no additional supports. There is only one external load point in z-direction, representing an elevator hinge location. Three lugs will be mounted on the side of the tailplane box's body. According to the designed loading schedule, a hydraulic jack will be applied to Lug P.																
<i>Loading schedule:</i>	The loads are tailored to be increased incrementally to prevent the testing structure from straining in each load case. <table border="1" style="margin-top: 10px;"> <thead> <tr> <th colspan="6"><i>Nominal load [N] (kg)</i></th> </tr> </thead> <tbody> <tr> <td>[220] (22.4)</td><td>[440] (44.9)</td><td>[660] (67.3)</td><td>[880] (89.7)</td><td>[1100] (112.1)</td><td>[1320] (134.6)</td></tr> </tbody> </table> <p style="text-align: center;"><u>Unit:</u> N = a (9.81 m/s^2) * m (kg)</p> <table border="1" style="margin-top: 10px;"> <thead> <tr> <th><i>Limit load [N] (kg)</i></th> <th><i>Ultimate load [N] (kg)</i></th> </tr> </thead> <tbody> <tr> <td>[880] (89.7)</td><td>[1320] (134.6)</td></tr> </tbody> </table>	<i>Nominal load [N] (kg)</i>						[220] (22.4)	[440] (44.9)	[660] (67.3)	[880] (89.7)	[1100] (112.1)	[1320] (134.6)	<i>Limit load [N] (kg)</i>	<i>Ultimate load [N] (kg)</i>	[880] (89.7)	[1320] (134.6)
<i>Nominal load [N] (kg)</i>																	
[220] (22.4)	[440] (44.9)	[660] (67.3)	[880] (89.7)	[1100] (112.1)	[1320] (134.6)												
<i>Limit load [N] (kg)</i>	<i>Ultimate load [N] (kg)</i>																
[880] (89.7)	[1320] (134.6)																
<i>Measurements to be taken & Measurement methods</i>	A force measurement device (a weighing digital scale) will be clamped firmly on one side, displaying the magnitude of compressive load at which the tailplane box is under. <u>Parameters to be measured are:</u> <ul style="list-style-type: none"> • Weight of the tailplane box 																

	<ul style="list-style-type: none"> Final dimensions of the test structure The magnitude of each loading Resultant deflection from each loading → Twisting 				
<i>Inspections to be carried out before, during & after the test</i>	<p><u>Before the test:</u></p> <ul style="list-style-type: none"> Inspect the sturdiness of the testing structure, ensuring no sections are falling apart, especially the fittings (bolts and lugs shall be safely secured). Inspect the tailplane box in x, y & z directions, checking for any cracks, breakage, or permanent deformation before proceeding with the next testing trial. Zero out the force measurement device (a weighing scale), which must be clamped firmly on one side. <p><u>During the test:</u></p> <ul style="list-style-type: none"> Observe the tailplane box to see any signs of damage or hear any ‘popping’ sound (which may indicate failure). <p><u>After the test:</u></p> <ul style="list-style-type: none"> Inspect whether there are any cracks, breakages or permanent deformations on the tailplane box. <p>Repeat this inspection procedure for each testing trial as the nominal load increases.</p>				
<i>Pass-Fail criteria for the test:</i>	<p>Limit and ultimate loads of the tailplane box are key determinants that define the pass-fail criteria.</p> <table border="1"> <thead> <tr> <th><i>Limit load [N] (kg)</i></th> <th><i>Ultimate load [N] (kg)</i></th> </tr> </thead> <tbody> <tr> <td>[880] (89.7)</td> <td>[1320] (134.6)</td> </tr> </tbody> </table> <p>The loading schedule will be followed on the ‘test day’.</p> <p>‘PASS’ will be considered when there are no cracks, breakage, or permanent deformation on the tailplane box after being subjected to the applied nominal load from the hydraulic jack on Lug P. Thus, the second nominal load will be tested in the following trial. Testing will continue in the same manner until the structures ‘FAIL’ – unable to survive the maximum loading. The highest loading reached will be recorded on the testing marking sheet.</p>	<i>Limit load [N] (kg)</i>	<i>Ultimate load [N] (kg)</i>	[880] (89.7)	[1320] (134.6)
<i>Limit load [N] (kg)</i>	<i>Ultimate load [N] (kg)</i>				
[880] (89.7)	[1320] (134.6)				
<i>Other information:</i>	<p><u>Precautions:</u></p> <ul style="list-style-type: none"> Personal protective equipment (PPE) must be worn at all times during the testing period to reduce exposure to hazards that may cause serious injuries. <p>All members will be present on ‘testing day’.</p>				

[MARKING SHEET] Test results:

Pre-test checklist:

Weight: 1382 g

- No sections of the right T-tail wingbox are falling apart.
- No cracks, breakage, or permanent deformation are observed.

Nominal Load [N] (kg)	Pass / Fail checklist	Load 1 [kg]	Load 2 [kg]	Relative deflection 1 (Rear Spar) [mm]	Relative deflection 2 (Front Spar) [mm]
[220] (22.4)	<input checked="" type="checkbox"/> Survived max. loading <input type="checkbox"/> Failed Highest loading reached: <u> </u>	38.1	21.2	5	12
[440] (44.9)	<input checked="" type="checkbox"/> Survived max. loading <input type="checkbox"/> Failed Highest loading reached: <u> </u>	30.4	14.3	10	9
[660] (67.3)	<input checked="" type="checkbox"/> Survived max. loading <input type="checkbox"/> Failed Highest loading reached: <u> </u>	42.9	23.8	16	14
[880] (89.7) [limit load]	<input checked="" type="checkbox"/> Survived max. loading <input type="checkbox"/> Failed Highest loading reached: <u> 88 </u>	52.1	35.9	21	18.5
[1100] (112.1)	<input type="checkbox"/> Survived max. loading <input checked="" type="checkbox"/> Failed Highest loading reached: <u> </u>	-	-	-	-
[1320] (134.6) [ultimate load]	<input type="checkbox"/> Survived max. loading <input checked="" type="checkbox"/> Failed Highest loading reached: <u> </u>	-	-	-	-

Results obtained after lug P failure:

Nominal Load [N] (kg)	Load 1 [kg]	Load 2 [kg]	Relative deflection 1 (Rear Spar) [mm]	Relative deflection 2 (Front Spar) [mm]
[900] (91.7)	47.2	44.6	25	20.5
[1100] (112.1)	53.5	57.4	45	31

[Comparison] Theoretical data from FEM model:

Nominal Load [N] (kg)	Deflection calculated for Nominal Load in FEM model [mm]	
	Front spar	Rear spar
[220] (22.4)	1.09	1.46
[440] (44.9)	2.18	2.93
[660] (67.3)	3.27	4.39
[880] (89.7) [limit load]	4.36	5.85
[1100] (112.1)	5.45	7.32
[1320] (134.6) [ultimate load]	6.54	8.78

*For analysis after the test: Comparing experimental results with the FEM model.

4 Test Report

4.1 Background

The final test of the completed tailplane box was conducted on the 27th of October 2023 (Friday) at 3 pm in the Bennett Lab, evaluating the static strength of the design structure. The tailplane box had a final weight of 1382 grams, after being weighed on a digital scale. It successfully passed each criterion delineated in the test plan, meeting the established pass/fail benchmarks until it reached the limit load of 88 kg (880 N), where it failed at lug P due to insufficient strength of the connection between lug P and the tip rib.

4.2 Method

Prior to testing, the mass of the tailplane box was obtained using a digital scale. An inspection was then carried out to ensure the structural integrity of the tailplane box before mounting it to the test station. The tailplane box was then mounted and secured tightly to the test station and two digital scales used for determining the load were placed under an MDF stand for the hydraulic jack. The hydraulic jack was then positioned on the MDF stand and shimmed to the correct height under lug P using wood scrap. Two metric rulers were clamped onto retort stands and positioned on either side of the tailplane box for reading deflections; photos of the testing station setup are given in figures 21 and 22. The digital scales were then zeroed and the structure was preloaded to 50 kg. Initial readings of the load and deflection were taken before releasing the preload and ensuring the jack was reset into its neutral position. The load was then gradually increased and load and deflection readings taken at each point specified in the test plan until failure.



Figure 21: Photos of the testing station setup showing (left) the tailplane box mounted in the test jig and (right) the connection between the tailplane box and test jig.



Figure 22: Photo of the full testing station setup, with jack, rulers for measuring deflections and digital scales for measuring the applied load.

4.3 Results & Discussion

The results of the static test are given in figure 23. It is clear from figure 23 that the deflections predicted by the FEM simulation do not match those obtained during the test prior to and after the failure of lug P. With respect to the deflections predicted by the FEM simulation, it is likely that the method used to approximate the spar cap areas has resulted in an underestimate of the deflection at each test load. As the spar cap areas change between ribs based on the particular spar cap configuration, a weighted area was computed for each of the connecting rods between each pair of ribs. This was done in order to simplify the setup for the FEM simulation, but this may have been at the expense of a valid set of predicted deflections. With respect to the deflections obtained during testing, a combination of factors may have affected the results given in figure 23. Inaccurate manufacturing and errors in visually determining the deflection of the tailplane box using rulers are possible sources of error in this regard. Another source of error as it relates to the deflections observed after the failure of lug P is the altered loading condition resulting from placement of the jack directly under the top-rear corner of the tailplane box. As the load was then concentrated on a single point, rather than distributed via the outboard tip rib, the difference in the rates at which the rear and front spars deflected increased, as seen in figure 23. Finally, whilst the initial deflection observed at the front spar is in line with the subsequent observed trend, the initial deflection observed at the rear spar is not. This is almost certainly due to either

a misreading of the deflection at the initial preload stage, or a premature release of preload and subsequent reading of the deflection at a lower jack load and hence should be treated as an outlier.

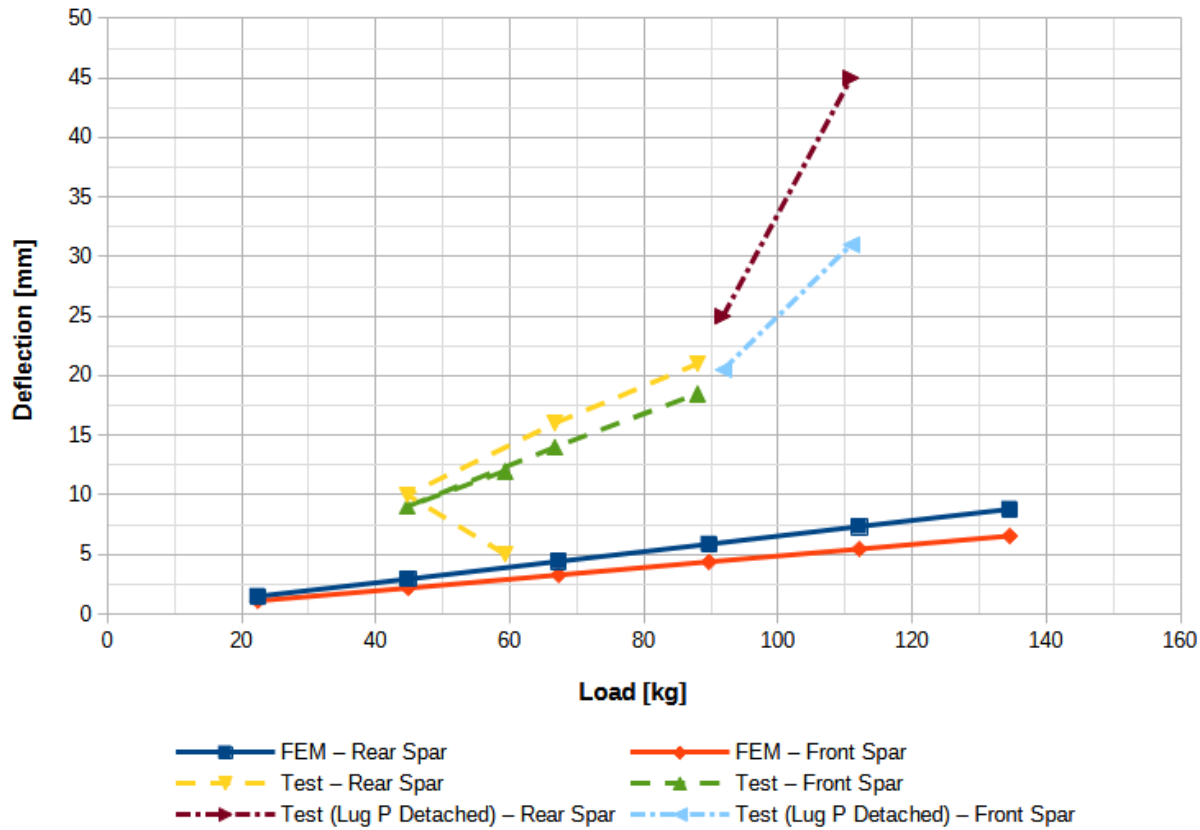


Figure 23: Tailplane box front and rear spar deflections with respect to loading at lug P.

The failure at 88 kg resulted from lug P detaching suddenly from the tip rib. Upon visual inspection of the failure, it was clear that a combination of an insufficient thickness of the designed tip rib of 0.41 mm, as well as shanking of lug P against the tip rib, prevented the CherryMax rivets from anchoring firmly to it, resulting in detachment at limit load; photos of the failure at lug P are given in figures 24 and 25. Testing subsequently continued without lug P, with the jack re-positioned directly under the top rear corner of the tip rib. Though this represented a different loading scenario, the load was increased up to 110 kg before the vertical tip rib flange and spar web began to exhibit buckling due to the direct compressive load, at which point the loading plateaued, indicating that the limit for sustaining further load in the structure in this arrangement had been reached.

The main factors that contributed to the failure at lug P were a combination of design and manufacturing errors. On the design side, recommendation of the use of thicker gauge sheet for the outboard tip and inboard closure ribs was not acknowledged, leading to 0.41 mm gauge being adopted for these critical components. On the manufacturing side, fastening of lug P to the outboard tip rib after the rib had been fastened to both spars resulted in a

gap forming between lug P and the tip rib (shanking) due to a slight overhang of the rear spar. Based on this, the design of the tailplane box should be modified such that the inboard closure and outboard tip rib thicknesses are increased to either 0.64 mm or 0.81 mm. The alignment and attachment of lug P will also require precise attention to ensure a flush and robust connection with the rib going forward and should be done prior to attachment of the tip rib to each spar.

Other potential sources of failure that did not manifest during testing were the lack of sheet metal work experience of all members of group 4, as well as manufacturing errors precipitated through the use of hand tools only. For example when drilling rivet holes for the lugs it was necessary to keep the drill bit as close to perpendicular as possible. A cooperative approach was adopted in this regard, where two team members were tasked with keeping an eye on the drilling angle and alerting the driller to any deviations. Of course this method is still subject to error, with the end result being enlarged rivet holes that are not perpendicular to the lug face, thus changing the loading on the rivets used to secure them to the tailplane box. Likewise, spot drilling holes in each rib imposed an additional challenge given that the actual placement of ribs within the tailplane box was not exact, though this was largely mitigated through the use of relatively wide rib flanges.

Through the course of manufacturing the tailplane box, it became apparent that CherryMax rivets would not be long enough to simultaneously penetrate lugs A and B and the spar cap reinforcement along the top and bottom rivet holes of lugs A and B respectively. As such, a change was made from CherryMax rivets to solid rivets for these rivet holes. This altered the design, and as such, was not accounted for in the preceding lug analyses. As the quality of the joint produced using solid rivets is dependant on the experience of the rivet gun operator, the strength of each joint could not be confidently verified, thus being another potential source of failure. Solid rivets were additionally used in a few rivet holes along the rear spar, with one rivet being fitted incorrectly, leading to damage of the rear spar cap reinforcement. As this was inboard of the rib at BL250 it was thought that this might not be an issue, given the loading along the rear spar was predicted to drop off relative to the loading on the rear spar closer to the tip rib.

4.4 Conclusion

The tailplane box presented in this report was tested to destruction in order to evaluate its static strength. Structural failure was observed at limit load, based on the requirements set out in the design brief, due to lug P detaching suddenly from the outboard tip rib. The primary cause of this failure was the combination of an inadequate tip rib design thickness of 0.41 mm and shanking of lug P against the tip rib due to an overhang of the rear spar after fastening the tip rib to both front and rear spars. The tailplane box design should thus be modified to incorporate a thicker gauge tip rib, with lug P fastened to it prior to fastening the tip rib to the front and rear spars. Additional sources of failure that did not manifest during the test include inexperience in sheet metal work of all members of group 4, leading to sub-optimal build quality, and the use of solid rivets in place of CherryMax rivets in lugs A and B and at the rear spar web near lug C.

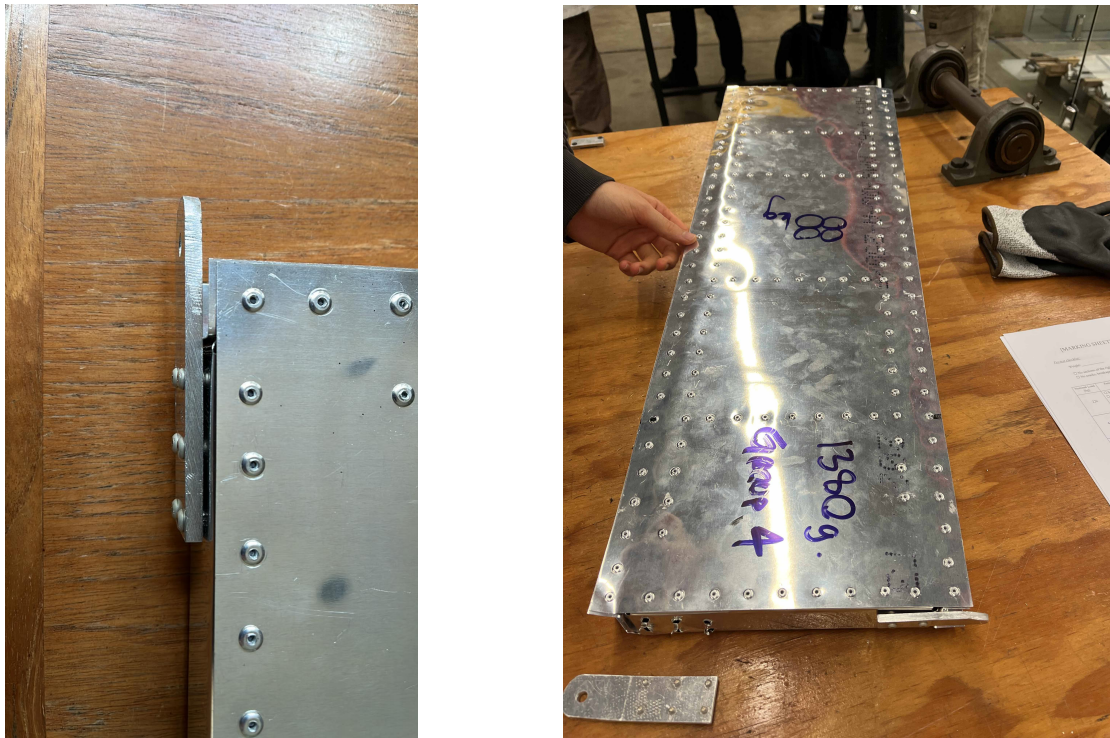


Figure 24: Photos of (left) shanking of lug P prior to testing and (right) the tailplane box post lug P failure.

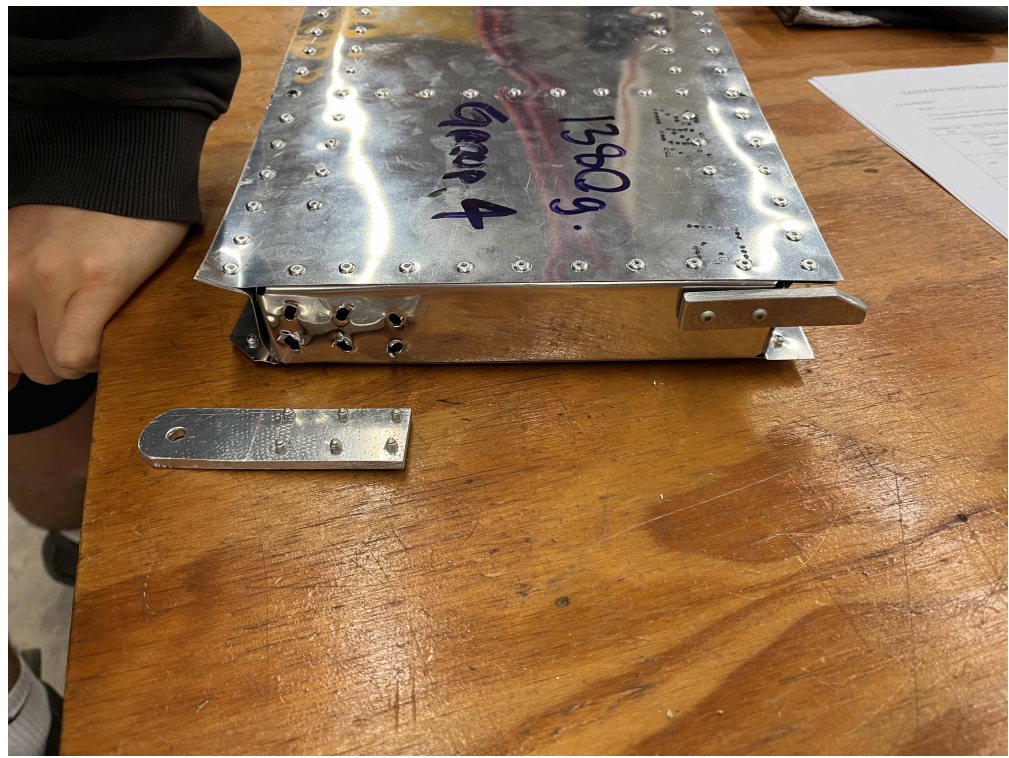


Figure 25: Photo of the outboard tip rib showing the lug P failure as a result of shanking.

5 Drawing List & Bill of Material

[SEE DRAWING LIST & BILL OF MATERIAL OVERLEAF]

Table 20: Left tailplane box bill of material (assembly 6011-001).

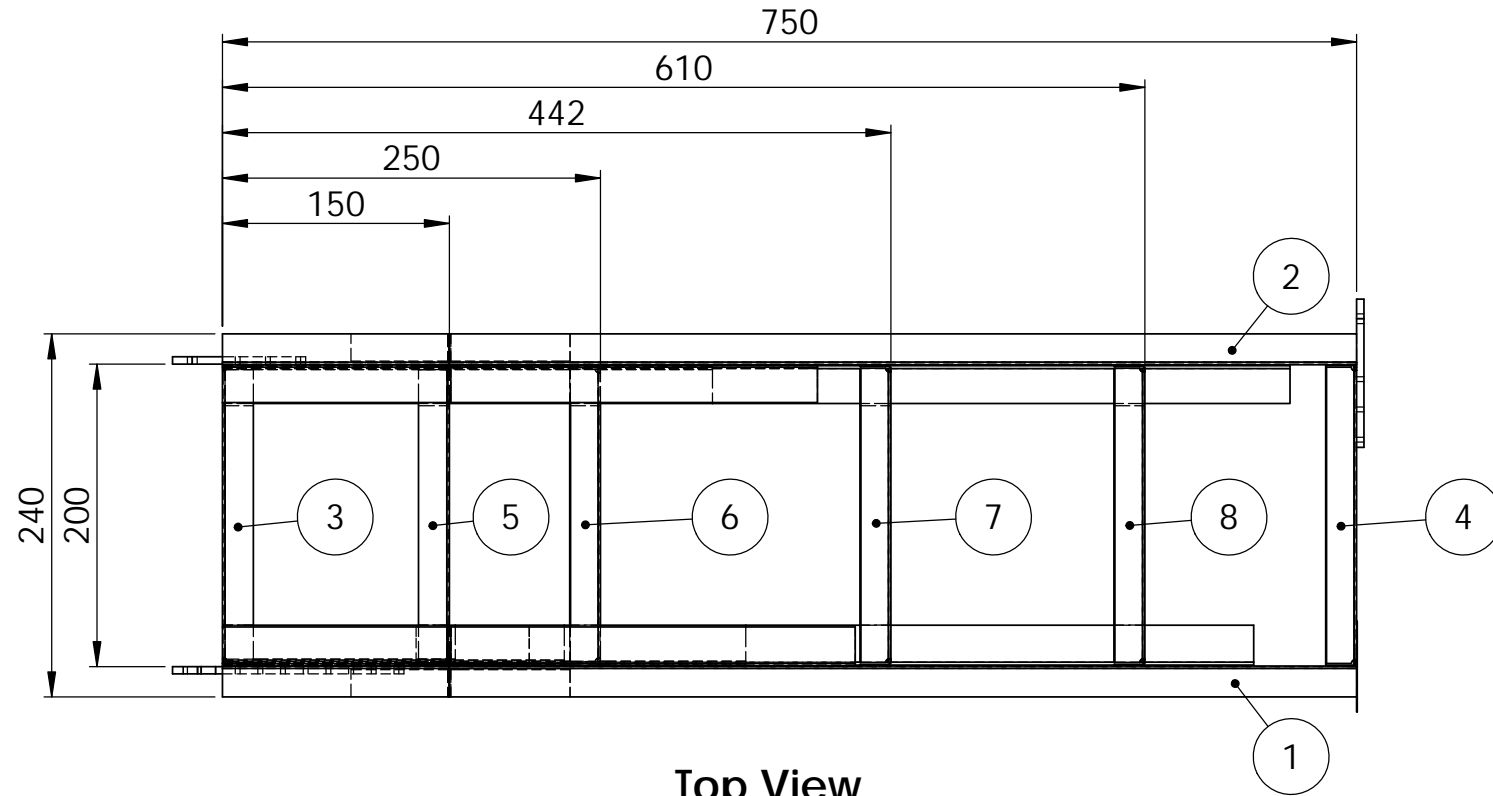
Part/Description	Part No.	Drawing No.	Issue	Date
Front Spar	6112-101	6112	A	22/09/23
Rear Spar	6112-103	6112	A	22/09/23
Inboard End Cap	6112-105	6112	A	22/09/23
Outboard End Cap	6112-107	6112	A	22/09/23
Rib BL250	6112-109	6112	A	22/09/23
Rib BL350	6112-111	6112	A	22/09/23
Rib BL542	6112-113	6112	A	22/09/23
Rib BL710	6112-115	6112	A	22/09/23
Lower Skin	6113-117	6113	A	28/09/23
Upper Skin	6113-119	6113	A	28/09/23
Lug P	6111-121	6111	A	21/09/23
Lugs A/B	6111-123	6111	A	21/09/23
Lug C	6111-125	6111	A	21/09/23
Front Top Stiffener 1	6114-127	6114	A	28/09/23
Front Top Stiffener 2	6114-129	6114	A	28/09/23
Front Top Stiffener 3	6114-131	6114	A	28/09/23
Rear Top Stiffener	6114-133	6114	A	28/09/23
Rear Bottom Stiffener 1	6114-135	6114	A	28/09/23
Rear Bottom Stiffener 2	6114-137	6114	A	28/09/23
Front Bottom Stiffener 1	6114-139	6114	A	28/09/23
Front Bottom Stiffener 2	6114-141	6114	A	28/09/23
Front Bottom Stiffener 3	6114-143	6114	A	28/09/23
Front Bottom Stiffener 4	6114-145	6114	A	28/09/23
3× End Cap Spacer	6115-147	6115	A	29/09/23
6× End Cap Spacer	6115-149	6115	A	29/09/23
3× Rib BL250 Spacer	6115-151	6115	A	29/09/23
2× Rib Long BL350 Spacer	6115-153	6115	A	29/09/23
2× Rib Short BL350 Spacer	6115-155	6115	A	29/09/23
2× Rib BL542 Spacer	6115-157	6115	A	29/09/23
2× Rib BL710 Spacer	6115-159	6115	A	29/09/23
3× Rib Upper Long Spacer	6115-161	6115	A	29/09/23
3× Rib Upper Short Spacer	6115-163	6115	A	29/09/23
4× Rib Lower Long Spacer	6115-165	6115	A	29/09/23
4× Rib Lower Short Spacer	6115-167	6115	A	29/09/23
2× Upper Spar Strap	6115-169	6115	A	29/09/23
3× Upper Stiffener Strap	6115-171	6115	A	29/09/23
Displacement Lug	6111-173	6111	A	21/09/23

Table 21: Right tailplane box bill of material (assembly 6011-002).

Part/Description	Part No.	Drawing No.	Issue	Date
Front Spar	6112-102	6112	A	22/09/23
Rear Spar	6112-104	6112	A	22/09/23
Inboard End Cap	6112-106	6112	A	22/09/23
Outboard End Cap	6112-108	6112	A	22/09/23
Rib BL250	6112-110	6112	A	22/09/23
Rib BL350	6112-112	6112	A	22/09/23
Rib BL542	6112-114	6112	A	22/09/23
Rib BL710	6112-116	6112	A	22/09/23
Lower Skin	6113-118	6113	A	28/09/23
Upper Skin	6113-120	6113	A	28/09/23
Lug P	6111-122	6111	A	21/09/23
Lugs A/B	6111-124	6111	A	21/09/23
Lug C	6111-126	6111	A	21/09/23
Front Top Stiffener 1	6114-128	6114	A	28/09/23
Front Top Stiffener 2	6114-130	6114	A	28/09/23
Front Top Stiffener 3	6114-132	6114	A	28/09/23
Rear Top Stiffener	6114-134	6114	A	28/09/23
Rear Bottom Stiffener 1	6114-136	6114	A	28/09/23
Rear Bottom Stiffener 2	6114-138	6114	A	28/09/23
Front Bottom Stiffener 1	6114-140	6114	A	28/09/23
Front Bottom Stiffener 2	6114-142	6114	A	28/09/23
Front Bottom Stiffener 3	6114-144	6114	A	28/09/23
Front Bottom Stiffener 4	6114-146	6114	A	28/09/23
3× End Cap Spacer	6115-148	6115	A	29/09/23
6× End Cap Spacer	6115-150	6115	A	29/09/23
3× Rib BL250 Spacer	6115-152	6115	A	29/09/23
2× Rib Long BL350 Spacer	6115-154	6115	A	29/09/23
2× Rib Short BL350 Spacer	6115-156	6115	A	29/09/23
2× Rib BL542 Spacer	6115-158	6115	A	29/09/23
2× Rib BL710 Spacer	6115-160	6115	A	29/09/23
3× Rib Upper Long Spacer	6115-162	6115	A	29/09/23
3× Rib Upper Short Spacer	6115-164	6115	A	29/09/23
4× Rib Lower Long Spacer	6115-166	6115	A	29/09/23
4× Rib Lower Short Spacer	6115-168	6115	A	29/09/23
2× Upper Spar Strap	6115-170	6115	A	29/09/23
3× Upper Stiffener Strap	6115-172	6115	A	29/09/23
Displacement Lug	6111-174	6111	A	21/09/23

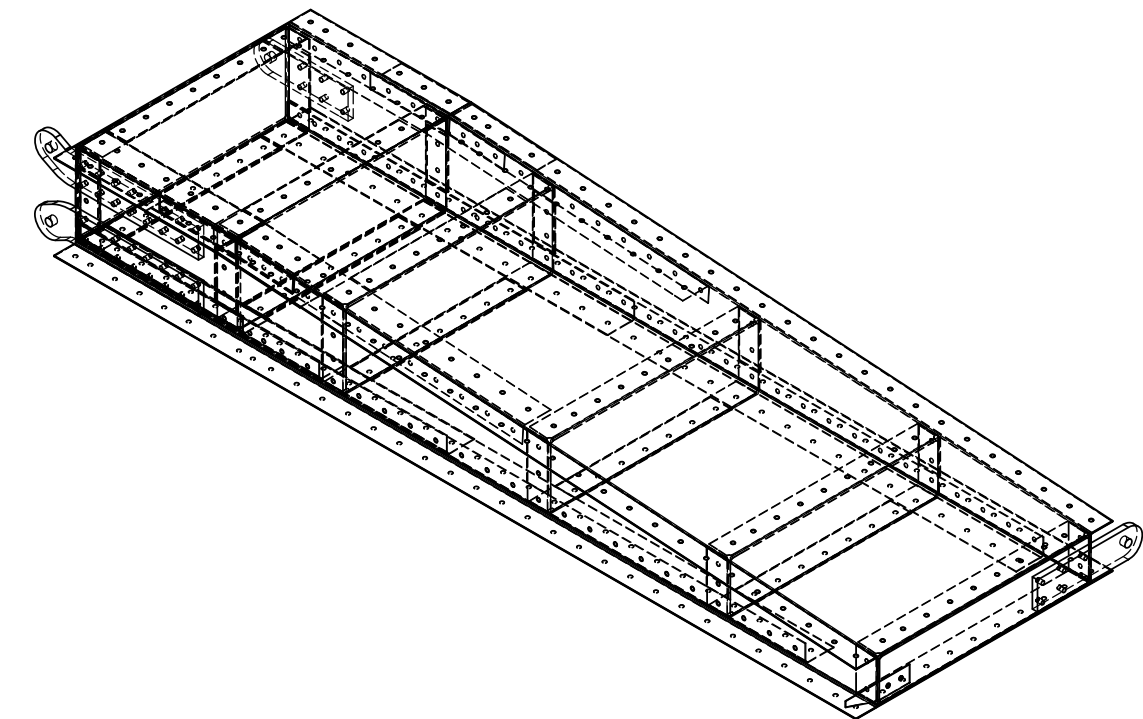
6 Drawings

[SEE DRAWINGS OVERLEAF]

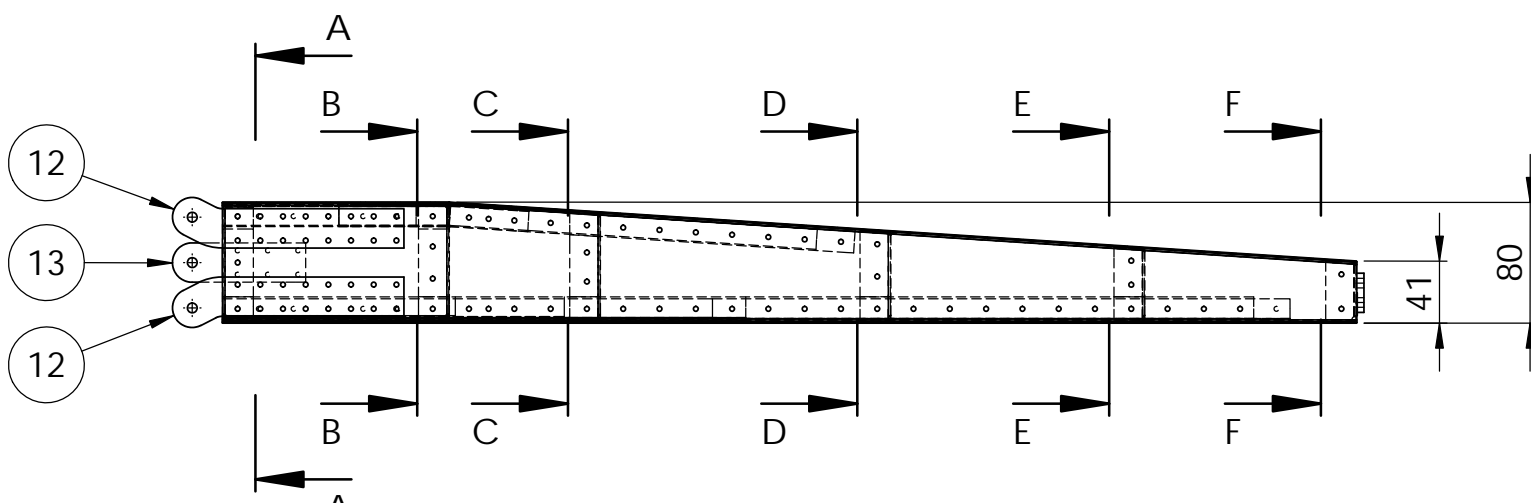


Top View

(Skin and Spacers Omitted for Clarity)
SCALE 1 : 5



Isometric View



Front View
SCALE 1 : 5

Left Tailplane Box Assembly

P/N: 6011-001

Right Tailplane Box Assembly (Opposite Hand)

P/N: 6011-002

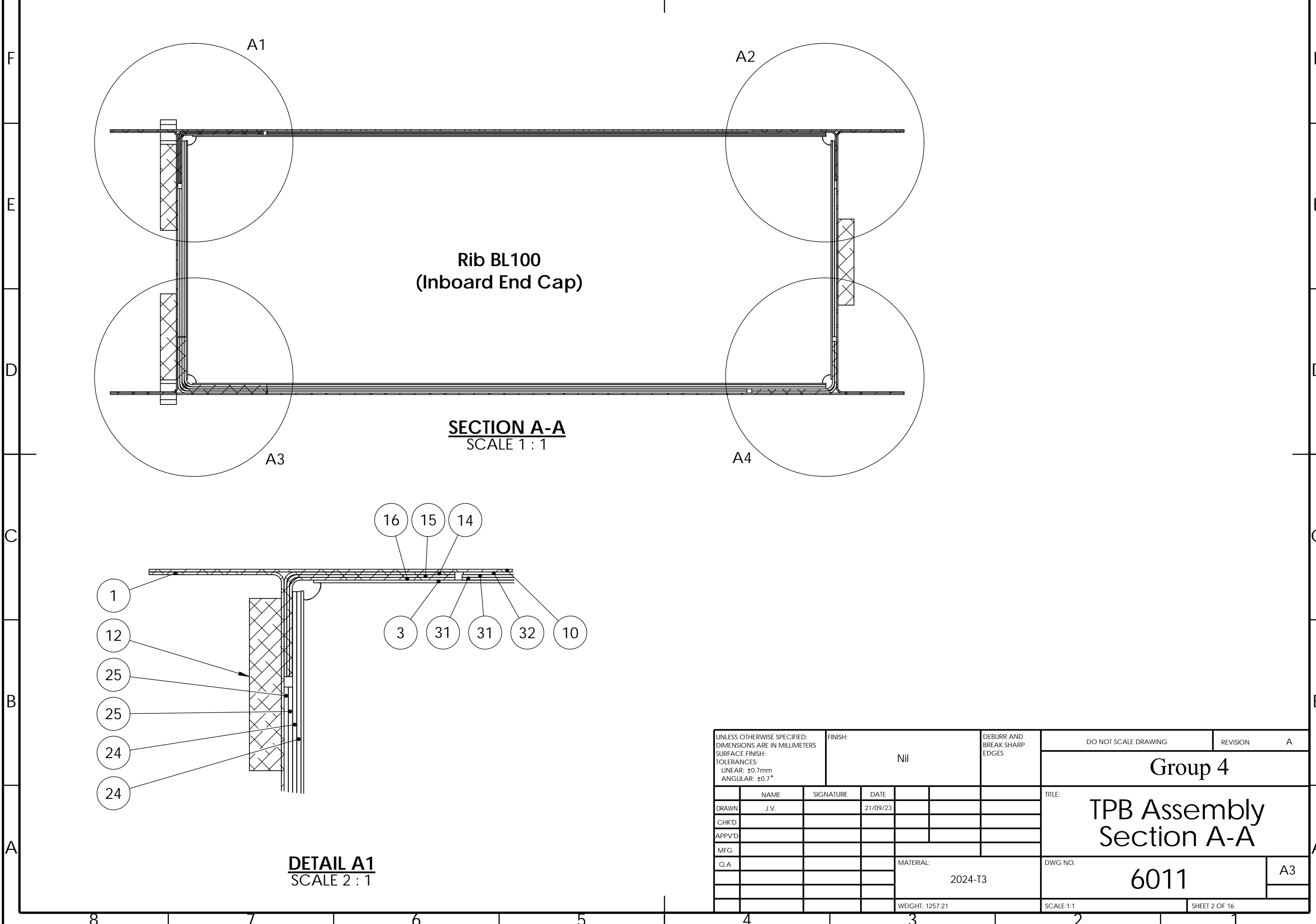
General Notes:

- General Notes:**

 1. Fittings shall be fastened to the TPB using CR3213-4 1/8" CherryMax rivets.
 2. All other structural connections shall be made using standard pop rivets.

UNLESS OTHERWISE SPECIFIED: DIMENSIONS ARE IN MILLIMETERS SURFACE FINISH: TOLERANCES: LINEAR: $\pm 0.7\text{mm}$ ANGULAR: $\pm 0.7^\circ$		FINISH: Nil			DEBURR AND BREAK SHARP EDGES	DO NOT SCALE DRAWING	REVISION	A
Group 4								
	NAME	SIGNATURE	DATE			TITLE: TPB Assembly Layout	DWG NO. 6011	A3
DRAWN	J.V.		21/09/23					
CHK'D								
APPV'D								
MFG								
Q.A								
				MATERIAL: 2024-T3				
				WEIGHT: 1257.21	SCALE: 1:5		SHEET 1 OF 16	

8 7 6 5 4 3 2 1



8

7

6

5

4

3

2

1

F

F

E

E

D

D

C

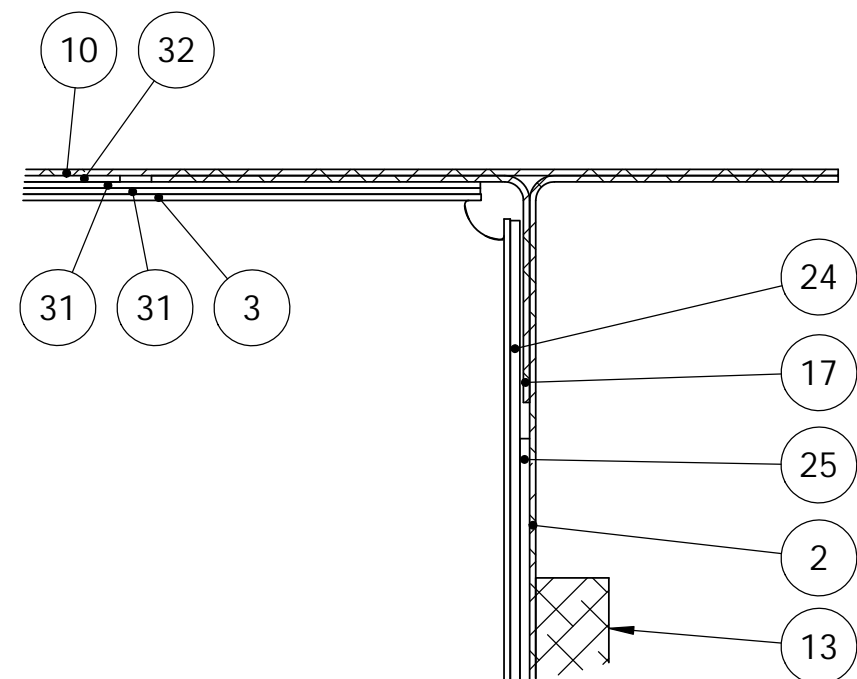
C

B

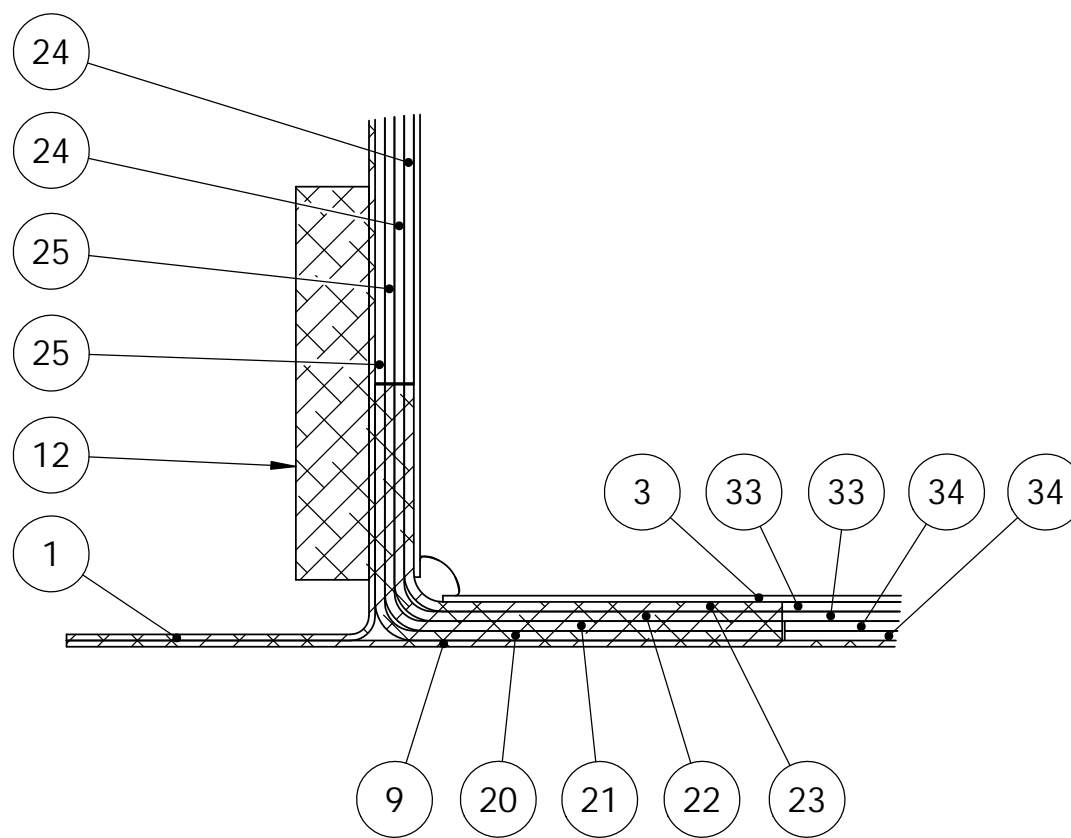
B

A

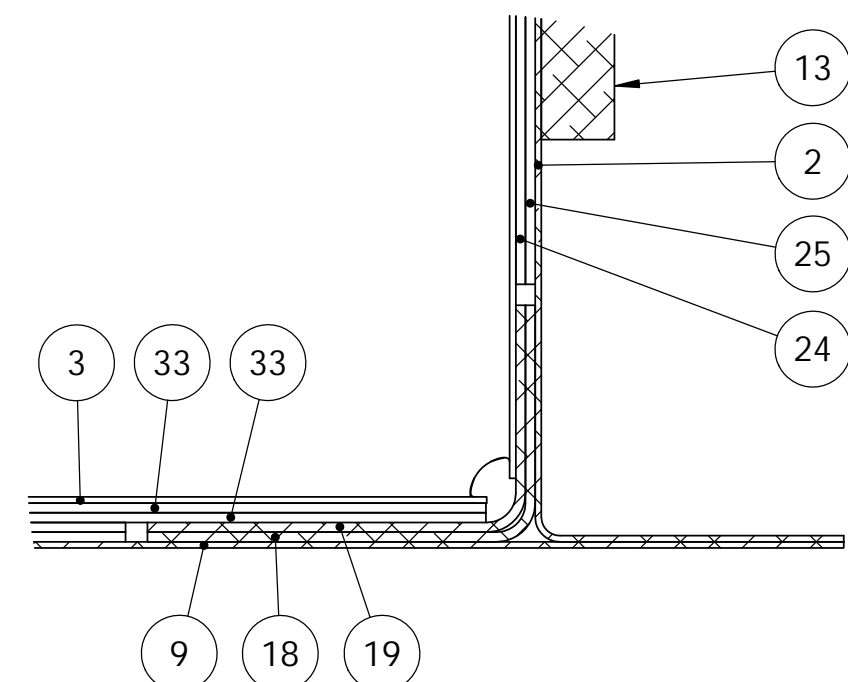
A



DETAIL A2
SCALE 2 : 1



DETAIL A3
SCALE 2 : 1



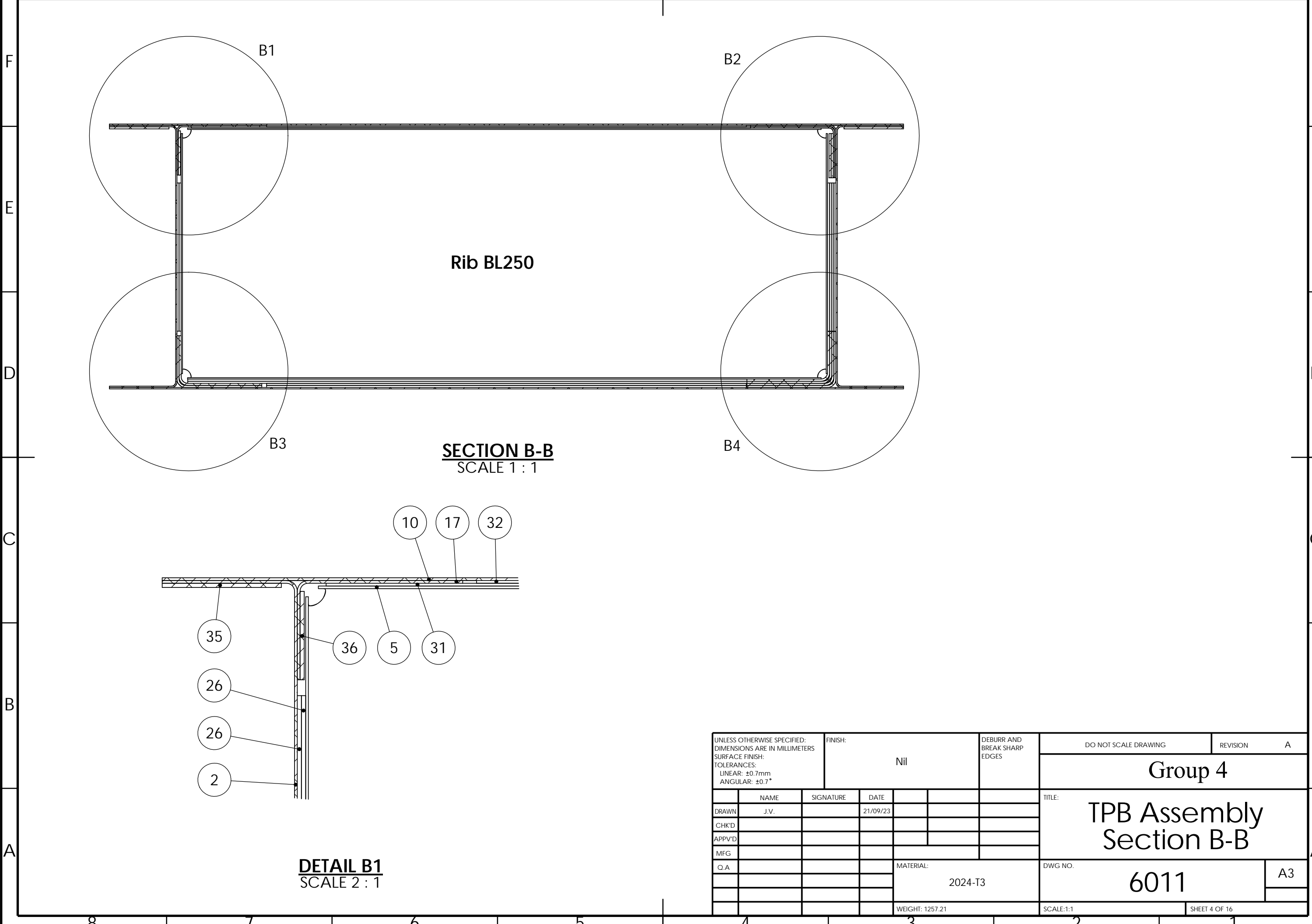
DETAIL A4
SCALE 2 : 1

UNLESS OTHERWISE SPECIFIED: DIMENSIONS ARE IN MILLIMETERS SURFACE FINISH: TOLERANCES: LINEAR: $\pm 0.7\text{mm}$ ANGULAR: $\pm 0.7^\circ$		FINISH: Nil			DEBURR AND BREAK SHARP EDGES	DO NOT SCALE DRAWING	REVISION
DRAWN	J.V.	NAME	SIGNATURE	DATE			A
CHK'D							
APP'D							
MFG							
Q.A					MATERIAL:	2024-T3	DWG NO.
							6011
					WEIGHT: 1257.21	SCALE: 2:1	A3
							SHEET 3 OF 16

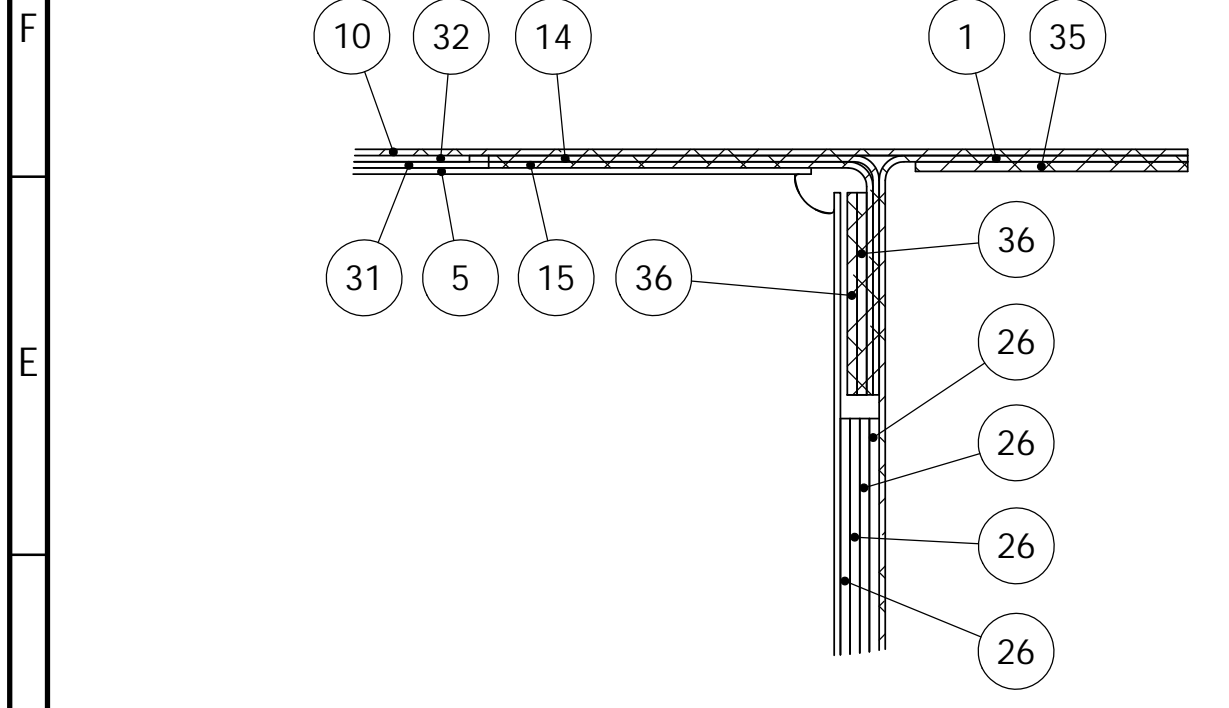
**TPB Assembly
Section A-A**

6011

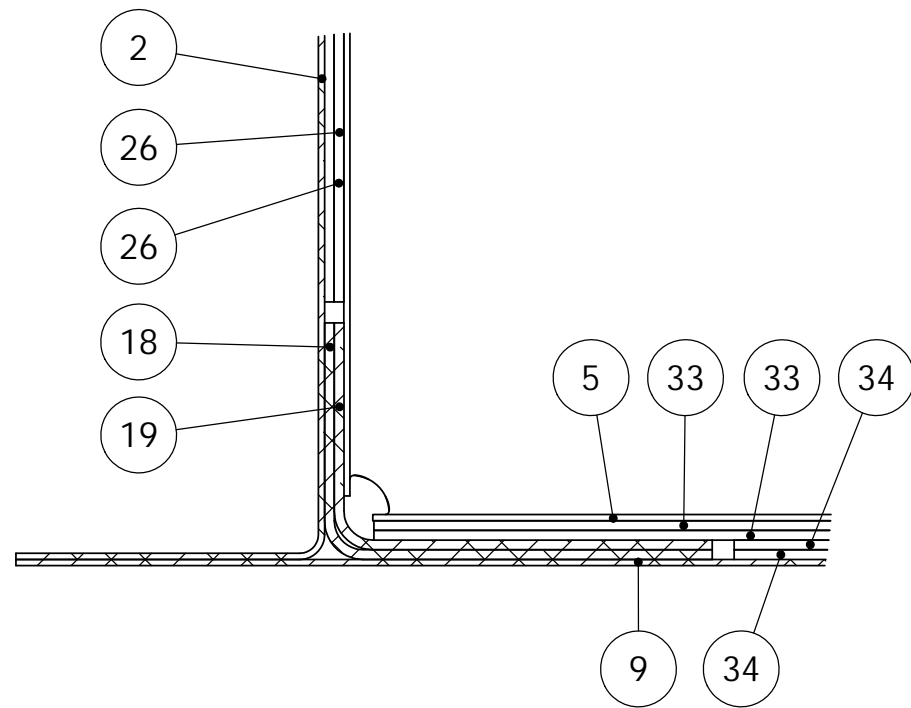
8 7 6 5 4 3 2 1



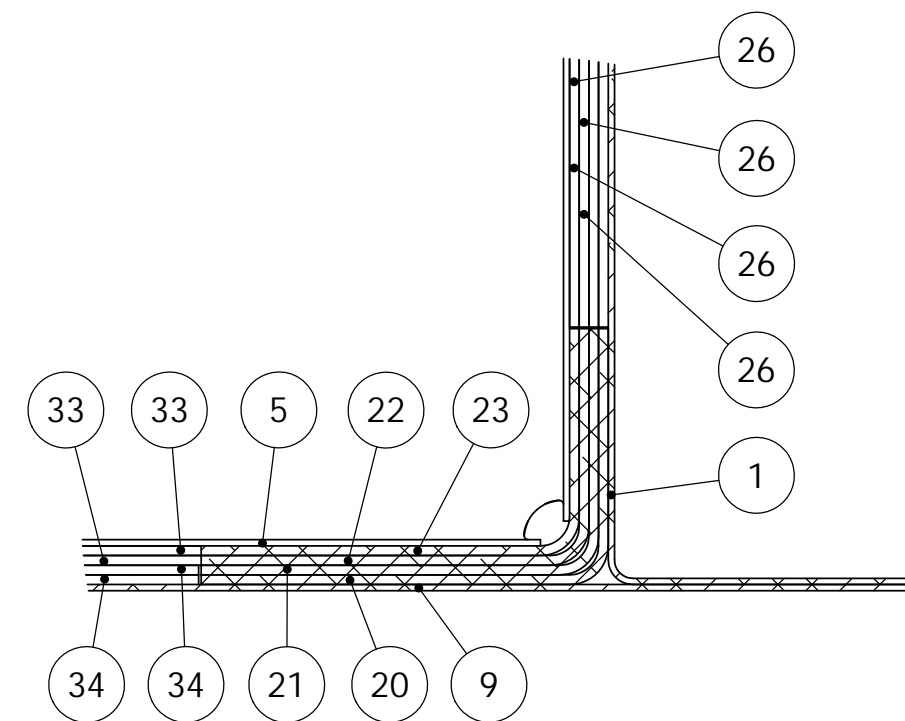
8 7 6 5 4 3 2 1



DETAIL B2
SCALE 2 : 1



DETAIL B3
SCALE 2 : 1



DETAIL B4
SCALE 2 : 1

UNLESS OTHERWISE SPECIFIED: DIMENSIONS ARE IN MILLIMETERS SURFACE FINISH: TOLERANCES: LINEAR: $\pm 0.7\text{mm}$ ANGULAR: $\pm 0.7^\circ$		FINISH: Nil			DEBURR AND BREAK SHARP EDGES	DO NOT SCALE DRAWING	REVISION A
DRAWN	J.V.	SIGNATURE	DATE				
CHK'D							
APP'D							
MFG							
Q.A					MATERIAL: 2024-T3	DWG NO. 6011	A3
					WEIGHT: 1257.21	SCALE: 2:1	
							SHEET 5 OF 16

**TPB Assembly
Section B-B**

6011

8 7 6 5 4 3 2 1

8 7 6 5 4 3 2 1

F

F

E

E

D

D

C

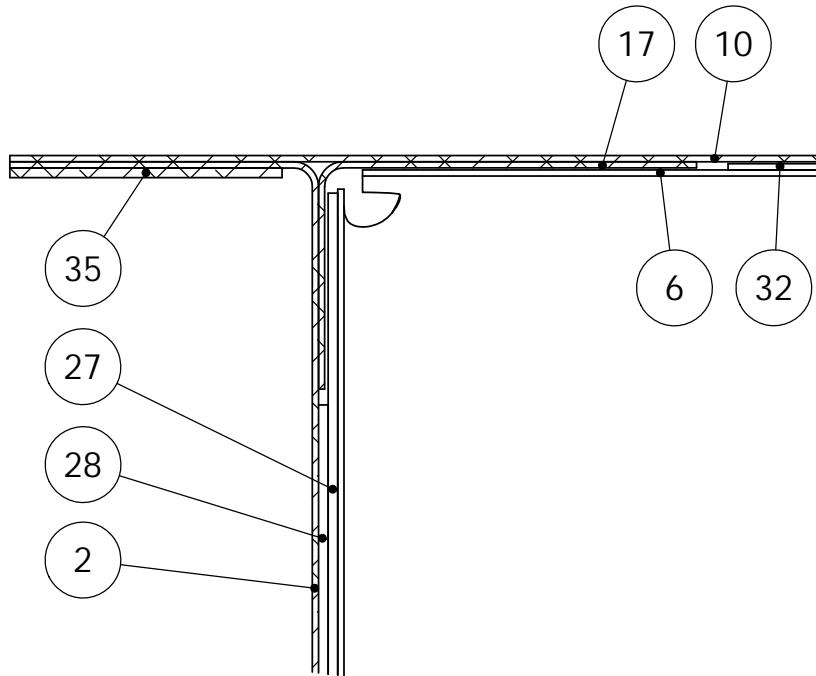
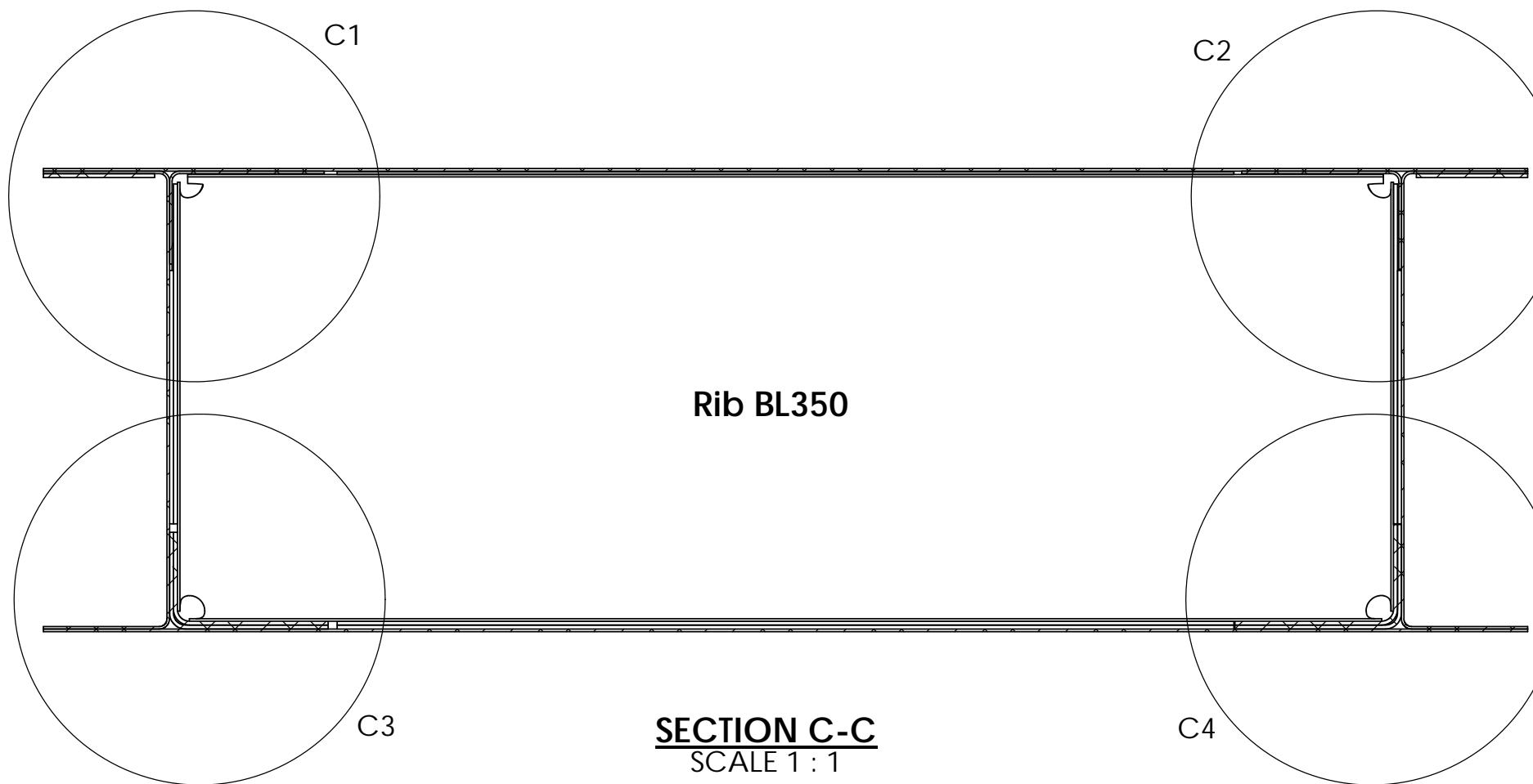
C

B

B

A

A



UNLESS OTHERWISE SPECIFIED: DIMENSIONS ARE IN MILLIMETERS SURFACE FINISH: TOLERANCES: LINEAR: $\pm 0.7\text{mm}$ ANGULAR: $\pm 0.7^\circ$		FINISH: Nil	DEBURR AND BREAK SHARP EDGES	DO NOT SCALE DRAWING	REVISION A
DRAWN	J.V.	SIGNATURE	DATE	21/09/23	
CHK'D					
APP'D					
MFG					
Q.A			MATERIAL:	2024-T3	DWG NO.
					6011
			WEIGHT: 1257.21	SCALE:1:1	A3
					SHEET 6 OF 16

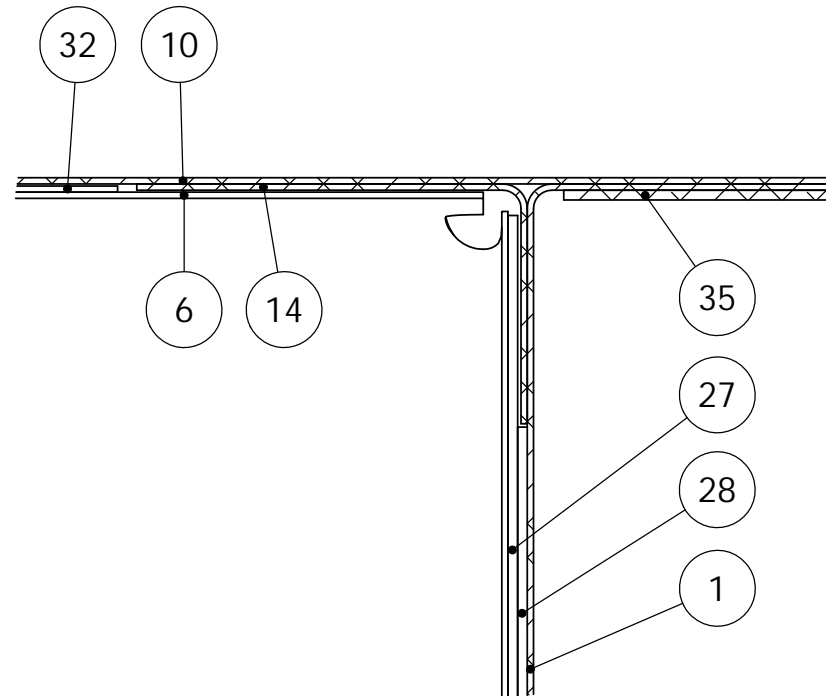
TPB Assembly
Section C-C

6011

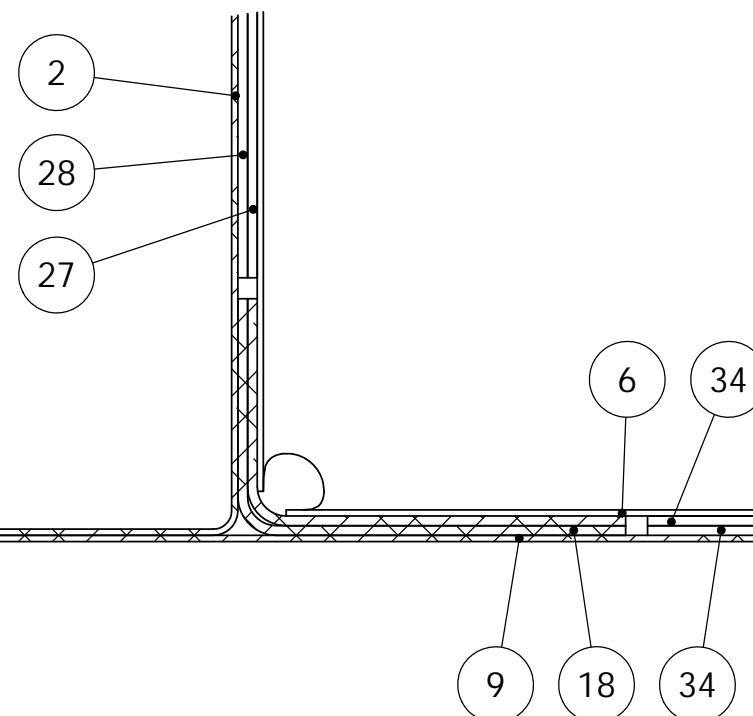
A3

8 7 6 5 4 3 2 1

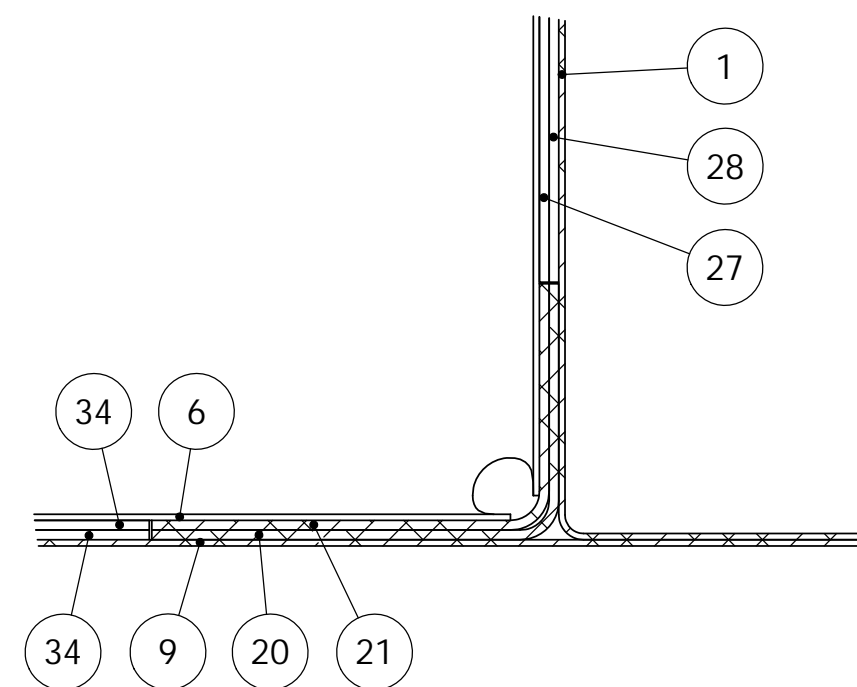
F F



DETAIL C2
SCALE 2 : 1



DETAIL C3
SCALE 2 : 1



DETAIL C4
SCALE 2 : 1

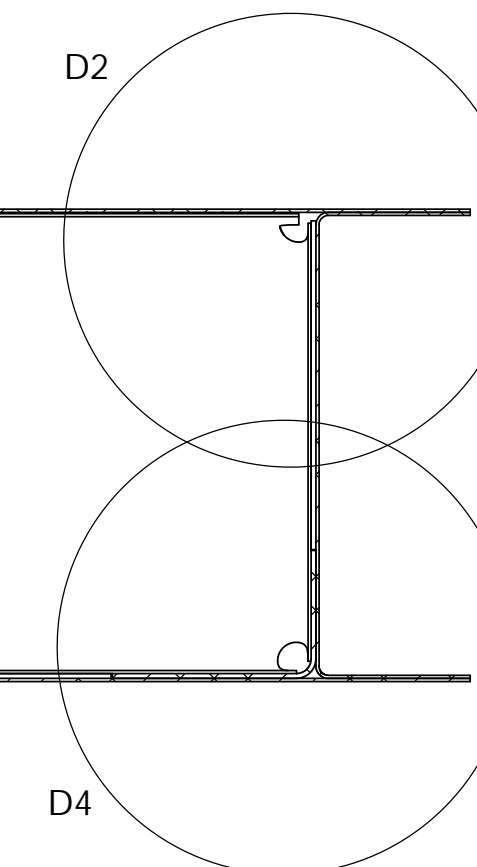
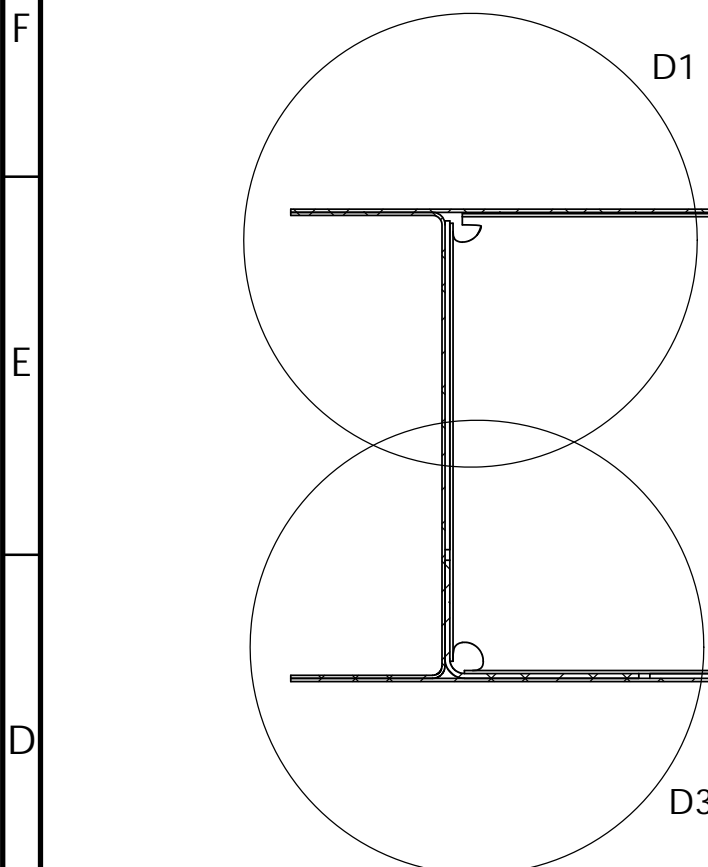
UNLESS OTHERWISE SPECIFIED: DIMENSIONS ARE IN MILLIMETERS SURFACE FINISH: TOLERANCES: LINEAR: $\pm 0.7\text{mm}$ ANGULAR: $\pm 0.7^\circ$		FINISH: Nil		DEBURR AND BREAK SHARP EDGES	DO NOT SCALE DRAWING		REVISION A
DRAWN	NAME J.V.	SIGNATURE	DATE 21/09/23				
CHK'D							
APP'D							
MFG							
Q.A				MATERIAL: 2024-T3		DWG NO. 6011	A3
					WEIGHT: 1257.21	SCALE: 2:1	
							SHEET 7 OF 16

**TPB Assembly
Section C-C**

6011

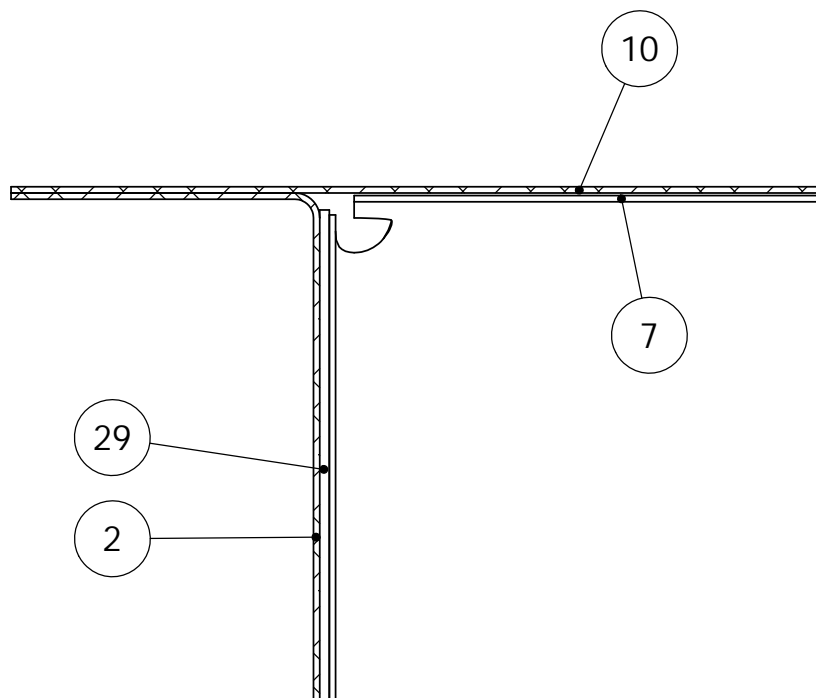
8 7 6 5 4 3 2 1

8 7 6 5 4 3 2 1



Rib BL542

SECTION D-D
SCALE 1 : 1



DETAIL D1
SCALE 2 : 1

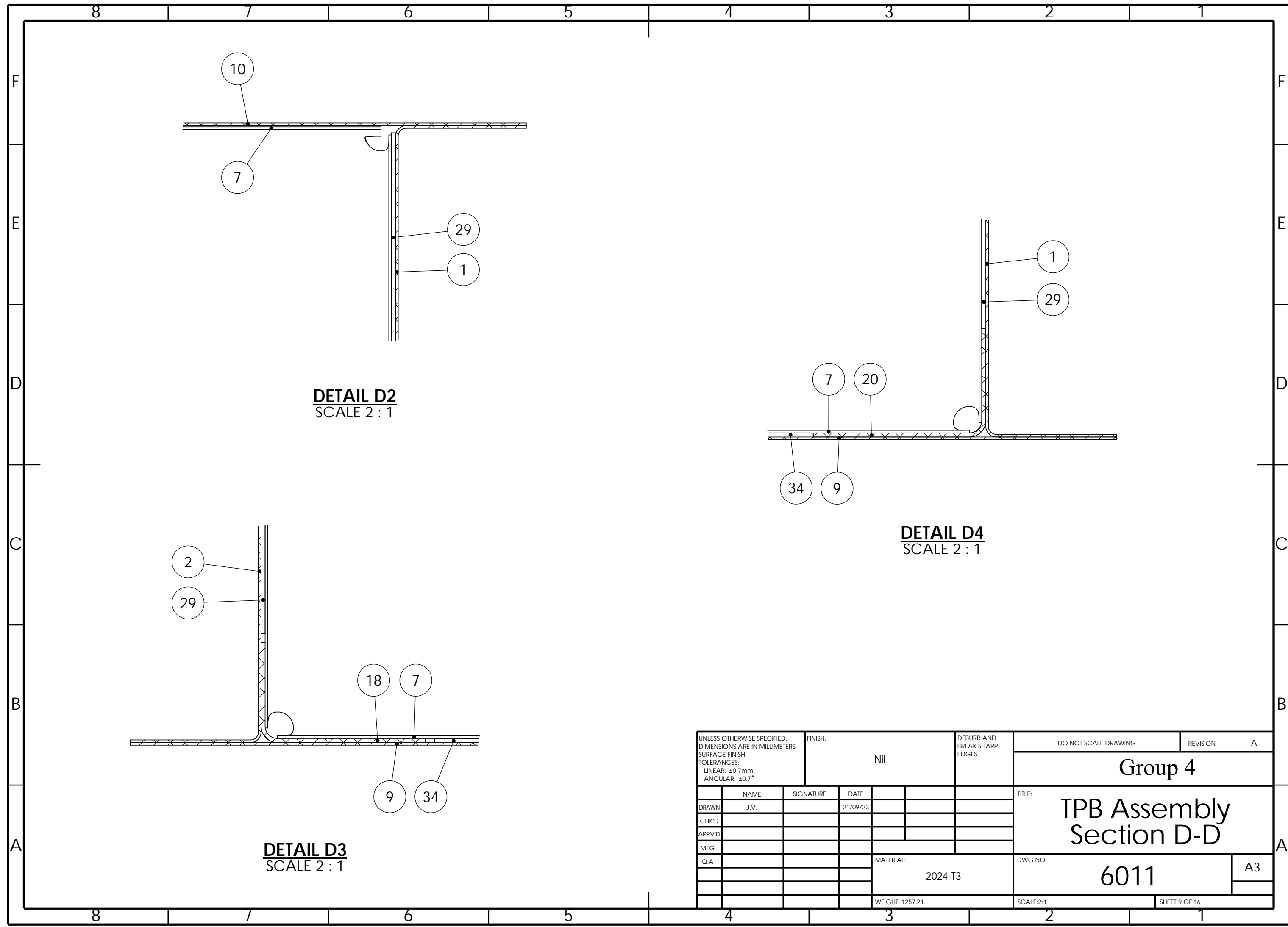
UNLESS OTHERWISE SPECIFIED: DIMENSIONS ARE IN MILLIMETERS SURFACE FINISH: TOLERANCES: LINEAR: $\pm 0.7\text{mm}$ ANGULAR: $\pm 0.7^\circ$		FINISH: Nil	DEBURR AND BREAK SHARP EDGES	DO NOT SCALE DRAWING	REVISION A
DRAWN	J.V.	SIGNATURE	DATE		
CHK'D					
APP'D					
MFG					
Q.A				MATERIAL:	DWG NO.
				2024-T3	6011
				WEIGHT: 1257.21	SCALE: 1:1
					Sheet 8 of 16

A3

TPB Assembly
Section D-D

6011

8 7 6 5 4 3 2 1



8 7 6 5 4 3 2 1

F

F

E

E

D

D

C

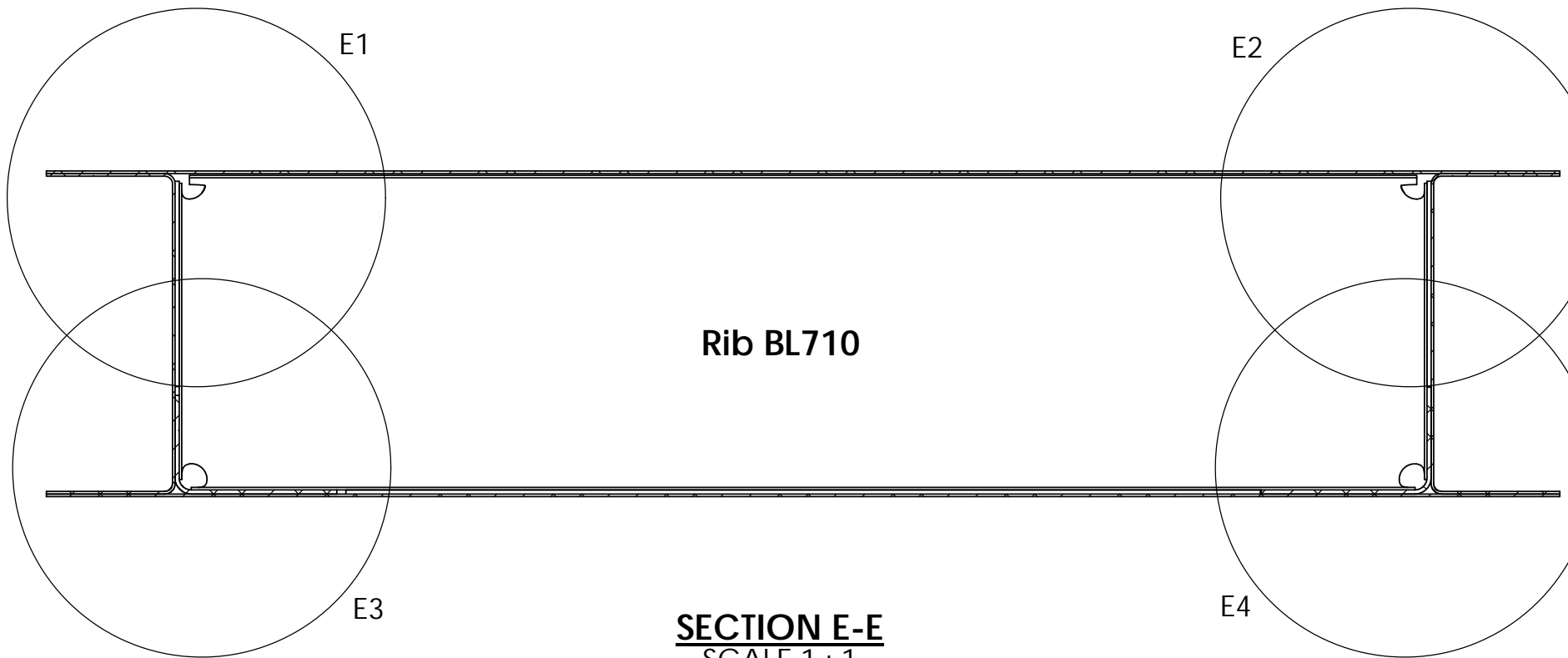
C

B

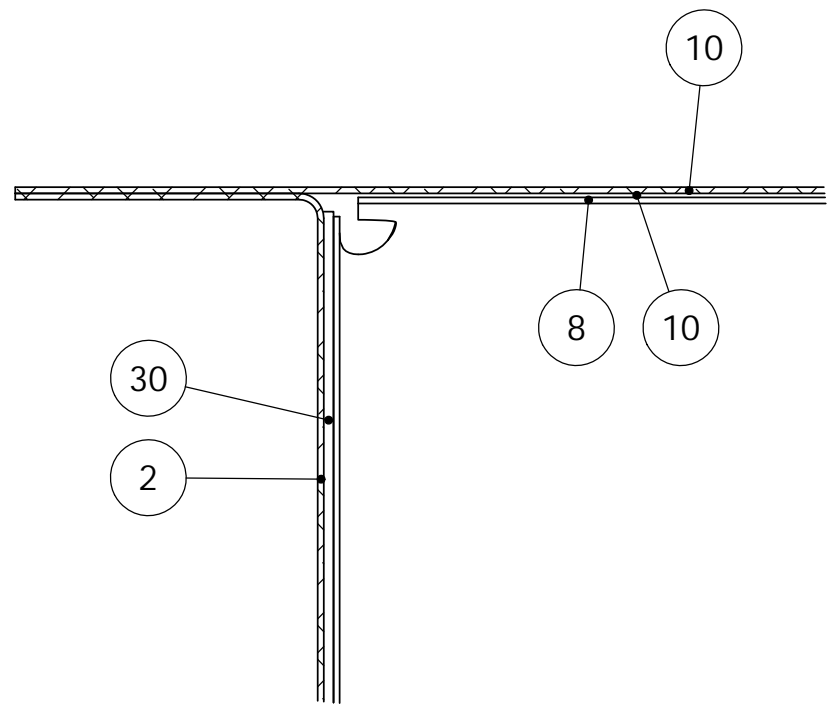
B

A

A

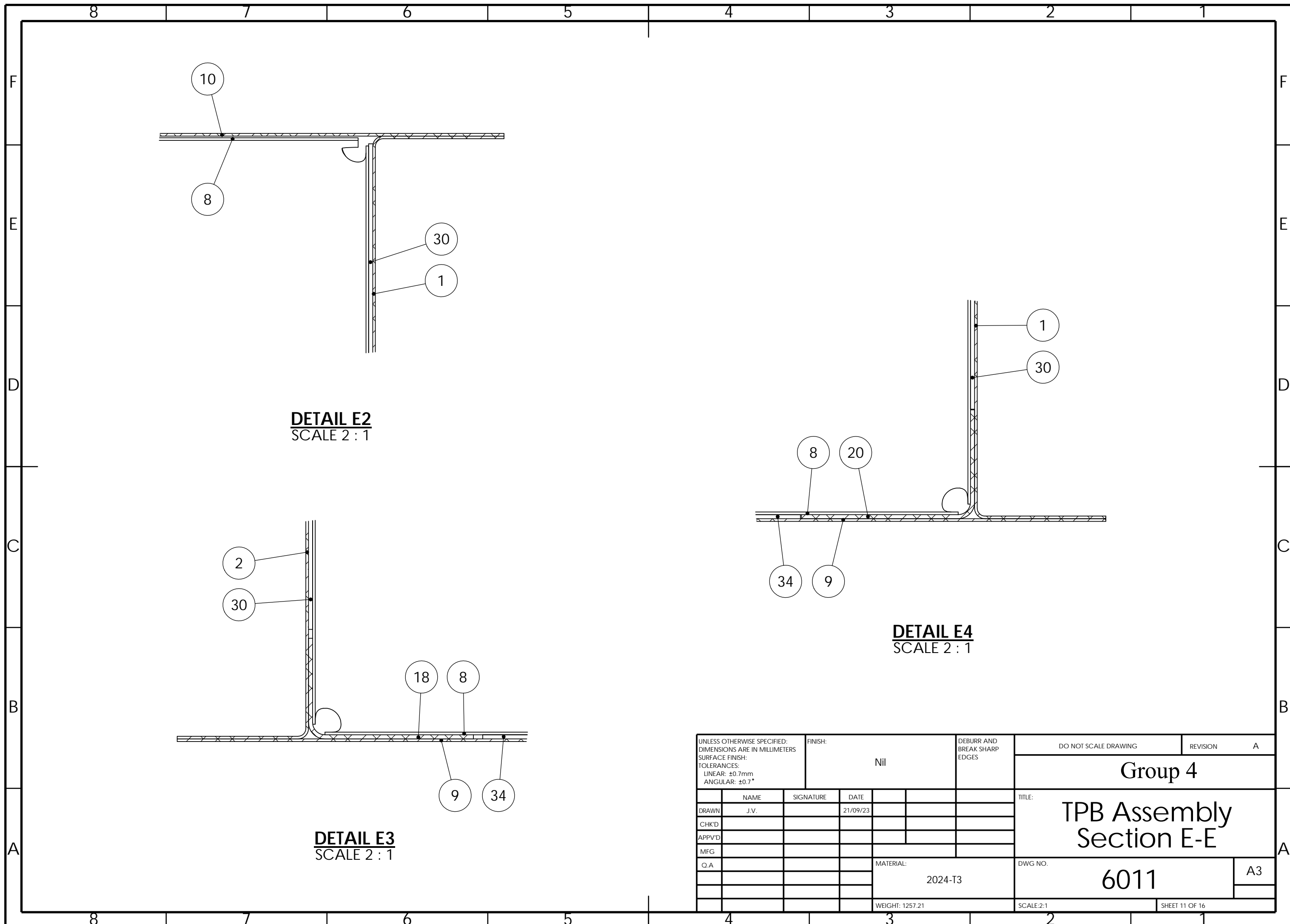


SECTION E-E
SCALE 1 : 1

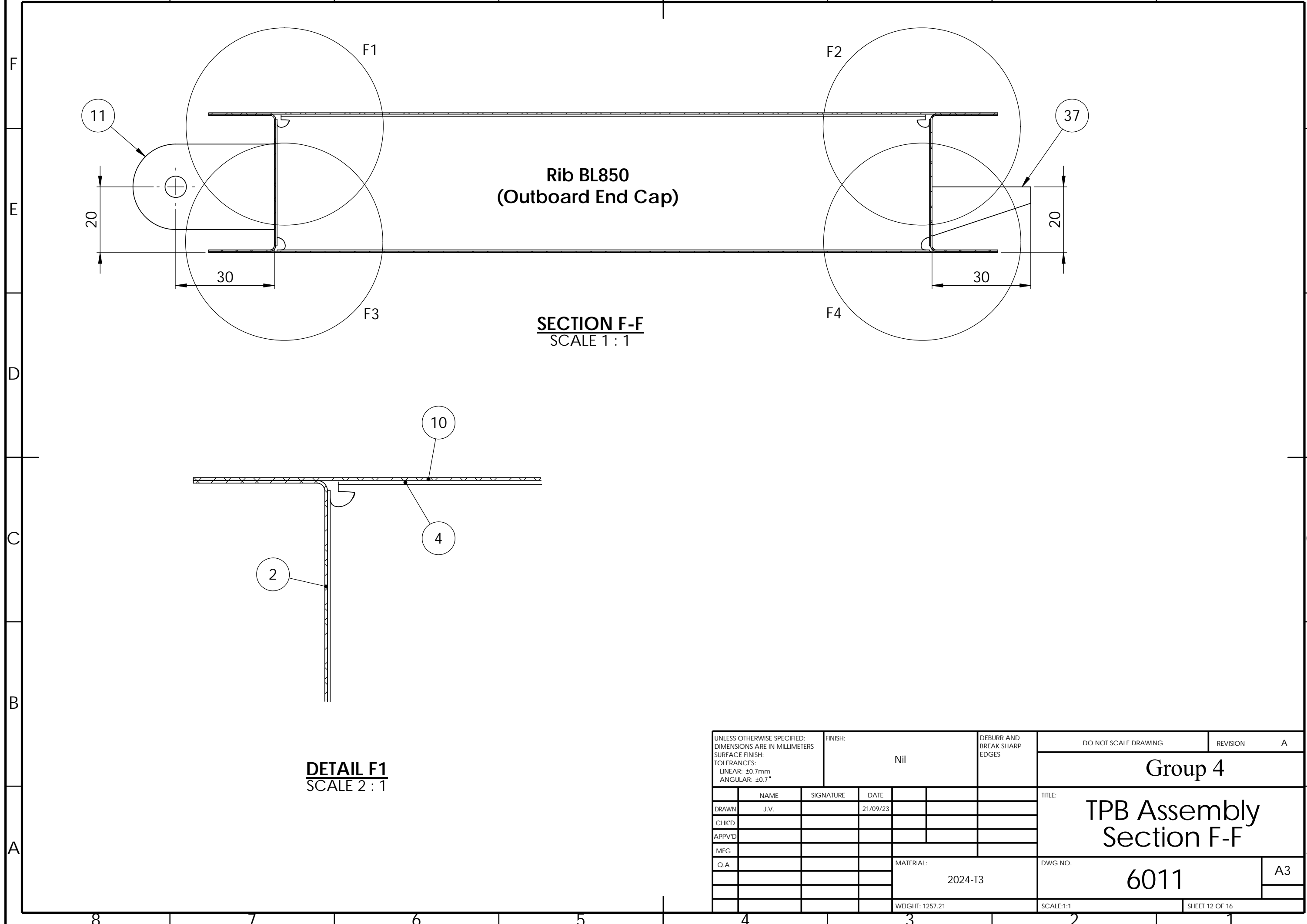


DETAIL E1
SCALE 2 : 1

UNLESS OTHERWISE SPECIFIED: DIMENSIONS ARE IN MILLIMETERS SURFACE FINISH: TOLERANCES: LINEAR: $\pm 0.7\text{mm}$ ANGULAR: $\pm 0.7^\circ$			FINISH: Nil	DEBURR AND BREAK SHARP EDGES	DO NOT SCALE DRAWING	REVISION A
DRAWN	NAME	SIGNATURE	DATE		TITLE:	Group 4
CHK'D			21/09/23			
APP'D						
MFG						
Q.A				MATERIAL:	DWG NO.	
				2024-T3	6011	A3
				WEIGHT: 1257.21	SCALE: 1:1	
						SHEET 10 OF 16

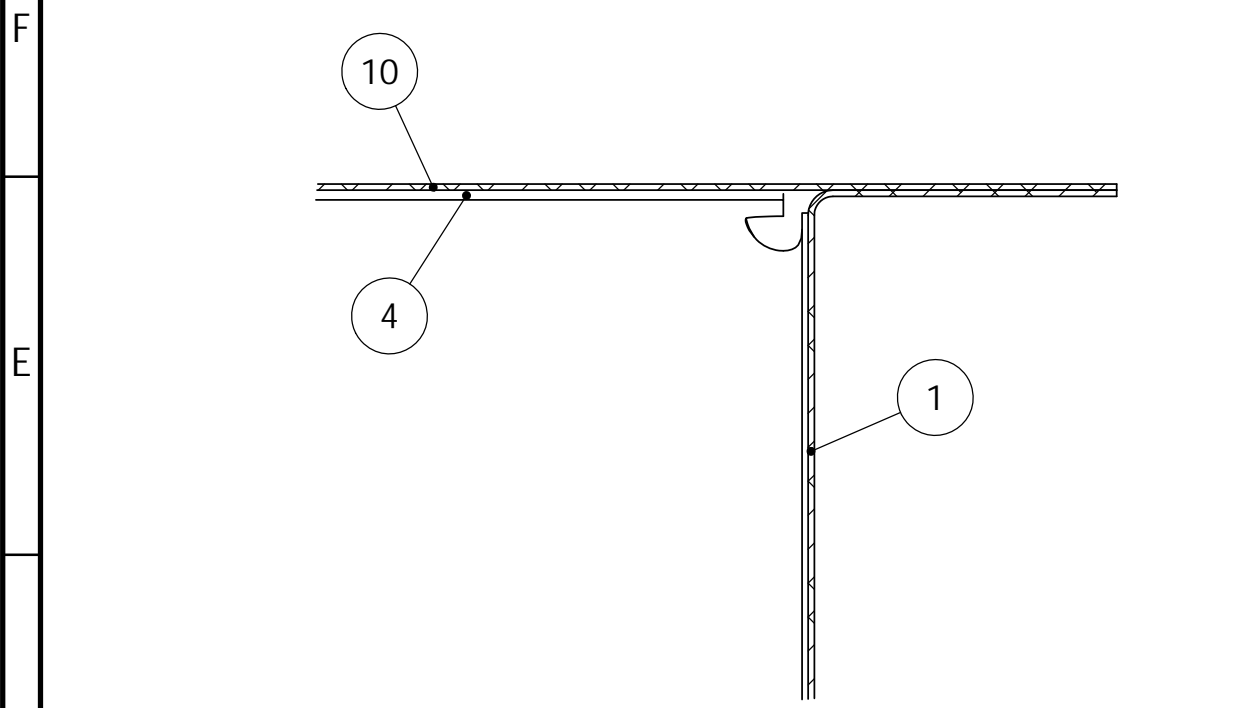


8 7 6 5 4 3 2 1

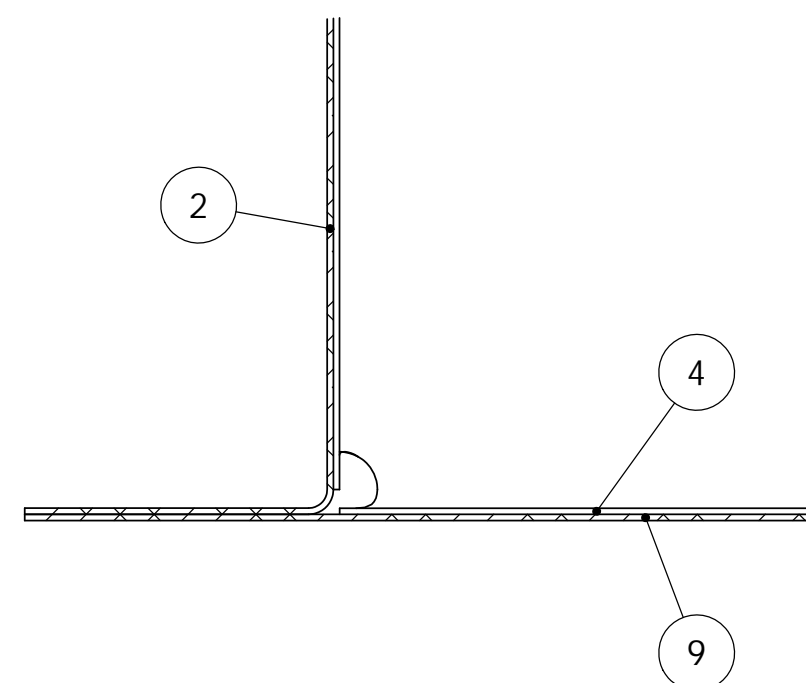


8 7 6 5 4 3 2 1

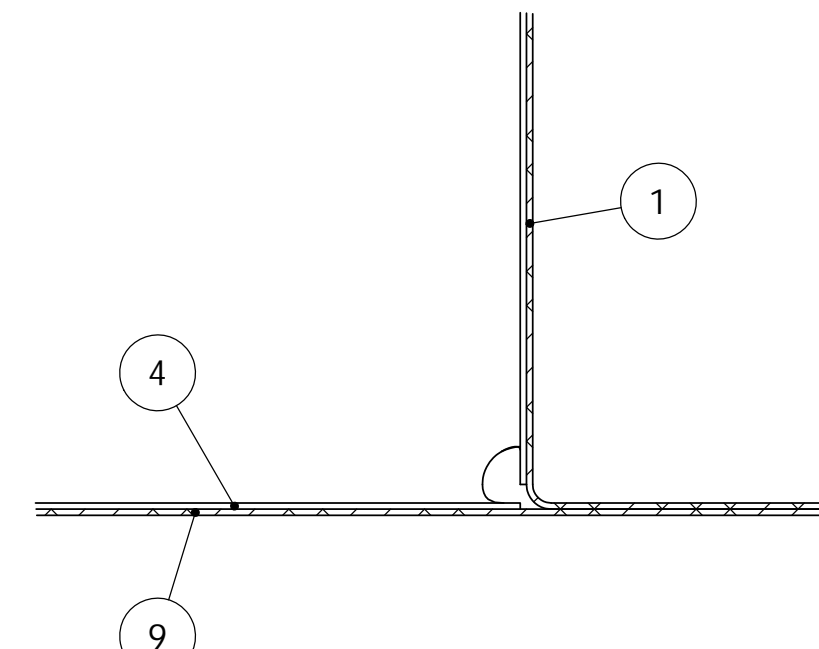
8 7 6 5 4 3 2 1



DETAIL F2
SCALE 2 : 1



DETAIL F3
SCALE 2 : 1



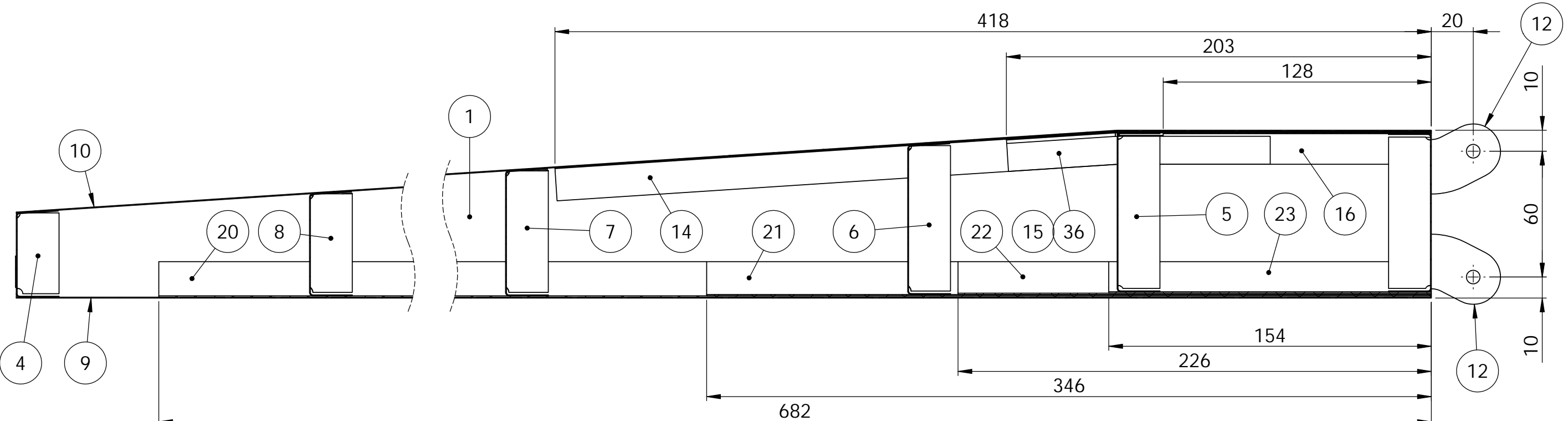
DETAIL F4
SCALE 2 : 1

UNLESS OTHERWISE SPECIFIED: DIMENSIONS ARE IN MILLIMETERS SURFACE FINISH: TOLERANCES: LINEAR: $\pm 0.7\text{mm}$ ANGULAR: $\pm 0.7^\circ$		FINISH: Nil	DEBURR AND BREAK SHARP EDGES	DO NOT SCALE DRAWING	REVISION
DRAWN	J.V.	SIGNATURE	DATE		A
CHK'D					
APP'D					
MFG					
Q.A				MATERIAL:	DWG NO.
				2024-T3	6011
				WEIGHT: 1257.21	SCALE: 2:1
					Sheet 13 of 16

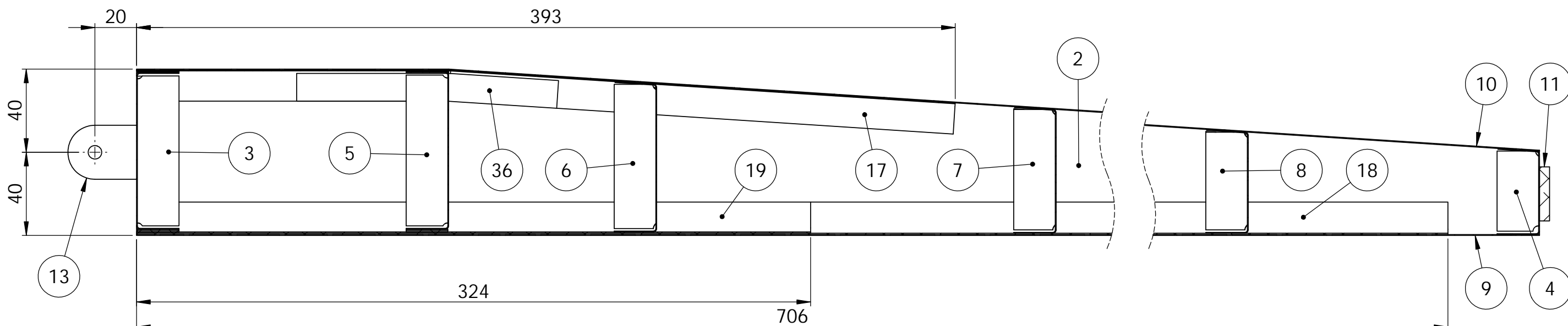
TPB Assembly
Section F-F

6011

A3



SECTION G-G
SCALE 1 : 2



SECTION H-H
SCALE 1 : 2

UNLESS OTHERWISE SPECIFIED: DIMENSIONS ARE IN MILLIMETERS SURFACE FINISH: TOLERANCES: LINEAR: $\pm 0.7\text{mm}$ ANGULAR: $\pm 0.7^\circ$			FINISH:	Nil	DEBURR AND BREAK SHARP EDGES	DO NOT SCALE DRAWING	REVISION
DRAWN	NAME	SIGNATURE	DATE				A
CHK'D			21/09/23				
APP'D							
MFG							
Q.A				MATERIAL:	2024-T3	DWG NO.	
						6011	A3
				WEIGHT: 1257.21		SCALE: 1:2	
							SHEET 14 OF 16

Note:

Spar cap reinforcing section lengths are shown as dimensioned in the above section views.

ITEM NO.	Qty	DESCRIPTION	PartNo	Material	Weight
1	1	Left Forward Spar	6112-101	2024-T3	86.77
2	1	Left Aft Spar	6112-103	2024-T3	86.91
3	1	Left Inboard End Cap	6112-105	2024-T3	28.14
4	1	Left Outboard End Cap	6112-107	2024-T3	19.15
5	1	Left Rib BL250	6112-109	2024-T3	28.25
6	1	Left Rib BL350	6112-111	2024-T3	27.12
7	1	Left Rib BL542	6112-113	2024-T3	24.22
8	1	Left Rib BL710	6112-115	2024-T3	21.30
9	1	Left Lower Skin	6113-117	2024-T3	203.60
10	1	Left Upper Skin	6113-119	2024-T3	204.13
11	1	Left Load Lug	6111-121	2024-T3	32.15
12	2	Left Inboard Forward Lug	6111-123	2024-T3	50.82
13	1	Left Inboard Aft Lug	6111-125	2024-T3	28.65
14	1	Left Front Top Spar Cap Stiffener 1	6114-127	2024-T3	19.36
15	1	Left Front Top Spar Cap Stiffener 2	6114-129	2024-T3	9.17
16	1	Left Front Top Spar Cap Stiffener 3	6114-131	2024-T3	5.69
17	1	Left Rear Top Spar Cap Stiffener 1	6114-133	2024-T3	17.47
18	1	Left Rear Bottom Spar Cap Stiffener 1	6114-135	2024-T3	49.84
19	1	Left Rear Bottom Spar Cap Stiffener 2	6114-137	2024-T3	22.14
20	1	Left Front Bottom Spar Cap Stiffener 1	6114-139	2024-T3	51.25
21	1	Left Front Bottom Spar Cap Stiffener 2	6114-141	2024-T3	25.21
22	1	Left Front Bottom Spar Cap Stiffener 3	6114-143	2024-T3	15.95
23	1	Left Front Bottom Spar Cap Stiffener 4	6114-145	2024-T3	10.52
24	3	Left Inboard End Cap Long Vertical Spacer	6115-147	2024-T3	2.11
25	3	Left Inboard End Cap Short Vertical Spacer	6115-149	2024-T3	1.59
26	6	Left Rib BL250 Vertical Spacer	6115-151	2024-T3	1.59
27	2	Left Rib BL350 Long Vertical Spacer	6115-153	2024-T3	1.93
28	2	Left Rib BL350 Short Vertical Spacer	6115-155	2024-T3	1.43
29	2	Left Rib BL542 Vertical Spacer	6115-157	2024-T3	1.52
30	2	Left Rib BL710 Vertical Spacer	6115-159	2024-T3	1.14
31	3	Left Rib Upper Long Horizontal Spacer	6115-161	2024-T3	3.85
32	3	Left Rib Upper Short Horizontal Spacer	6115-163	2024-T3	3.31
33	4	Left Rib Lower Long Horizontal Spacer	6115-165	2024-T3	6.01
34	8	Left Rib Lower Short Horizontal Spacer	6115-167	2024-T3	5.16
35	2	Left Upper Spar Flange Strap	6115-169	2024-T3	4.64
36	3	Left Upper Stiffener Strap	6115-171	2024-T3	2.98
37	1	Left Displacement Lug	6111-173	2024-T3	0.84

UNLESS OTHERWISE SPECIFIED: DIMENSIONS ARE IN MILLIMETERS SURFACE FINISH: TOLERANCES: LINEAR: $\pm 0.7\text{mm}$ ANGULAR: $\pm 0.7^\circ$		FINISH: Nil		DEBURR AND BREAK SHARP EDGES	DO NOT SCALE DRAWING		REVISION	A
Group 4								
Left TPB Assembly BOM								
DRAWN	NAME	SIGNATURE	DATE				TITLE:	
CHK'D							DWG NO.	
APP'D								
MFG							A3	
Q.A								
				MATERIAL:		2024-T3		
				WEIGHT:		1257.21		
				SHEET 15 OF 16				

ITEM NO.	Qty	DESCRIPTION	PartNo	Material	Weight	
1	1	Right Forward Spar	6112-102	2024-T3	86.77	
2	1	Right Aft Spar	6112-104	2024-T3	86.91	
3	1	Right Inboard End Cap	6112-106	2024-T3	28.14	
4	1	Right Outboard End Cap	6112-108	2024-T3	19.15	
5	1	Right Rib BL250	6112-110	2024-T3	28.25	
6	1	Right Rib BL350	6112-112	2024-T3	27.12	
7	1	Right Rib BL542	6112-114	2024-T3	24.22	
8	1	Right Rib BL710	6112-116	2024-T3	21.30	
9	1	Right Lower Skin	6113-118	2024-T3	203.60	
10	1	Right Upper Skin	6113-120	2024-T3	204.13	
11	1	Right Load Lug	6111-122	2024-T3	32.15	
12	2	Right Inboard Forward Lug	6111-124	2024-T3	50.82	
13	1	Right Inboard Aft Lug	6111-126	2024-T3	28.65	
14	1	Right Front Top Spar Cap Stiffener 1	6114-128	2024-T3	19.36	
15	1	Right Front Top Spar Cap Stiffener 2	6114-130	2024-T3	9.17	
16	1	Right Front Top Spar Cap Stiffener 3	6114-132	2024-T3	5.69	
17	1	Right Rear Top Spar Cap Stiffener 1	6114-134	2024-T3	17.47	
18	1	Right Rear Bottom Spar Cap Stiffener 1	6114-136	2024-T3	49.84	
19	1	Right Rear Bottom Spar Cap Stiffener 2	6114-138	2024-T3	22.14	
20	1	Right Front Bottom Spar Cap Stiffener 1	6114-140	2024-T3	51.25	
21	1	Right Front Bottom Spar Cap Stiffener 2	6114-142	2024-T3	25.21	
22	1	Right Front Bottom Spar Cap Stiffener 3	6114-144	2024-T3	15.95	
23	1	Right Front Bottom Spar Cap Stiffener 4	6114-146	2024-T3	10.52	
24	3	Right Inboard End Cap Long Vertical Spacer	6115-148	2024-T3	2.11	
25	3	Right Inboard End Cap Short Vertical Spacer	6115-150	2024-T3	1.59	
26	6	Right Rib BL250 Vertical Spacer	6115-152	2024-T3	1.59	
27	2	Right Rib BL350 Long Vertical Spacer	6115-154	2024-T3	1.93	
28	2	Right Rib BL350 Short Vertical Spacer	6115-156	2024-T3	1.43	
29	2	Right Rib BL542 Vertical Spacer	6115-158	2024-T3	1.52	
30	2	Right Rib BL710 Vertical Spacer	6115-160	2024-T3	1.14	
31	3	Right Rib Upper Long Horizontal Spacer	6115-162	2024-T3	3.85	
32	3	Right Rib Upper Short Horizontal Spacer	6115-164	2024-T3	3.31	
33	4	Right Rib Lower Long Horizontal Spacer	6115-166	2024-T3	6.01	
34	8	Right Rib Lower Short Horizontal Spacer	6115-168	2024-T3	5.16	
35	2	Right Upper Spar Flange Strap	6115-170	2024-T3	4.64	
36	3	Right Upper Stiffener Strap	6115-172	2024-T3	2.98	
37	1	Right Displacement Lug	6111-174	2024-T3	0.84	

UNLESS OTHERWISE SPECIFIED: DIMENSIONS ARE IN MILLIMETERS SURFACE FINISH: TOLERANCES: LINEAR: $\pm 0.7\text{mm}$ ANGULAR: $\pm 0.7^\circ$		FINISH: Nil		DEBURR AND BREAK SHARP EDGES	DO NOT SCALE DRAWING	REVISION A
Group 4						
DRAWN	J.V.	SIGNATURE	DATE			TITLE: Right TPB Assembly BOM
CHK'D			21/09/23			
APPV'D						
MFG						
Q.A				MATERIAL: 2024-T3	DWG NO. 6011	A3
				WEIGHT: 1257.21		SHEET 16 OF 16

A3

Right TPB Assembly BOM

A3

8

1

1

1

4

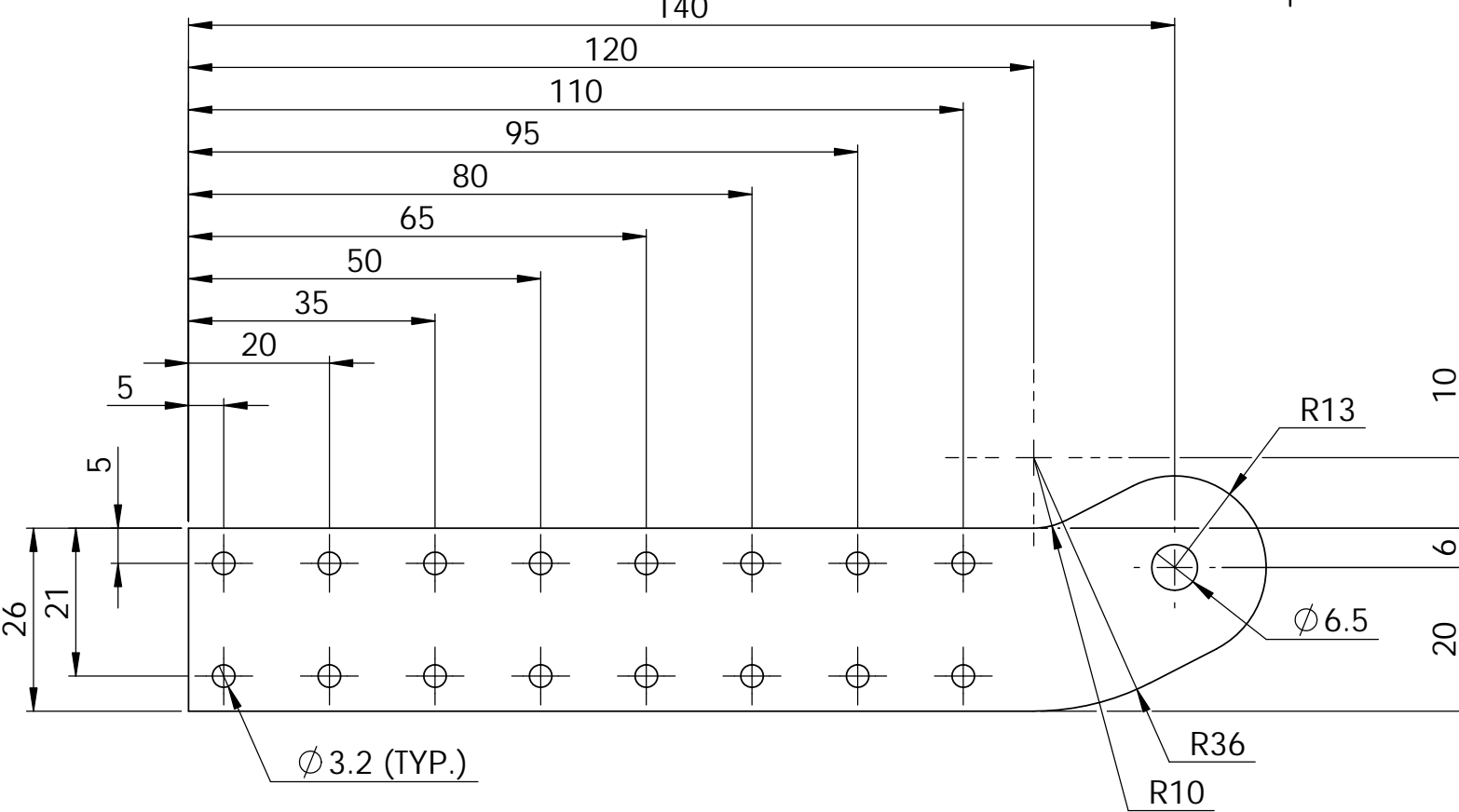
WEIGHT: 1257.21

—

6011

A3

SHEET 16 OF 16



Left Inboard Forward Lug (Lugs A and B)

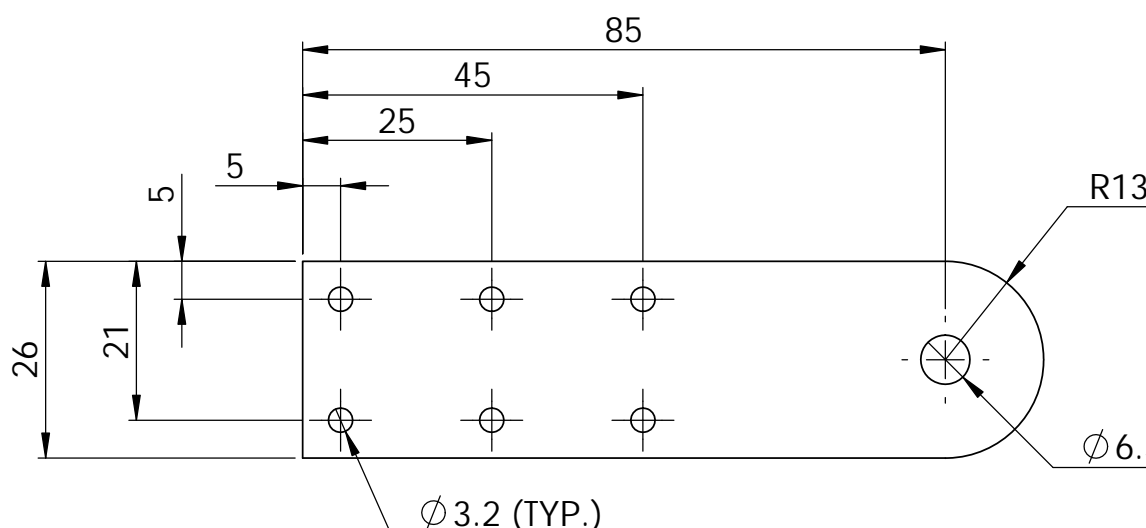
P/N: 6111-123

Right Inboard Forward Lug (Lugs A and B)

P/N: 6111-124

Material: 4.83x31x153 2023-T3 Clad Plate

Scale 1:1



Left Outboard Load Lug (Lug P)

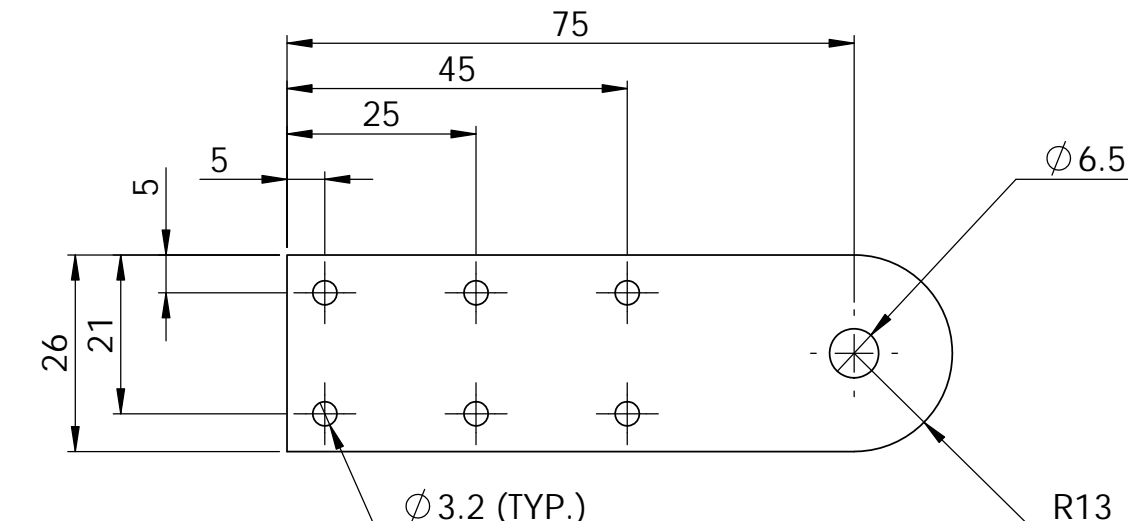
P/N: 6111-121

Right Outboard Load Lug (Lug P)

P/N: 6111-122

Material: 4.83x26x98 2023-T3 Clad Plate

Scale 1:1



Left Inboard Aft Lug (Lug C)

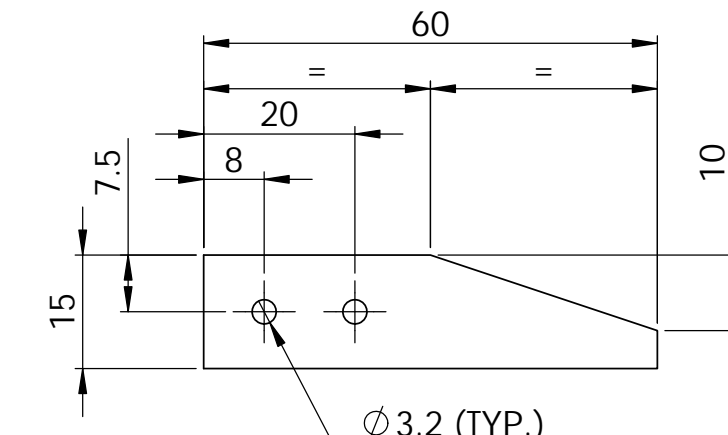
P/N: 6111-125

Right Inboard Aft Lug (Lug C)

P/N: 6111-126

Material: 4.83x26x88 2023-T3 Clad Plate

Scale 1:1



Left Displacement Lug

P/N: 6111-173

Right Displacement Lug

P/N: 6111-174

Material: 0.41x15x60 2023-T3 Clad Plate

Scale 1:1

UNLESS OTHERWISE SPECIFIED: DIMENSIONS ARE IN MILLIMETERS SURFACE FINISH: TOLERANCES: LINEAR: $\pm 0.7\text{mm}$ ANGULAR: $\pm 0.7^\circ$		FINISH: Nil		DEBURR AND BREAK SHARP EDGES	DO NOT SCALE DRAWING	REVISION
DRAWN	J.V.	SIGNATURE	DATE			A
CHK'D						
APP'D						
MFG						
Q.A				MATERIAL: 2024-T3	DWG NO. 6111	
				WEIGHT: 32.15	SCALE: 1:1	A3
						SHEET 1 OF 1

1

8

7

6

5

4

3

2

1

F

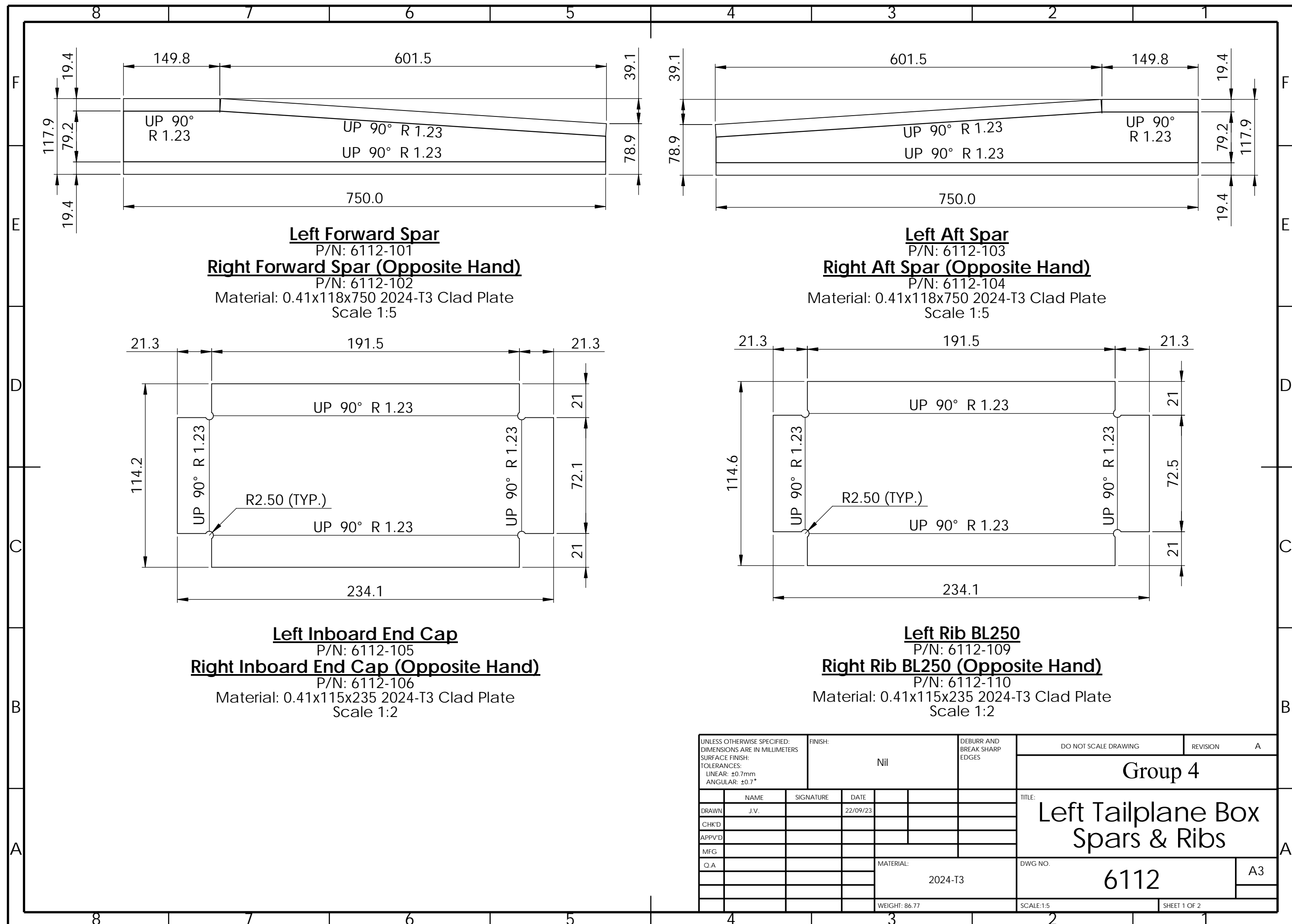
E

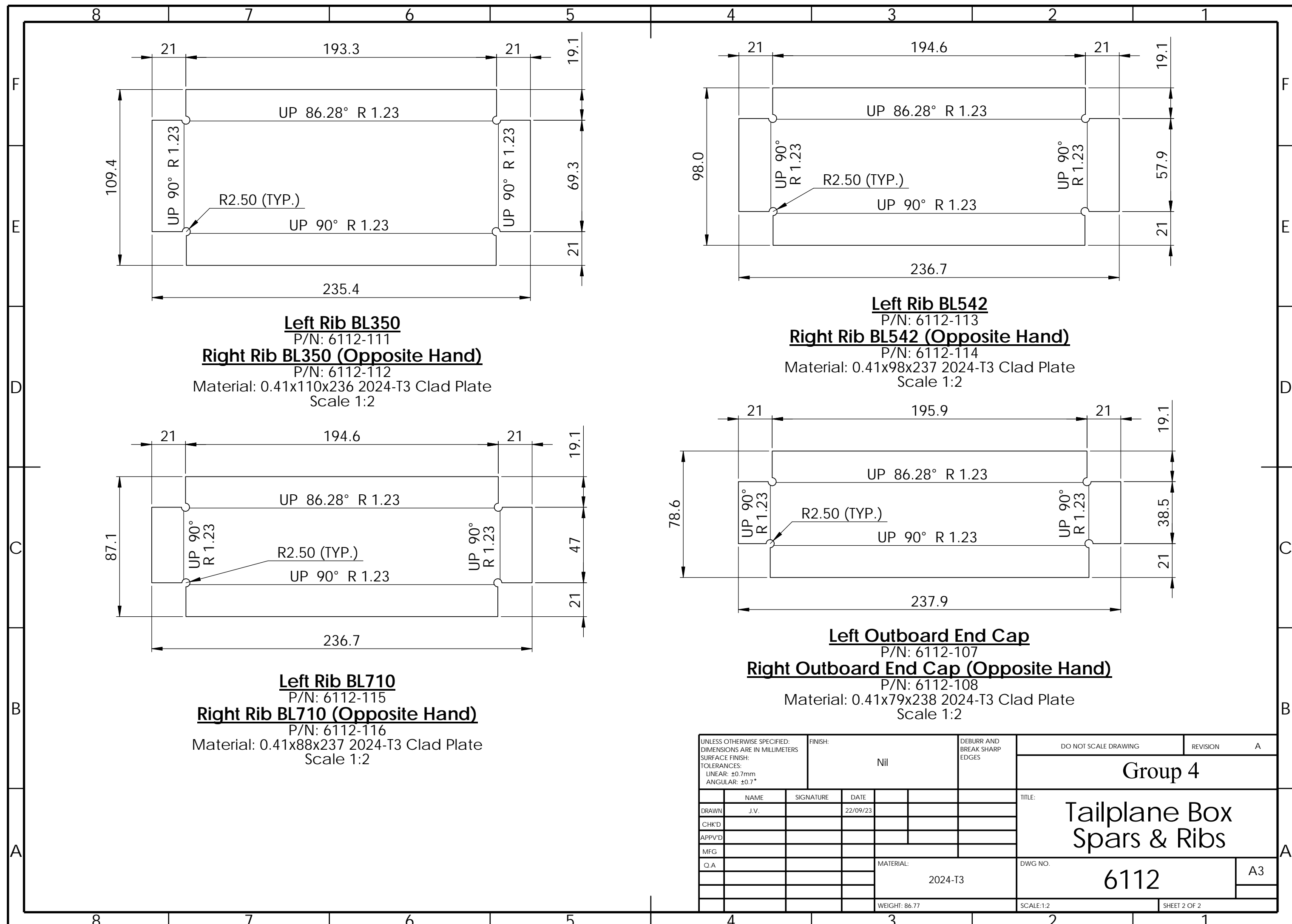
D

C

B

A





8

7

6

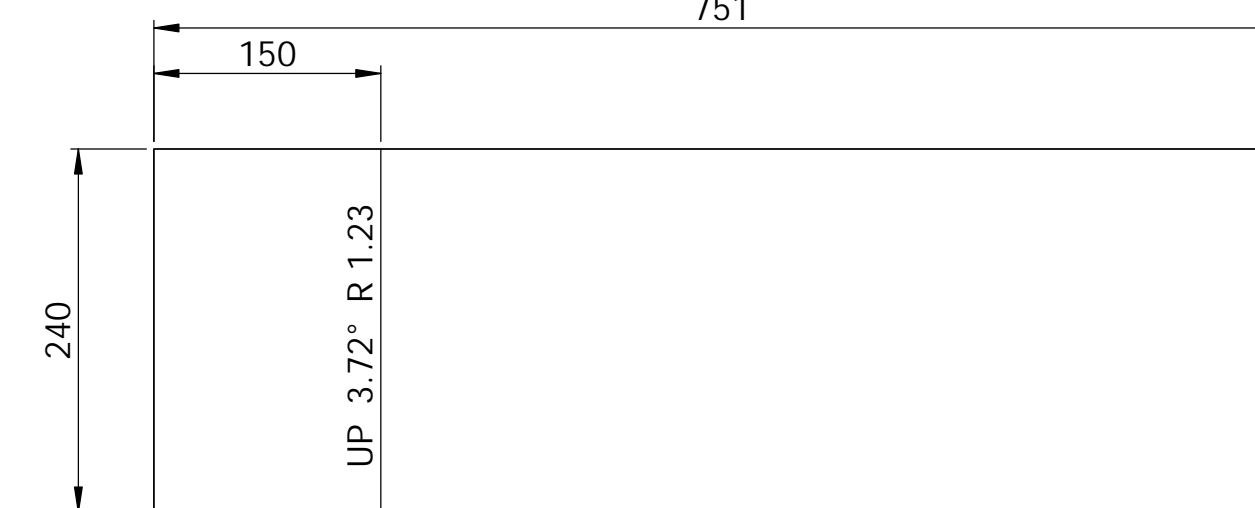
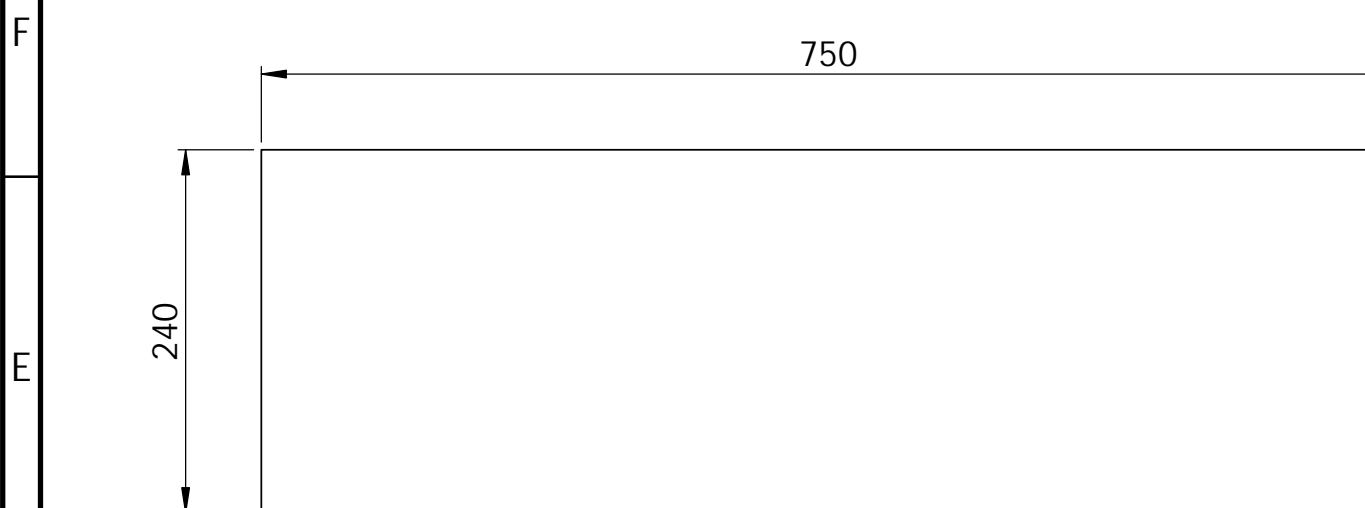
5

4

3

2

1



Left Lower Skin

P/N: 6113-117

Right Lower Skin (Opposite Hand)

P/N: 6113-118

Material: 0.41x240x750 2024-T3 Clad Plate

Scale 1:5

Left Upper Skin

P/N: 6113-119

Right Upper Skin (Opposite Hand)

P/N: 6113-120

Material: 0.41x240x751 2024-T3 Clad Plate

Scale 1:5

UNLESS OTHERWISE SPECIFIED: DIMENSIONS ARE IN MILLIMETERS SURFACE FINISH: TOLERANCES: LINEAR: ±0.7mm ANGULAR: ±0.7°		FINISH: Nil			DEBURR AND BREAK SHARP EDGES	DO NOT SCALE DRAWING		REVISION	A
DRAWN	J.V.			28/09/23					
CHK'D									
APP'D									
MFG									
Q.A					MATERIAL: 2024-T3		DWG NO. 6113		
						WEIGHT: 204.99	SCALE: 1:5		
								SHEET 1 OF 1	

Group 4
Tailplane Box
Skins

6113

A3

8

7

6

5

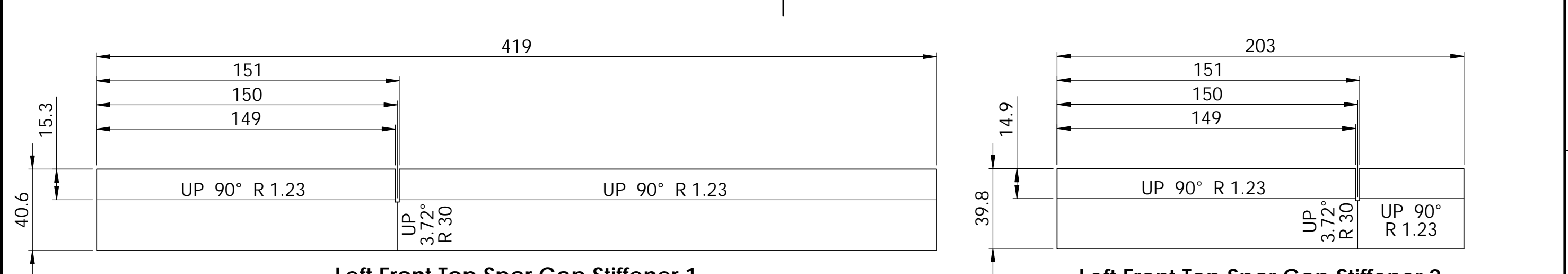
4

3

2

1

8 7 6 5 4 3 2 1



Left Front Top Spar Cap Stiffener 1

P/N: 6114-127

Right Front Top Spar Cap Stiffener 1 (Opposite Hand)

P/N: 6114-128

Material: 0.41x41x419 2024-T3 Clad Plate

Scale 1:2

Left Front Top Spar Cap Stiffener 2

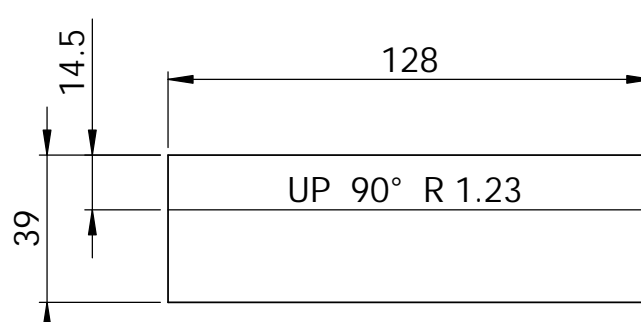
P/N: 6114-129

Right Front Top Spar Cap Stiffener 2 (Opposite Hand)

P/N: 6114-130

Material: 0.41x40x203 2024-T3 Clad Plate

Scale 1:2



Left Front Top Spar Cap Stiffener 3

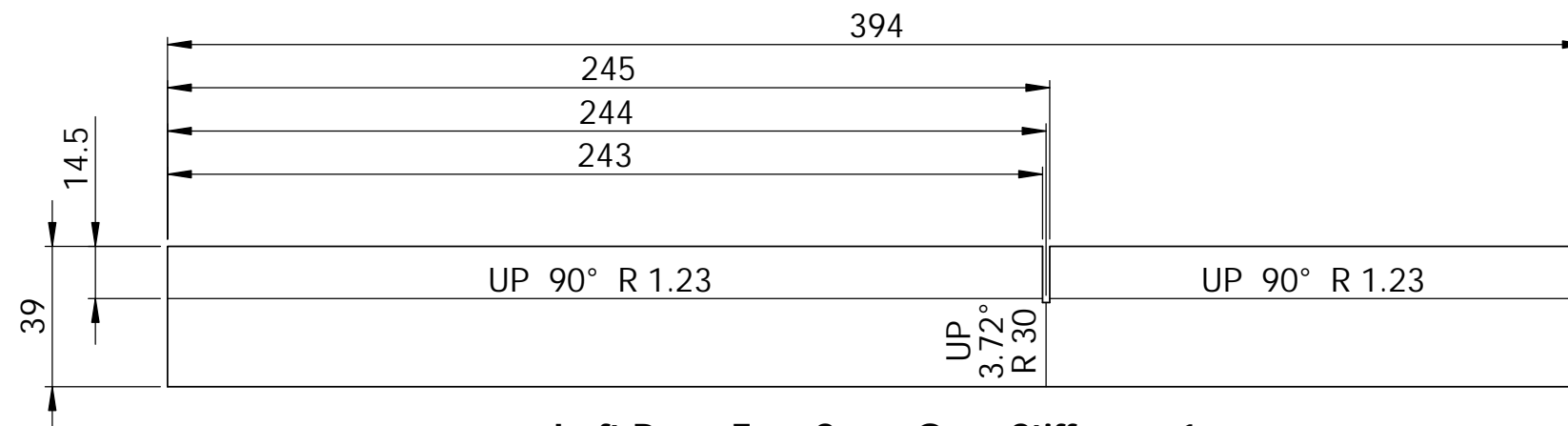
P/N: 6114-131

Right Front Top Spar Cap Stiffener 3 (Opposite Hand)

P/N: 6114-132

Material: 0.41x39x128 2024-T3 Clad Plate

Scale 1:2



Left Rear Top Spar Cap Stiffener 1

P/N: 6114-133

Right Rear Top Spar Cap Stiffener 1 (Opposite Hand)

P/N: 6114-134

Material: 0.41x39x394 2024-T3 Clad Plate

Scale 1:2

UNLESS OTHERWISE SPECIFIED: DIMENSIONS ARE IN MILLIMETERS SURFACE FINISH: TOLERANCES: LINEAR: $\pm 0.7\text{mm}$ ANGULAR: $\pm 0.7^\circ$				FINISH: Nil	DEBURR AND BREAK SHARP EDGES	DO NOT SCALE DRAWING	REVISION A
DRAWN	NAME J.V.	SIGNATURE	DATE 28/09/23			TITLE: Tailplane Box Spar Cap Stiffeners	Group 4
CHK'D						DWG NO. 6114	A3
APP'D						SCALE: 1:2	
MFG				MATERIAL: 2024-T3			
Q.A				WEIGHT: 9.17			
							SHEET 1 OF 3

8 7 6 5 4 3 2 1

8 7 6 5 4 3 2 1

F
39.7
14.8

706

UP 90° R 1.92

Left Rear Bottom Spar Cap Stiffener 1

P/N: 6114-135

Right Rear Bottom Spar Cap Stiffener 1 (Opposite Hand)

P/N: 6114-136

Material: 0.64x40x706 2024-T3 Clad Plate

Scale 1:2

D
42.2
16.1

682

UP 90° R 1.92

Left Front Bottom Spar Cap Stiffener 1

P/N: 6114-139

Right Front Bottom Spar Cap Stiffener 1 (Opposite Hand)

P/N: 6114-140

Material: 0.64x43x682 2024-T3 Clad Plate

Scale 1:2

B
38.4
14.2

324

UP 90° R 1.92

Left Rear Bottom Spar Cap Stiffener 2

P/N: 6114-137

Right Rear Bottom Spar Cap Stiffener 2 (Opposite Hand)

P/N: 6114-138

Material: 0.64x39x324 2024-T3 Clad Plate

Scale 1:2

UNLESS OTHERWISE SPECIFIED: DIMENSIONS ARE IN MILLIMETERS SURFACE FINISH: TOLERANCES: LINEAR: ±0.7mm ANGULAR: ±0.7°			FINISH: Nil	DEBURR AND BREAK SHARP EDGES	DO NOT SCALE DRAWING	REVISION
DRAWN	J.V.		28/09/23			A
CHK'D						
APP'D						
MFG						
Q.A				MATERIAL: 2024-T3	DWG NO. 6114	A3
				WEIGHT: 9.17	SCALE: 1:2	
						SHEET 2 OF 3

Group 4
Tailplane Box
Spar Cap Stiffeners

6114

8 7 6 5 4 3 2 1

8

7

6

5

4

3

2

1

F

F

E

E

D

D

C

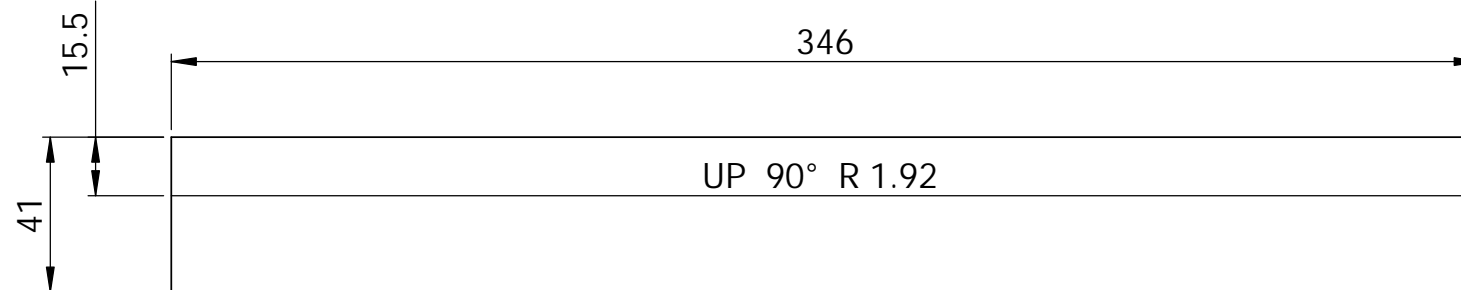
C

B

B

A

A



Left Front Bottom Spar Cap Stiffener 2

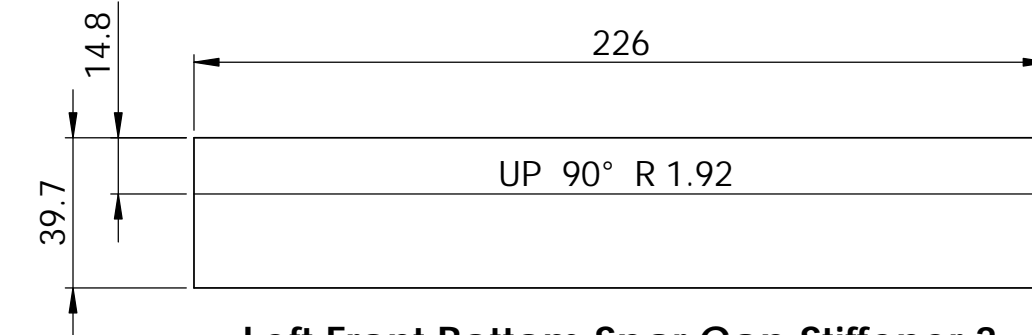
P/N: 6114-141

Right Front Bottom Spar Cap Stiffener 2 (Opposite Hand)

P/N: 6114-142

Material: 0.64x41x346 2024-T3 Clad Plate

Scale 1:2



Left Front Bottom Spar Cap Stiffener 3

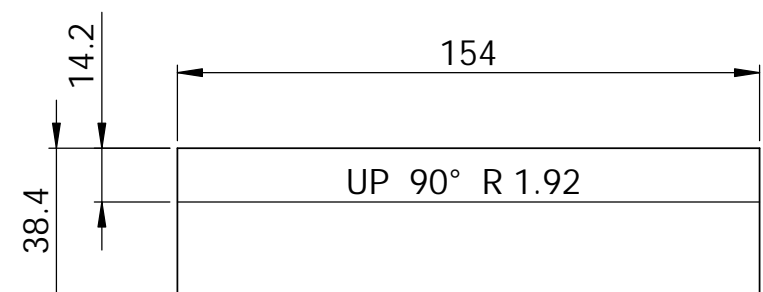
P/N: 6114-143

Right Front Bottom Spar Cap Stiffener 3 (Opposite Hand)

P/N: 6114-144

Material: 0.64x40x226 2024-T3 Clad Plate

Scale 1:2



Left Front Bottom Spar Cap Stiffener 4

P/N: 6114-145

Right Front Bottom Spar Cap Stiffener 4 (Opposite Hand)

P/N: 6114-146

Material: 0.64x39x154 2024-T3 Clad Plate

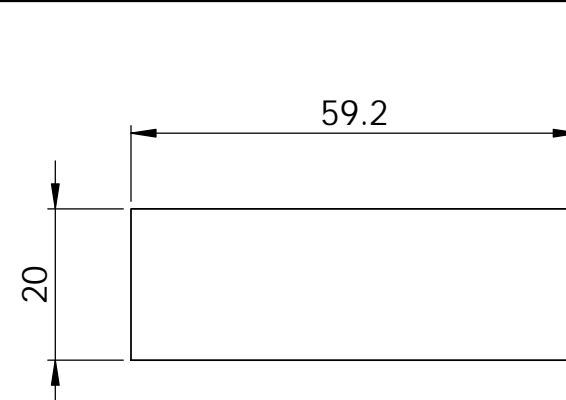
Scale 1:2

UNLESS OTHERWISE SPECIFIED: DIMENSIONS ARE IN MILLIMETERS SURFACE FINISH: TOLERANCES: LINEAR: $\pm 0.7\text{mm}$ ANGULAR: $\pm 0.7^\circ$		FINISH: Nil		DEBURR AND BREAK SHARP EDGES	DO NOT SCALE DRAWING	REVISION	A
DRAWN	J.V.	SIGNATURE	DATE				
CHK'D							
APP'D							
MFG							
Q.A				MATERIAL:	2024-T3	DWG NO.	
						6114	A3
				WEIGHT: 9.17		SCALE: 1:2	
							SHEET 3 OF 3

Tailplane Box
Spar Cap Stiffeners

6114

8 7 6 5 4 3 2 1



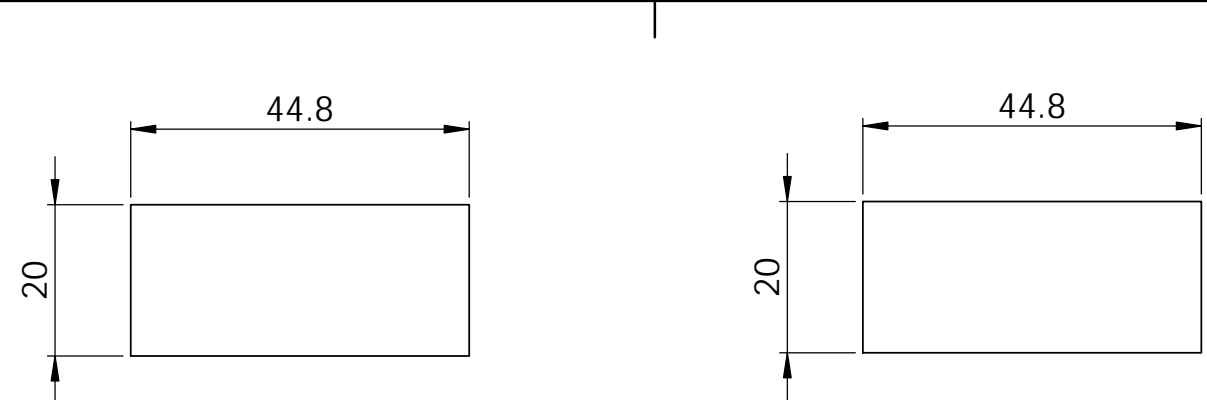
Left Inboard End Cap
Long Vertical Spacer

P/N: 6115-147

Right Inboard End Cap
Long Vertical Spacer
(Opposite Hand)

P/N: 6115-148

Material: 0.64x20x60 2024-T3 Clad Plate
Scale 1:1



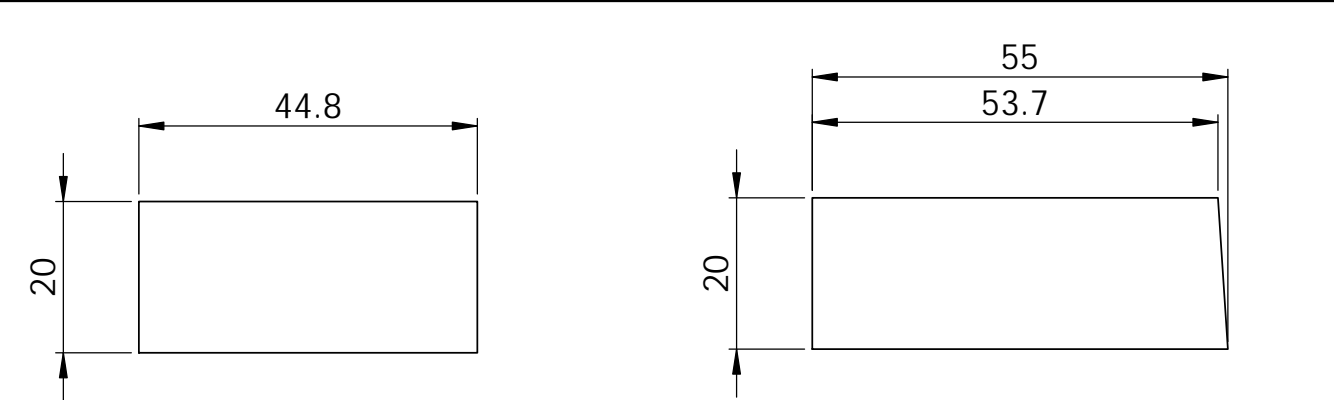
Left Inboard End Cap
Short Vertical Spacer

P/N: 6115-149

Right Inboard End Cap
Short Vertical Spacer
(Opposite Hand)

P/N: 6115-150

Material: 0.64x20x45 2024-T3 Clad Plate
Scale 1:1



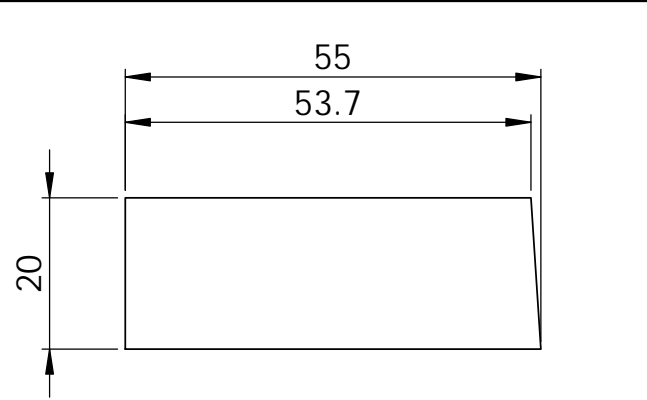
Left Rib BL250
Vertical Spacer

P/N: 6115-151

Right Rib BL250
Vertical Spacer
(Opposite Hand)

P/N: 6115-152

Material: 0.64x20x45 2024-T3 Clad Plate
Scale 1:1



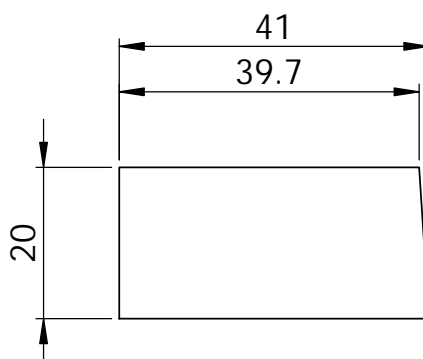
Left Rib BL350
Long Vertical Spacer

P/N: 6115-153

Right Rib BL350
Long Vertical Spacer
(Opposite Hand)

P/N: 6115-154

Material: 0.64x20x55 2024-T3 Clad Plate
Scale 1:1



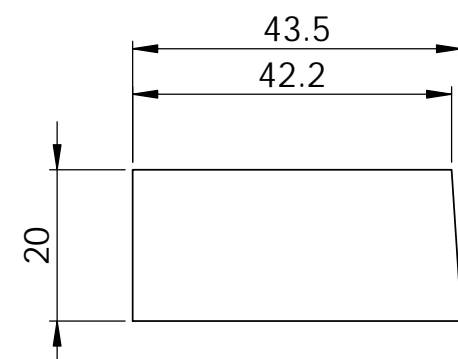
Left Rib BL350
Short Vertical Spacer

P/N: 6115-155

Right Rib BL350
Short Vertical Spacer
(Opposite Hand)

P/N: 6115-156

Material: 0.64x20x41 2024-T3 Clad Plate
Scale 1:1



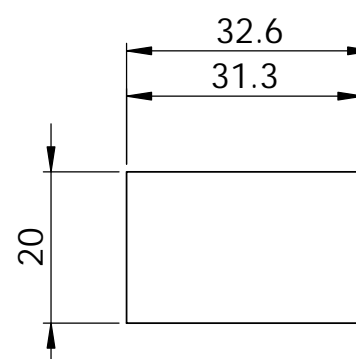
Left Rib BL542
Vertical Spacer

P/N: 6115-157

Right Rib BL542
Vertical Spacer
(Opposite Hand)

P/N: 6115-158

Material: 0.64x20x44 2024-T3 Clad Plate
Scale 1:1



Left Rib BL710
Vertical Spacer

P/N: 6115-159

Right Rib BL710
Vertical Spacer
(Opposite Hand)

P/N: 6115-160

Material: 0.64x20x33 2024-T3 Clad Plate
Scale 1:1

UNLESS OTHERWISE SPECIFIED: DIMENSIONS ARE IN MILLIMETERS SURFACE FINISH: TOLERANCES: LINEAR: $\pm 0.7\text{mm}$ ANGULAR: $\pm 0.7^\circ$		FINISH: Nil		DEBURR AND BREAK SHARP EDGES	DO NOT SCALE DRAWING	REVISION	A
Group 4							
DRAWN	J.V.	SIGNATURE	DATE				
CHK'D			29/09/23				
APP'D							
MFG							
Q.A				MATERIAL:	2024-T3	DWG NO.	
						6115	A3
				WEIGHT: 2.11		SCALE: 1:1	
							Sheet 1 of 2

Tailplane Box
Vertical Spacers

6115

8 7 6 5 4 3 2 1

8

7

6

5

4

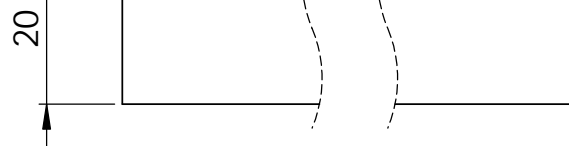
3

2

1

F

169



Left Rib Upper
Long Horizontal Spacer

P/N: 6115-161

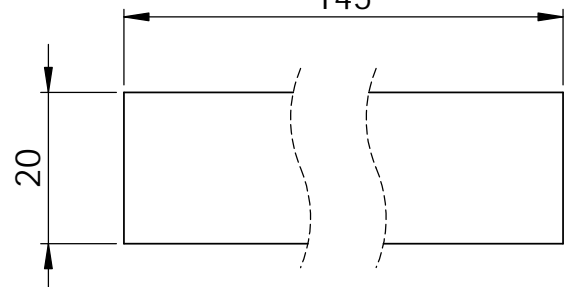
Right Rib Upper
Long Horizontal Spacer
(Opposite Hand)

P/N: 6115-162

Material: 0.41x20x169 2024-T3 Clad Plate
Scale 1:1

F

145



Left Rib Upper
Short Horizontal Spacer

P/N: 6115-163

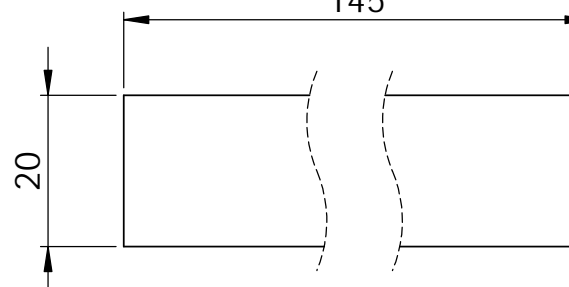
Right Rib Upper
Short Horizontal Spacer
(Opposite Hand)

P/N: 6115-164

Material: 0.41x20x145 2024-T3 Clad Plate
Scale 1:1

F

145



Left Rib Lower
Short Horizontal Spacer

P/N: 6115-167

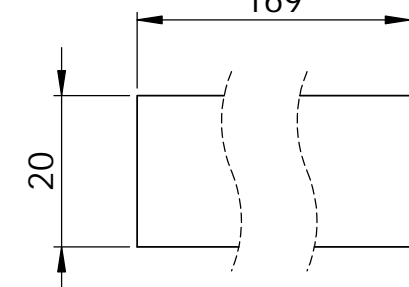
Right Rib Lower
Short Horizontal Spacer
(Opposite Hand)

P/N: 6115-168

Material: 0.64x20x145 2024-T3 Clad Plate
Scale 1:1

F

169



Left Rib Lower
Long Horizontal Spacer

P/N: 6115-165

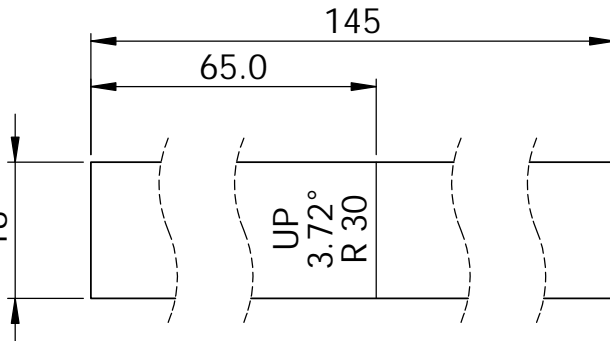
Right Rib Lower
Long Horizontal Spacer
(Opposite Hand)

P/N: 6115-166

Material: 0.64x20x169 2024-T3 Clad Plate
Scale 1:1

E

D



Left Upper
Spar Flange Strap

P/N: 6115-169

Right Upper
Spar Flange Strap
(Opposite Hand)

P/N: 6115-170

Material: 0.64x18x145 2024-T3 Clad Plate
Scale 1:1

C

Left Upper
Stiffener Strap

P/N: 6115-171

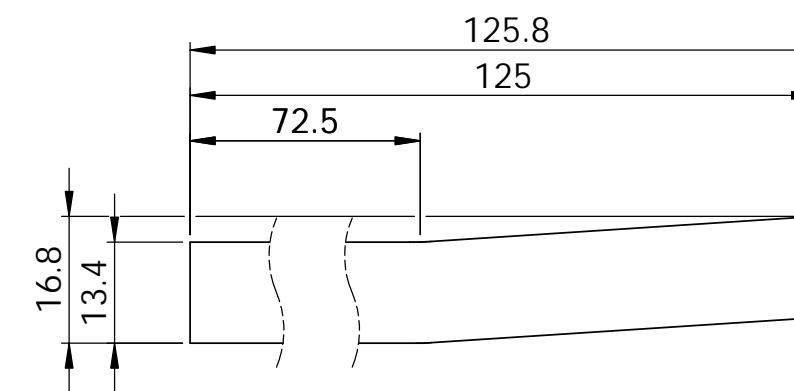
Right Upper
Stiffener Strap
(Opposite Hand)

P/N: 6115-172

Material: 0.64x17x126 2024-T3 Clad Plate
Scale 1:1

B

A



UNLESS OTHERWISE SPECIFIED:
DIMENSIONS ARE IN MILLIMETERS
SURFACE FINISH:
TOLERANCES:
LINEAR: ±0.7mm
ANGULAR: ±0.7°

FINISH:
Nil

DEBURR AND
BREAK SHARP
EDGES

DO NOT SCALE DRAWING

REVISION A

Group 4

DRAWN	NAME	SIGNATURE	DATE			TITLE:	DWG NO.	
CHK'D							6115	
APP'D							A3	
MFG								
Q.A				MATERIAL:	2024-T3			
				WEIGHT:	2.11		SCALE:1:1	SHEET 2 OF 2

Tailplane Box
Horizontal Spacers

6115

8

7

6

5

4

3

2

1

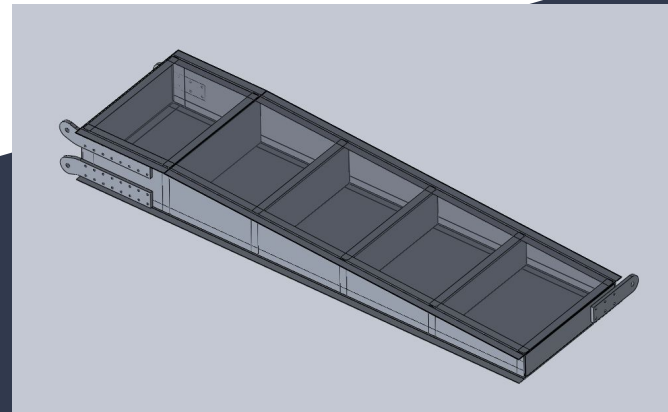
7 Preliminary Design Review

[SEE PDR OVERLEAF]

Group 4 PDR

AERO3465 - Tailplane Box DBT

James, Chris, Tom, Jorge, Kelly, Kay, Cham



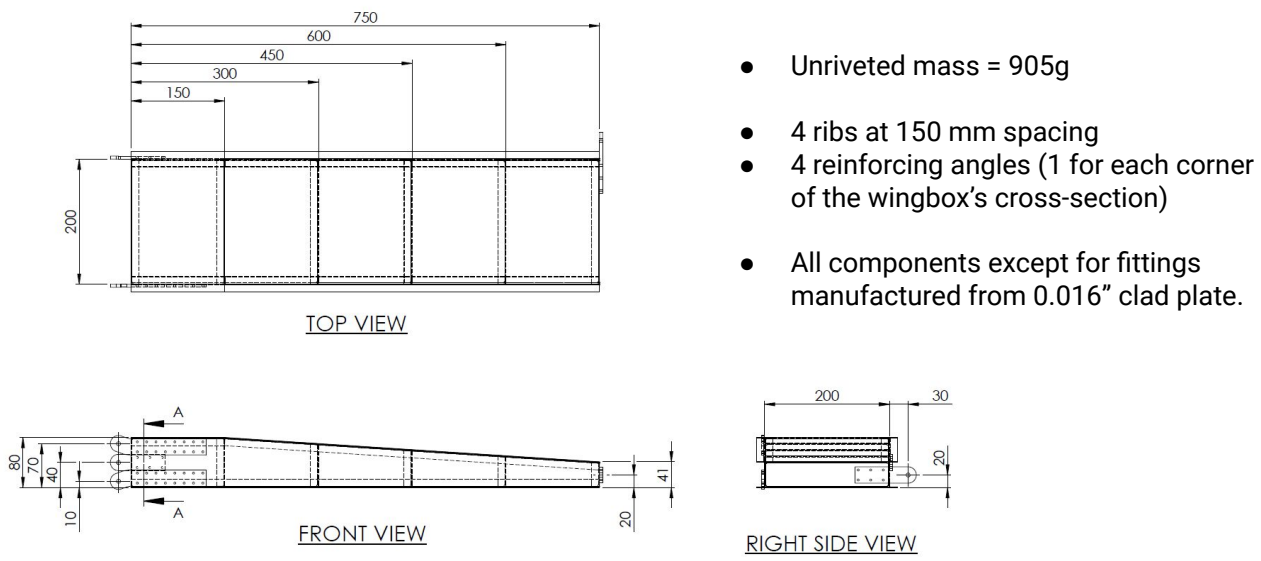
Interface Loads - Limit

	Test Case 1 [N]	Test Case 2 [N]	Test Case 3 [N]	Test Case 4 [N]
Ax	0	0	-33	0
Ay	11293	-5133	193	41
Az	-66	30	5	0
Bx	0	0	-33	0
By	-11293	5133	193	-26
Bz	-66	30	5	0
Cx	0	0	-33	0
Cy	0	0	-385	-115
Cz	1012	-460	-10	0
Px	0	0	100	0
Py	-880	400	0	100
Pz	0	0	0	0

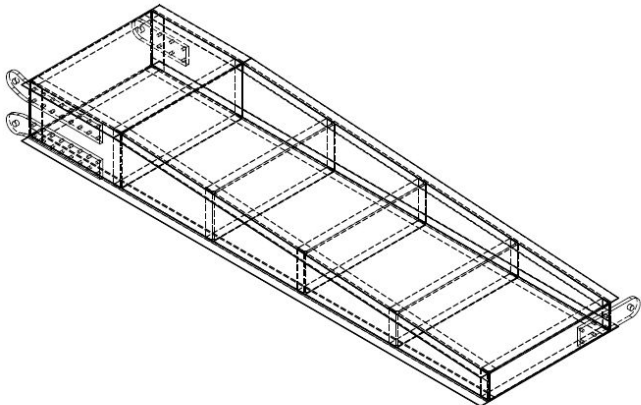
Interface Loads - Ultimate

	Test Case 1 [N]	Test Case 2 [N]	Test Case 3 [N]	Test Case 4 [N]
Ax	0	0	-50	0
Ay	16940	-7700	289	61
Az	-99	45	8	0
Bx	0	0	-50	0
By	-16940	7700	289	-39
Bz	-99	45	8	0
Cx	0	0	-50	0
Cy	0	0	-578	-173
Cz	1518	-690	-15	0
Px	0	0	150	0
Py	-1320	600	0	150
Pz	0	0	0	0

Preliminary Layout Drawing



Preliminary Layout Drawing



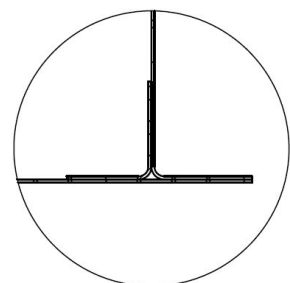
ISOMETRIC VIEW

- Lugs A and B have a 2x8 rivet pattern, 16x15 mm typical separation.
- Lugs C and P have a 2x3 rivet pattern, 16x20 mm typical separation.
- Typical lug width is 26mm, for $e/D = 2$.
- Critical failure mode for lugs found to be 'rivet shear' at load case 1.
- Rivet shear MS > 0.01 for all lugs using CherryMax rivets for all load cases.
- MS for other failure modes > MS for rivet shear for all lugs and load cases.

Layout Cross Section at BL120

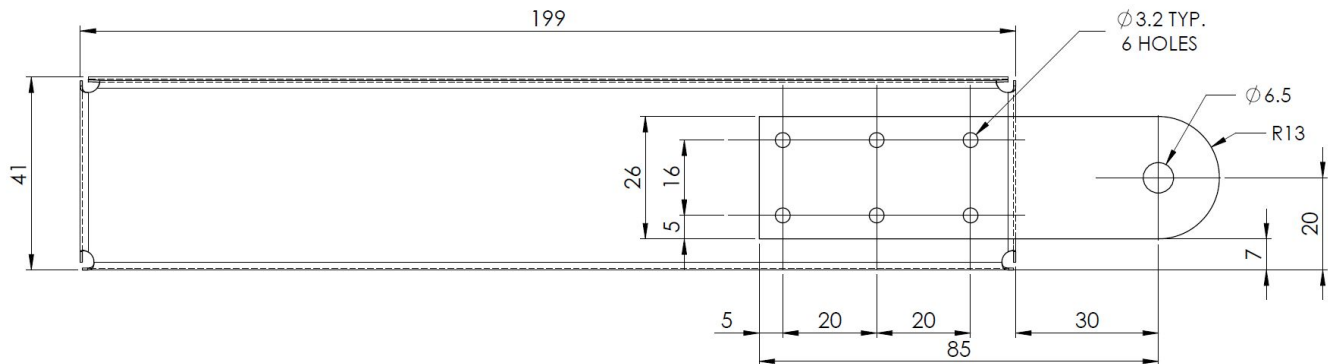


DETAIL 1

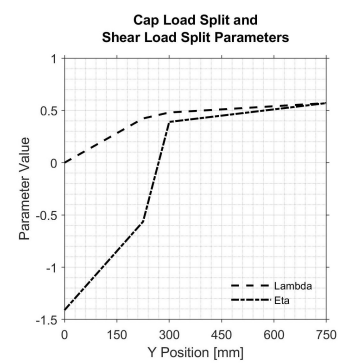
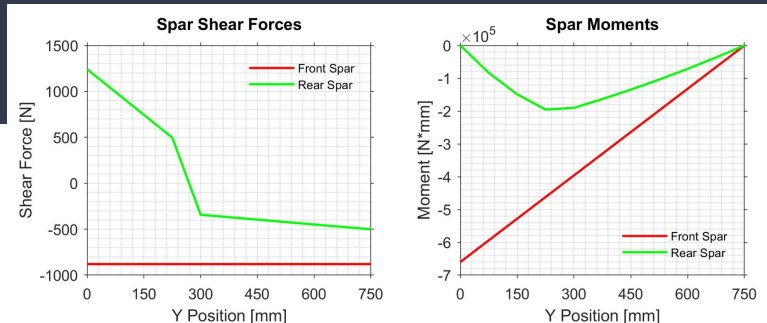
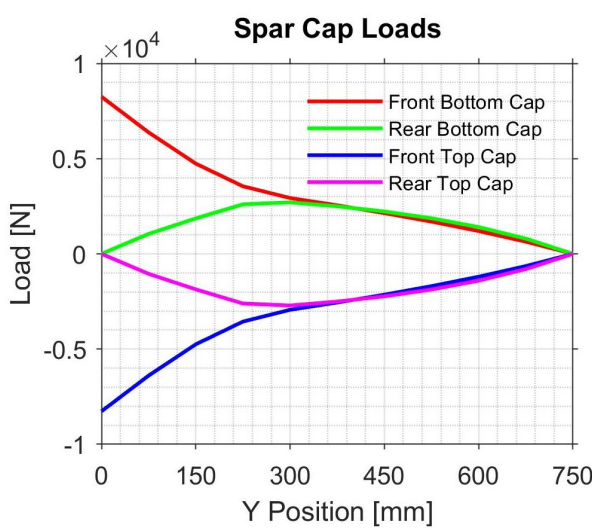


DETAIL 1

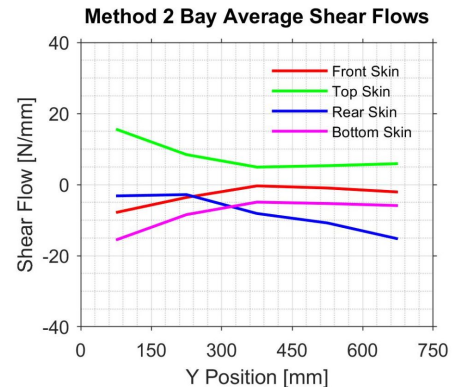
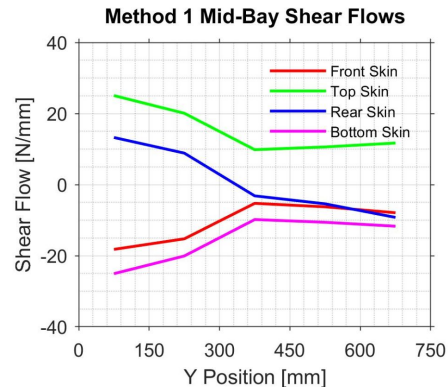
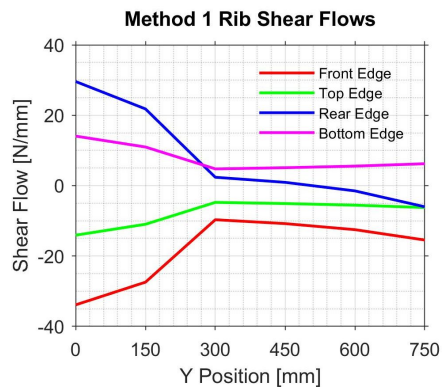
Layout Drawing of Tip Rib (Outboard End Cap)



Spar Cap Loads



Shear Flows



8 Critical Design Review

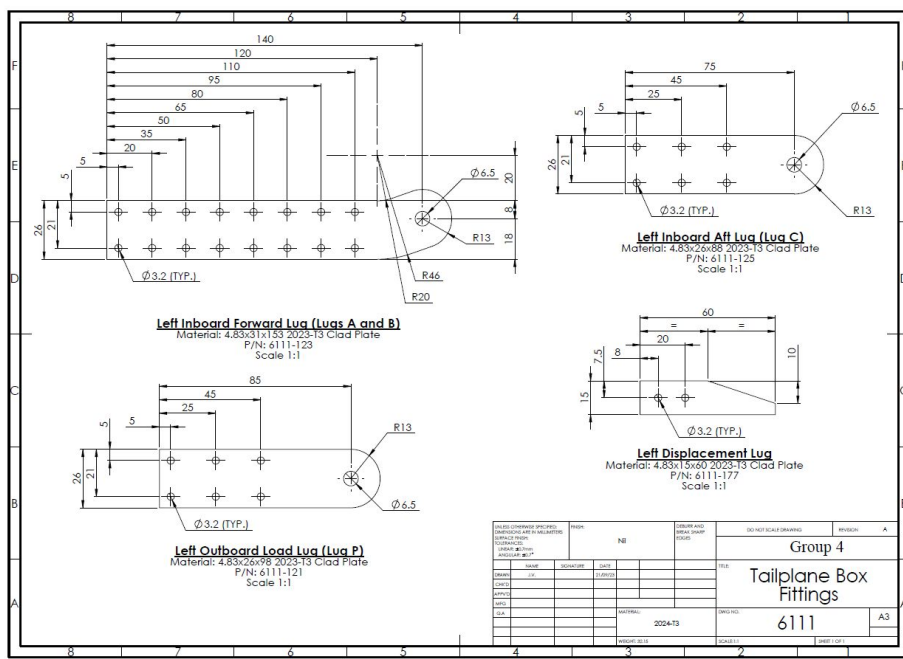
[SEE CDR OVERLEAF]

Critical design review (CDR)

AERO3465 / Aerospace design 2

Team 4 - James, Chris, Tom, Jorge, Kelly, Kay, Cham

Final drawings of fittings #1 - Lugs

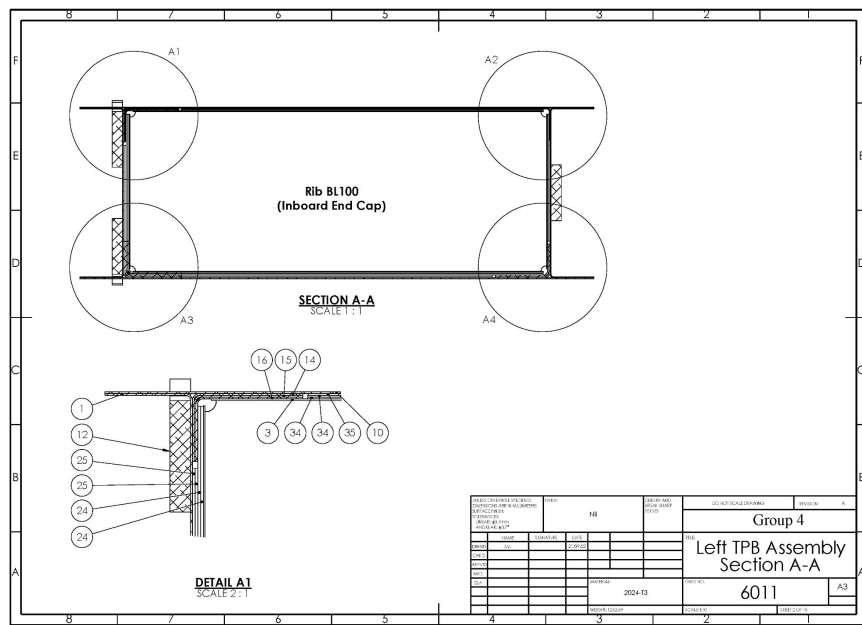


Final drawings of fittings #2

Section A-A

At BL150

Added stiffeners

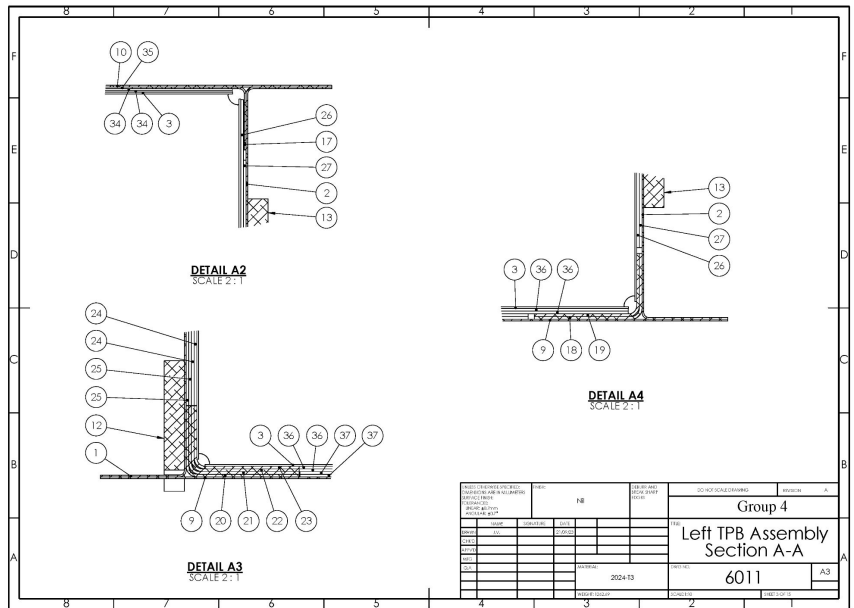


IC
MAGE

Preliminary drawings of other components #1

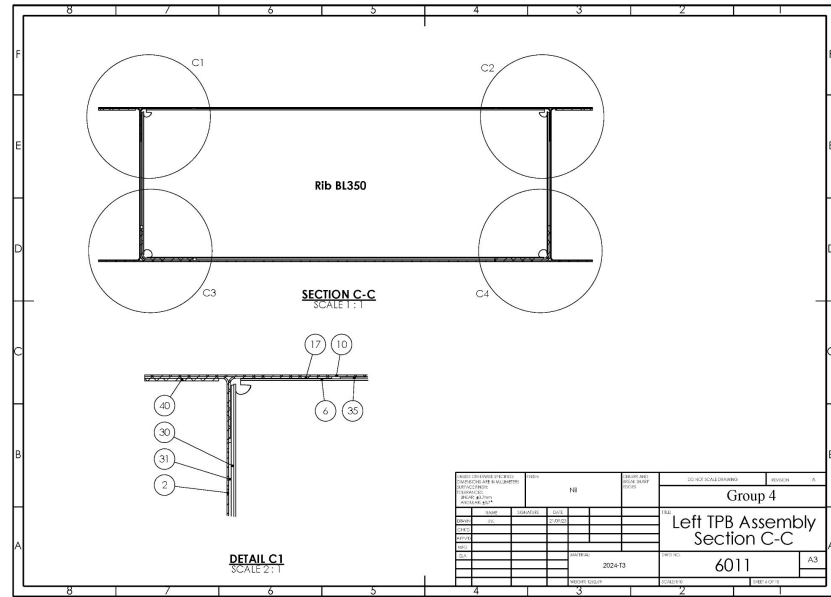
Details

Showing stiffener angles



Preliminary drawings of other components #2

Section C-C at BL350

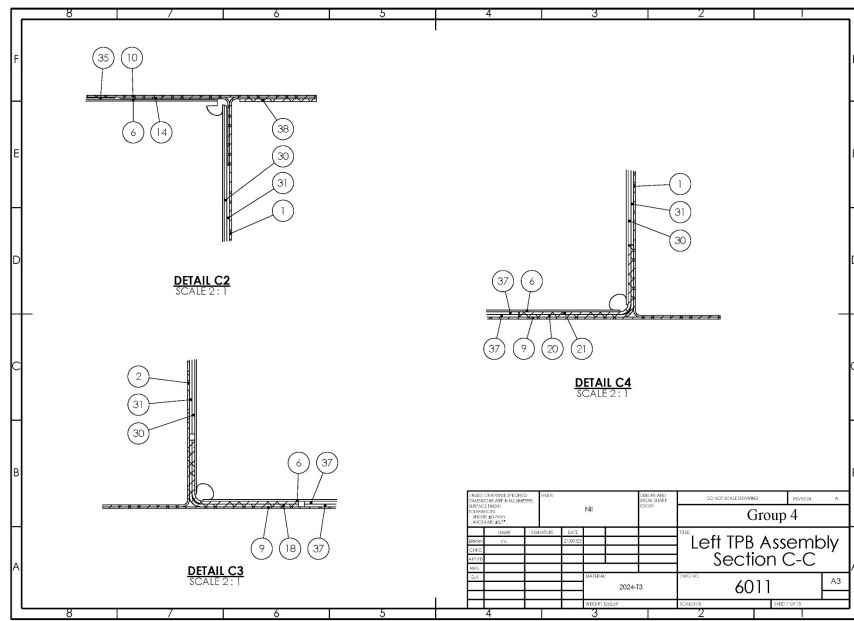


Preliminary drawings of other components #3

Details

At BL350

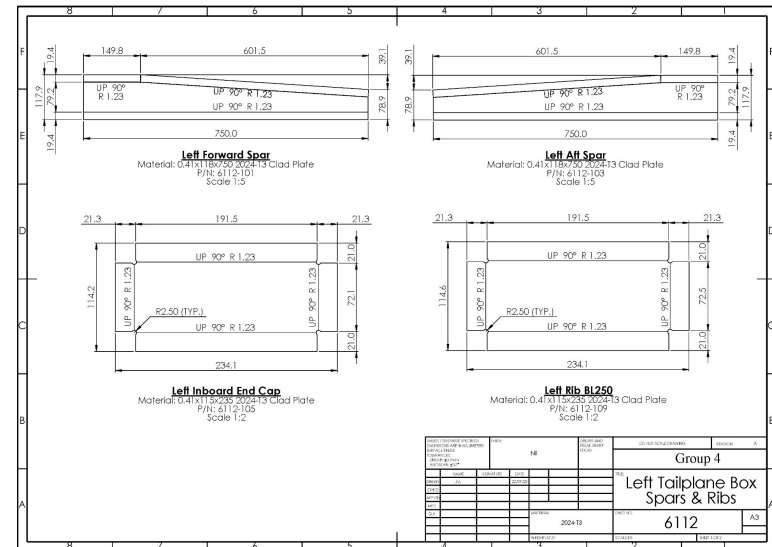
Rib/spar connection.



Preliminary drawings of other components #4

Spars end cap and BL250 rib

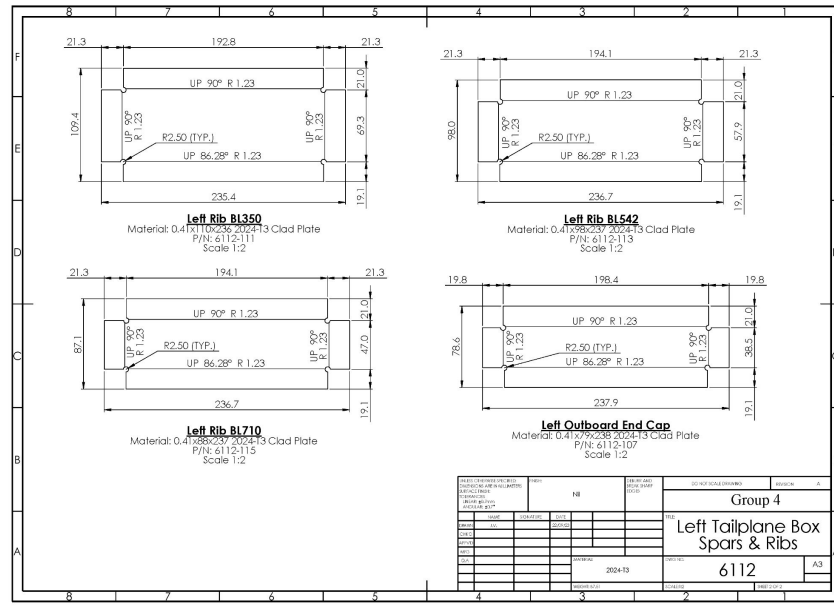
Pattern and bend locations



Preliminary drawings of other components #5

3 Ribs and end cap

Pattern and bend locations



Lug A - Example calculation

Load for each rivet = 706N (shear and moment)

CherryMax ult = 1246N

MoS = 0.023 for (706N per rivet)

Lug: Tension

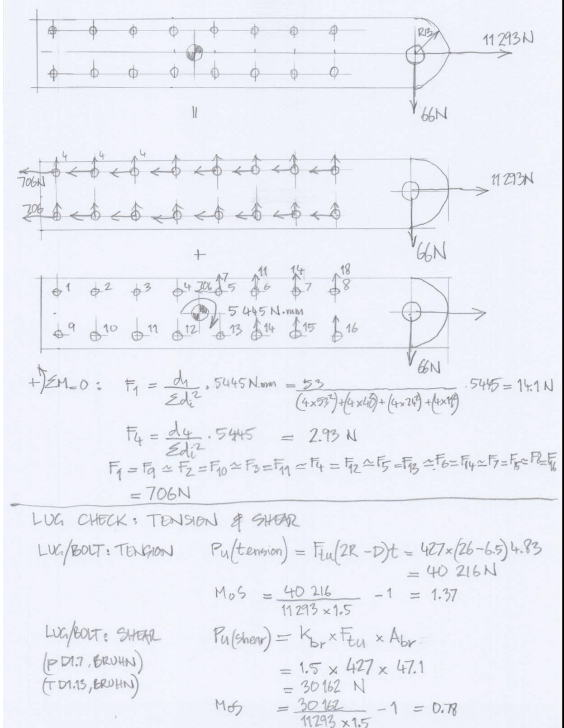
$$P_{ult} = F_{tu} * (2R - D)t = 427(26-6.5)4.83 = 40,216N$$

MoS = 1.37 for (11,293N)

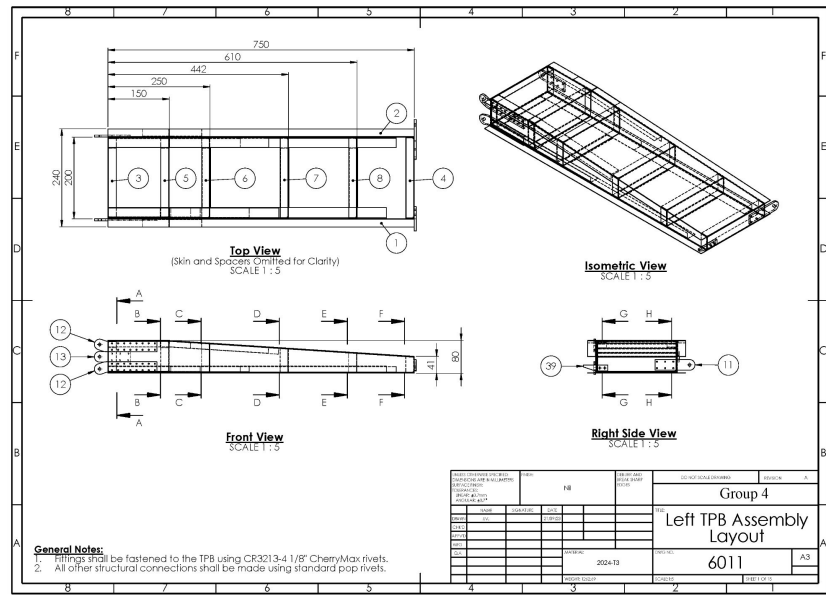
Lug: Shear

$$P_u(\text{shear}) = k_{br} \times F_{tu} \times A_{br} = 1.5 * 427 * 9.75 * 4.8 = 30,162N$$

MoS = 0.78 for (11,293N)



Layout drawing of TPB #1

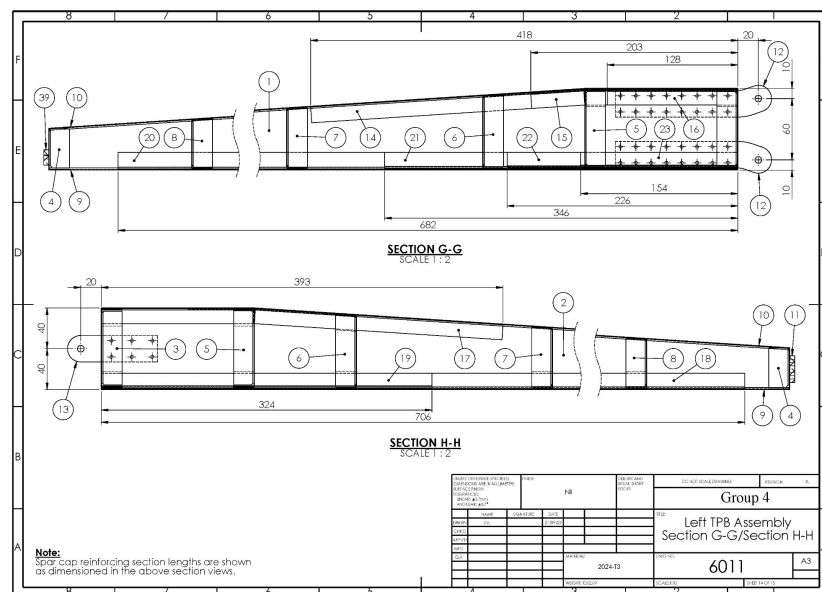


Layout drawing of TPB #2

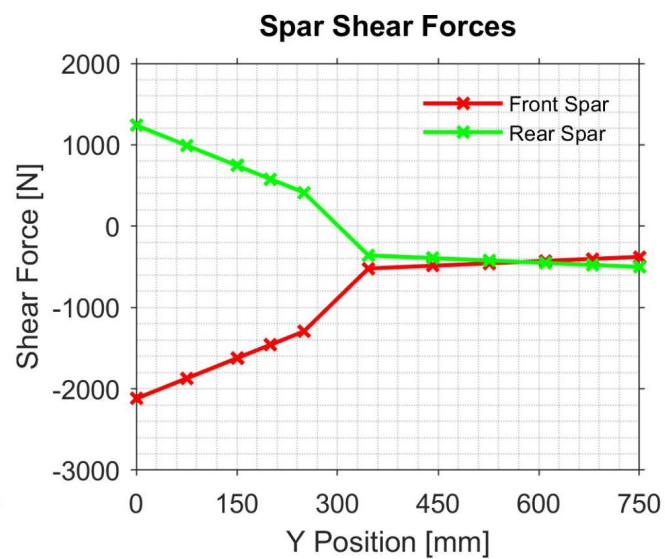
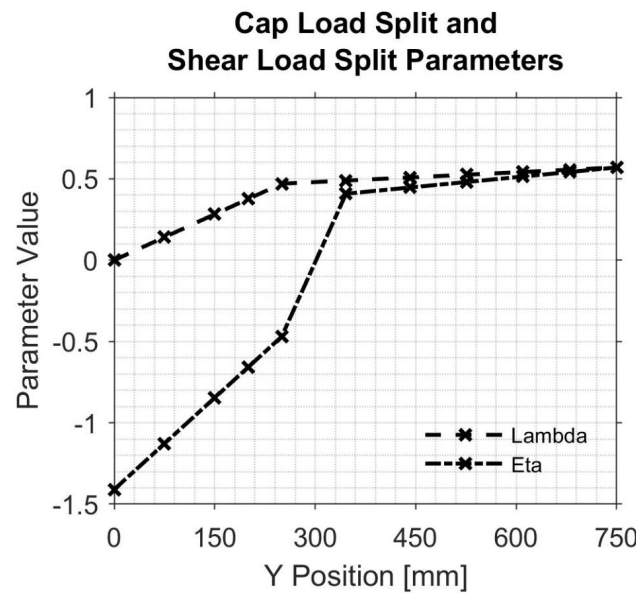
Sectional Elevation

Front and rear spars

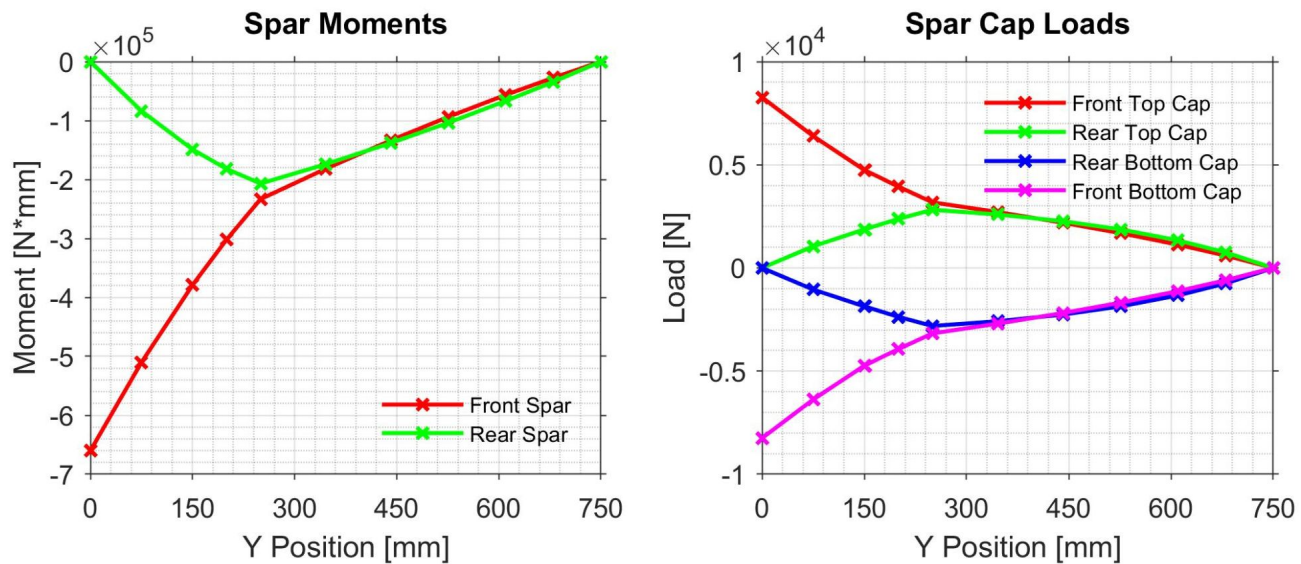
Stiffener angles - front/rear



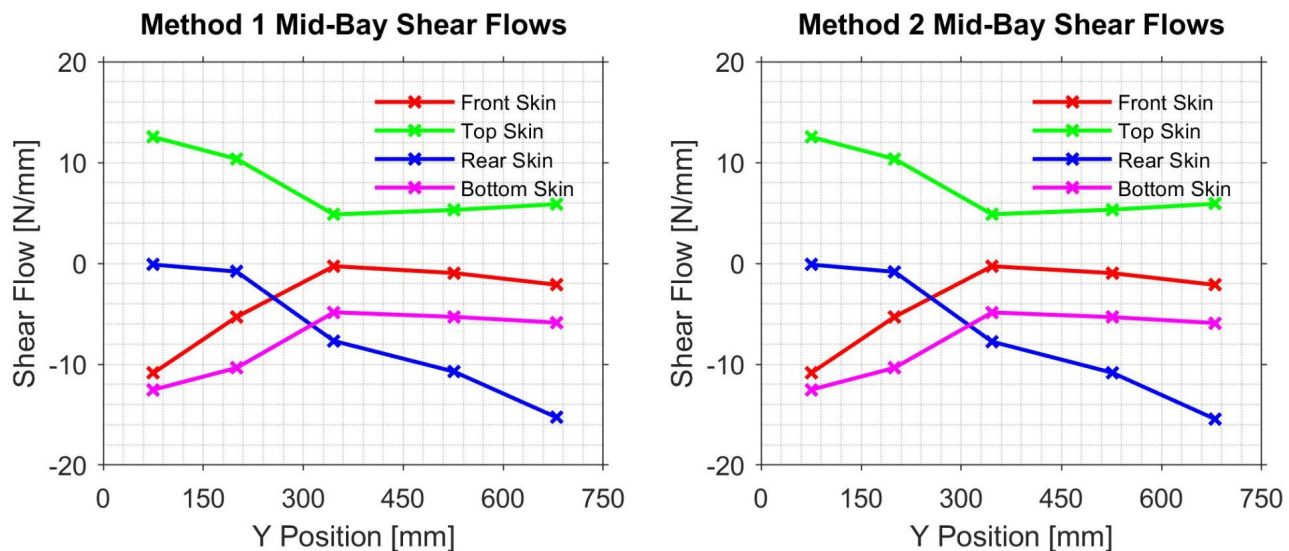
Calculation of Limit Cap Loads #1



Calculation of Limit Cap Loads #2



Limit Skin & Spar-web Shear Flows



Limit Skin Shear Buckling Ratios

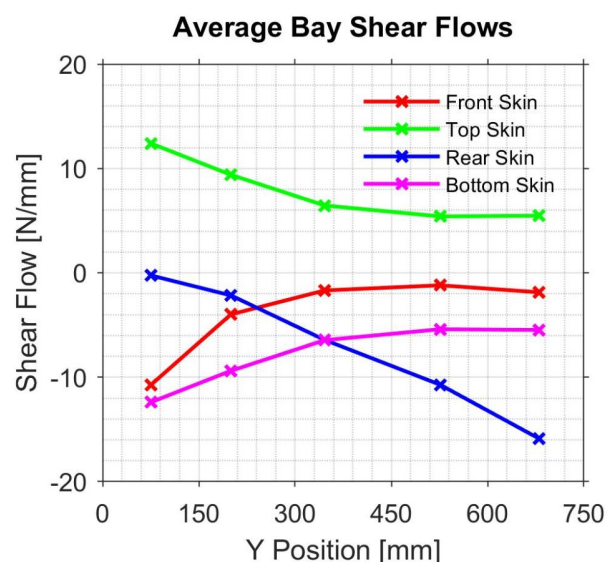
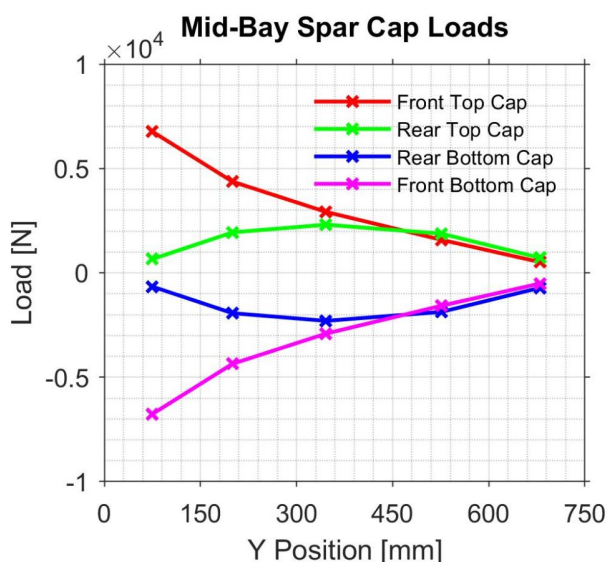
===== Load Case 1 Shear Buckling Ratios =====

	Bay 5	Bay 4	Bay 3	Bay 2	Bay 1
Front	0.16753	0.11204	0.047912	0.86458	2.1352
Top	3.7938	4.2841	4.6819	3.4061	5.455
Rear	1.2131	1.2594	1.3098	0.13607	0.023748
Bottom	3.7938	4.2841	4.6819	3.4061	5.455

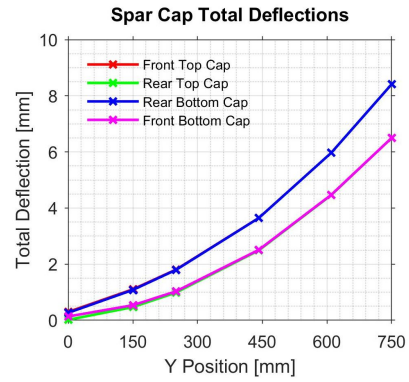
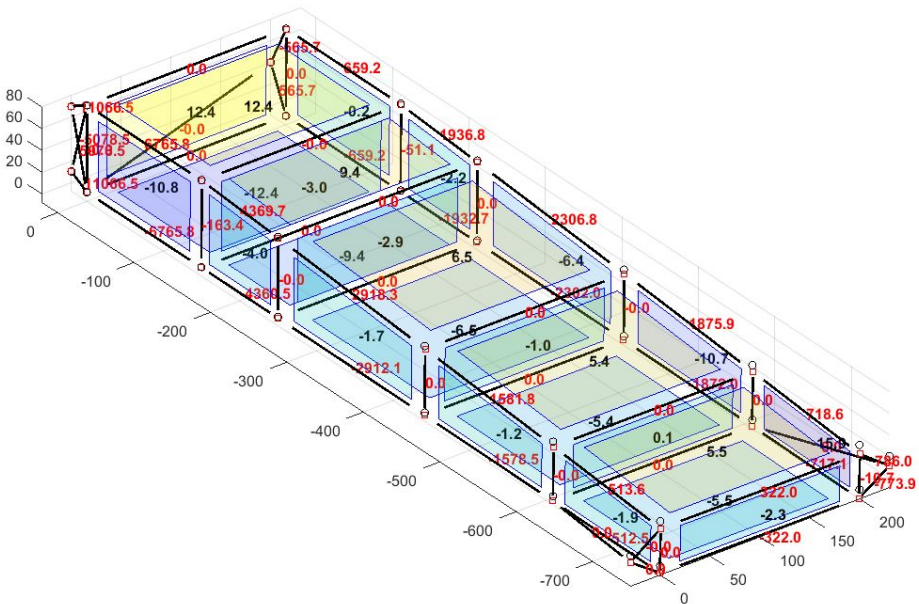
===== Load Case 2 Shear Buckling Ratios =====

	Bay 5	Bay 4	Bay 3	Bay 2	Bay 1
Front	0.076155	0.050931	0.021771	0.393	0.97053
Top	1.7244	1.9473	2.1281	1.5482	2.4795
Rear	0.55139	0.57244	0.59534	0.061855	0.010795
Bottom	1.7244	1.9473	2.1281	1.5482	2.4795

FEM Analysis of Internal Limit Loads #1



FEM Analysis of Internal Limit Loads #2



Deflection lug ds = 6.25mm
(limit load)

Spar Caps Crippling with No Diagonal Tension

===== Crippling Failure =====

===== Top Front Spar Cap =====

	Section 4	Section 3	Section 2	Section 1
Section MS Minimum	0.023318	0.13153	0.050155	0.21195
Applied Load/Stress	1196.9	2024.7	2937.3	3200
Failure Load/Stress	1837.2	3436.5	4627	5817.4
Failure Point [mm]	360	168	72	48

===== Bottom Front Spar Cap =====

	Section 5	Section 4	Section 3	Section 2	Section 1
Section MS Minimum	0.1937	0.056294	0.091732	0.111191	0.17631
Applied Load/Stress	1026.1	2990.1	4445	5895.6	7025.2
Failure Load/Stress	1837.2	4737.6	7279.1	9833.1	12396
Failure Point [mm]	624	288	168	96	48

===== Top Rear Spar Cap =====

	Section 2	Section 1
Section MS Minimum	0.028784	0.80558
Applied Load/Stress	1190.6	1268.9
Failure Load/Stress	1837.2	3436.5
Failure Point [mm]	336	264

===== Bottom Rear Spar Cap =====

	Section 3	Section 2	Section 1
Section MS Minimum	0.18257	0.13384	0.92533
Applied Load/Stress	1035.7	2785.6	2520.5
Failure Load/Stress	1837.2	4737.6	7279.1
Failure Point [mm]	648	264	216

- Minimum MS shown for each reinforcing section.
- Crippling failure load computed using Needham's method.

Spar Caps Crippling with Skin Diagonal Tension

Crippling Failure w/ Skin DT					Bottom Front Spar Cap					
	Section 4	Section 3	Section 2	Section 1		Section 5	Section 4	Section 3	Section 2	Section 1
Section MS Minimum	0.44406	0.16677	NaN	0.25699	Section MS Minimum	3.5434	0.06129	0.044239	0.32785	0.1217
Applied Load/Stress	36.862	43.889	NaN	39.55	Applied Load/Stress	11.716	59.186	61.666	48.619	57.271
Failure Load/Stress	79.847	76.812	NaN	74.571	Failure Load/Stress	79.847	94.22	96.59	96.837	96.362
Failure Point [mm]	432	144	NaN	24	Failure Point [mm]	744	432	240	144	24
Top Rear Spar Cap					Bottom Rear Spar Cap					
	Section 2	Section 1				Section 3	Section 2	Section 1		
Section MS Minimum	0.4116	0.45712			Section MS Minimum	3.3353	0.04635	0.16263		
Applied Load/Stress	37.71	35.143			Applied Load/Stress	12.279	60.031	55.386		
Failure Load/Stress	79.847	76.812			Failure Load/Stress	79.847	94.22	96.59		
Failure Point [mm]	432	240			Failure Point [mm]	744	432	240		

- Minimum MS shown for each reinforcing section.
- Crippling failure stress computed using Needham's method.
- Applied stress correct for diagonal tension at edge of spar cap.
- NaN values in table indicate no ribs present in reinforcing section.

Margin of Safety Summary

Top Front Spar Cap

	Section 4	Section 3	Section 2	Section 1
Critical Failure Mode	Crippling, no DT	Crippling, no DT	Crippling, no DT	Crippling, no DT
Minimum MS	0.023318	0.13153	0.050155	0.21195
Failure Point [mm]	360	168	72	48
Load Case	2	2	2	2

Top Rear Spar Cap

	Section 2	Section 1
Critical Failure Mode	Crippling, no DT	Rivet shear, skin
Minimum MS	0.028784	0.33025
Failure Point [mm]	336	216
Load Case	2	1 (no DT shear)

Bottom Front Spar Cap

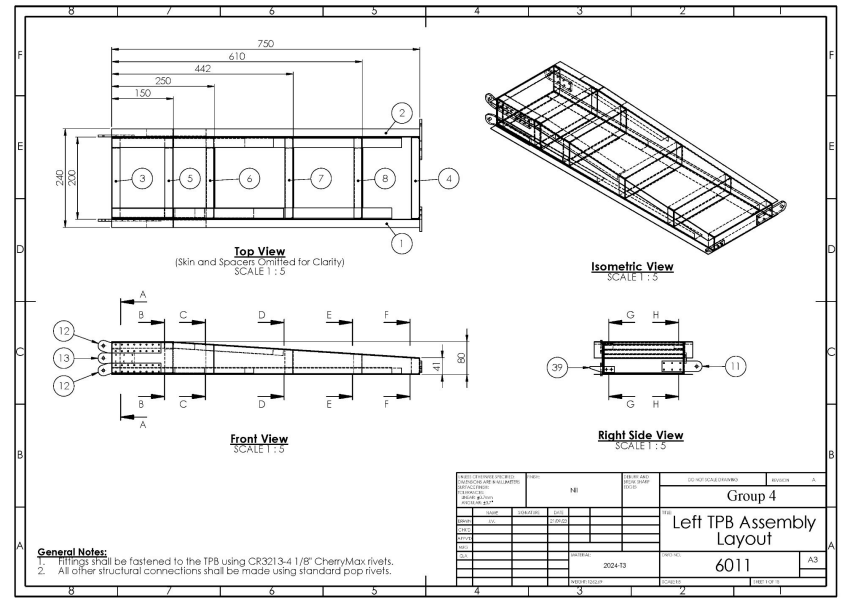
	Section 5	Section 4	Section 3	Section 2	Section 1
Critical Failure Mode	Crippling, no DT	Crippling, no DT	Crippling, bottom skin DT	Crippling, no DT	Crippling, skin DT
Minimum MS	0.1937	0.056294	0.044239	0.11191	0.1217
Failure Point [mm]	624	288	240	96	24
Load Case	1	1	1	1	1

Lugs

	Lug A	Lug B	Lug C	Lug P
Critical Failure Mode	Rivet shear, load case 1			
Minimum MS	0.019879	0.019879	0.019144	0.015171

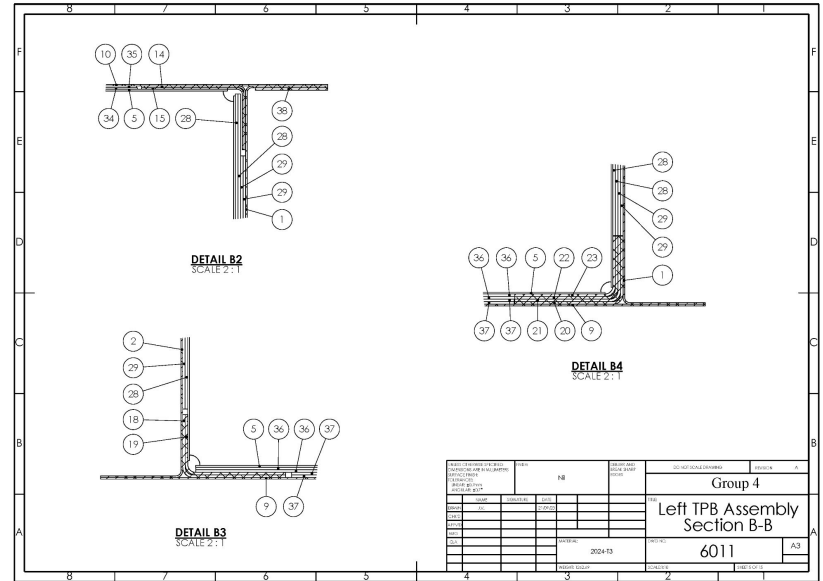
Description & Pictures of Main design features #1

Rib spacing set to reduce BR

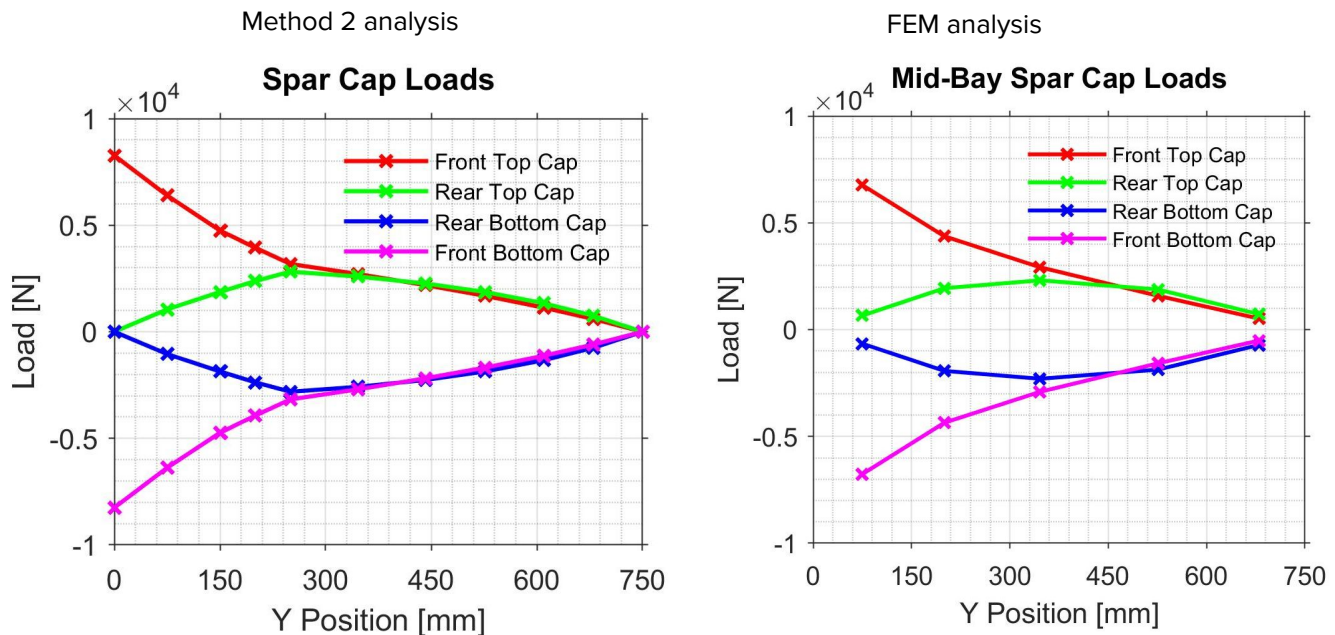


Description & Pictures of Main design features #2

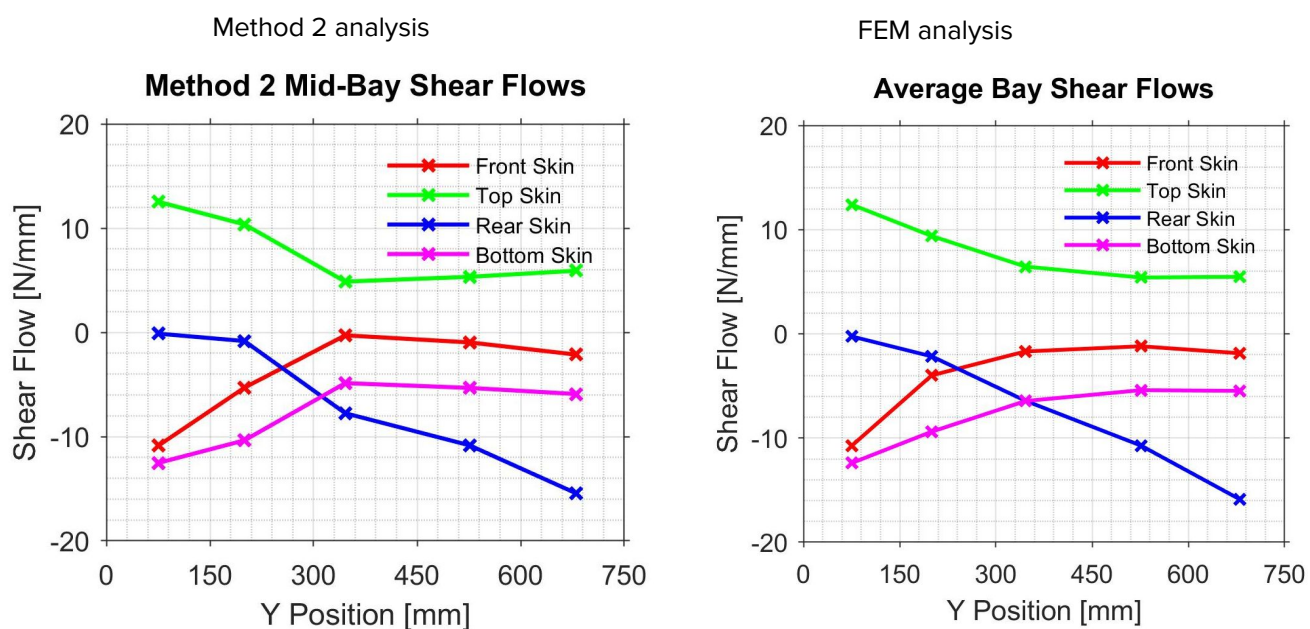
Added stiffener angles to resist buckling forces for load case 1 and 2.



FEM Comparison With Other Calculation - Cap Loads

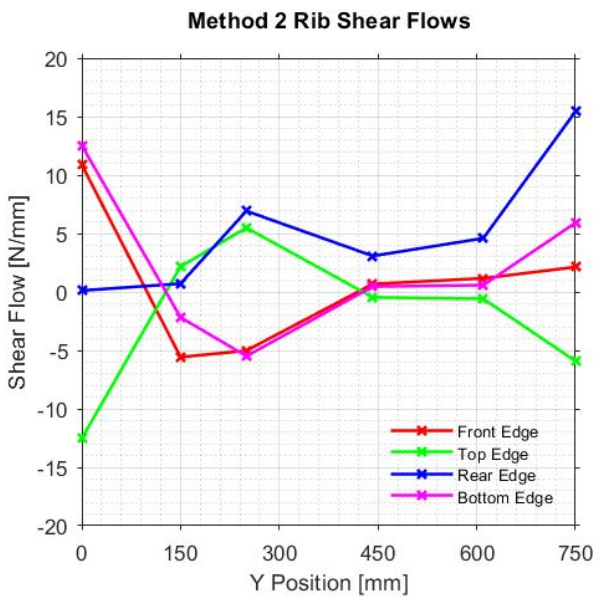


FEM Comparison With Other Calculation - Shear Flows

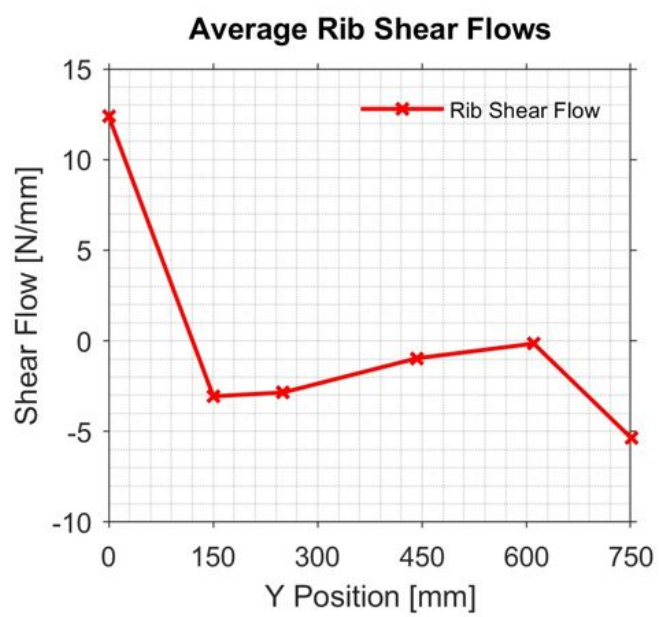


FEM Comparison With Other Calculation - Rib Shear Flows

Method 2 analysis



FEM analysis



Questions

A Detailed Geometry Calculations

A.1 Spar Cap Component Geometry Calculations

A.1.1 Spar Cap Reinforcement 1

A diagram of the cross sectional area of the spar cap reinforcement is given in figure 14(b). For a bend radius of $3t$, the bend areas for 0.64 mm clad sheet was computed as,

$$A_{r(0.64)} = \frac{\pi}{4}(16t_{st1}^2 - 9t_{st1}^2) = \frac{7}{4}\pi \times (0.64)^2 = 2.252 \text{ mm}^2 \quad (128)$$

The horizontal and vertical areas of the spar cap reinforcement were computed as,

$$A_{w_{st1}} = t_{st1}(w_{st1} - 4t_{st1}) = 0.64 \times (25 - 4 \times 0.64) = 14.36 \text{ mm}^2 \quad (129)$$

$$A_{h_{st1}} = t_{st1}(h_{st1} - 4t_{st1}) = 0.64 \times (15 - 4 \times 0.64) = 7.962 \text{ mm}^2 \quad (130)$$

The total spar cap reinforcement area was thus computed as,

$$\begin{aligned} A_{st1} &= A_{w_{st1}} + A_{h_{st1}} + A_{r(0.64)} \\ &= 14.36 + 7.962 + 2.252 = 24.57 \text{ mm}^2 \end{aligned} \quad (131)$$

The mid-line area of the spar cap reinforcement was computed as,

$$\begin{aligned} A_{st1m} &= (w_{st1} + h_{st1} - t_{st1})t_{st1} \\ &= (25 + 15 - 0.64) \times 0.64 = 25.19 \text{ mm}^2 \end{aligned} \quad (132)$$

The average side length divided by thickness of the spar cap reinforcement for crippling calculations was computed as,

$$c_{st1} = \frac{w_{st1} + h_{st1} - t}{2t} = \frac{25 + 15 - 0.64}{2 \times 0.64} = 30.75 \quad (133)$$

Taking the x and y ordinate directions to be those shown in figure 14(b), the centroid was computed relative to the edges of the angle as shown in figure 14(b). For a bend radius of $3t$, the bend centroid for 0.64 mm clad sheet was computed as,

$$\begin{aligned} \bar{x}_{r(0.64)} &= \bar{y}_{r(0.64)} = 4t_{st1} - \frac{8}{3\pi} \sin\left(\frac{\pi}{4}\right) \frac{64t_{st1}^3 - 27t_{st1}^3}{16t_{st1}^2 - 9t_{st1}^2} \\ &= 4 \times 0.64 - \frac{8 \times 37 \times (0.64)^3}{\sqrt{18\pi} \times 7 \times (0.64)^2} \\ &= 0.5296 \text{ mm} \end{aligned} \quad (134)$$

The centroid of the horizontal edge of the spar cap reinforcement was computed as,

$$\bar{x}_{w_{st1}} = \frac{w_{st1} - 4t}{2} + 4t_{st1} = \frac{25 - 4 \times 0.64}{2} + 4 \times 0.64 = 13.78 \text{ mm} \quad (135)$$

$$\bar{y}_{w_{st1}} = \frac{t}{2} = \frac{0.64}{2} = 0.3200 \text{ mm} \quad (136)$$

The centroid of the vertical edge of the spar cap reinforcement was computed as,

$$\bar{x}_{h_{st1}} = \bar{y}_{w_{st1}} = 0.3200 \text{ mm} \quad (137)$$

$$\bar{y}_{h_{st1}} = \frac{h_{st1} - 4t}{2} + 4t_{st1} = \frac{15 - 4 \times 0.64}{2} + 4 \times 0.64 = 8.780 \text{ mm} \quad (138)$$

The total spar cap reinforcement centroid was thus computed as,

$$\begin{aligned} \bar{x}_{st1} &= \frac{\sum \bar{x}_{st1(i)} A_{st1(i)}}{\sum A_{st1(i)}} \\ &= \frac{\bar{x}_{w_{st1}} A_{w_{st1}} + \bar{x}_{h_{st1}} A_{h_{st1}} + \bar{x}_{r(0.64)} A_{r(0.64)}}{A_{st1}} \\ &= \frac{13.78 \times 14.36 + 0.3200 \times 7.962 + 0.5296 \times 2.252}{24.57} \\ &= 8.206 \text{ mm} \end{aligned} \quad (139)$$

$$\begin{aligned} \bar{y}_{st1} &= \frac{\sum \bar{y}_{st1(i)} A_{st1(i)}}{\sum A_{st1(i)}} \\ &= \frac{\bar{y}_{w_{st1}} A_{w_{st1}} + \bar{y}_{h_{st1}} A_{h_{st1}} + \bar{y}_{r(0.64)} A_{r(0.64)}}{A_{st1}} \\ &= \frac{0.3200 \times 14.36 + 8.780 \times 7.962 + 0.5296 \times 2.252}{24.57} \\ &= 3.081 \text{ mm} \end{aligned} \quad (140)$$

For a bend radius of $3t$, the bend second moment of area for 0.64 mm clad sheet was computed as,

$$I_{rxx(0.64)} = I_{ryy(0.64)} = \frac{\pi}{16} (256t_{st1}^4 - 81t_{st1}^4) = \frac{175\pi \times (0.64)^4}{16} = 5.765 \text{ mm}^4 \quad (141)$$

The horizontal second moments of area of the spar cap reinforcement were computed as,

$$I_{w1xx} = \frac{(w_{st1} - 4t_{st1})t_{st1}^3}{12} = \frac{(25 - 4 \times 0.64)(0.64)^3}{12} = 0.4902 \text{ mm}^4 \quad (142)$$

$$I_{w1yy} = \frac{t(w_{st1} - 4t_{st1})^3}{12} = \frac{0.64 \times (25 - 4 \times 0.64)^3}{12} = 602.7 \text{ mm}^4 \quad (143)$$

The vertical second moments of area of the spar cap reinforcement were computed as,

$$I_{h1xx} = \frac{t(h_{st1} - 4t_{st1})^3}{12} = \frac{0.64 \times (15 - 4 \times 0.64)^3}{12} = 102.7 \text{ mm}^4 \quad (144)$$

$$I_{h1yy} = \frac{(h_{st1} - 4t_{st1})t_{st1}^3}{12} = \frac{(15 - 4 \times 0.64)(0.64)^3}{12} = 0.2718 \text{ mm}^4 \quad (145)$$

Hence the total second moments of area of the spar cap reinforcement were computed as,

$$\begin{aligned} I_{st1xx} &= I_{w1xx} + I_{h1xx} + I_{rxx(0.64)} + (\bar{y}_{st1} - \bar{y}_{w_{st1}})^2 A_{w_{st1}} + (\bar{y}_{st1} - \bar{y}_{h_{st1}})^2 A_{h_{st1}} \\ &\quad + (\bar{y}_{st1} - \bar{y}_{r(0.64)})^2 A_{r(0.64)} \\ &= 0.4902 + 102.7 + 5.765 + (3.081 - 0.3200)^2 \times 14.36 \\ &\quad + (3.081 - 8.780)^2 \times 7.962 + (3.081 - 0.5296)^2 \times 2.252 \\ &= 491.7 \text{ mm}^4 \end{aligned} \quad (146)$$

$$\begin{aligned} I_{st1yy} &= I_{w1yy} + I_{h1yy} + I_{ryy(0.64)} + (\bar{x}_{st1} - \bar{x}_{w_{st1}})^2 A_{w_{st1}} + (\bar{x}_{st1} - \bar{x}_{h_{st1}})^2 A_{h_{st1}} \\ &\quad + (\bar{x}_{st1} - \bar{x}_{r(0.64)})^2 A_{r(0.64)} \\ &= 602.7 + 0.2718 + 5.765 + (8.206 - 13.78)^2 \times 14.36 \\ &\quad + (8.206 - 0.3200)^2 \times 7.962 + (8.206 - 0.5296)^2 \times 2.252 \\ &= 1683 \text{ mm}^4 \end{aligned} \quad (147)$$

A.1.2 Spar Cap Reinforcement 2

A diagram of the cross sectional area of the spar cap reinforcement is given in figure 14(c). The total spar cap reinforcement area was computed as,

$$A_{st2} = A_{st1} + 2t_{st1}^2 = 24.57 + 2 \times (0.64)^2 = 25.39 \text{ mm}^2 \quad (148)$$

The width and height of the spar cap reinforcement were computed as,

$$\begin{aligned} w_{st2} &= w_{st1} + t_{st1} = 25 + 0.64 = 25.64 \text{ mm} \\ h_{st2} &= h_{st1} + t_{st1} = 15 + 0.64 = 15.64 \text{ mm} \end{aligned} \quad (149)$$

The mid-line area of the spar cap reinforcement was thus computed as,

$$\begin{aligned} A_{st2m} &= (w_{st2} + h_{st2} - t_{st1})t_{st1} \\ &= (25.64 + 15.64 - 0.64) \times 0.64 = 26.01 \text{ mm}^2 \end{aligned} \quad (150)$$

The average side length divided by thickness of the spar cap reinforcement for crippling calculations was computed as,

$$c_{st2} = \frac{w_{st2} + h_{st2} - t}{2t} = \frac{25.64 + 15.64 - 0.64}{2 \times 0.64} = 31.75 \quad (151)$$

The centroid of the additional horizontal area of the spar cap reinforcement was computed as,

$$\bar{x}_{w_{st2}} = w_{st1} + \frac{t}{2} = 25 + \frac{0.64}{2} = 25.32 \text{ mm} \quad (152)$$

$$\bar{y}_{w_{st2}} = \bar{y}_{w_{st1}} = 0.3200 \text{ mm} \quad (153)$$

The centroid of the additional vertical area of the spar cap reinforcement was computed as,

$$\bar{x}_{h_{st2}} = \bar{x}_{h_{st1}} = 0.3200 \text{ mm} \quad (154)$$

$$\bar{y}_{h_{st2}} = h_{st1} + \frac{t}{2} = 15 + \frac{0.64}{2} = 15.32 \text{ mm} \quad (155)$$

The total spar cap reinforcement centroid was thus computed as,

$$\begin{aligned} \bar{x}_{st2} &= \frac{\sum \bar{x}_{st2(i)} A_{st2(i)}}{\sum A_{st2(i)}} \\ &= \frac{\bar{x}_{st1} A_{st1} + (\bar{x}_{w_{st2}} + \bar{x}_{h_{st2}}) t_{st1}^2}{A_{st2}} \\ &= \frac{8.206 \times 24.57 + (25.32 + 0.3200)(0.64)^2}{25.39} \\ &= 8.355 \text{ mm} \end{aligned} \quad (156)$$

$$\begin{aligned}
\bar{y}_{st2} &= \frac{\sum \bar{y}_{st2(i)} A_{st2(i)}}{\sum A_{st2(i)}} \\
&= \frac{\bar{y}_{st1} A_{st1} + (\bar{y}_{w_{st2}} + \bar{y}_{h_{st2}}) t_{st1}^2}{A_{st2}} \\
&= \frac{3.081 \times 24.57 + (0.3200 + 15.32)(0.64)^2}{25.39} \\
&= 3.234 \text{ mm}
\end{aligned} \tag{157}$$

Hence the total second moments of area of the spar cap reinforcement were computed as,

$$\begin{aligned}
I_{st2xx} &= I_{st1xx} + \frac{1}{6} t_{st1}^4 + (\bar{y}_{st2} - \bar{y}_{st1})^2 A_{st1} \\
&\quad + [(\bar{y}_{st2} - \bar{y}_{w_{st2}})^2 + (\bar{y}_{st2} - \bar{y}_{h_{st2}})^2] t_{st1}^2 \\
&= 491.7 + \frac{1}{6} (0.64)^4 + (3.234 - 3.081)^2 \times 24.57 \\
&\quad + [(3.234 - 0.3200)^2 + (3.234 - 15.32)^2] (0.64)^2 \\
&= 555.6 \text{ mm}^4
\end{aligned} \tag{158}$$

$$\begin{aligned}
I_{st2yy} &= I_{st1yy} + \frac{1}{6} t_{st1}^4 + (\bar{x}_{st2} - \bar{x}_{st1})^2 A_{st1} \\
&\quad + [(\bar{x}_{st2} - \bar{x}_{w_{st2}})^2 + (\bar{x}_{st2} - \bar{x}_{h_{st2}})^2] t_{st1}^2 \\
&= 1683 + \frac{1}{6} (0.64)^4 + (8.355 - 8.206)^2 \times 24.57 \\
&\quad + [(8.355 - 25.32)^2 + (8.355 - 0.3200)^2] (0.64)^2 \\
&= 1828 \text{ mm}^4
\end{aligned} \tag{159}$$

A.1.3 Spar Cap Reinforcement 3

A diagram of the cross sectional area of the spar cap reinforcement is given in figure 14(d). The total spar cap reinforcement area was computed as,

$$A_{st3} = A_{st2} + 2t_{st1}^2 = 25.39 + 2 \times (0.64)^2 = 26.21 \text{ mm}^2 \tag{160}$$

The width and height of the spar cap reinforcement were computed as,

$$\begin{aligned} w_{st3} &= w_{st2} + t_{st1} = 25.64 + 0.64 = 26.28 \text{ mm} \\ h_{st3} &= h_{st2} + t_{st1} = 15.64 + 0.64 = 16.28 \text{ mm} \end{aligned} \quad (161)$$

The mid-line area of the spar cap reinforcement was thus computed as,

$$\begin{aligned} A_{st3m} &= (w_{st3} + h_{st3} - t_{st1})t_{st1} \\ &= (26.28 + 16.28 - 0.64) \times 0.64 = 26.83 \text{ mm}^2 \end{aligned} \quad (162)$$

The average side length divided by thickness of the spar cap reinforcement for crippling calculations was computed as,

$$c_{st3} = \frac{w_{st3} + h_{st3} - t}{2t} = \frac{26.28 + 16.28 - 0.64}{2 \times 0.64} = 32.75 \quad (163)$$

The centroid of the additional horizontal area of the spar cap reinforcement was computed as,

$$\bar{x}_{w_{st3}} = \bar{x}_{w_{st2}} + t_{st1} = 25.32 + 0.64 = 25.96 \text{ mm} \quad (164)$$

$$\bar{y}_{w_{st3}} = \bar{y}_{w_{st2}} = 0.3200 \text{ mm} \quad (165)$$

The centroid of the additional vertical area of the spar cap reinforcement was computed as,

$$\bar{x}_{h_{st3}} = \bar{x}_{h_{st2}} = 0.3200 \text{ mm} \quad (166)$$

$$\bar{y}_{h_{st3}} = \bar{y}_{h_{st2}} + t_{st1} = 15.32 + 0.64 = 15.96 \text{ mm} \quad (167)$$

The total spar cap reinforcement centroid was thus computed as,

$$\begin{aligned} \bar{x}_{st3} &= \frac{\sum \bar{x}_{st3(i)} A_{st3(i)}}{\sum A_{st3(i)}} \\ &= \frac{\bar{x}_{st2} A_{st2} + (\bar{x}_{w_{st3}} + \bar{x}_{h_{st3}}) t_{st1}^2}{A_{st3}} \\ &= \frac{8.355 \times 25.39 + (25.96 + 0.3200)(0.64)^2}{26.21} \\ &= 8.504 \text{ mm} \end{aligned} \quad (168)$$

$$\begin{aligned}
\bar{y}_{st3} &= \frac{\sum \bar{y}_{st3(i)} A_{st3(i)}}{\sum A_{st3(i)}} \\
&= \frac{\bar{y}_{st2} A_{st2} + (\bar{y}_{w_{st3}} + \bar{y}_{h_{st3}}) t_{st1}^2}{A_{st3}} \\
&= \frac{3.234 \times 25.39 + (0.3200 + 15.96)(0.64)^2}{26.21} \\
&= 3.387 \text{ mm}
\end{aligned} \tag{169}$$

Hence the total second moments of area of the spar cap reinforcement were computed as,

$$\begin{aligned}
I_{st3xx} &= I_{st2xx} + \frac{1}{6} t_{st1}^4 + (\bar{y}_{st3} - \bar{y}_{st2})^2 A_{st2} \\
&\quad + [(\bar{y}_{st3} - \bar{y}_{w_{st3}})^2 + (\bar{y}_{st3} - \bar{y}_{h_{st3}})^2] t_{st1}^2 \\
&= 555.6 + \frac{1}{6} (0.64)^4 + (3.387 - 3.234)^2 \times 25.39 \\
&\quad + [(3.387 - 0.3200)^2 + (3.387 - 15.96)^2] (0.64)^2 \\
&= 624.8 \text{ mm}^4
\end{aligned} \tag{170}$$

$$\begin{aligned}
I_{st3yy} &= I_{st2yy} + \frac{1}{6} t_{st1}^4 + (\bar{x}_{st3} - \bar{x}_{st2})^2 A_{st2} \\
&\quad + [(\bar{x}_{st3} - \bar{x}_{w_{st3}})^2 + (\bar{x}_{st3} - \bar{x}_{h_{st3}})^2] t_{st1}^2 \\
&= 1828 + \frac{1}{6} (0.64)^4 + (8.504 - 8.355)^2 \times 25.39 \\
&\quad + [(8.504 - 25.96)^2 + (8.504 - 0.3200)^2] (0.64)^2 \\
&= 1981 \text{ mm}^4
\end{aligned} \tag{171}$$

A.1.4 Spar Cap Reinforcement 5

A diagram of the cross sectional area of the spar cap reinforcement is given in figure 14(f). The horizontal and vertical areas of the spar cap reinforcement were computed as,

$$A_{w5_{st}} = t_{st2}(w_{st1} - 4t_{st2}) = 0.41 \times (25 - 4 \times 0.41) = 9.578 \text{ mm}^2 \tag{172}$$

$$A_{h5_{st}} = t_{st2}(h_{st1} - 4t_{st2}) = 0.41 \times (15 - 4 \times 0.41) = 5.478 \text{ mm}^2 \tag{173}$$

The total spar cap reinforcement area was thus computed as,

$$\begin{aligned} A_{st5} &= A_{w5_{st}} + A_{h5_{st}} + A_{r(0.41)} \\ &= 9.578 + 5.478 + 0.9242 = 15.98 \text{ mm}^2 \end{aligned} \quad (174)$$

The mid-line area of the spar cap reinforcement was computed as,

$$\begin{aligned} A_{st5m} &= (w_{st1} + h_{st1} - t_{st2})t_{st2} \\ &= (25 + 15 - 0.41) \times 0.41 = 16.23 \text{ mm}^2 \end{aligned} \quad (175)$$

The average side length divided by thickness of the spar cap reinforcement for crippling calculations was computed as,

$$c_{st5} = \frac{w_{st1} + h_{st1} - t}{2t} = \frac{25 + 15 - 0.41}{2 \times 0.41} = 48.28 \quad (176)$$

The centroid of the horizontal edge of the spar cap reinforcement was computed as,

$$\bar{x}_{w5_{st}} = \frac{w_{st1} - 4t}{2} + 4t_{st2} = \frac{25 - 4 \times 0.41}{2} + 4 \times 0.41 = 13.32 \text{ mm} \quad (177)$$

$$\bar{y}_{w5_{st}} = \bar{y}_{w5_{sp}} = 0.2050 \text{ mm} \quad (178)$$

The centroid of the vertical edge of the spar cap reinforcement was computed as,

$$\bar{x}_{h5_{st}} = \bar{y}_{w5_{sp}} = 0.2050 \text{ mm} \quad (179)$$

$$\bar{y}_{h5_{st}} = \frac{h_{st1} - 4t}{2} + 4t_{st2} = \frac{15 - 4 \times 0.41}{2} + 4 \times 0.41 = 8.320 \text{ mm} \quad (180)$$

The total spar cap reinforcement centroid was thus computed as,

$$\begin{aligned} \bar{x}_{st5} &= \frac{\sum \bar{x}_{st5(i)} A_{st5(i)}}{\sum A_{st5(i)}} \\ &= \frac{\bar{x}_{w5_{st}} A_{w5_{st}} + \bar{x}_{h5_{st}} A_{h5_{st}} + \bar{x}_{r(0.41)} A_{r(0.41)}}{A_{st5}} \\ &= \frac{13.32 \times 9.578 + 0.2050 \times 5.478 + 0.3393 \times 0.9242}{15.98} \\ &= 8.074 \text{ mm} \end{aligned} \quad (181)$$

$$\begin{aligned}
\bar{y}_{st5} &= \frac{\sum \bar{y}_{st5(i)} A_{st5(i)}}{\sum A_{st5(i)}} \\
&= \frac{\bar{y}_{w5_{st}} A_{w5_{st}} + \bar{y}_{h5_{st}} A_{h5_{st}} + \bar{y}_{r(0.41)} A_{r(0.41)}}{A_{st5}} \\
&= \frac{0.2050 \times 9.578 + 8.320 \times 5.478 + 0.3393 \times 0.9242}{15.98} \\
&= 2.995 \text{ mm}
\end{aligned} \tag{182}$$

The horizontal second moments of area of the spar cap reinforcement were computed as,

$$I_{w5xx} = \frac{(w_{st1} - 4t_{st2}) t_{st2}^3}{12} = \frac{(25 - 4 \times 0.41)(0.41)^3}{12} = 0.1342 \text{ mm}^4 \tag{183}$$

$$I_{w5yy} = \frac{t(w_{st1} - 4t_{st2})^3}{12} = \frac{0.41 \times (25 - 4 \times 0.41)^3}{12} = 435.5 \text{ mm}^4 \tag{184}$$

The vertical second moments of area of the spar cap reinforcement were computed as,

$$I_{h5xx} = \frac{t(h_{st1} - 4t_{st2})^3}{12} = \frac{0.41 \times (15 - 4 \times 0.41)^3}{12} = 81.47 \text{ mm}^4 \tag{185}$$

$$I_{h5yy} = \frac{(h_{st1} - 4t_{st2}) t_{st2}^3}{12} = \frac{(15 - 4 \times 0.41)(0.41)^3}{12} = 0.07673 \text{ mm}^4 \tag{186}$$

Hence the total second moments of area of the spar cap reinforcement were computed as,

$$\begin{aligned}
I_{st5xx} &= I_{w5xx} + I_{h5xx} + I_{rxx(0.41)} + (\bar{y}_{st5} - \bar{y}_{w5_{st}})^2 A_{w5_{st}} + (\bar{y}_{st5} - \bar{y}_{h5_{st}})^2 A_{h5_{st}} \\
&\quad + (\bar{y}_{st5} - \bar{y}_{r(0.41)})^2 A_{r(0.41)} \\
&= 0.1342 + 81.47 + 0.9710 + (2.995 - 0.2050)^2 \times 9.578 \\
&\quad + (2.995 - 8.320)^2 \times 5.478 + (2.995 - 0.3393)^2 \times 0.9242 \\
&= 319.0 \text{ mm}^4
\end{aligned} \tag{187}$$

$$\begin{aligned}
I_{st5yy} &= I_{w5yy} + I_{h5yy} + I_{ryy(0.41)} + (\bar{x}_{st5} - \bar{x}_{w5st})^2 A_{w5st} + (\bar{x}_{st5} - \bar{x}_{h5st})^2 A_{h5st} \\
&\quad + (\bar{x}_{st5} - \bar{x}_{r(0.41)})^2 A_{r(0.41)} \\
&= 435.5 + 0.07673 + 0.9710 + (8.074 - 13.32)^2 \times 9.578 \\
&\quad + (8.074 - 0.2050)^2 \times 5.478 + (8.074 - 0.3393)^2 \times 0.9242 \\
&= 1095 \text{ mm}^4
\end{aligned} \tag{188}$$

A.1.5 Spar Cap Reinforcement 6

A diagram of the cross sectional area of the spar cap reinforcement is given in figure 14(g). The total spar cap reinforcement area was computed as,

$$A_{st6} = A_{st5} + 2t_{st2}^2 = 15.98 + 2 \times (0.41)^2 = 16.32 \text{ mm}^2 \tag{189}$$

The width and height of the spar cap reinforcement were computed as,

$$\begin{aligned}
w_{st6} &= w_{st1} + t_{st2} = 25 + 0.41 = 25.41 \text{ mm} \\
h_{st6} &= h_{st1} + t_{st2} = 15 + 0.41 = 15.41 \text{ mm}
\end{aligned} \tag{190}$$

The mid-line area of the spar cap reinforcement was thus computed as,

$$\begin{aligned}
A_{st6m} &= (w_{st6} + h_{st6} - t_{st2})t_{st2} \\
&= (25.41 + 15.41 - 0.41) \times 0.41 = 16.57 \text{ mm}^2
\end{aligned} \tag{191}$$

The average side length divided by thickness of the spar cap reinforcement for crippling calculations was computed as,

$$c_{st6} = \frac{w_{st6} + h_{st6} - t}{2t} = \frac{25.41 + 15.41 - 0.41}{2 \times 0.41} = 49.28 \tag{192}$$

The centroid of the additional horizontal area of the spar cap reinforcement was computed as,

$$\bar{x}_{w_{st6}} = w_{st1} + \frac{t}{2} = 25 + \frac{0.41}{2} = 25.21 \text{ mm} \tag{193}$$

$$\bar{y}_{w_{st6}} = \bar{y}_{w_{st5}} = 0.2050 \text{ mm} \tag{194}$$

The centroid of the additional vertical area of the spar cap reinforcement was computed as,

$$\bar{x}_{h_{st6}} = \bar{x}_{h_{st5}} = 0.2050 \text{ mm} \tag{195}$$

$$\bar{y}_{h_{st6}} = h_{st1} + \frac{t}{2} = 15 + \frac{0.41}{2} = 15.21 \text{ mm} \quad (196)$$

The total spar cap reinforcement centroid was thus computed as,

$$\begin{aligned} \bar{x}_{st6} &= \frac{\sum \bar{x}_{st6(i)} A_{st6(i)}}{\sum A_{st6(i)}} \\ &= \frac{\bar{x}_{st5} A_{st5} + (\bar{x}_{w_{st6}} + \bar{x}_{h_{st6}}) t_{st2}^2}{A_{st6}} \\ &= \frac{8.074 \times 15.98 + (25.21 + 0.2050)(0.41)^2}{16.32} \\ &= 8.168 \text{ mm} \end{aligned} \quad (197)$$

$$\begin{aligned} \bar{y}_{st6} &= \frac{\sum \bar{y}_{st6(i)} A_{st6(i)}}{\sum A_{st6(i)}} \\ &= \frac{\bar{y}_{st5} A_{st5} + (\bar{y}_{w_{st6}} + \bar{y}_{h_{st6}}) t_{st2}^2}{A_{st6}} \\ &= \frac{2.995 \times 15.98 + (0.2050 + 15.21)(0.41)^2}{16.32} \\ &= 3.091 \text{ mm} \end{aligned} \quad (198)$$

Hence the total second moments of area of the spar cap reinforcement were computed as,

$$\begin{aligned} I_{st6xx} &= I_{st5xx} + \frac{1}{6} t_{st2}^4 + (\bar{y}_{st6} - \bar{y}_{st5})^2 A_{st5} + [(\bar{y}_{st6} - \bar{y}_{w_{st6}})^2 + (\bar{y}_{st6} - \bar{y}_{h_{st6}})^2] t_{st2}^2 \\ &= 319.0 + \frac{1}{6}(0.41)^4 + (3.091 - 2.995)^2 \times 15.98 \\ &\quad + [(3.091 - 0.2050)^2 + (3.091 - 15.21)^2] (0.41)^2 \\ &= 345.2 \text{ mm}^4 \end{aligned} \quad (199)$$

$$\begin{aligned} I_{st6yy} &= I_{st5yy} + \frac{1}{6} t_{st2}^4 + (\bar{x}_{st6} - \bar{x}_{st5})^2 A_{st5} + [(\bar{x}_{st6} - \bar{x}_{w_{st6}})^2 + (\bar{x}_{st6} - \bar{x}_{h_{st6}})^2] t_{st2}^2 \\ &= 1095 + \frac{1}{6}(0.41)^4 + (8.168 - 8.074)^2 \times 15.98 \\ &\quad + [(8.168 - 25.21)^2 + (8.168 - 0.2050)^2] (0.41)^2 \\ &= 1155 \text{ mm}^4 \end{aligned} \quad (200)$$

A.1.6 Spar Cap Reinforcement 7

A diagram of the cross sectional area of the spar cap reinforcement is given in figure 14(h). The total spar cap reinforcement area was computed as,

$$A_{st7} = A_{st6} + 2t_{st2}^2 = 16.32 + 2 \times (0.41)^2 = 16.66 \text{ mm}^2 \quad (201)$$

The width and height of the spar cap reinforcement were computed as,

$$\begin{aligned} w_{st7} &= w_{st6} + t_{st2} = 25.41 + 0.41 = 25.82 \text{ mm} \\ h_{st7} &= h_{st6} + t_{st2} = 15.41 + 0.41 = 15.82 \text{ mm} \end{aligned} \quad (202)$$

The mid-line area of the spar cap reinforcement was thus computed as,

$$\begin{aligned} A_{st7m} &= (w_{st7} + h_{st7} - t_{st2})t_{st2} \\ &= (25.82 + 15.82 - 0.41) \times 0.41 = 16.90 \text{ mm}^2 \end{aligned} \quad (203)$$

The average side length divided by thickness of the spar cap reinforcement for crippling calculations was computed as,

$$c_{st7} = \frac{w_{st7} + h_{st7} - t}{2t} = \frac{25.82 + 15.82 - 0.41}{2 \times 0.41} = 50.28 \quad (204)$$

The centroid of the additional horizontal area of the spar cap reinforcement was computed as,

$$\bar{x}_{w_{st7}} = \bar{x}_{w_{st6}} + t_{st2} = 25.21 + 0.41 = 25.62 \text{ mm} \quad (205)$$

$$\bar{y}_{w_{st7}} = \bar{y}_{w_{st6}} = 0.2050 \text{ mm} \quad (206)$$

The centroid of the additional vertical area of the spar cap reinforcement was computed as,

$$\bar{x}_{h_{st7}} = \bar{x}_{h_{st6}} = 0.2050 \text{ mm} \quad (207)$$

$$\bar{y}_{h_{st7}} = \bar{y}_{h_{st6}} + t_{st2} = 15 + 0.41 = 15.62 \text{ mm} \quad (208)$$

The total spar cap reinforcement centroid was thus computed as,

$$\begin{aligned}
\bar{x}_{st7} &= \frac{\sum \bar{x}_{st7(i)} A_{st7(i)}}{\sum A_{st7(i)}} \\
&= \frac{\bar{x}_{st6} A_{st6} + (\bar{x}_{w_{st7}} + \bar{x}_{h_{st7}}) t_{st2}^2}{A_{st7}} \\
&= \frac{8.168 \times 16.32 + (25.62 + 0.2050)(0.41)^2}{16.66} \\
&= 8.262 \text{ mm}
\end{aligned} \tag{209}$$

$$\begin{aligned}
\bar{y}_{st7} &= \frac{\sum \bar{y}_{st7(i)} A_{st7(i)}}{\sum A_{st7(i)}} \\
&= \frac{\bar{y}_{st6} A_{st6} + (\bar{y}_{w_{st7}} + \bar{y}_{h_{st7}}) t_{st2}^2}{A_{st7}} \\
&= \frac{3.091 \times 16.32 + (0.2050 + 15.62)(0.41)^2}{16.66} \\
&= 3.188 \text{ mm}
\end{aligned} \tag{210}$$

Hence the total second moments of area of the spar cap reinforcement were computed as,

$$\begin{aligned}
I_{st7xx} &= I_{st6xx} + \frac{1}{6} t_{st2}^4 + (\bar{y}_{st7} - \bar{y}_{st6})^2 A_{st6} + [(\bar{y}_{st7} - \bar{y}_{w_{st7}})^2 + (\bar{y}_{st7} - \bar{y}_{h_{st7}})^2] t_{st2}^2 \\
&= 345.2 + \frac{1}{6} (0.41)^4 + (3.188 - 3.091)^2 \times 16.32 \\
&\quad + [(3.188 - 0.2050)^2 + (3.188 - 15.62)^2] (0.41)^2 \\
&= 372.8 \text{ mm}^4
\end{aligned} \tag{211}$$

$$\begin{aligned}
I_{st7yy} &= I_{st6yy} + \frac{1}{6} t_{st2}^4 + (\bar{x}_{st7} - \bar{x}_{st6})^2 A_{st6} + [(\bar{x}_{st7} - \bar{x}_{w_{st7}})^2 + (\bar{x}_{st7} - \bar{x}_{h_{st7}})^2] t_{st2}^2 \\
&= 1155 + \frac{1}{6} (0.41)^4 + (8.262 - 8.168)^2 \times 16.32 \\
&\quad + [(8.262 - 25.62)^2 + (8.262 - 0.2050)^2] (0.41)^2 \\
&= 1217 \text{ mm}^4
\end{aligned} \tag{212}$$

A.2 Spar Cap Configuration Geometry Calculations

A.2.1 Spar Cap Configuration 1

A diagram of the cross sectional area of the spar cap configuration is given in figure 15(a). The true area of the configuration, excluding the skin,

$$A_{t1} = A_{sp} = 15.98 \text{ mm}^2 \quad (213)$$

The total width and height of the configuration were computed as,

$$\begin{aligned} W_{c1} &= w_{sp} = 20 \text{ mm} \\ H_{c1} &= w_{sp} + t_{sk} = 20 + 0.41 = 20.41 \text{ mm} \end{aligned} \quad (214)$$

The true skin area was computed as,

$$A_{sk1} = W_{c1}t_{sk} = 20 \times 0.41 = 8.200 \text{ mm}^2 \quad (215)$$

The centroids of the skin and spar flange and web, relative to the global configuration coordinates shown in figure 15(a), were computed, respectively, as,

$$\begin{aligned} \bar{X}_{sk1} &= \frac{W_{c1}}{2} = 10 \text{ mm} \\ \bar{Y}_{sk1} &= H_{c1} - \frac{t_{sk}}{2} = 20.41 - \frac{0.41}{2} = 20.21 \text{ mm} \\ \bar{X}_{sp1} &= \bar{x}_{sp} = 5.213 \text{ mm} \\ \bar{Y}_{sp1} &= H_{c1} - (\bar{y}_{sp} + t_{sk}) = 20.41 - (5.213 + 0.41) = 14.79 \text{ mm} \end{aligned} \quad (216)$$

The total centroid of the configuration, relative to the global configuration coordinates shown in figure 15(a), was thus computed as,

$$\begin{aligned} \bar{X}_{c1} &= \frac{\sum \bar{X}_{c1(i)} A_{c1(i)}}{\sum A_{c1(i)}} \\ &= \frac{\bar{X}_{sk1} A_{sk1} + \bar{X}_{sp1} A_{sp}}{A_{sk1} + A_{sp}} \\ &= \frac{10 \times 8.200 + 5.213 \times 15.98}{8.200 + 15.98} \\ &= 6.836 \text{ mm} \end{aligned} \quad (217)$$

$$\begin{aligned}
\bar{Y}_{c1} &= \frac{\sum \bar{Y}_{c1(i)} A_{c1(i)}}{\sum A_{c1(i)}} \\
&= \frac{\bar{Y}_{sk1} A_{sk1} + \bar{Y}_{sp1} A_{sp}}{A_{sk1} + A_{sp}} \\
&= \frac{20.21 \times 8.200 + 14.79 \times 15.98}{8.200 + 15.98} \\
&= 16.63 \text{ mm}
\end{aligned} \tag{218}$$

Hence the total second moments of area of the configuration were computed as,

$$\begin{aligned}
I_{c1xx} &= I_{spxx} + \frac{W_{c1} t_{sk}^3}{12} + (\bar{Y}_{c1} - \bar{Y}_{sp1})^2 A_{sp} + (\bar{Y}_{c1} - \bar{Y}_{sk1})^2 A_{sk1} \\
&= 660.0 + \frac{20 \times (0.41)^3}{12} + (16.63 - 14.79)^2 \times 15.98 + (16.63 - 20.21)^2 \times 8.200 \\
&= 819.3 \text{ mm}^4
\end{aligned} \tag{219}$$

$$\begin{aligned}
I_{c1yy} &= I_{spyy} + \frac{t_{sk} W_{c1}^3}{12} + (\bar{X}_{c1} - \bar{X}_{sp1})^2 A_{sp} + (\bar{X}_{c1} - \bar{X}_{sk1})^2 A_{sk1} \\
&= 660.0 + \frac{0.41 \times (20)^3}{12} + (6.836 - 5.213)^2 \times 15.98 + (6.836 - 10)^2 \times 8.200 \\
&= 1058 \text{ mm}^4
\end{aligned} \tag{220}$$

A.2.2 Spar Cap Configuration 3

A diagram of the cross sectional area of the spar cap configuration is given in figure 15(c). Detailed calculations of all quantities relating to the spar cap configuration 2 geometry (denoted by a subscript 2) that are referenced in the calculation of the spar cap configuration 3 geometry can be found in section 2.7.3. The true area of the configuration, excluding the skin, was computed as,

$$A_{t3} = A_{t2} + A_{st3} = 43.01 + 26.21 = 69.22 \text{ mm}^2 \tag{221}$$

The centroid of the additional spar cap reinforcement, relative to the global configuration coordinates shown in figure 15(c), was computed as,

$$\begin{aligned}
\bar{X}_{st3} &= W_{c2} - (w_{sp} + \bar{x}_{st3} + t_{st1}) = 46.92 - (20 + 8.504 + 0.64) = 17.78 \text{ mm} \\
\bar{Y}_{st3} &= H_{c2} - (\bar{y}_{st3} + t_{sk} + t_{st1}) = 20.41 - (3.387 + 0.41 + 0.64) = 15.97 \text{ mm}
\end{aligned} \tag{222}$$

The total centroid of the configuration, relative to the global configuration coordinates shown in figure 15(c), was thus computed as,

$$\begin{aligned}\bar{X}_{c3} &= \frac{\sum \bar{X}_{c3(i)} A_{c3(i)}}{\sum A_{c3(i)}} \\ &= \frac{\bar{X}_{c2}(A_{sk2} + A_{t2}) + \bar{X}_{st3} A_{st3}}{A_{sk2} + A_{t3}} \\ &= \frac{23.43 \times (19.24 + 43.01) + 17.78 \times 26.21}{19.24 + 69.22} \\ &= 21.76 \text{ mm}\end{aligned}\tag{223}$$

$$\begin{aligned}\bar{Y}_{c3} &= \frac{\sum \bar{Y}_{c3(i)} A_{c3(i)}}{\sum A_{c3(i)}} \\ &= \frac{\bar{Y}_{c2}(A_{sk2} + A_{t2}) + \bar{Y}_{st3} A_{st3}}{A_{sk2} + A_{t3}} \\ &= \frac{17.19 \times (19.24 + 43.01) + 15.97 \times 26.21}{19.24 + 69.22} \\ &= 16.83 \text{ mm}\end{aligned}\tag{224}$$

Hence the total second moments of area of the configuration were computed as,

$$\begin{aligned}I_{c3xx} &= I_{c2xx} + I_{st3xx} + (\bar{Y}_{c3} - \bar{Y}_{c2})^2 (A_{sk2} + A_{t2}) + (\bar{Y}_{c3} - \bar{Y}_{st3})^2 A_{st3} \\ &= 1642 + 624.8 + (16.83 - 17.19)^2 \times (19.24 + 43.01) + (16.83 - 15.97)^2 \times 26.21 \\ &= 2294 \text{ mm}^4\end{aligned}\tag{225}$$

$$\begin{aligned}I_{c3yy} &= I_{c2yy} + I_{st3yy} + (\bar{X}_{c3} - \bar{X}_{c2})^2 (A_{sk2} + A_{t2}) + (\bar{X}_{c3} - \bar{X}_{st3})^2 A_{st3} \\ &= 8260 + 1981 + (21.76 - 23.43)^2 \times (19.24 + 43.01) + (21.76 - 17.78)^2 \times 26.21 \\ &= 10830 \text{ mm}^4\end{aligned}\tag{226}$$

A.2.3 Spar Cap Configuration 4

A diagram of the cross sectional area of the spar cap configuration is given in figure 15(d). The true area of the configuration, excluding the skin, was computed as,

$$A_{t4} = A_{t3} + A_{st2} = 69.22 + 25.39 = 94.61 \text{ mm}^2\tag{227}$$

The centroid of the additional spar cap reinforcement, relative to the global configuration coordinates shown in figure 15(d), was computed as,

$$\begin{aligned}\bar{X}_{st4} &= W_{c2} - (w_{sp} + \bar{x}_{st2} + 2t_{st1}) = 46.92 - (20 + 8.355 + 2 \times 0.64) = 17.29 \text{ mm} \\ \bar{Y}_{st4} &= H_{c2} - (\bar{y}_{st2} + t_{sk} + 2t_{st1}) = 20.41 - (3.234 + 0.41 + 2 \times 0.64) = 15.49 \text{ mm}\end{aligned}\quad (228)$$

The total centroid of the configuration, relative to the global configuration coordinates shown in figure 15(d), was thus computed as,

$$\begin{aligned}\bar{X}_{c4} &= \frac{\sum \bar{X}_{c4(i)} A_{c4(i)}}{\sum A_{c4(i)}} \\ &= \frac{\bar{X}_{c3}(A_{sk2} + A_{t3}) + \bar{X}_{st4} A_{st2}}{A_{sk2} + A_{t4}} \\ &= \frac{21.76 \times (19.24 + 69.22) + 17.29 \times 25.39}{19.24 + 94.61} \\ &= 20.76 \text{ mm}\end{aligned}\quad (229)$$

$$\begin{aligned}\bar{Y}_{c4} &= \frac{\sum \bar{Y}_{c4(i)} A_{c4(i)}}{\sum A_{c4(i)}} \\ &= \frac{\bar{Y}_{c3}(A_{sk2} + A_{t3}) + \bar{Y}_{st4} A_{st2}}{A_{sk2} + A_{t4}} \\ &= \frac{16.83 \times (19.24 + 69.22) + 15.49 \times 25.39}{19.24 + 94.61} \\ &= 16.53 \text{ mm}\end{aligned}\quad (230)$$

Hence the total second moments of area of the configuration were computed as,

$$\begin{aligned}I_{c4xx} &= I_{c3xx} + I_{st2xx} + (\bar{Y}_{c4} - \bar{Y}_{c3})^2 (A_{sk2} + A_{t3}) + (\bar{Y}_{c4} - \bar{Y}_{st4})^2 A_{st2} \\ &= 2294 + 555.6 + (16.53 - 16.83)^2 \times (19.24 + 69.22) + (16.53 - 15.49)^2 \times 25.39 \\ &= 2885 \text{ mm}^4\end{aligned}\quad (231)$$

$$\begin{aligned}I_{c4yy} &= I_{c3yy} + I_{st2yy} + (\bar{X}_{c4} - \bar{X}_{c3})^2 (A_{sk2} + A_{t3}) + (\bar{X}_{c4} - \bar{X}_{st4})^2 A_{st2} \\ &= 10830 + 1828 + (20.76 - 21.76)^2 \times (19.24 + 69.22) + (20.76 - 17.29)^2 \times 25.39 \\ &= 13052 \text{ mm}^4\end{aligned}\quad (232)$$

A.2.4 Spar Cap Configuration 5

A diagram of the cross sectional area of the spar cap configuration is given in figure 15(e). The true area of the configuration, excluding the skin, was computed as,

$$A_{t5} = A_{t4} + A_{st1} = 94.61 + 24.57 = 119.2 \text{ mm}^2 \quad (233)$$

The centroid of the additional spar cap reinforcement, relative to the global configuration coordinates shown in figure 15(e), was computed as,

$$\begin{aligned} \bar{X}_{st5} &= W_{c2} - (w_{sp} + \bar{x}_{st1} + 3t_{st1}) = 46.92 - (20 + 8.206 + 3 \times 0.64) = 16.79 \text{ mm} \\ \bar{Y}_{st5} &= H_{c2} - (\bar{y}_{st1} + t_{sk} + 3t_{st1}) = 20.41 - (3.081 + 0.41 + 3 \times 0.64) = 15.00 \text{ mm} \end{aligned} \quad (234)$$

The total centroid of the configuration, relative to the global configuration coordinates shown in figure 15(e), was thus computed as,

$$\begin{aligned} \bar{X}_{c5} &= \frac{\sum \bar{X}_{c5(i)} A_{c5(i)}}{\sum A_{c5(i)}} \\ &= \frac{\bar{X}_{c4}(A_{sk2} + A_{t4}) + \bar{X}_{st5} A_{st1}}{A_{sk2} + A_{t5}} \\ &= \frac{20.76 \times (19.24 + 94.61) + 16.79 \times 24.57}{19.24 + 119.2} \\ &= 20.05 \text{ mm} \end{aligned} \quad (235)$$

$$\begin{aligned} \bar{Y}_{c5} &= \frac{\sum \bar{Y}_{c5(i)} A_{c5(i)}}{\sum A_{c5(i)}} \\ &= \frac{\bar{Y}_{c4}(A_{sk2} + A_{t4}) + \bar{Y}_{st5} A_{st1}}{A_{sk2} + A_{t5}} \\ &= \frac{16.53 \times (19.24 + 94.61) + 15.00 \times 24.57}{19.24 + 119.2} \\ &= 16.26 \text{ mm} \end{aligned} \quad (236)$$

Hence the total second moments of area of the configuration were computed as,

$$\begin{aligned} I_{c5xx} &= I_{c4xx} + I_{st1xx} + (\bar{Y}_{c5} - \bar{Y}_{c4})^2 (A_{sk2} + A_{t4}) + (\bar{Y}_{c5} - \bar{Y}_{st5})^2 A_{st1} \\ &= 2885 + 491.7 + (16.26 - 16.53)^2 \times (19.24 + 94.61) + (16.26 - 15.00)^2 \times 24.57 \\ &= 3424 \text{ mm}^4 \end{aligned} \quad (237)$$

$$\begin{aligned}
I_{c5yy} &= I_{c4yy} + I_{st1yy} + (\bar{X}_{c5} - \bar{X}_{c4})^2(A_{sk2} + A_{t4}) + (\bar{X}_{c5} - \bar{X}_{st5})^2A_{st1} \\
&= 13052 + 1683 + (20.05 - 20.76)^2 \times (19.24 + 94.61) + (20.05 - 16.79)^2 \times 24.57 \\
&= 15054 \text{ mm}^4
\end{aligned} \tag{238}$$

A.2.5 Spar Cap Configuration 6

A diagram of the cross sectional area of the spar cap configuration is given in figure 15(f). The true area of the configuration, excluding the skin, was computed as,

$$A_{t6} = A_{sp} + A_{st2} = 15.98 + 25.39 = 41.37 \text{ mm}^2 \tag{239}$$

The total width and height of the configuration were computed as,

$$\begin{aligned}
W_{c6} &= W_{c1} + w_{st2} = 20 + 25.64 = 45.64 \text{ mm} \\
H_{c6} &= H_{c1} = 20.41 \text{ mm}
\end{aligned} \tag{240}$$

The true skin area was computed as,

$$A_{sk6} = W_{c6}t_{sk} = 45.64 \times 0.41 = 18.71 \text{ mm}^2 \tag{241}$$

The centroids of the skin, spar flange and web and spar cap reinforcement, relative to the global configuration coordinates shown in figure 15(f), were computed, respectively, as,

$$\begin{aligned}
\bar{X}_{sk6} &= \frac{W_{c6}}{2} = \frac{45.64}{2} = 22.82 \text{ mm} \\
\bar{Y}_{sk6} &= \bar{Y}_{sk1} = 20.21 \text{ mm} \\
\bar{X}_{sp6} &= \bar{x}_{sp} + w_{st2} = 5.213 + 25.64 = 30.85 \text{ mm} \\
\bar{Y}_{sp6} &= \bar{Y}_{sp1} = 14.79 \text{ mm} \\
\bar{X}_{st6} &= W_{c6} - (w_{sp} + \bar{x}_{st2}) = 45.64 - (20 + 8.355) = 17.29 \text{ mm} \\
\bar{Y}_{st6} &= H_{c6} - (\bar{y}_{st2} + t_{sk}) = 20.41 - (3.234 + 0.41) = 16.77 \text{ mm}
\end{aligned} \tag{242}$$

The total centroid of the configuration, relative to the global configuration coordinates shown in figure 15(f), was thus computed as,

$$\begin{aligned}
\bar{X}_{c6} &= \frac{\sum \bar{X}_{c6(i)} A_{c6(i)}}{\sum A_{c6(i)}} \\
&= \frac{\bar{X}_{sk6} A_{sk6} + \bar{X}_{sp6} A_{sp} + \bar{X}_{st6} A_{st2}}{A_{sk6} + A_{sp} + A_{st2}} \\
&= \frac{22.82 \times 18.71 + 30.85 \times 15.98 + 17.29 \times 25.39}{18.71 + 15.98 + 25.39} \\
&= 22.62 \text{ mm}
\end{aligned} \tag{243}$$

$$\begin{aligned}
\bar{Y}_{c6} &= \frac{\sum \bar{Y}_{c6(i)} A_{c6(i)}}{\sum A_{c6(i)}} \\
&= \frac{\bar{Y}_{sk6} A_{sk6} + \bar{Y}_{sp6} A_{sp} + \bar{Y}_{st6} A_{st2}}{A_{sk6} + A_{sp} + A_{st2}} \\
&= \frac{20.21 \times 18.71 + 14.79 \times 15.98 + 16.77 \times 25.39}{18.71 + 15.98 + 25.39} \\
&= 17.31 \text{ mm}
\end{aligned} \tag{244}$$

Hence the total second moments of area of the configuration were computed as,

$$\begin{aligned}
I_{c6xx} &= I_{spxx} + I_{st2xx} + \frac{W_{c6} t_{sk}^3}{12} + (\bar{Y}_{c6} - \bar{Y}_{sp6})^2 A_{sp} \\
&\quad + (\bar{Y}_{c6} - \bar{Y}_{st6})^2 A_{st2} + (\bar{Y}_{c6} - \bar{Y}_{sk6})^2 A_{sk6} \\
&= 660.0 + 555.6 + \frac{45.64 \times (0.41)^3}{12} + (17.31 - 14.79)^2 \times 15.98 \\
&\quad + (17.31 - 16.77)^2 \times 25.39 + (17.31 - 20.21)^2 \times 18.71 \\
&= 1482 \text{ mm}^4
\end{aligned} \tag{245}$$

$$\begin{aligned}
I_{c6yy} &= I_{spyy} + I_{st2yy} + \frac{t_{sk} W_{c6}^3}{12} + (\bar{X}_{c6} - \bar{X}_{sp6})^2 A_{sp} \\
&\quad + (\bar{X}_{c6} - \bar{X}_{st6})^2 A_{st2} + (\bar{X}_{c6} - \bar{X}_{sk6})^2 A_{sk6} \\
&= 660.0 + 1828 + \frac{0.41 \times (45.64)^3}{12} + (22.62 - 30.85)^2 \times 15.98 \\
&\quad + (22.62 - 17.29)^2 \times 25.39 + (22.62 - 22.82)^2 \times 19.24 \\
&= 7541 \text{ mm}^4
\end{aligned} \tag{246}$$

A.2.6 Spar Cap Configuration 7

A diagram of the cross sectional area of the spar cap configuration is given in figure 15(g). The true area of the configuration, excluding the skin, was computed as,

$$A_{t7} = A_{t6} + A_{st1} = 41.37 + 24.57 = 65.94 \text{ mm}^2 \quad (247)$$

The centroid of the additional spar cap reinforcement, relative to the global configuration coordinates shown in figure 15(g), was computed as,

$$\begin{aligned} \bar{X}_{st7} &= W_{c6} - (w_{sp} + \bar{x}_{st1} + t_{st1}) = 45.64 - (20 + 8.206 + 0.64) = 16.79 \text{ mm} \\ \bar{Y}_{st7} &= H_{c6} - (\bar{y}_{st1} + t_{sk} + t_{st1}) = 20.41 - (3.081 + 0.41 + 0.64) = 16.28 \text{ mm} \end{aligned} \quad (248)$$

The total centroid of the configuration, relative to the global configuration coordinates shown in figure 15(g), was thus computed as,

$$\begin{aligned} \bar{X}_{c7} &= \frac{\sum \bar{X}_{c7(i)} A_{c7(i)}}{\sum A_{c7(i)}} \\ &= \frac{\bar{X}_{c6}(A_{sk6} + A_{t6}) + \bar{X}_{st7} A_{st1}}{A_{sk6} + A_{t7}} \\ &= \frac{22.62 \times (18.71 + 41.37) + 16.79 \times 24.57}{18.71 + 65.94} \\ &= 20.93 \text{ mm} \end{aligned} \quad (249)$$

$$\begin{aligned} \bar{Y}_{c7} &= \frac{\sum \bar{Y}_{c7(i)} A_{c7(i)}}{\sum A_{c7(i)}} \\ &= \frac{\bar{Y}_{c6}(A_{sk6} + A_{t6}) + \bar{Y}_{st7} A_{st1}}{A_{sk6} + A_{t7}} \\ &= \frac{17.31 \times (18.71 + 41.37) + 16.28 \times 24.57}{18.71 + 65.94} \\ &= 17.01 \text{ mm} \end{aligned} \quad (250)$$

Hence the total second moments of area of the configuration were computed as,

$$\begin{aligned} I_{c7xx} &= I_{c6xx} + I_{st1xx} + (\bar{Y}_{c7} - \bar{Y}_{c6})^2 (A_{sk6} + A_{t6}) + (\bar{Y}_{c7} - \bar{Y}_{st7})^2 A_{st1} \\ &= 1482 + 491.7 + (17.01 - 17.31)^2 \times (18.71 + 41.37) + (17.01 - 16.28)^2 \times 24.57 \\ &= 1992 \text{ mm}^4 \end{aligned} \quad (251)$$

$$\begin{aligned}
I_{c7yy} &= I_{c6yy} + I_{st1yy} + (\bar{X}_{c7} - \bar{X}_{c6})^2(A_{sk6} + A_{t6}) + (\bar{X}_{c7} - \bar{X}_{st7})^2A_{st1} \\
&= 7541 + 1683 + (20.93 - 22.62)^2 \times (18.71 + 41.37) + (20.93 - 16.79)^2 \times 24.57 \quad (252) \\
&= 9817 \text{ mm}^4
\end{aligned}$$

A.2.7 Spar Cap Configuration 8

A diagram of the cross sectional area of the spar cap configuration is given in figure 15(h). The true area of the configuration, excluding the skin, was computed as,

$$A_{t8} = A_{sp} + A_{st7} = 15.98 + 16.66 = 32.64 \text{ mm}^2 \quad (253)$$

The total width and height of the configuration were computed as,

$$\begin{aligned}
W_{c8} &= W_{c1} + w_{st7} = 20 + 25.82 = 45.82 \text{ mm} \\
H_{c8} &= H_{c1} = 20.41 \text{ mm}
\end{aligned} \quad (254)$$

The true skin area was computed as,

$$A_{sk8} = W_{c8}t_{sk} = 45.82 \times 0.41 = 18.79 \text{ mm}^2 \quad (255)$$

The centroids of the skin, spar flange and web and spar cap reinforcement, relative to the global configuration coordinates shown in figure 15(h), were computed, respectively, as,

$$\begin{aligned}
\bar{X}_{sk8} &= \frac{W_{c8}}{2} = \frac{45.82}{2} = 22.91 \text{ mm} \\
\bar{Y}_{sk8} &= \bar{Y}_{sk1} = 20.21 \text{ mm} \\
\bar{X}_{sp8} &= \bar{x}_{sp} + w_{st7} = 5.213 + 25.82 = 30.03 \text{ mm} \\
\bar{Y}_{sp8} &= \bar{Y}_{sp1} = 14.79 \text{ mm} \\
\bar{X}_{st8} &= W_{c8} - (w_{sp} + \bar{x}_{st7}) = 45.64 - (20 + 8.262) = 17.38 \text{ mm} \\
\bar{Y}_{st8} &= H_{c8} - (\bar{y}_{st7} + t_{sk}) = 20.41 - (3.188 + 0.41) = 16.81 \text{ mm}
\end{aligned} \quad (256)$$

The total centroid of the configuration, relative to the global configuration coordinates shown in figure 15(h), was thus computed as,

$$\begin{aligned}
\bar{X}_{c8} &= \frac{\sum \bar{X}_{c8(i)} A_{c8(i)}}{\sum A_{c8(i)}} \\
&= \frac{\bar{X}_{sk8} A_{sk8} + \bar{X}_{sp8} A_{sp} + \bar{X}_{st8} A_{st7}}{A_{sk8} + A_{sp} + A_{st7}} \\
&= \frac{22.91 \times 18.79 + 30.03 \times 15.98 + 17.38 \times 16.66}{18.79 + 15.98 + 16.66} \\
&= 23.33 \text{ mm}
\end{aligned} \tag{257}$$

$$\begin{aligned}
\bar{Y}_{c8} &= \frac{\sum \bar{Y}_{c8(i)} A_{c8(i)}}{\sum A_{c8(i)}} \\
&= \frac{\bar{Y}_{sk8} A_{sk8} + \bar{Y}_{sp8} A_{sp} + \bar{Y}_{st8} A_{st7}}{A_{sk8} + A_{sp} + A_{st7}} \\
&= \frac{20.21 \times 18.79 + 14.79 \times 15.98 + 16.81 \times 16.66}{18.79 + 15.98 + 16.66} \\
&= 17.42 \text{ mm}
\end{aligned} \tag{258}$$

Hence the total second moments of area of the configuration were computed as,

$$\begin{aligned}
I_{c8xx} &= I_{spxx} + I_{st7xx} + \frac{W_{c8} t_{sk}^3}{12} + (\bar{Y}_{c8} - \bar{Y}_{sp8})^2 A_{sp} \\
&\quad + (\bar{Y}_{c8} - \bar{Y}_{st8})^2 A_{st7} + (\bar{Y}_{c8} - \bar{Y}_{sk8})^2 A_{sk8} \\
&= 660.0 + 372.8 + \frac{45.82 \times (0.41)^3}{12} + (17.42 - 14.79)^2 \times 15.98 \\
&\quad + (17.42 - 16.81)^2 \times 16.66 + (17.42 - 20.21)^2 \times 18.71 \\
&= 1295 \text{ mm}^4
\end{aligned} \tag{259}$$

$$\begin{aligned}
I_{c8yy} &= I_{spyy} + I_{st7yy} + \frac{t_{sk} W_{c8}^3}{12} + (\bar{X}_{c8} - \bar{X}_{sp8})^2 A_{sp} \\
&\quad + (\bar{X}_{c8} - \bar{X}_{st8})^2 A_{st7} + (\bar{X}_{c8} - \bar{X}_{sk8})^2 A_{sk8} \\
&= 660.0 + 1217 + \frac{0.41 \times (45.82)^3}{12} + (23.33 - 30.03)^2 \times 15.98 \\
&\quad + (23.33 - 17.38)^2 \times 16.66 + (23.33 - 22.91)^2 \times 18.71 \\
&= 6474 \text{ mm}^4
\end{aligned} \tag{260}$$

A.2.8 Spar Cap Configuration 9

A diagram of the cross sectional area of the spar cap configuration is given in figure 16(i). The true area of the configuration, excluding the skin, was computed as,

$$A_{t9} = A_{t8} + A_{st6} = 32.64 + 16.32 = 48.96 \text{ mm}^2 \quad (261)$$

The centroid of the additional spar cap reinforcement, relative to the global configuration coordinates shown in figure 16(i), was computed as,

$$\begin{aligned} \bar{X}_{st9} &= W_{c8} - (w_{sp} + \bar{x}_{st6} + t_{st2}) = 45.82 - (20 + 8.168 + 0.41) = 17.24 \text{ mm} \\ \bar{Y}_{st9} &= H_{c8} - (\bar{y}_{st6} + t_{sk} + t_{st2}) = 20.41 - (3.091 + 0.41 + 0.41) = 16.50 \text{ mm} \end{aligned} \quad (262)$$

The total centroid of the configuration, relative to the global configuration coordinates shown in figure 16(i), was thus computed as,

$$\begin{aligned} \bar{X}_{c9} &= \frac{\sum \bar{X}_{c9(i)} A_{c9(i)}}{\sum A_{c9(i)}} \\ &= \frac{\bar{X}_{c8}(A_{sk8} + A_{t8}) + \bar{X}_{st9} A_{st6}}{A_{sk8} + A_{t9}} \\ &= \frac{23.33 \times (18.79 + 32.64) + 17.24 \times 16.32}{18.79 + 48.96} \\ &= 21.86 \text{ mm} \end{aligned} \quad (263)$$

$$\begin{aligned} \bar{Y}_{c9} &= \frac{\sum \bar{Y}_{c9(i)} A_{c9(i)}}{\sum A_{c9(i)}} \\ &= \frac{\bar{Y}_{c8}(A_{sk8} + A_{t8}) + \bar{Y}_{st9} A_{st6}}{A_{sk8} + A_{t9}} \\ &= \frac{17.42 \times (18.79 + 32.64) + 16.50 \times 16.32}{18.79 + 48.96} \\ &= 17.20 \text{ mm} \end{aligned} \quad (264)$$

Hence the total second moments of area of the configuration were computed as,

$$\begin{aligned} I_{c9xx} &= I_{c8xx} + I_{st6xx} + (\bar{Y}_{c9} - \bar{Y}_{c8})^2 (A_{sk8} + A_{t8}) + (\bar{Y}_{c9} - \bar{Y}_{st9})^2 A_{st6} \\ &= 1295 + 345.2 + (17.20 - 17.42)^2 \times (18.79 + 32.64) + (17.20 - 16.50)^2 \times 16.32 \quad (265) \\ &= 1651 \text{ mm}^4 \end{aligned}$$

$$\begin{aligned}
I_{c9yy} &= I_{c8yy} + I_{st6yy} + (\bar{X}_{c9} - \bar{X}_{c8})^2(A_{sk8} + A_{t8}) + (\bar{X}_{c9} - \bar{X}_{st9})^2A_{st6} \\
&= 6474 + 1155 + (21.86 - 23.33)^2 \times (18.79 + 32.64) + (21.86 - 17.24)^2 \times 16.32 \quad (266) \\
&= 8089 \text{ mm}^4
\end{aligned}$$

A.2.9 Spar Cap Configuration 10

A diagram of the cross sectional area of the spar cap configuration is given in figure 16(j). The true area of the configuration, excluding the skin, was computed as,

$$A_{t10} = A_{t9} + A_{st5} = 48.96 + 15.98 = 64.94 \text{ mm}^2 \quad (267)$$

The centroid of the additional spar cap reinforcement, relative to the global configuration coordinates shown in figure 16(j), was computed as,

$$\begin{aligned}
\bar{X}_{st10} &= W_{c8} - (w_{sp} + \bar{x}_{st5} + 2t_{st2}) = 45.82 - (20 + 8.074 + 2 \times 0.41) = 16.93 \text{ mm} \\
\bar{Y}_{st10} &= H_{c8} - (\bar{y}_{st5} + t_{sk} + 2t_{st2}) = 20.41 - (2.995 + 0.41 + 2 \times 0.41) = 16.19 \text{ mm} \quad (268)
\end{aligned}$$

The total centroid of the configuration, relative to the global configuration coordinates shown in figure 16(j), was thus computed as,

$$\begin{aligned}
\bar{X}_{c10} &= \frac{\sum \bar{X}_{c10(i)} A_{c10(i)}}{\sum A_{c10(i)}} \\
&= \frac{\bar{X}_{c9}(A_{sk8} + A_{t9}) + \bar{X}_{st10} A_{st5}}{A_{sk8} + A_{t10}} \\
&= \frac{21.86 \times (18.79 + 48.96) + 16.93 \times 15.98}{18.79 + 64.94} \\
&= 20.92 \text{ mm}
\end{aligned} \quad (269)$$

$$\begin{aligned}
\bar{Y}_{c10} &= \frac{\sum \bar{Y}_{c10(i)} A_{c10(i)}}{\sum A_{c10(i)}} \\
&= \frac{\bar{Y}_{c9}(A_{sk8} + A_{t9}) + \bar{Y}_{st10} A_{st5}}{A_{sk8} + A_{t10}} \\
&= \frac{17.20 \times (18.79 + 48.96) + 16.19 \times 15.98}{18.79 + 64.94} \\
&= 17.01 \text{ mm}
\end{aligned} \quad (270)$$

Hence the total second moments of area of the configuration were computed as,

$$\begin{aligned}
 I_{c10xx} &= I_{c9xx} + I_{st5xx} + (\bar{Y}_{c10} - \bar{Y}_{c9})^2(A_{sk8} + A_{t9}) + (\bar{Y}_{c10} - \bar{Y}_{st10})^2 A_{st5} \\
 &= 1651 + 319.0 + (17.01 - 17.20)^2 \times (18.79 + 48.96) + (17.01 - 16.19)^2 \times 15.98 \\
 &= 1983 \text{ mm}^4
 \end{aligned} \tag{271}$$

$$\begin{aligned}
 I_{c10yy} &= I_{c9yy} + I_{st5yy} + (\bar{X}_{c10} - \bar{X}_{c9})^2(A_{sk8} + A_{t9}) + (\bar{X}_{c10} - \bar{X}_{st10})^2 A_{st5} \\
 &= 8089 + 1095 + (20.92 - 21.86)^2 \times (18.79 + 48.96) + (20.92 - 16.93)^2 \times 15.98 \\
 &= 9498 \text{ mm}^4
 \end{aligned} \tag{272}$$

A.2.10 Spar Cap Configuration 11

A diagram of the cross sectional area of the spar cap configuration is given in figure 16(k). The true area of the configuration, excluding the skin, was computed as,

$$A_{t11} = A_{sp} + A_{st5} = 15.98 + 15.98 = 31.96 \text{ mm}^2 \tag{273}$$

The total width and height of the configuration were computed as,

$$\begin{aligned}
 W_{c11} &= W_{c1} + w_{st1} = 20 + 25 = 45 \text{ mm} \\
 H_{c11} &= H_{c1} = 20.41 \text{ mm}
 \end{aligned} \tag{274}$$

The true skin area was computed as,

$$A_{sk11} = W_{c11} t_{sk} = 45 \times 0.41 = 18.45 \text{ mm}^2 \tag{275}$$

The centroids of the skin, spar flange and web and spar cap reinforcement, relative to the global configuration coordinates shown in figure 16(k), were computed, respectively, as,

$$\begin{aligned}\bar{X}_{sk11} &= \frac{W_{c11}}{2} = \frac{45}{2} = 22.5 \text{ mm} \\ \bar{Y}_{sk11} &= \bar{Y}_{sk1} = 20.21 \text{ mm} \\ \bar{X}_{sp11} &= \bar{x}_{sp} + w_{st1} = 5.213 + 25 = 30.21 \text{ mm} \\ \bar{Y}_{sp11} &= \bar{Y}_{sp1} = 14.79 \text{ mm}\end{aligned}\tag{276}$$

$$\begin{aligned}\bar{X}_{st11} &= W_{c11} - (w_{sp} + \bar{x}_{st5}) = 45 - (20 + 8.074) = 16.93 \text{ mm} \\ \bar{Y}_{st11} &= H_{c11} - (\bar{y}_{st5} + t_{sk}) = 20.41 - (2.995 + 0.41) = 17.01 \text{ mm}\end{aligned}$$

The total centroid of the configuration, relative to the global configuration coordinates shown in figure 16(k), was thus computed as,

$$\begin{aligned}\bar{X}_{c11} &= \frac{\sum \bar{X}_{c11(i)} A_{c11(i)}}{\sum A_{c11(i)}} \\ &= \frac{\bar{X}_{sk11} A_{sk11} + \bar{X}_{sp11} A_{sp} + \bar{X}_{st11} A_{st5}}{A_{sk11} + A_{sp} + A_{st5}} \\ &= \frac{22.5 \times 18.45 + 30.21 \times 15.98 + 16.93 \times 15.98}{18.45 + 15.98 + 15.98} \\ &= 23.18 \text{ mm}\end{aligned}\tag{277}$$

$$\begin{aligned}\bar{Y}_{c11} &= \frac{\sum \bar{Y}_{c11(i)} A_{c11(i)}}{\sum A_{c11(i)}} \\ &= \frac{\bar{Y}_{sk11} A_{sk11} + \bar{Y}_{sp11} A_{sp} + \bar{Y}_{st11} A_{st5}}{A_{sk11} + A_{sp} + A_{st5}} \\ &= \frac{20.21 \times 18.45 + 14.79 \times 15.98 + 17.01 \times 15.98}{18.45 + 15.98 + 15.98} \\ &= 17.48 \text{ mm}\end{aligned}\tag{278}$$

Hence the total second moments of area of the configuration were computed as,

$$\begin{aligned}
I_{c11xx} &= I_{spxx} + I_{st5xx} + \frac{W_{c11}t_{sk}^3}{12} + (\bar{Y}_{c11} - \bar{Y}_{sp11})^2 A_{sp} \\
&\quad + (\bar{Y}_{c11} - \bar{Y}_{st11})^2 A_{st5} + (\bar{Y}_{c11} - \bar{Y}_{sk11})^2 A_{sk11} \\
&= 660.0 + 319.0 + \frac{45 \times (0.41)^3}{12} + (17.48 - 14.79)^2 \times 15.98 \quad (279) \\
&\quad + (17.48 - 17.01)^2 \times 15.98 + (17.48 - 20.21)^2 \times 18.45 \\
&= 1236 \text{ mm}^4
\end{aligned}$$

$$\begin{aligned}
I_{c11yy} &= I_{spyy} + I_{st5yy} + \frac{t_{sk}W_{c11}^3}{12} + (\bar{X}_{c11} - \bar{X}_{sp11})^2 A_{sp} \\
&\quad + (\bar{X}_{c11} - \bar{X}_{st11})^2 A_{st5} + (\bar{X}_{c11} - \bar{X}_{sk11})^2 A_{sk11} \\
&= 660.0 + 1095 + \frac{0.41 \times (45)^3}{12} + (23.18 - 30.21)^2 \times 15.98 \quad (280) \\
&\quad + (23.18 - 16.93)^2 \times 15.98 + (23.18 - 22.5)^2 \times 18.45 \\
&= 6291 \text{ mm}^4
\end{aligned}$$

B Spar Cap Stress Analysis Calculations

B.1 Spar Cap Configuration 1 Stress Analysis

B.1.1 Tension Failure

Spar cap configuration 1 is located in all four corners of the tailplane box, however it experiences the most critical tensile loading in the top-front corner as a result of load case 1. The critical failure point is at BL460, where, according to the analysis of section 2.5, the direct limit load, $P_{load} = 2633$ N. From the area computed for spar cap configuration 1 in appendix A.2.1, the allowable load, given a rivet hole diameter, $d_r = 3.2$ mm,

$$\begin{aligned} P_{allow} &= A_{nett} F_{tu} = [A_{t1} + A_{sk1} - d_r(t_{sp} + t_{sk})] F_{tu} \\ &= [15.98 + 8.200 - 3.2 \times (0.41 + 0.41)] \times 406.5 \\ &= 8763 \text{ N} \end{aligned} \quad (281)$$

Hence the margin of safety,

$$MS = \frac{P_{allow}}{F_{uf} P_{load}} - 1 = \frac{8763}{1.5 \times 2633} - 1 = 1.219 \quad (282)$$

B.1.2 Compression Yield Failure

Spar cap configuration 1 is located in all four corners of the tailplane box, however it experiences the most critical compressive loading in the top-front corner as a result of load case 2. The critical failure point is at BL460, where, according to the analysis of section 2.5, the direct limit load, $P_{load} = 1197$ N. From the area computed for spar cap configuration 1 in appendix A.2.1, the allowable load,

$$P_{allow} = A_{gross} F_{cy} = (A_{t1} + A_{sk1}) F_{cy} = (15.98 + 8.200) \times 248.0 = 5997 \text{ N} \quad (283)$$

Hence the margin of safety,

$$MS = \frac{P_{allow}}{F_{uf} P_{load}} - 1 = \frac{5997}{1.5 \times 1197} - 1 = 2.340 \quad (284)$$

B.1.3 Crippling Failure

Spar cap configuration 1 is located in all four corners of the tailplane box, however it experiences the most critical crippling load without diagonal tension in the top-front corner as a result of load case 2. The critical failure point is at BL460, where, according to the analysis of section 2.5, the direct limit load, $P_{load} = 1197$ N. Needham's method was first used to compute the allowable stress. As the only angled element in spar cap configuration 1 is the spar flange and web, the allowable stress, as computed in section 2.8.2.2 and given in table

16, is $F_{allow} = 103.5 \text{ N/mm}^2$. From the allowable stress, the effective inter-rivet and edge skin widths were computed, respectively, as,

$$\begin{aligned} w_{eff_{ir}} &= 1.7 t_{sk} \sqrt{\frac{E_c}{F_{allow}}} = 1.7 \times 0.41 \times \sqrt{\frac{7.372 \times 10^4}{103.5}} = 18.60 \text{ mm} \\ w_{eff_{edge}} &= 0.6 t_{sk} \sqrt{\frac{E_c}{F_{allow}}} = \frac{0.6}{1.7} \times 18.60 = 6.565 \text{ mm} \end{aligned} \quad (285)$$

From these, the total effective skin width was obtained as the sum of the non-overlapping portions of effective skin width, from which the effective skin area, A_{eff} , was obtained. Given the inter-rivet distance between spar flange rivet lines is $> 200 \text{ mm}$, the total effective skin width was computed as,

$$w_{eff} = w_{eff_{edge}} + \frac{1}{2} w_{eff_{ir}} = 6.565 + \frac{1}{2} \times 18.60 = 15.87 \text{ mm} \quad (286)$$

Accounting for longitudinal inter-rivet buckling, for an inter-rivet distance to thickness ratio of $R_{ir} = d_{ir}/t = 24/0.41 \approx 59$, from figure 32 in appendix D, the inter-rivet buckling stress for a universal head rivet, $F_{ir} \approx 11 \text{ ksi} = 75.79 \text{ N/mm}^2$. Hence the total effective skin width was corrected to be,

$$w_{corrected} = \min \left(\frac{F_{ir}}{F_{allow}} w_{eff}, w_{eff} \right) = \frac{75.79}{103.5} \times 15.87 = 11.62 \text{ mm} \quad (287)$$

Hence the effective skin area,

$$A_{eff} = w_{corrected} t_{sk} = 11.62 \times 0.41 = 4.764 \text{ mm}^2 \quad (288)$$

Hence the allowable crippling load was computed, for spar cap configuration 1, as,

$$P_{allow} = (A_{t1} + A_{eff}) F_{allow} = (15.98 + 4.764) \times 103.5 = 2147 \text{ N} \quad (289)$$

Hence the margin of safety,

$$MS = \frac{P_{allow}}{F_{uf} P_{load}} - 1 = \frac{2147}{1.5 \times 1197} - 1 = 0.1958 \quad (290)$$

B.1.4 Crippling Failure with Diagonal Tension

Spar cap configuration 1 is located in all four corners of the tailplane box, however it experiences the most critical crippling load with diagonal tension in the top-rear corner as a result of load case 2. The critical failure point is at BL532, where, according to the analysis of section 2.5, the direct limit load, $P_{load} = 1047 \text{ N}$. The largest contribution resulting from diagonal tension at BL532 originates from the upper skin of the tailplane box. The skin shear buckling ratio at this point was taken to be the maximum skin shear buckling ratio

either side of the corresponding rib, $BR = 2.128$, as given in table 12. Likewise, the skin shear flow and inter-rib distance were taken to be the maximum either side of the rib at BL532, $q_{sk} = 2.423 \text{ N/mm}$ and $b = 192 \text{ mm}$ respectively. Hence the diagonal tension factor was found from figure 33 in appendix D to be $k \approx 0.15$, and thus the maximum bending moment experienced by the spar cap was computed as,

$$M_{max} = \frac{kq_{sk}b^2}{12} = \frac{0.15 \times 2.423 \times (192)^2}{12} = 1117 \text{ N} \cdot \text{mm} \quad (291)$$

Hence the total applied stress at the critical point was computed as,

$$\begin{aligned} F_{total} &= \frac{P_{load}}{(A_{t1} + A_{sk1})} + M_{max} \frac{\bar{X}_{c1}}{I_{c1yy}} \\ &= \frac{1047}{15.98 + 8.200} + 1117 \times \frac{6.836}{1058} \\ &= 50.52 \text{ N/mm}^2 \end{aligned} \quad (292)$$

Hence the margin of safety,

$$MS = \frac{F_{allow}}{F_{uf}F_{total}} - 1 = \frac{103.5}{1.5 \times 50.52} - 1 = 0.3658 \quad (293)$$

B.1.5 Shear Failure

Spar cap configuration 1 is located in all four corners of the tailplane box, however it experiences the most critical shear flow in the bottom-rear corner as a result of diagonal tension from load case 1. The critical failure point is at BL844, where, according to the analysis of section 2.5, the rear spar shear flow, $q_{sp} = 15.43 \text{ N/mm}$. The skin shear buckling ratio at this point is $BR = 1.213$, as given in table 11. Hence the diagonal tension factor was found from figure 33 in appendix D to be $k \approx 0.04$, and thus the increase in shear flow in the spar cap at BL844 was computed as,

$$q_{inc} = q_{sp}\sqrt{1+k} = 15.43 \times \sqrt{1+0.04} = 15.74 \text{ N/mm} \quad (294)$$

Hence, for a shear ultimate strength, $F_{su} = 254.9 \text{ N/mm}^2$ and inter-rivet distance, $d_{ir} = 24 \text{ mm}$, the margin of safety was computed as,

$$\begin{aligned} MS &= \frac{F_{su}(d_{ir} - d_r)(t_{sk} + t_{sp})}{F_{uf}q_{inc}d_{ir}} - 1 \\ &= \frac{254.9 \times (24 - 3.2)(0.41 + 0.41)}{1.5 \times 15.74 \times 24} - 1 \\ &= 6.673 \end{aligned} \quad (295)$$

Rivet Shear Failure

Spar cap configuration 1 is located in all four corners of the tailplane box, however it experiences the most critical shear flow in the bottom-rear corner as a result of diagonal tension from load case 1. The critical failure point is at BL844, where, according to the analysis of section 2.5, the rear spar shear flow, $q_{sp} = 15.43 \text{ N/mm}$. From the increase in shear flow given in (294), the fastener load in the spar cap at BL844 was computed as,

$$P_{fast} = d_{ir}q_{inc} = 24 \times 15.74 = 377.8 \text{ N} \quad (296)$$

Hence, for a pop rivet ultimate load, $P_{ru} = 600 \text{ N}$, taken from figure 3, the margin of safety was computed as,

$$MS = \frac{P_{ru}}{F_{uf}P_{fast}} - 1 = \frac{600}{1.5 \times 377.8} - 1 = 0.05876 \quad (297)$$

B.2 Spar Cap Configuration 3 Stress Analysis

B.2.1 Tension Failure

Spar cap configuration 3 is located in the bottom-front corner of the tailplane box and, as such, experiences the most critical tensile loading as a result of load case 2. The critical failure point is at BL268, where, according to the analysis of section 2.5, the direct limit load, $P_{load} = 2021 \text{ N}$. From the area computed for spar cap configuration 3 in appendix A.2.2, the allowable load, given a rivet hole diameter, $d_r = 3.2 \text{ mm}$,

$$\begin{aligned} P_{allow} &= A_{nett}F_{tu} = [A_{t3} + A_{sk2} - 2d_r(2t_{st1} + t_{sp} + t_{sk})] F_{tu} \\ &= [69.22 + 19.24 - 2 \times 3.2 \times (2 \times 0.64 + 0.41 + 0.41)] \times 406.5 \\ &= 30496 \text{ N} \end{aligned} \quad (298)$$

Hence the margin of safety,

$$MS = \frac{P_{allow}}{F_{uf}P_{load}} - 1 = \frac{30496}{1.5 \times 2021} - 1 = 9.060 \quad (299)$$

B.2.2 Compression Yield Failure

Spar cap configuration 3 is located in the bottom-front corner of the tailplane box and, as such, experiences the most critical compressive loading as a result of load case 1. The critical failure point is at BL268, where, according to the analysis of section 2.5, the direct limit load, $P_{load} = 4445 \text{ N}$. From the area computed for spar cap configuration 3 in appendix A.2.2, the allowable load,

$$P_{allow} = A_{gross}F_{cy} = (A_{t3} + A_{sk2})F_{cy} = (69.22 + 19.24) \times 248.0 = 21938 \text{ N} \quad (300)$$

Hence the margin of safety,

$$MS = \frac{P_{allow}}{F_{uf}P_{load}} - 1 = \frac{21938}{1.5 \times 4445} - 1 = 2.290 \quad (301)$$

B.2.3 Crippling Failure

Spar cap configuration 3 is located in the bottom-front corner of the tailplane box and, as such, experiences the most critical crippling load without diagonal tension as a result of load case 1. The critical failure point is at BL268, where, according to the analysis of section 2.5, the direct limit load, $P_{load} = 4445$ N. Needham's method was first used to compute the allowable stress. Derived data used to compute the allowable crippling stress at BL268 for spar cap configuration 3 is given in table 22.

Table 22: Derived data used to compute the allowable crippling stress at BL268 for spar cap configuration 3 (appendix A.2.2).

Component	c	t [mm]	C_e	A_m [mm 2]	A_t [mm 2]	E_c [N/mm 2]	F_{cy} [N/mm 2]	F_{cs} [N/mm 2]	$A_m F_{cs}$ [N]		
Spar Flange and Web	30.75	0.41	0.316	16.23	15.98	7.372×10^4	248.0	103.5	1680		
Spar Cap Reinforcement 3	32.75	0.64	0.316	26.83	26.21	7.372×10^4	248.0	98.70	2648		
Spar Cap Reinforcement 4	33.75	0.64	0.316	27.65	27.03	7.372×10^4	248.0	96.49	2668		
Σ					70.71	69.22	Σ				

Dividing the spar cap into individual angled components, the crippling stress for each angled element was computed as,

$$F_{cs} = C_e \frac{\sqrt{E_c F_{cy}}}{c^{0.75}} \quad (302)$$

where $C_e = 0.316$ for angled elements with two free edges, E_c is the compressive modulus, F_{cy} is the compressive yield strength, and c is the average side length divided by thickness of the angled element, as computed in section 2.7.2 and appendix A.1. The allowable stress was then computed as,

$$F_{allow} = \frac{\sum A_{m(i)} F_{cs(i)}}{\sum A_{m(i)}} = \frac{6996}{70.71} = 98.94 \text{ N/mm}^2 \quad (303)$$

where $A_{m(i)}$ and $F_{cs(i)}$ are the mid-line areas, as computed in section 2.7.2 and appendix A.1, and crippling stresses respectively of each angled element. From the allowable stress, the effective inter-rivet and edge skin widths were computed, respectively, as,

$$w_{eff_{ir}} = 1.7 t_{sk} \sqrt{\frac{E_c}{F_{allow}}} = 1.7 \times 0.41 \times \sqrt{\frac{7.372 \times 10^4}{98.94}} = 19.03 \text{ mm}$$

$$(304)$$

$$w_{eff_{edge}} = 0.6 t_{sk} \sqrt{\frac{E_c}{F_{allow}}} = \frac{0.6}{1.7} \times 19.03 = 6.717 \text{ mm}$$

From these, the total effective skin width was obtained as the sum of the non-overlapping portions of effective skin width, from which the effective skin area, A_{eff} , was obtained. Given the inter-rivet distance between the spar flange and spar cap reinforcement rivet lines is 25 mm, the total effective skin width was computed as,

$$w_{eff} = w_{eff_{edge}} + \frac{3}{2} w_{eff_{ir}} = 6.717 + \frac{3}{2} \times 19.03 = 35.26 \text{ mm} \quad (305)$$

Accounting for longitudinal inter-rivet buckling, for an inter-rivet distance to thickness ratio of $R_{ir} = d_{ir}/t = 24/0.41 \approx 59$, from figure 32 in appendix D, the inter-rivet buckling stress for a universal head rivet, $F_{ir} \approx 11 \text{ ksi} = 75.79 \text{ N/mm}^2$. Hence the total effective skin width was corrected to be,

$$w_{corrected} = \min \left(\frac{F_{ir}}{F_{allow}} w_{eff}, w_{eff} \right) = \frac{75.79}{98.94} \times 35.26 = 27.01 \text{ mm} \quad (306)$$

Hence the effective skin area,

$$A_{eff} = w_{corrected} t_{sk} = 27.01 \times 0.41 = 11.07 \text{ mm}^2 \quad (307)$$

Hence the allowable crippling load was computed, for spar cap configuration 3, as,

$$P_{allow} = (A_{t3} + A_{eff}) F_{allow} = (69.22 + 11.07) \times 98.94 = 7944 \text{ N} \quad (308)$$

Hence the margin of safety,

$$MS = \frac{P_{allow}}{F_{uf} P_{load}} - 1 = \frac{7944}{1.5 \times 4445} - 1 = 0.1915 \quad (309)$$

B.2.4 Crippling Failure with Diagonal Tension

Spar cap configuration 3 is located in the bottom-front corner of the tailplane box and, as such, experiences the most critical crippling load with diagonal tension as a result of load case 1. The critical failure point is at BL340, where, according to the analysis of section 2.5, the direct limit load, $P_{load} = 3322 \text{ N}$. The allowable crippling stress is given in (303) for spar cap configuration 3 and the largest contribution resulting from diagonal tension at BL340 originates from the lower skin of the tailplane box. The skin shear buckling ratio at this point was taken to be the maximum skin shear buckling ratio either side of the corresponding rib, $BR = 4.682$, as given in table 11. Likewise, the skin shear flow and inter-rib distance

were taken to be the maximum either side of the rib at BL340, $q_{sk} = 10.36 \text{ N/mm}$ and $b = 192 \text{ mm}$ respectively. Hence the diagonal tension factor was found from figure 33 in appendix D to be $k \approx 0.32$, and thus the maximum bending moment experienced by the spar cap was computed as,

$$M_{max} = \frac{kq_{sk}b^2}{12} = \frac{0.32 \times 10.36 \times (192)^2}{12} = 10184 \text{ N} \cdot \text{mm} \quad (310)$$

Hence the total applied stress at the critical point was computed as,

$$\begin{aligned} F_{total} &= \frac{P_{load}}{(A_{t3} + A_{sk2})} + M_{max} \frac{\bar{X}_{c3}}{I_{c3yy}} \\ &= \frac{3322}{69.22 + 19.24} + 10184 \times \frac{21.76}{10830} \\ &= 58.02 \text{ N/mm}^2 \end{aligned} \quad (311)$$

Hence the margin of safety,

$$MS = \frac{F_{allow}}{F_{uf}F_{total}} - 1 = \frac{98.94}{1.5 \times 58.02} - 1 = 0.1368 \quad (312)$$

B.2.5 Shear Failure

Spar cap configuration 3 is located in the bottom-front corner of the tailplane box and experiences the most critical shear flow as a result of load case 1. The critical failure point is at BL316, where, according to the analysis of section 2.5, the bottom skin shear flow, $q_{sk} = 12.53 \text{ N/mm}$. For a shear ultimate strength, $F_{su} = 254.9 \text{ N/mm}^2$ and inter-rivet distance, $d_{ir} = 24 \text{ mm}$, the margin of safety was computed as,

$$\begin{aligned} MS &= \frac{F_{su}(d_{ir} - d_r)(t_{sk} + 2t_{st1})}{F_{uf}q_{sk}d_{ir}} - 1 \\ &= \frac{254.9 \times (24 - 3.2)(0.41 + 2 \times 0.64)}{1.5 \times 12.53 \times 24} - 1 \\ &= 18.86 \end{aligned} \quad (313)$$

B.2.6 Rivet Shear Failure

Spar cap configuration 3 is located in the bottom-front corner of the tailplane box and experiences the most critical shear flow as a result of load case 1. The critical failure point is at BL316, where, according to the analysis of section 2.5, the bottom skin shear flow, $q_{sk} = 12.53 \text{ N/mm}$. For a pop rivet ultimate load, $P_{ru} = 600 \text{ N}$, taken from figure 3, the margin of safety was computed as,

$$MS = \frac{P_{ru}}{F_{uf}q_{sk}d_{ir}} - 1 = \frac{600}{1.5 \times 12.53 \times 24} - 1 = 0.3301 \quad (314)$$

B.3 Spar Cap Configuration 4 Stress Analysis

B.3.1 Tension Failure

Spar cap configuration 4 is located in the bottom-front corner of the tailplane box and, as such, experiences the most critical tensile loading as a result of load case 2. The critical failure point is at BL196, where, according to the analysis of section 2.5, the direct limit load, $P_{load} = 2680$ N. From the area computed for spar cap configuration 4 in appendix A.2.3, the allowable load, given a rivet hole diameter, $d_r = 3.2$ mm,

$$\begin{aligned} P_{allow} &= A_{nett}F_{tu} = [A_{t4} + A_{sk2} - 2d_r(3t_{st1} + t_{sp} + t_{sk})] F_{tu} \\ &= [94.61 + 19.24 - 2 \times 3.2 \times (3 \times 0.64 + 0.41 + 0.41)] \times 406.5 \\ &= 39152 \text{ N} \end{aligned} \quad (315)$$

Hence the margin of safety,

$$MS = \frac{P_{allow}}{F_{uf}P_{load}} - 1 = \frac{39152}{1.5 \times 2680} - 1 = 8.739 \quad (316)$$

Compression Yield Failure

Spar cap configuration 4 is located in the bottom-front corner of the tailplane box and, as such, experiences the most critical compressive loading as a result of load case 1. The critical failure point is at BL196, where, according to the analysis of section 2.5, the direct limit load, $P_{load} = 5896$ N. From the area computed for spar cap configuration 4 in appendix A.2.3, the allowable load,

$$P_{allow} = A_{gross}F_{cy} = (A_{t4} + A_{sk2})F_{cy} = (94.61 + 19.24) \times 248.0 = 28235 \text{ N} \quad (317)$$

Hence the margin of safety,

$$MS = \frac{P_{allow}}{F_{uf}P_{load}} - 1 = \frac{28235}{1.5 \times 5896} - 1 = 2.193 \quad (318)$$

B.3.2 Crippling Failure

Spar cap configuration 4 is located in the bottom-front corner of the tailplane box and, as such, experiences the most critical crippling load without diagonal tension as a result of load case 1. The critical failure point is at BL196, where, according to the analysis of section 2.5, the direct limit load, $P_{load} = 5896$ N. Needham's method was first used to compute the

allowable stress. Derived data used to compute the allowable crippling stress at BL196 for spar cap configuration 4 is given in table 23.

Table 23: Derived data used to compute the allowable crippling stress at BL196 for spar cap configuration 4 (appendix A.2.3).

Component	c	t [mm]	C_e	A_m [mm 2]	A_t [mm 2]	E_c [N/mm 2]	F_{cy} [N/mm 2]	F_{cs} [N/mm 2]	$A_m F_{cs}$ [N]
Spar Flange and Web	30.75	0.41	0.316	16.23	15.98	7.372×10^4	248.0	103.5	1680
Spar Cap Reinforcement 2	31.75	0.64	0.316	26.01	25.39	7.372×10^4	248.0	101.0	2627
Spar Cap Reinforcement 3	32.75	0.64	0.316	26.83	26.21	7.372×10^4	248.0	98.70	2648
Spar Cap Reinforcement 4	33.75	0.64	0.316	27.65	27.03	7.372×10^4	248.0	96.49	2668
			Σ	96.72	94.61			Σ	9623

Dividing the spar cap into individual angled components, the crippling stress for each angled element was computed as,

$$F_{cs} = C_e \frac{\sqrt{E_c F_{cy}}}{c^{0.75}} \quad (319)$$

where $C_e = 0.316$ for angled elements with two free edges, E_c is the compressive modulus, F_{cy} is the compressive yield strength, and c is the average side length divided by thickness of the angled element, as computed in section 2.7.2 and appendix A.1. The allowable stress was then computed as,

$$F_{allow} = \frac{\sum A_{m(i)} F_{cs(i)}}{\sum A_{m(i)}} = \frac{9623}{96.72} = 99.49 \text{ N/mm}^2 \quad (320)$$

where $A_{m(i)}$ and $F_{cs(i)}$ are the mid-line areas, as computed in section 2.7.2 and appendix A.1, and crippling stresses respectively of each angled element. From the allowable stress, the effective inter-rivet and edge skin widths were computed, respectively, as,

$$\begin{aligned} w_{eff_{ir}} &= 1.7 t_{sk} \sqrt{\frac{E_c}{F_{allow}}} = 1.7 \times 0.41 \times \sqrt{\frac{7.372 \times 10^4}{99.49}} = 18.97 \text{ mm} \\ w_{eff_{edge}} &= 0.6 t_{sk} \sqrt{\frac{E_c}{F_{allow}}} = \frac{0.6}{1.7} \times 18.97 = 6.695 \text{ mm} \end{aligned} \quad (321)$$

From these, the total effective skin width was obtained as the sum of the non-overlapping portions of effective skin width, from which the effective skin area, A_{eff} , was obtained. Given the inter-rivet distance between the spar flange and spar cap reinforcement rivet lines is 25 mm, the total effective skin width was computed as,

$$w_{eff} = w_{eff_{edge}} + \frac{3}{2} w_{eff_{ir}} = 6.695 + \frac{3}{2} \times 18.97 = 35.15 \text{ mm} \quad (322)$$

Accounting for longitudinal inter-rivet buckling, for an inter-rivet distance to thickness ratio of $R_{ir} = d_{ir}/t = 24/0.41 \approx 59$, from figure 32 in appendix D, the inter-rivet buckling stress for a universal head rivet, $F_{ir} \approx 11 \text{ ksi} = 75.79 \text{ N/mm}^2$. Hence the total effective skin width was corrected to be,

$$w_{corrected} = \min \left(\frac{F_{ir}}{F_{allow}} w_{eff}, w_{eff} \right) = \frac{75.79}{99.49} \times 35.15 = 26.78 \text{ mm} \quad (323)$$

Hence the effective skin area,

$$A_{eff} = w_{corrected} t_{sk} = 26.78 \times 0.41 = 10.98 \text{ mm}^2 \quad (324)$$

Hence the allowable crippling load was computed, for spar cap configuration 4, as,

$$P_{allow} = (A_{t4} + A_{eff}) F_{allow} = (94.61 + 10.98) \times 99.49 = 10505 \text{ N} \quad (325)$$

Hence the margin of safety,

$$MS = \frac{P_{allow}}{F_{uf} P_{load}} - 1 = \frac{10505}{1.5 \times 5896} - 1 = 0.1878 \quad (326)$$

B.3.3 Crippling Failure with Diagonal Tension

Spar cap configuration 4 is located in the bottom-front corner of the tailplane box and, as such, experiences the most critical crippling load with diagonal tension as a result of load case 1. The critical failure point is at BL244, where, according to the analysis of section 2.5, the direct limit load, $P_{load} = 4861 \text{ N}$. The allowable crippling stress is given in (320) for spar cap configuration 4 and the largest contribution resulting from diagonal tension at BL244 originates from the front spar of the tailplane box. The spar shear buckling ratio at this point was taken to be the maximum spar shear buckling ratio either side of the corresponding rib, $BR = 2.135$, as given in table 11. Likewise, the skin shear flow and inter-rib distance were taken to be the maximum either side of the rib at BL244, $q_{sp} = 10.88 \text{ N/mm}$ and $b = 120 \text{ mm}$ respectively. Hence the diagonal tension factor was found from figure 33 in appendix D to be $k \approx 0.16$, and thus the maximum bending moment experienced by the spar cap was computed as,

$$M_{max} = \frac{k q_{sp} b^2}{12} = \frac{0.16 \times 10.88 \times (120)^2}{12} = 2089 \text{ N} \cdot \text{mm} \quad (327)$$

Hence the total applied stress at the critical point was computed as,

$$\begin{aligned}
F_{total} &= \frac{P_{load}}{(A_{t4} + A_{sk2})} + M_{max} \frac{\bar{Y}_{c4}}{I_{c4xx}} \\
&= \frac{4861}{94.61 + 19.24} + 2089 \times \frac{16.53}{2885} \\
&= 54.67 \text{ N/mm}^2
\end{aligned} \tag{328}$$

Hence the margin of safety,

$$MS = \frac{F_{allow}}{F_{uf}F_{total}} - 1 = \frac{99.49}{1.5 \times 54.67} - 1 = 0.2132 \tag{329}$$

B.3.4 Shear Failure

Spar cap configuration 4 is located in the bottom-front corner of the tailplane box and, as such, experiences the most critical shear flow as a result of diagonal tension from load case 1. The critical failure point is at BL244, where, according to the analysis of section 2.5, the bottom skin shear flow was taken to be the maximum shear flow either side of the corresponding rib, $q_{sk} = 12.53 \text{ N/mm}$. Likewise, the skin shear buckling ratio at this point was taken to be the maximum either side of the rib at BL244, $BR = 5.455$, as given in table 11. Hence the diagonal tension factor was found from figure 33 in appendix D to be $k \approx 0.35$, and thus the increase in shear flow in the spar cap at BL244 was computed as,

$$q_{inc} = q_{sk}\sqrt{1+k} = 12.53 \times \sqrt{1+0.35} = 14.56 \text{ N/mm} \tag{330}$$

Hence, for a shear ultimate strength, $F_{su} = 254.9 \text{ N/mm}^2$ and inter-rivet distance, $d_{ir} = 24 \text{ mm}$, the margin of safety was computed as,

$$\begin{aligned}
MS &= \frac{F_{su}(d_{ir} - d_r)(t_{sk} + 3t_{st1})}{F_{uf}q_{inc}d_{ir}} - 1 \\
&= \frac{254.9 \times (24 - 3.2)(0.41 + 3 \times 0.64)}{1.5 \times 14.56 \times 24} - 1 \\
&= 22.57
\end{aligned} \tag{331}$$

B.3.5 Rivet Shear Failure

Spar cap configuration 4 is located in the bottom-front corner of the tailplane box and, as such, experiences the most critical shear flow as a result of diagonal tension from load case 1. The critical failure point is at BL244, where, according to the analysis of section 2.5, the bottom skin shear flow, $q_{sk} = 12.53 \text{ N/mm}$. From the increase in shear flow given in (330), the fastener load in the spar cap at BL244 was computed as,

$$P_{fast} = d_{ir}q_{inc} = 24 \times 14.56 = 349.4 \text{ N} \quad (332)$$

Hence, for a pop rivet ultimate load, $P_{ru} = 600 \text{ N}$, taken from figure 3, the margin of safety was computed as,

$$MS = \frac{P_{ru}}{F_{uf}P_{fast}} - 1 = \frac{600}{1.5 \times 349.4} - 1 = 0.1448 \quad (333)$$

B.4 Spar Cap Configuration 5 Stress Analysis

B.4.1 Tension Failure

Spar cap configuration 5 is located in the bottom-front corner of the tailplane box and, as such, experiences the most critical tensile loading as a result of load case 2. The critical failure point is at BL124, where, according to the analysis of section 2.5, the direct limit load, $P_{load} = 3466 \text{ N}$. From the area computed for spar cap configuration 5 in appendix A.2.4, the allowable load, given a rivet hole diameter, $d_r = 3.2 \text{ mm}$,

$$\begin{aligned} P_{allow} &= A_{nett}F_{tu} = [A_{t5} + A_{sk2} - 2d_r(4t_{st1} + t_{sp} + t_{sk})] F_{tu} \\ &= [119.2 + 19.24 - 2 \times 3.2 \times (4 \times 0.64 + 0.41 + 0.41)] \times 406.5 \\ &= 47482 \text{ N} \end{aligned} \quad (334)$$

Hence the margin of safety,

$$MS = \frac{P_{allow}}{F_{uf}P_{load}} - 1 = \frac{47482}{1.5 \times 3466} - 1 = 8.133 \quad (335)$$

B.4.2 Compression Yield Failure

Spar cap configuration 5 is located in the bottom-front corner of the tailplane box and, as such, experiences the most critical compressive loading as a result of load case 1. The critical failure point is at BL124, where, according to the analysis of section 2.5, the direct limit load, $P_{load} = 7626 \text{ N}$. From the area computed for spar cap configuration 5 in appendix A.2.4, the allowable load,

$$P_{allow} = A_{gross}F_{cy} = (A_{t5} + A_{sk2})F_{cy} = (119.2 + 19.24) \times 248.0 = 34333 \text{ N} \quad (336)$$

Hence the margin of safety,

$$MS = \frac{P_{allow}}{F_{uf}P_{load}} - 1 = \frac{34333}{1.5 \times 7626} - 1 = 2.001 \quad (337)$$

B.4.3 Crippling Failure

Spar cap configuration 5 is located in the bottom-front corner of the tailplane box and, as such, experiences the most critical crippling load without diagonal tension as a result of load case 1. The critical failure point is at BL148, where, according to the analysis of section 2.5, the direct limit load, $P_{load} = 7025$ N. Needham's method was first used to compute the allowable stress. Derived data used to compute the allowable crippling stress at BL148 for spar cap configuration 5 is given in table 24.

Table 24: Derived data used to compute the allowable crippling stress at BL148 for spar cap configuration 5 (appendix A.2.4).

Component	c	t [mm]	C_e	A_m [mm 2]	A_t [mm 2]	E_c [N/mm 2]	F_{cy} [N/mm 2]	F_{cs} [N/mm 2]	$A_m F_{cs}$ [N]
Spar Flange and Web	30.75	0.41	0.316	16.23	15.98	7.372×10^4	248.0	103.5	1680
Spar Cap Reinforcement 1	30.75	0.64	0.316	25.19	24.57	7.372×10^4	248.0	103.5	2607
Spar Cap Reinforcement 2	31.75	0.64	0.316	26.01	25.39	7.372×10^4	248.0	101.0	2627
Spar Cap Reinforcement 3	32.75	0.64	0.316	26.83	26.21	7.372×10^4	248.0	98.70	2648
Spar Cap Reinforcement 4	33.75	0.64	0.316	27.65	27.03	7.372×10^4	248.0	96.49	2668
				Σ	121.9	119.2		Σ	12230

Dividing the spar cap into individual angled components, the crippling stress for each angled element was computed as,

$$F_{cs} = C_e \frac{\sqrt{E_c F_{cy}}}{c^{0.75}} \quad (338)$$

where $C_e = 0.316$ for angled elements with two free edges, E_c is the compressive modulus, F_{cy} is the compressive yield strength, and c is the average side length divided by thickness of the angled element, as computed in section 2.7.2 and appendix A.1. The allowable stress was then computed as,

$$F_{allow} = \frac{\sum A_{m(i)} F_{cs(i)}}{\sum A_{m(i)}} = \frac{12230}{121.9} = 100.3 \text{ N/mm}^2 \quad (339)$$

where $A_{m(i)}$ and $F_{cs(i)}$ are the mid-line areas, as computed in section 2.7.2 and appendix A.1, and crippling stresses respectively of each angled element. From the allowable stress, the effective inter-rivet and edge skin widths were computed, respectively, as,

$$\begin{aligned} w_{eff_{ir}} &= 1.7 t_{sk} \sqrt{\frac{E_c}{F_{allow}}} = 1.7 \times 0.41 \times \sqrt{\frac{7.372 \times 10^4}{100.3}} = 18.90 \text{ mm} \\ w_{eff_{edge}} &= 0.6 t_{sk} \sqrt{\frac{E_c}{F_{allow}}} = \frac{0.6}{1.7} \times 18.90 = 6.671 \text{ mm} \end{aligned} \quad (340)$$

From these, the total effective skin width was obtained as the sum of the non-overlapping portions of effective skin width, from which the effective skin area, A_{eff} , was obtained. Given

the inter-rivet distance between the spar flange and spar cap reinforcement rivet lines is 25 mm, the total effective skin width was computed as,

$$w_{eff} = w_{eff_{edge}} + \frac{3}{2}w_{eff_{ir}} = 6.671 + \frac{3}{2} \times 18.90 = 35.02 \text{ mm} \quad (341)$$

Accounting for longitudinal inter-rivet buckling, for an inter-rivet distance to thickness ratio of $R_{ir} = d_{ir}/t = 24/0.41 \approx 59$, from figure 32 in appendix D, the inter-rivet buckling stress for a universal head rivet, $F_{ir} \approx 11 \text{ ksi} = 75.79 \text{ N/mm}^2$. Hence the total effective skin width was corrected to be,

$$w_{corrected} = \min \left(\frac{F_{ir}}{F_{allow}} w_{eff}, w_{eff} \right) = \frac{75.79}{100.3} \times 35.02 = 26.46 \text{ mm} \quad (342)$$

Hence the effective skin area,

$$A_{eff} = w_{corrected} t_{sk} = 26.46 \times 0.41 = 10.85 \text{ mm}^2 \quad (343)$$

Hence the allowable crippling load was computed, for spar cap configuration 5, as,

$$P_{allow} = (A_{t5} + A_{eff})F_{allow} = (119.2 + 10.85) \times 100.3 = 13044 \text{ N} \quad (344)$$

Hence the margin of safety,

$$MS = \frac{P_{allow}}{F_{uf}P_{load}} - 1 = \frac{13044}{1.5 \times 7025} - 1 = 0.2379 \quad (345)$$

B.4.4 Crippling Failure with Diagonal Tension

Spar cap configuration 5 is located in the bottom-front corner of the tailplane box and, as such, experiences the most critical crippling load with diagonal tension as a result of load case 1. The critical failure point is at BL124, where, according to the analysis of section 2.5, the direct limit load, $P_{load} = 7626 \text{ N}$. The allowable crippling stress is given in (339) for spar cap configuration 5 and the largest contribution resulting from diagonal tension at BL124 originates from the front spar of the tailplane box. The spar shear buckling ratio at this point was taken to be the maximum spar shear buckling ratio either side of the corresponding rib, $BR = 2.135$, as given in table 11. Likewise, the skin shear flow and inter-rib distance were taken to be the maximum either side of the rib at BL124, $q_{sp} = 10.88 \text{ N/mm}$ and $b = 120 \text{ mm}$ respectively. Hence the diagonal tension factor was found from figure 33 in appendix D to be $k \approx 0.16$, and thus the maximum bending moment experienced by the spar cap is identical to that in (327) computed for spar cap configuration 4, $M_{max} = 2089 \text{ N} \cdot \text{mm}$. Hence the total applied stress at the critical point was computed as,

$$\begin{aligned}
F_{total} &= \frac{P_{load}}{(A_{t5} + A_{sk2})} + M_{max} \frac{\bar{Y}_{c5}}{I_{c5xx}} \\
&= \frac{7626}{119.2 + 19.24} + 2089 \times \frac{16.26}{3424} \\
&= 65.01 \text{ N/mm}^2
\end{aligned} \tag{346}$$

Hence the margin of safety,

$$MS = \frac{F_{allow}}{F_{uf}F_{total}} - 1 = \frac{100.3}{1.5 \times 65.01} - 1 = 0.02856 \tag{347}$$

B.4.5 Shear Failure

Spar cap configuration 5 is located in the bottom-front corner of the tailplane box and, as such, experiences the most critical shear flow as a result of diagonal tension from load case 1. The critical failure point is at BL124, where, according to the analysis of section 2.5, the bottom skin shear flow was taken to be the maximum shear flow either side of the corresponding rib, $q_{sk} = 12.53 \text{ N/mm}$. Likewise, the skin shear buckling ratio at this point was taken to be the maximum either side of the rib at BL124, $BR = 5.455$, as given in table 11. Hence the diagonal tension factor was found from figure 33 in appendix D to be $k \approx 0.35$, and thus the increase in shear flow in the spar cap at BL124 is identical to that in (330) computed for spar cap configuration 4, $q_{inc} = 14.56 \text{ N/mm}$. Hence, for a shear ultimate strength, $F_{su} = 254.9 \text{ N/mm}^2$ and inter-rivet distance, $d_{ir} = 24 \text{ mm}$, the margin of safety was computed as,

$$\begin{aligned}
MS &= \frac{F_{su}(d_{ir} - d_r)(t_{sk} + 4t_{st1})}{F_{uf}q_{inc}d_{ir}} - 1 \\
&= \frac{254.9 \times (24 - 3.2)(0.41 + 4 \times 0.64)}{1.5 \times 14.56 \times 24} - 1 \\
&= 29.04
\end{aligned} \tag{348}$$

B.4.6 Rivet Shear Failure

Spar cap configuration 5 is located in the bottom-front corner of the tailplane box and, as such, experiences the most critical shear flow as a result of diagonal tension from load case 1. The critical failure point is at BL124, where, according to the analysis of section 2.5, the bottom skin shear flow, $q_{sk} = 12.53 \text{ N/mm}$. Given the increase in shear flow in (330) is identical for both spar cap configurations 4 and 5, the fastener load in the spar cap at BL124 is also identical to that in (332) computed for spar cap configuration 4, $P_{fast} = 349.4 \text{ N}$. Hence, for a pop rivet ultimate load, $P_{ru} = 600 \text{ N}$, taken from figure 3, the margin of safety was computed as,

$$MS = \frac{P_{ru}}{F_{uf}P_{fast}} - 1 = \frac{600}{1.5 \times 349.4} - 1 = 0.1448 \quad (349)$$

B.5 Spar Cap Configuration 6 Stress Analysis

B.5.1 Tension Failure

Spar cap configuration 6 is located in the bottom-rear corner of the tailplane box and, as such, experiences the most critical tensile loading as a result of load case 2. The critical failure point is at BL364, where, according to the analysis of section 2.5, the direct limit load, $P_{load} = 1266$ N. From the area computed for spar cap configuration 6 in appendix A.2.5, the allowable load, given a rivet hole diameter, $d_r = 3.2$ mm,

$$\begin{aligned} P_{allow} &= A_{nett}F_{tu} = [A_{t6} + A_{sk6} - 2d_r(t_{st1} + t_{sp} + t_{sk})] F_{tu} \\ &= [41.37 + 18.71 - 2 \times 3.2 \times (0.64 + 0.41 + 0.41)] \times 406.5 \\ &= 20624 \text{ N} \end{aligned} \quad (350)$$

Hence the margin of safety,

$$MS = \frac{P_{allow}}{F_{uf}P_{load}} - 1 = \frac{20624}{1.5 \times 1266} - 1 = 9.861 \quad (351)$$

B.5.2 Compression Yield Failure

Spar cap configuration 6 is located in the bottom-rear corner of the tailplane box and, as such, experiences the most critical compressive loading as a result of load case 1. The critical failure point is at BL364, where, according to the analysis of section 2.5, the direct limit load, $P_{load} = 2786$ N. From the area computed for spar cap configuration 6 in appendix A.2.5, the allowable load,

$$P_{allow} = A_{gross}F_{cy} = (A_{t6} + A_{sk6})F_{cy} = (41.37 + 18.71) \times 248.0 = 14900 \text{ N} \quad (352)$$

Hence the margin of safety,

$$MS = \frac{P_{allow}}{F_{uf}P_{load}} - 1 = \frac{14900}{1.5 \times 2786} - 1 = 2.565 \quad (353)$$

B.5.3 Crippling Failure

Spar cap configuration 6 is located in the bottom-rear corner of the tailplane box and, as such, experiences the most critical crippling load without diagonal tension as a result of load case 1. The critical failure point is at BL364, where, according to the analysis of section

2.5, the direct limit load, $P_{load} = 2786$ N. Needham's method was first used to compute the allowable stress. Derived data used to compute the allowable crippling stress at BL364 for spar cap configuration 6 is given in table 25.

Table 25: Derived data used to compute the allowable crippling stress at BL364 for spar cap configuration 6 (appendix A.2.5).

Component	c	t [mm]	C_e	A_m [mm 2]	A_t [mm 2]	E_c [N/mm 2]	F_{cy} [N/mm 2]	F_{cs} [N/mm 2]	$A_m F_{cs}$ [N]
Spar Flange and Web	30.75	0.41	0.316	16.23	15.98	7.372×10^4	248.0	103.5	1680
Spar Cap Reinforcement 2	31.75	0.64	0.316	26.01	25.39	7.372×10^4	248.0	101.0	2627
			Σ	42.24	41.37			Σ	4307

Dividing the spar cap into individual angled components, the crippling stress for each angled element was computed as,

$$F_{cs} = C_e \frac{\sqrt{E_c F_{cy}}}{c^{0.75}} \quad (354)$$

where $C_e = 0.316$ for angled elements with two free edges, E_c is the compressive modulus, F_{cy} is the compressive yield strength, and c is the average side length divided by thickness of the angled element, as computed in section 2.7.2 and appendix A.1. The allowable stress was then computed as,

$$F_{allow} = \frac{\sum A_{m(i)} F_{cs(i)}}{\sum A_{m(i)}} = \frac{4307}{42.24} = 102.0 \text{ N/mm}^2 \quad (355)$$

where $A_{m(i)}$ and $F_{cs(i)}$ are the mid-line areas, as computed in section 2.7.2 and appendix A.1, and crippling stresses respectively of each angled element. From the allowable stress, the effective inter-rivet and edge skin widths were computed, respectively, as,

$$\begin{aligned} w_{eff_{ir}} &= 1.7 t_{sk} \sqrt{\frac{E_c}{F_{allow}}} = 1.7 \times 0.41 \times \sqrt{\frac{7.372 \times 10^4}{102.0}} = 18.74 \text{ mm} \\ w_{eff_{edge}} &= 0.6 t_{sk} \sqrt{\frac{E_c}{F_{allow}}} = \frac{0.6}{1.7} \times 18.74 = 6.614 \text{ mm} \end{aligned} \quad (356)$$

From these, the total effective skin width was obtained as the sum of the non-overlapping portions of effective skin width, from which the effective skin area, A_{eff} , was obtained. Given the inter-rivet distance between the spar flange and spar cap reinforcement rivet lines is 25 mm, the total effective skin width was computed as,

$$w_{eff} = w_{eff_{edge}} + \frac{3}{2} w_{eff_{ir}} = 6.614 + \frac{3}{2} \times 18.74 = 34.72 \text{ mm} \quad (357)$$

Accounting for longitudinal inter-rivet buckling, for an inter-rivet distance to thickness ratio of $R_{ir} = d_{ir}/t = 24/0.41 \approx 59$, from figure 32 in appendix D, the inter-rivet buckling stress

for a universal head rivet, $F_{ir} \approx 11 \text{ ksi} = 75.79 \text{ N/mm}^2$. Hence the total effective skin width was corrected to be,

$$w_{corrected} = \min \left(\frac{F_{ir}}{F_{allow}} w_{eff}, w_{eff} \right) = \frac{75.79}{102.0} \times 34.72 = 25.80 \text{ mm} \quad (358)$$

Hence the effective skin area,

$$A_{eff} = w_{corrected} t_{sk} = 25.80 \times 0.41 = 10.58 \text{ mm}^2 \quad (359)$$

Hence the allowable crippling load was computed, for spar cap configuration 6, as,

$$P_{allow} = (A_{t6} + A_{eff}) F_{allow} = (41.37 + 10.58) \times 102.0 = 5299 \text{ N} \quad (360)$$

Hence the margin of safety,

$$MS = \frac{P_{allow}}{F_{uf} P_{load}} - 1 = \frac{5299}{1.5 \times 2786} - 1 = 0.2680 \quad (361)$$

B.5.4 Crippling Failure with Diagonal Tension

Spar cap configuration 6 is located in the bottom-rear corner of the tailplane box and, as such, experiences the most critical crippling load with diagonal tension as a result of load case 1. The critical failure point is at BL532, where, according to the analysis of section 2.5, the direct limit load, $P_{load} = 2298 \text{ N}$. The allowable crippling stress is given in (355) for spar cap configuration 6 and the largest contribution resulting from diagonal tension at BL532 originates from the rear spar of the tailplane box. The spar shear buckling ratio at this point was taken to be the maximum spar shear buckling ratio either side of the corresponding rib, $BR = 1.310$, as given in table 11. Likewise, the spar shear flow and inter-rib distance were taken to be the maximum either side of the rib at BL532, $q_{sp} = 10.84 \text{ N/mm}$ and $b = 192 \text{ mm}$ respectively. Hence the diagonal tension factor was found from figure 33 in appendix D to be $k \approx 0.05$, and thus the maximum bending moment experienced by the spar cap was computed as,

$$M_{max} = \frac{k q_{sk} b^2}{12} = \frac{0.05 \times 10.84 \times (192)^2}{12} = 1665 \text{ N} \cdot \text{mm} \quad (362)$$

Hence the total applied stress at the critical point was computed as,

$$\begin{aligned} F_{total} &= \frac{P_{load}}{(A_{t6} + A_{sk6})} + M_{max} \frac{\bar{Y}_{c6}}{I_{c6xx}} \\ &= \frac{2298}{41.37 + 18.71} + 1665 \times \frac{17.31}{1482} \\ &= 57.70 \text{ N/mm}^2 \end{aligned} \quad (363)$$

Hence the margin of safety,

$$MS = \frac{F_{allow}}{F_{uf}F_{total}} - 1 = \frac{102.0}{1.5 \times 57.70} - 1 = 0.1785 \quad (364)$$

B.5.5 Shear Failure

Spar cap configuration 6 is located in the bottom-rear corner of the tailplane box and, as such, experiences the most critical shear flow as a result of diagonal tension from load case 1. The critical failure point is at BL700, where, according to the analysis of section 2.5, the rear spar shear flow was taken to be the maximum shear flow either side of the corresponding rib, $q_{sp} = 15.43 \text{ N/mm}$. Likewise, the spar shear buckling ratio at this point was taken to be the maximum either side of the rib at BL700, $BR = 1.259$, as given in table 11. Hence the diagonal tension factor was found from figure 33 in appendix D to be $k \approx 0.05$, and thus the increase in shear flow in the spar cap at BL700 was computed as,

$$q_{inc} = q_{sp}\sqrt{1+k} = 15.43 \times \sqrt{1+0.05} = 15.81 \text{ N/mm} \quad (365)$$

Hence, for a shear ultimate strength, $F_{su} = 254.9 \text{ N/mm}^2$ and inter-rivet distance, $d_{ir} = 24 \text{ mm}$, the margin of safety was computed as,

$$\begin{aligned} MS &= \frac{F_{su}(d_{ir} - d_r)(t_{sp} + t_{st1})}{F_{uf}q_{inc}d_{ir}} - 1 \\ &= \frac{254.9 \times (24 - 3.2)(0.41 + 0.64)}{1.5 \times 15.81 \times 24} - 1 \\ &= 8.781 \end{aligned} \quad (366)$$

B.5.6 Rivet Shear Failure

Spar cap configuration 6 is located in the bottom-rear corner of the tailplane box and, as such, experiences the most critical shear flow as a result of diagonal tension from load case 1. The critical failure point is at BL700, where, according to the analysis of section 2.5, the rear spar shear flow, $q_{sp} = 15.43 \text{ N/mm}$. From the increase in shear flow given in (365), the fastener load in the spar cap at BL700 was computed as,

$$P_{fast} = d_{ir}q_{inc} = 24 \times 15.81 = 379.4 \text{ N} \quad (367)$$

Hence, for a pop rivet ultimate load, $P_{ru} = 600 \text{ N}$, taken from figure 3, the margin of safety was computed as,

$$MS = \frac{P_{ru}}{F_{uf}P_{fast}} - 1 = \frac{600}{1.5 \times 379.4} - 1 = 0.05430 \quad (368)$$

B.6 Spar Cap Configuration 7 Stress Analysis

B.6.1 Tension Failure

Spar cap configuration 7 is located in the bottom-rear corner of the tailplane box and, as such, experiences the most critical tensile loading as a result of load case 2. The critical failure point is at BL340, where, according to the analysis of section 2.5, the direct limit load, $P_{load} = 1241$ N. From the area computed for spar cap configuration 7 in appendix A.2.6, the allowable load, given a rivet hole diameter, $d_r = 3.2$ mm,

$$\begin{aligned} P_{allow} &= A_{nett} F_{tu} = [A_{t7} + A_{sk6} - 2d_r(2t_{st1} + t_{sp} + t_{sk})] F_{tu} \\ &= [65.94 + 18.71 - 2 \times 3.2 \times (2 \times 0.64 + 0.41 + 0.41)] \times 406.5 \\ &= 28947 \text{ N} \end{aligned} \quad (369)$$

Hence the margin of safety,

$$MS = \frac{P_{allow}}{F_{uf} P_{load}} - 1 = \frac{28947}{1.5 \times 1241} - 1 = 14.55 \quad (370)$$

B.6.2 Compression Yield Failure

Spar cap configuration 7 is located in the bottom-rear corner of the tailplane box and, as such, experiences the most critical compressive loading as a result of load case 1. The critical failure point is at BL340, where, according to the analysis of section 2.5, the direct limit load, $P_{load} = 2731$ N. From the area computed for spar cap configuration 7 in appendix A.2.6, the allowable load,

$$P_{allow} = A_{gross} F_{cy} = (A_{t7} + A_{sk6}) F_{cy} = (65.94 + 18.71) \times 248.0 = 20993 \text{ N} \quad (371)$$

Hence the margin of safety,

$$MS = \frac{P_{allow}}{F_{uf} P_{load}} - 1 = \frac{20993}{1.5 \times 2731} - 1 = 4.125 \quad (372)$$

B.6.3 Crippling Failure

Spar cap configuration 7 is located in the bottom-rear corner of the tailplane box and, as such, experiences the most critical crippling load without diagonal tension as a result of load case 1. The critical failure point is at BL316, where, according to the analysis of section 2.5, the direct limit load, $P_{load} = 2521$ N. Needham's method was first used to compute the allowable stress. Derived data used to compute the allowable crippling stress at BL316 for spar cap configuration 7 is given in table 26.

Table 26: Derived data used to compute the allowable crippling stress at BL316 for spar cap configuration 7 (appendix A.2.6).

Component	c	t [mm]	C_e	A_m [mm 2]	A_t [mm 2]	E_c [N/mm 2]	F_{cy} [N/mm 2]	F_{cs} [N/mm 2]	$A_m F_{cs}$ [N]
Spar Flange and Web	30.75	0.41	0.316	16.23	15.98	7.372×10^4	248.0	103.5	1680
Spar Cap Reinforcement 1	30.75	0.64	0.316	25.19	24.57	7.372×10^4	248.0	103.5	2607
Spar Cap Reinforcement 2	31.75	0.64	0.316	26.01	25.39	7.372×10^4	248.0	101.0	2627
Σ				67.43	65.94	Σ			6914

Dividing the spar cap into individual angled components, the crippling stress for each angled element was computed as,

$$F_{cs} = C_e \frac{\sqrt{E_c F_{cy}}}{c^{0.75}} \quad (373)$$

where $C_e = 0.316$ for angled elements with two free edges, E_c is the compressive modulus, F_{cy} is the compressive yield strength, and c is the average side length divided by thickness of the angled element, as computed in section 2.7.2 and appendix A.1. The allowable stress was then computed as,

$$F_{allow} = \frac{\sum A_{m(i)} F_{cs(i)}}{\sum A_{m(i)}} = \frac{6914}{67.43} = 102.5 \text{ N/mm}^2 \quad (374)$$

where $A_{m(i)}$ and $F_{cs(i)}$ are the mid-line areas, as computed in section 2.7.2 and appendix A.1, and crippling stresses respectively of each angled element. From the allowable stress, the effective inter-rivet and edge skin widths were computed, respectively, as,

$$\begin{aligned} w_{eff_{ir}} &= 1.7 t_{sk} \sqrt{\frac{E_c}{F_{allow}}} = 1.7 \times 0.41 \times \sqrt{\frac{7.372 \times 10^4}{102.5}} = 18.69 \text{ mm} \\ w_{eff_{edge}} &= 0.6 t_{sk} \sqrt{\frac{E_c}{F_{allow}}} = \frac{0.6}{1.7} \times 18.69 = 6.597 \text{ mm} \end{aligned} \quad (375)$$

From these, the total effective skin width was obtained as the sum of the non-overlapping portions of effective skin width, from which the effective skin area, A_{eff} , was obtained. Given the inter-rivet distance between the spar flange and spar cap reinforcement rivet lines is 25 mm, the total effective skin width was computed as,

$$w_{eff} = w_{eff_{edge}} + \frac{3}{2} w_{eff_{ir}} = 6.597 + \frac{3}{2} \times 18.69 = 34.63 \text{ mm} \quad (376)$$

Accounting for longitudinal inter-rivet buckling, for an inter-rivet distance to thickness ratio of $R_{ir} = d_{ir}/t = 24/0.41 \approx 59$, from figure 32 in appendix D, the inter-rivet buckling stress for a universal head rivet, $F_{ir} \approx 11 \text{ ksi} = 75.79 \text{ N/mm}^2$. Hence the total effective skin width was corrected to be,

$$w_{corrected} = \min \left(\frac{F_{ir}}{F_{allow}} w_{eff}, w_{eff} \right) = \frac{75.79}{102.5} \times 34.63 = 25.61 \text{ mm} \quad (377)$$

Hence the effective skin area,

$$A_{eff} = w_{corrected} t_{sk} = 25.61 \times 0.41 = 10.50 \text{ mm}^2 \quad (378)$$

Hence the allowable crippling load was computed, for spar cap configuration 7, as,

$$P_{allow} = (A_{t7} + A_{eff}) F_{allow} = (65.94 + 10.50) \times 102.5 = 7835 \text{ N} \quad (379)$$

Hence the margin of safety,

$$MS = \frac{P_{allow}}{F_{uf} P_{load}} - 1 = \frac{7835}{1.5 \times 2521} - 1 = 1.072 \quad (380)$$

B.6.4 Crippling Failure with Diagonal Tension

Spar cap configuration 7 is located in the bottom-rear corner of the tailplane box and, as such, experiences the most critical crippling load with diagonal tension as a result of load case 1. The critical failure point is at BL340, where, according to the analysis of section 2.5, the direct limit load, $P_{load} = 2731 \text{ N}$. The allowable crippling stress is given in (374) for spar cap configuration 7 and the largest contribution resulting from diagonal tension at BL340 originates from the bottom skin of the tailplane box. The skin shear buckling ratio at this point was taken to be the maximum skin shear buckling ratio either side of the corresponding rib, $BR = 4.682$, as given in table 11. Likewise, the spar shear flow and inter-rib distance were taken to be the maximum either side of the rib at BL340, $q_{sk} = 10.36 \text{ N/mm}$ and $b = 192 \text{ mm}$ respectively. Hence the diagonal tension factor was found from figure 33 in appendix D to be $k \approx 0.33$, and thus the maximum bending moment experienced by the spar cap was computed as,

$$M_{max} = \frac{k q_{sk} b^2}{12} = \frac{0.33 \times 10.36 \times (192)^2}{12} = 10503 \text{ N} \cdot \text{mm} \quad (381)$$

Hence the total applied stress at the critical point was computed as,

$$\begin{aligned} F_{total} &= \frac{P_{load}}{(A_{t7} + A_{sk6})} + M_{max} \frac{\bar{X}_{c7}}{I_{c7yy}} \\ &= \frac{2731}{65.94 + 18.71} + 10503 \times \frac{20.93}{9817} \\ &= 54.65 \text{ N/mm}^2 \end{aligned} \quad (382)$$

Hence the margin of safety,

$$MS = \frac{F_{allow}}{F_{uf}F_{total}} - 1 = \frac{102.5}{1.5 \times 54.65} - 1 = 0.2504 \quad (383)$$

B.6.5 Shear Failure

Spar cap configuration 7 is located in the bottom-rear corner of the tailplane box and, as such, experiences the most critical shear flow as a result of diagonal tension from load case 1. The critical failure point is at BL244, where, according to the analysis of section 2.5, the bottom skin shear flow was taken to be the maximum shear flow either side of the corresponding rib, $q_{sk} = 12.53 \text{ N/mm}$. Likewise, the skin shear buckling ratio at this point was taken to be the maximum either side of the rib at BL244, $BR = 5.455$, as given in table 11. Hence the diagonal tension factor was found from figure 33 in appendix D to be $k \approx 0.35$, and thus the increase in shear flow in the spar cap at BL244 is identical to that in (330) computed for spar cap configuration 4, $q_{inc} = 14.56 \text{ N/mm}$. Hence, for a shear ultimate strength, $F_{su} = 254.9 \text{ N/mm}^2$ and inter-rivet distance, $d_{ir} = 24 \text{ mm}$, the margin of safety was computed as,

$$\begin{aligned} MS &= \frac{F_{su}(d_{ir} - d_r)(t_{sk} + 2t_{st1})}{F_{uf}q_{inc}d_{ir}} - 1 \\ &= \frac{254.9 \times (24 - 3.2)(0.41 + 2 \times 0.64)}{1.5 \times 14.56 \times 24} - 1 \\ &= 16.09 \end{aligned} \quad (384)$$

B.6.6 Rivet Shear Failure

Spar cap configuration 7 is located in the bottom-rear corner of the tailplane box and, as such, experiences the most critical shear flow as a result of diagonal tension from load case 1. The critical failure point is at BL244, where, according to the analysis of section 2.5, the bottom skin shear flow, $q_{sk} = 12.53 \text{ N/mm}$. Given the increase in shear flow in (330) is identical for both spar cap configurations 4 and 7, the fastener load in the spar cap at BL244 is also identical to that in (332) computed for spar cap configuration 4, $P_{fast} = 349.4 \text{ N}$. Hence, for a pop rivet ultimate load, $P_{ru} = 600 \text{ N}$, taken from figure 3, the margin of safety was computed as,

$$MS = \frac{P_{ru}}{F_{uf}P_{fast}} - 1 = \frac{600}{1.5 \times 349.4} - 1 = 0.1448 \quad (385)$$

B.7 Spar Cap Configuration 8 Stress Analysis

B.7.1 Tension Failure

Spar cap configuration 8 is located in the top-front corner of the tailplane box and, as such, experiences the most critical tensile loading as a result of load case 1. The critical failure point is at BL244, where, according to the analysis of section 2.5, the direct limit load, $P_{load} = 4872$ N. From the area computed for spar cap configuration 8 in appendix A.2.7, the allowable load, given a rivet hole diameter, $d_r = 3.2$ mm,

$$\begin{aligned} P_{allow} &= A_{nett} F_{tu} = [A_{t8} + A_{sk8} - 2d_r(t_{st2} + t_{sp} + t_{sk})] F_{tu} \\ &= [32.64 + 18.79 - 2 \times 3.2 \times (0.41 + 0.41 + 0.41)] \times 406.5 \\ &= 17706 \text{ N} \end{aligned} \quad (386)$$

Hence the margin of safety,

$$MS = \frac{P_{allow}}{F_{uf} P_{load}} - 1 = \frac{17706}{1.5 \times 4872} - 1 = 1.423 \quad (387)$$

B.7.2 Compression Yield Failure

Spar cap configuration 8 is located in the top-front corner of the tailplane box and, as such, experiences the most critical compressive loading as a result of load case 2. The critical failure point is at BL244, where, according to the analysis of section 2.5, the direct limit load, $P_{load} = 2214$ N. From the area computed for spar cap configuration 8 in appendix A.2.7, the allowable load,

$$P_{allow} = A_{gross} F_{cy} = (A_{t8} + A_{sk8}) F_{cy} = (32.64 + 18.79) \times 248.0 = 12755 \text{ N} \quad (388)$$

Hence the margin of safety,

$$MS = \frac{P_{allow}}{F_{uf} P_{load}} - 1 = \frac{12755}{1.5 \times 2214} - 1 = 2.841 \quad (389)$$

B.7.3 Crippling Failure

Spar cap configuration 8 is located in the top-front corner of the tailplane box and, as such, experiences the most critical crippling load without diagonal tension as a result of load case 2. The critical failure point is at BL268, where, according to the analysis of section 2.5, the direct limit load, $P_{load} = 2025$ N. Needham's method was first used to compute the allowable stress. Derived data used to compute the allowable crippling stress at BL268 for spar cap configuration 8 is given in table 27.

Table 27: Derived data used to compute the allowable crippling stress at BL268 for spar cap configuration 8 (appendix A.2.7).

Component	c	t [mm]	C_e	A_m [mm 2]	A_t [mm 2]	E_c [N/mm 2]	F_{cy} [N/mm 2]	F_{cs} [N/mm 2]	$A_m F_{cs}$ [N]
Spar Flange and Web	30.75	0.41	0.316	16.23	15.98	7.372×10^4	248.0	103.5	1680
Spar Cap Reinforcement 7	50.28	0.41	0.316	16.90	16.66	7.372×10^4	248.0	71.56	1209
			Σ	33.13	32.64			Σ	2889

Dividing the spar cap into individual angled components, the crippling stress for each angled element was computed as,

$$F_{cs} = C_e \frac{\sqrt{E_c F_{cy}}}{c^{0.75}} \quad (390)$$

where $C_e = 0.316$ for angled elements with two free edges, E_c is the compressive modulus, F_{cy} is the compressive yield strength, and c is the average side length divided by thickness of the angled element, as computed in section 2.7.2 and appendix A.1. The allowable stress was then computed as,

$$F_{allow} = \frac{\sum A_{m(i)} F_{cs(i)}}{\sum A_{m(i)}} = \frac{2889}{33.13} = 87.20 \text{ N/mm}^2 \quad (391)$$

where $A_{m(i)}$ and $F_{cs(i)}$ are the mid-line areas, as computed in section 2.7.2 and appendix A.1, and crippling stresses respectively of each angled element. From the allowable stress, the effective inter-rivet and edge skin widths were computed, respectively, as,

$$\begin{aligned} w_{eff_{ir}} &= 1.7 t_{sk} \sqrt{\frac{E_c}{F_{allow}}} = 1.7 \times 0.41 \times \sqrt{\frac{7.372 \times 10^4}{87.20}} = 20.27 \text{ mm} \\ w_{eff_{edge}} &= 0.6 t_{sk} \sqrt{\frac{E_c}{F_{allow}}} = \frac{0.6}{1.7} \times 20.27 = 7.154 \text{ mm} \end{aligned} \quad (392)$$

From these, the total effective skin width was obtained as the sum of the non-overlapping portions of effective skin width, from which the effective skin area, A_{eff} , was obtained. Given the inter-rivet distance between the spar flange and spar cap reinforcement rivet lines is 25 mm, the total effective skin width was computed as,

$$w_{eff} = w_{eff_{edge}} + \frac{3}{2} w_{eff_{ir}} = 7.154 + \frac{3}{2} \times 20.27 = 37.56 \text{ mm} \quad (393)$$

Accounting for longitudinal inter-rivet buckling, for an inter-rivet distance to thickness ratio of $R_{ir} = d_{ir}/t = 24/0.41 \approx 59$, from figure 32 in appendix D, the inter-rivet buckling stress for a universal head rivet, $F_{ir} \approx 11 \text{ ksi} = 75.79 \text{ N/mm}^2$. Hence the total effective skin width was corrected to be,

$$w_{corrected} = \min \left(\frac{F_{ir}}{F_{allow}} w_{eff}, w_{eff} \right) = \frac{75.79}{87.20} \times 37.56 = 32.65 \text{ mm} \quad (394)$$

Hence the effective skin area,

$$A_{eff} = w_{corrected} t_{sk} = 32.65 \times 0.41 = 13.39 \text{ mm}^2 \quad (395)$$

Hence the allowable crippling load was computed, for spar cap configuration 8, as,

$$P_{allow} = (A_{t8} + A_{eff})F_{allow} = (32.64 + 13.39) \times 87.20 = 4014 \text{ N} \quad (396)$$

Hence the margin of safety,

$$MS = \frac{P_{allow}}{F_{uf}P_{load}} - 1 = \frac{4014}{1.5 \times 2025} - 1 = 0.3215 \quad (397)$$

B.7.4 Crippling Failure with Diagonal Tension

Spar cap configuration 8 is located in the top-front corner of the tailplane box and, as such, experiences the most critical crippling load with diagonal tension as a result of load case 2. The critical failure point is at BL244, where, according to the analysis of section 2.5, the direct limit load, $P_{load} = 2214 \text{ N}$. The allowable crippling stress is given in (391) for spar cap configuration 8 and the largest contribution resulting from diagonal tension at BL244 originates from the top skin of the tailplane box. The skin shear buckling ratio at this point was taken to be the maximum skin shear buckling ratio either side of the corresponding rib, $BR = 2.480$, as given in table 12. Likewise, the spar shear flow and inter-rib distance were taken to be the maximum either side of the rib at BL244, $q_{sk} = 5.695 \text{ N/mm}$ and $b = 120 \text{ mm}$ respectively. Hence the diagonal tension factor was found from figure 33 in appendix D to be $k \approx 0.2$, and thus the maximum bending moment experienced by the spar cap was computed as,

$$M_{max} = \frac{kq_{sk}b^2}{12} = \frac{0.2 \times 5.695 \times (120)^2}{12} = 1367 \text{ N} \cdot \text{mm} \quad (398)$$

Hence the total applied stress at the critical point was computed as,

$$\begin{aligned} F_{total} &= \frac{P_{load}}{(A_{t8} + A_{sk8})} + M_{max} \frac{\bar{X}_{c8}}{I_{c8yy}} \\ &= \frac{2214}{32.64 + 18.79} + 1367 \times \frac{23.33}{6474} \\ &= 47.98 \text{ N/mm}^2 \end{aligned} \quad (399)$$

Hence the margin of safety,

$$MS = \frac{F_{allow}}{F_{uf}F_{total}} - 1 = \frac{87.20}{1.5 \times 47.98} - 1 = 0.2116 \quad (400)$$

B.7.5 Shear Failure

Spar cap configuration 8 is located in the top-front corner of the tailplane box and experiences the most critical shear flow as a result of load case 1. The critical failure point is at BL316, where, according to the analysis of section 2.5, the top skin shear flow, $q_{sk} = 10.36 \text{ N/mm}$. For a shear ultimate strength, $F_{su} = 254.9 \text{ N/mm}^2$ and inter-rivet distance, $d_{ir} = 24 \text{ mm}$, the margin of safety was computed as,

$$\begin{aligned} MS &= \frac{F_{su}(d_{ir} - d_r)(t_{sk} + t_{st2})}{F_{uf}q_{sk}d_{ir}} - 1 \\ &= \frac{254.9 \times (24 - 3.2)(0.41 + 0.41)}{1.5 \times 10.36 \times 24} - 1 \\ &= 11.66 \end{aligned} \quad (401)$$

B.7.6 Rivet Shear Failure

Spar cap configuration 8 is located in the top-front corner of the tailplane box and experiences the most critical shear flow as a result of load case 1. The critical failure point is at BL316, where, according to the analysis of section 2.5, the top skin shear flow, $q_{sk} = 10.36 \text{ N/mm}$. For a pop rivet ultimate load, $P_{ru} = 600 \text{ N}$, taken from figure 3, the margin of safety was computed as,

$$MS = \frac{P_{ru}}{F_{uf}q_{sk}d_{ir}} - 1 = \frac{600}{1.5 \times 10.36 \times 24} - 1 = 0.6088 \quad (402)$$

B.8 Spar Cap Configuration 9 Stress Analysis

B.8.1 Tension Failure

Spar cap configuration 9 is located in the top-front corner of the tailplane box and, as such, experiences the most critical tensile loading as a result of load case 1. The critical failure point is at BL172, where, according to the analysis of section 2.5, the direct limit load, $P_{load} = 6462 \text{ N}$. From the area computed for spar cap configuration 9 in appendix A.2.8, the allowable load, given a rivet hole diameter, $d_r = 3.2 \text{ mm}$,

$$\begin{aligned} P_{allow} &= A_{nett}F_{tu} = [A_{t9} + A_{sk8} - 2d_r(2t_{st2} + t_{sp} + t_{sk})] F_{tu} \\ &= [48.96 + 18.79 - 2 \times 3.2 \times (2 \times 0.41 + 0.41 + 0.41)] \times 406.5 \\ &= 23274 \text{ N} \end{aligned} \quad (403)$$

Hence the margin of safety,

$$MS = \frac{P_{allow}}{F_{uf}P_{load}} - 1 = \frac{23274}{1.5 \times 6462} - 1 = 1.401 \quad (404)$$

B.8.2 Compression Yield Failure

Spar cap configuration 9 is located in the top-front corner of the tailplane box and, as such, experiences the most critical compressive loading as a result of load case 2. The critical failure point is at BL172, where, according to the analysis of section 2.5, the direct limit load, $P_{load} = 2937$ N. From the area computed for spar cap configuration 9 in appendix A.2.8, the allowable load,

$$P_{allow} = A_{gross}F_{cy} = (A_{t9} + A_{sk8})F_{cy} = (48.96 + 18.79) \times 248.0 = 16802 \text{ N} \quad (405)$$

Hence the margin of safety,

$$MS = \frac{P_{allow}}{F_{uf}P_{load}} - 1 = \frac{16802}{1.5 \times 2937} - 1 = 2.814 \quad (406)$$

B.8.3 Crippling Failure

Spar cap configuration 9 is located in the top-front corner of the tailplane box and, as such, experiences the most critical crippling load without diagonal tension as a result of load case 2. The critical failure point is at BL172, where, according to the analysis of section 2.5, the direct limit load, $P_{load} = 2937$ N. Needham's method was first used to compute the allowable stress. Derived data used to compute the allowable crippling stress at BL172 for spar cap configuration 9 is given in table 28.

Table 28: Derived data used to compute the allowable crippling stress at BL172 for spar cap configuration 9 (appendix A.2.8).

Component	c	t [mm]	C_e	A_m [mm 2]	A_t [mm 2]	E_c [N/mm 2]	F_{cy} [N/mm 2]	F_{cs} [N/mm 2]	$A_m F_{cs}$ [N]
Spar Flange and Web	30.75	0.41	0.316	16.23	15.98	7.372×10^4	248.0	103.5	1680
Spar Cap Reinforcement 6	49.28	0.41	0.316	16.57	16.32	7.372×10^4	248.0	72.64	1204
Spar Cap Reinforcement 7	50.28	0.41	0.316	16.90	16.66	7.372×10^4	248.0	71.56	1209
				Σ	49.70	48.96		Σ	4093

Dividing the spar cap into individual angled components, the crippling stress for each angled element was computed as,

$$F_{cs} = C_e \frac{\sqrt{E_c F_{cy}}}{c^{0.75}} \quad (407)$$

where $C_e = 0.316$ for angled elements with two free edges, E_c is the compressive modulus, F_{cy} is the compressive yield strength, and c is the average side length divided by thickness of the angled element, as computed in section 2.7.2 and appendix A.1. The allowable stress was then computed as,

$$F_{allow} = \frac{\sum A_{m(i)} F_{cs(i)}}{\sum A_{m(i)}} = \frac{4093}{49.70} = 82.35 \text{ N/mm}^2 \quad (408)$$

where $A_{m(i)}$ and $F_{cs(i)}$ are the mid-line areas, as computed in section 2.7.2 and appendix A.1, and crippling stresses respectively of each angled element. From the allowable stress, the effective inter-rivet and edge skin widths were computed, respectively, as,

$$\begin{aligned} w_{eff_{ir}} &= 1.7 t_{sk} \sqrt{\frac{E_c}{F_{allow}}} = 1.7 \times 0.41 \times \sqrt{\frac{7.372 \times 10^4}{82.35}} = 20.85 \text{ mm} \\ w_{eff_{edge}} &= 0.6 t_{sk} \sqrt{\frac{E_c}{F_{allow}}} = \frac{0.6}{1.7} \times 20.85 = 7.359 \text{ mm} \end{aligned} \quad (409)$$

From these, the total effective skin width was obtained as the sum of the non-overlapping portions of effective skin width, from which the effective skin area, A_{eff} , was obtained. Given the inter-rivet distance between the spar flange and spar cap reinforcement rivet lines is 25 mm, the total effective skin width was computed as,

$$w_{eff} = w_{eff_{edge}} + \frac{3}{2} w_{eff_{ir}} = 7.359 + \frac{3}{2} \times 20.85 = 38.63 \text{ mm} \quad (410)$$

Accounting for longitudinal inter-rivet buckling, for an inter-rivet distance to thickness ratio of $R_{ir} = d_{ir}/t = 24/0.41 \approx 59$, from figure 32 in appendix D, the inter-rivet buckling stress for a universal head rivet, $F_{ir} \approx 11 \text{ ksi} = 75.79 \text{ N/mm}^2$. Hence the total effective skin width was corrected to be,

$$w_{corrected} = \min \left(\frac{F_{ir}}{F_{allow}} w_{eff}, w_{eff} \right) = \frac{75.79}{82.35} \times 38.63 = 35.55 \text{ mm} \quad (411)$$

Hence the effective skin area,

$$A_{eff} = w_{corrected} t_{sk} = 35.55 \times 0.41 = 14.58 \text{ mm}^2 \quad (412)$$

Hence the allowable crippling load was computed, for spar cap configuration 9, as,

$$P_{allow} = (A_{t9} + A_{eff}) F_{allow} = (48.96 + 14.58) \times 82.35 = 5233 \text{ N} \quad (413)$$

Hence the margin of safety,

$$MS = \frac{P_{allow}}{F_{uf} P_{load}} - 1 = \frac{5233}{1.5 \times 2937} - 1 = 0.1878 \quad (414)$$

B.8.4 Crippling Failure with Diagonal Tension

Spar cap configuration 9 is located in the top-front corner of the tailplane box between ribs BL124 and BL244, hence there are no secondary effects due to diagonal tension within the span occupied by this configuration.

B.8.5 Shear Failure

Spar cap configuration 9 is located in the top-front corner of the tailplane box and experiences the most critical shear flow as a result of load case 1. The critical failure point is at BL220, where, according to the analysis of section 2.5, the top skin shear flow, $q_{sk} = 12.53 \text{ N/mm}$. For a shear ultimate strength, $F_{su} = 254.9 \text{ N/mm}^2$ and inter-rivet distance, $d_{ir} = 24 \text{ mm}$, the margin of safety was computed as,

$$\begin{aligned} MS &= \frac{F_{su}(d_{ir} - d_r)(t_{sk} + 2t_{st2})}{F_{uf}q_{sk}d_{ir}} - 1 \\ &= \frac{254.9 \times (24 - 3.2)(0.41 + 2 \times 0.41)}{1.5 \times 12.53 \times 24} - 1 \\ &= 13.46 \end{aligned} \quad (415)$$

B.8.6 Rivet Shear Failure

Spar cap configuration 9 is located in the top-front corner of the tailplane box and experiences the most critical shear flow as a result of load case 1. The critical failure point is at BL220, where, according to the analysis of section 2.5, the top skin shear flow, $q_{sk} = 12.53 \text{ N/mm}$. For a pop rivet ultimate load, $P_{ru} = 600 \text{ N}$, taken from figure 3, the margin of safety was computed as,

$$MS = \frac{P_{ru}}{F_{uf}q_{sk}d_{ir}} - 1 = \frac{600}{1.5 \times 12.53 \times 24} - 1 = 0.3301 \quad (416)$$

B.9 Spar Cap Configuration 10 Stress Analysis

B.9.1 Tension Failure

Spar cap configuration 10 is located in the top-front corner of the tailplane box and, as such, experiences the most critical tensile loading as a result of load case 1. The critical failure point is at BL124, where, according to the analysis of section 2.5, the direct limit load, $P_{load} = 7642 \text{ N}$. From the area computed for spar cap configuration 10 in appendix A.2.9, the allowable load, given a rivet hole diameter, $d_r = 3.2 \text{ mm}$,

$$\begin{aligned} P_{allow} &= A_{nett}F_{tu} = [A_{t10} + A_{sk8} - 2d_r(3t_{st2} + t_{sp} + t_{sk})] F_{tu} \\ &= [64.94 + 18.79 - 2 \times 3.2 \times (3 \times 0.41 + 0.41 + 0.41)] \times 406.5 \\ &= 28703 \text{ N} \end{aligned} \quad (417)$$

Hence the margin of safety,

$$MS = \frac{P_{allow}}{F_{uf}P_{load}} - 1 = \frac{28703}{1.5 \times 7642} - 1 = 1.504 \quad (418)$$

B.9.2 Compression Yield Failure

Spar cap configuration 10 is located in the top-front corner of the tailplane box and, as such, experiences the most critical compressive loading as a result of load case 2. The critical failure point is at BL124, where, according to the analysis of section 2.5, the direct limit load, $P_{load} = 3474$ N. From the area computed for spar cap configuration 10 in appendix A.2.9, the allowable load,

$$P_{allow} = A_{gross}F_{cy} = (A_{t10} + A_{sk8})F_{cy} = (64.94 + 18.79) \times 248.0 = 20765 \text{ N} \quad (419)$$

Hence the margin of safety,

$$MS = \frac{P_{allow}}{F_{uf}P_{load}} - 1 = \frac{20765}{1.5 \times 3474} - 1 = 2.985 \quad (420)$$

B.9.3 Crippling Failure

Spar cap configuration 10 is located in the top-front corner of the tailplane box and, as such, experiences the most critical crippling load without diagonal tension as a result of load case 2. The critical failure point is at BL148, where, according to the analysis of section 2.5, the direct limit load, $P_{load} = 3200$ N. Needham's method was first used to compute the allowable stress. Derived data used to compute the allowable crippling stress at BL148 for spar cap configuration 10 is given in table 29.

Table 29: Derived data used to compute the allowable crippling stress at BL148 for spar cap configuration 10 (appendix A.2.9).

Component	c	t [mm]	C_e	A_m [mm 2]	A_t [mm 2]	E_c [N/mm 2]	F_{cy} [N/mm 2]	F_{cs} [N/mm 2]	$A_m F_{cs}$ [N]
Spar Flange and Web	30.75	0.41	0.316	16.23	15.98	7.372×10^4	248.0	103.5	1680
Spar Cap Reinforcement 5	48.28	0.41	0.316	16.23	15.98	7.372×10^4	248.0	73.77	1197
Spar Cap Reinforcement 6	49.28	0.41	0.316	16.57	16.32	7.372×10^4	248.0	72.64	1204
Spar Cap Reinforcement 7	50.28	0.41	0.316	16.90	16.66	7.372×10^4	248.0	71.56	1209
			Σ	65.93	64.94			Σ	5290

Dividing the spar cap into individual angled components, the crippling stress for each angled element was computed as,

$$F_{cs} = C_e \frac{\sqrt{E_c F_{cy}}}{c^{0.75}} \quad (421)$$

where $C_e = 0.316$ for angled elements with two free edges, E_c is the compressive modulus, F_{cy} is the compressive yield strength, and c is the average side length divided by thickness of the angled element, as computed in section 2.7.2 and appendix A.1. The allowable stress was then computed as,

$$F_{allow} = \frac{\sum A_{m(i)} F_{cs(i)}}{\sum A_{m(i)}} = \frac{5290}{65.93} = 80.24 \text{ N/mm}^2 \quad (422)$$

where $A_{m(i)}$ and $F_{cs(i)}$ are the mid-line areas, as computed in section 2.7.2 and appendix A.1, and crippling stresses respectively of each angled element. From the allowable stress, the effective inter-rivet and edge skin widths were computed, respectively, as,

$$\begin{aligned} w_{eff_{ir}} &= 1.7 t_{sk} \sqrt{\frac{E_c}{F_{allow}}} = 1.7 \times 0.41 \times \sqrt{\frac{7.372 \times 10^4}{80.24}} = 21.13 \text{ mm} \\ w_{eff_{edge}} &= 0.6 t_{sk} \sqrt{\frac{E_c}{F_{allow}}} = \frac{0.6}{1.7} \times 21.13 = 7.458 \text{ mm} \end{aligned} \quad (423)$$

From these, the total effective skin width was obtained as the sum of the non-overlapping portions of effective skin width, from which the effective skin area, A_{eff} , was obtained. Given the inter-rivet distance between the spar flange and spar cap reinforcement rivet lines is 25 mm, the total effective skin width was computed as,

$$w_{eff} = w_{eff_{edge}} + \frac{3}{2} w_{eff_{ir}} = 7.458 + \frac{3}{2} \times 21.13 = 39.15 \text{ mm} \quad (424)$$

Accounting for longitudinal inter-rivet buckling, for an inter-rivet distance to thickness ratio of $R_{ir} = d_{ir}/t = 24/0.41 \approx 59$, from figure 32 in appendix D, the inter-rivet buckling stress for a universal head rivet, $F_{ir} \approx 11 \text{ ksi} = 75.79 \text{ N/mm}^2$. Hence the total effective skin width was corrected to be,

$$w_{corrected} = \min \left(\frac{F_{ir}}{F_{allow}} w_{eff}, w_{eff} \right) = \frac{75.79}{80.24} \times 39.15 = 36.98 \text{ mm} \quad (425)$$

Hence the effective skin area,

$$A_{eff} = w_{corrected} t_{sk} = 36.98 \times 0.41 = 15.16 \text{ mm}^2 \quad (426)$$

Hence the allowable crippling load was computed, for spar cap configuration 9, as,

$$P_{allow} = (A_{t10} + A_{eff}) F_{allow} = (64.94 + 15.16) \times 80.24 = 6427 \text{ N} \quad (427)$$

Hence the margin of safety,

$$MS = \frac{P_{allow}}{F_{uf} P_{load}} - 1 = \frac{6427}{1.5 \times 3200} - 1 = 0.3390 \quad (428)$$

B.9.4 Crippling Failure with Diagonal Tension

Spar cap configuration 10 is located in the top-front corner of the tailplane box and, as such, experiences the most critical crippling load with diagonal tension as a result of load case 2. The critical failure point is at BL124, where, according to the analysis of section 2.5, the direct limit load, $P_{load} = 3474$ N. The allowable crippling stress is given in (422) for spar cap configuration 10 and the largest contribution resulting from diagonal tension at BL124 originates from the top skin of the tailplane box. The skin shear buckling ratio at this point was taken to be the maximum skin shear buckling ratio either side of the corresponding rib, $BR = 2.480$, as given in table 12. Likewise, the spar shear flow and inter-rib distance were taken to be the maximum either side of the rib at BL124, $q_{sk} = 5.695$ N/mm and $b = 120$ mm respectively. Hence the diagonal tension factor was found from figure 33 in appendix D to be $k \approx 0.2$, and thus the maximum bending moment experienced by the spar cap is identical to that in (398) computed for spar cap configuration 8, $M_{max} = 1367$ N · mm. Hence the total applied stress at the critical point was computed as,

$$\begin{aligned} F_{total} &= \frac{P_{load}}{(A_{t10} + A_{sk8})} + M_{max} \frac{\bar{X}_{c10}}{I_{c10yy}} \\ &= \frac{3474}{64.94 + 18.79} + 1367 \times \frac{20.92}{9498} \\ &= 44.50 \text{ N/mm}^2 \end{aligned} \quad (429)$$

Hence the margin of safety,

$$MS = \frac{F_{allow}}{F_{uf}F_{total}} - 1 = \frac{80.24}{1.5 \times 44.50} - 1 = 0.2021 \quad (430)$$

B.9.5 Shear Failure

Spar cap configuration 10 is located in the top-front corner of the tailplane box and experiences the most critical shear flow as a result of load case 1. The critical failure point is at BL148, where, according to the analysis of section 2.5, the top skin shear flow, $q_{sk} = 12.53$ N/mm. For a shear ultimate strength, $F_{su} = 254.9$ N/mm² and inter-rivet distance, $d_{ir} = 24$ mm, the margin of safety was computed as,

$$\begin{aligned} MS &= \frac{F_{su}(d_{ir} - d_r)(t_{sk} + 3t_{st2})}{F_{uf}q_{sk}d_{ir}} - 1 \\ &= \frac{254.9 \times (24 - 3.2)(0.41 + 3 \times 0.41)}{1.5 \times 12.53 \times 24} - 1 \\ &= 18.28 \end{aligned} \quad (431)$$

B.9.6 Rivet Shear Failure

Spar cap configuration 10 is located in the top-front corner of the tailplane box and experiences the most critical shear flow as a result of load case 1. The critical failure point is at BL148, where, according to the analysis of section 2.5, the top skin shear flow, $q_{sk} = 12.53 \text{ N/mm}$. For a pop rivet ultimate load, $P_{ru} = 600 \text{ N}$, taken from figure 3, the margin of safety was computed as,

$$MS = \frac{P_{ru}}{F_{uf}q_{sk}d_{ir}} - 1 = \frac{600}{1.5 \times 12.53 \times 24} - 1 = 0.3301 \quad (432)$$

B.10 Spar Cap Configuration 11 Stress Analysis

B.10.1 Tension Failure

Spar cap configuration 11 is located in the top-rear corner of the tailplane box and, as such, experiences the most critical tensile loading as a result of load case 1. The critical failure point is at BL364, where, according to the analysis of section 2.5, the direct limit load, $P_{load} = 2792 \text{ N}$. From the area computed for spar cap configuration 11 in appendix A.2.10, the allowable load, given a rivet hole diameter, $d_r = 3.2 \text{ mm}$,

$$\begin{aligned} P_{allow} &= A_{nett}F_{tu} = [A_{t11} + A_{sk11} - 2d_r(t_{st2} + t_{sp} + t_{sk})] F_{tu} \\ &= [31.96 + 18.45 - 2 \times 3.2 \times (0.41 + 0.41 + 0.41)] \times 406.5 \\ &= 17292 \text{ N} \end{aligned} \quad (433)$$

Hence the margin of safety,

$$MS = \frac{P_{allow}}{F_{uf}P_{load}} - 1 = \frac{17292}{1.5 \times 2792} - 1 = 3.129 \quad (434)$$

B.10.2 Compression Yield Failure

Spar cap configuration 11 is located in the top-rear corner of the tailplane box and, as such, experiences the most critical compressive loading as a result of load case 2. The critical failure point is at BL364, where, according to the analysis of section 2.5, the direct limit load, $P_{load} = 1269 \text{ N}$. From the area computed for spar cap configuration 11 in appendix A.2.10, the allowable load,

$$P_{allow} = A_{gross}F_{cy} = (A_{t11} + A_{sk11})F_{cy} = (31.96 + 18.45) \times 248.0 = 12502 \text{ N} \quad (435)$$

Hence the margin of safety,

$$MS = \frac{P_{allow}}{F_{uf}P_{load}} - 1 = \frac{12502}{1.5 \times 1269} - 1 = 5.568 \quad (436)$$

B.10.3 Crippling Failure

Spar cap configuration 11 is located in the top-rear corner of the tailplane box and, as such, experiences the most critical crippling load without diagonal tension as a result of load case 2. The critical failure point is at BL364, where, according to the analysis of section 2.5, the direct limit load, $P_{load} = 1269$ N. Needham's method was first used to compute the allowable stress. Derived data used to compute the allowable crippling stress at BL364 for spar cap configuration 11 is given in table 30.

Table 30: Derived data used to compute the allowable crippling stress at BL364 for spar cap configuration 11 (appendix A.2.10).

Component	c	t [mm]	C_e	A_m [mm 2]	A_t [mm 2]	E_c [N/mm 2]	F_{cy} [N/mm 2]	F_{cs} [N/mm 2]	$A_m F_{cs}$ [N]
Spar Flange and Web	30.75	0.41	0.316	16.23	15.98	7.372×10^4	248.0	103.5	1680
Spar Cap Reinforcement 5	48.28	0.41	0.316	16.23	15.98	7.372×10^4	248.0	73.77	1197
			Σ	32.46	31.96			Σ	2877

Dividing the spar cap into individual angled components, the crippling stress for each angled element was computed as,

$$F_{cs} = C_e \frac{\sqrt{E_c F_{cy}}}{c^{0.75}} \quad (437)$$

where $C_e = 0.316$ for angled elements with two free edges, E_c is the compressive modulus, F_{cy} is the compressive yield strength, and c is the average side length divided by thickness of the angled element, as computed in section 2.7.2 and appendix A.1. The allowable stress was then computed as,

$$F_{allow} = \frac{\sum A_{m(i)} F_{cs(i)}}{\sum A_{m(i)}} = \frac{2877}{32.46} = 88.63 \text{ N/mm}^2 \quad (438)$$

where $A_{m(i)}$ and $F_{cs(i)}$ are the mid-line areas, as computed in section 2.7.2 and appendix A.1, and crippling stresses respectively of each angled element. From the allowable stress, the effective inter-rivet and edge skin widths were computed, respectively, as,

$$\begin{aligned} w_{eff_{ir}} &= 1.7 t_{sk} \sqrt{\frac{E_c}{F_{allow}}} = 1.7 \times 0.41 \times \sqrt{\frac{7.372 \times 10^4}{88.63}} = 20.10 \text{ mm} \\ w_{eff_{edge}} &= 0.6 t_{sk} \sqrt{\frac{E_c}{F_{allow}}} = \frac{0.6}{1.7} \times 20.10 = 7.094 \text{ mm} \end{aligned} \quad (439)$$

From these, the total effective skin width was obtained as the sum of the non-overlapping portions of effective skin width, from which the effective skin area, A_{eff} , was obtained. Given the inter-rivet distance between the spar flange and spar cap reinforcement rivet lines is 25 mm, the total effective skin width was computed as,

$$w_{eff} = w_{eff_{edge}} + \frac{3}{2}w_{eff_{ir}} = 7.094 + \frac{3}{2} \times 20.10 = 37.24 \text{ mm} \quad (440)$$

Accounting for longitudinal inter-rivet buckling, for an inter-rivet distance to thickness ratio of $R_{ir} = d_{ir}/t = 24/0.41 \approx 59$, from figure 32 in appendix D, the inter-rivet buckling stress for a universal head rivet, $F_{ir} \approx 11 \text{ ksi} = 75.79 \text{ N/mm}^2$. Hence the total effective skin width was corrected to be,

$$w_{corrected} = \min \left(\frac{F_{ir}}{F_{allow}} w_{eff}, w_{eff} \right) = \frac{75.79}{88.63} \times 37.24 = 31.85 \text{ mm} \quad (441)$$

Hence the effective skin area,

$$A_{eff} = w_{corrected} t_{sk} = 31.85 \times 0.41 = 13.06 \text{ mm}^2 \quad (442)$$

Hence the allowable crippling load was computed, for spar cap configuration 11, as,

$$P_{allow} = (A_{t11} + A_{eff}) F_{allow} = (31.96 + 13.06) \times 88.63 = 3990 \text{ N} \quad (443)$$

Hence the margin of safety,

$$MS = \frac{P_{allow}}{F_{uf} P_{load}} - 1 = \frac{3990}{1.5 \times 1269} - 1 = 1.096 \quad (444)$$

B.10.4 Crippling Failure with Diagonal Tension

Spar cap configuration 11 is located in the top-rear corner of the tailplane box and, as such, experiences the most critical crippling load with diagonal tension as a result of load case 2. The critical failure point is at BL340, where, according to the analysis of section 2.5, the direct limit load, $P_{load} = 1244 \text{ N}$. The allowable crippling stress is given in (438) for spar cap configuration 11 and the largest contribution resulting from diagonal tension at BL340 originates from the top skin of the tailplane box. The skin shear buckling ratio at this point was taken to be the maximum skin shear buckling ratio either side of the corresponding rib, $BR = 2.128$, as given in table 12. Likewise, the spar shear flow and inter-rib distance were taken to be the maximum either side of the rib at BL340, $q_{sk} = 4.708 \text{ N/mm}$ and $b = 192 \text{ mm}$ respectively. Hence the diagonal tension factor was found from figure 33 in appendix D to be $k \approx 0.16$, and thus the maximum bending moment experienced by the spar cap was computed as,

$$M_{max} = \frac{k q_{sk} b^2}{12} = \frac{0.16 \times 2.128 \times (192)^2}{12} = 1046 \text{ N} \cdot \text{mm} \quad (445)$$

Hence the total applied stress at the critical point was computed as,

$$\begin{aligned}
F_{total} &= \frac{P_{load}}{(A_{t11} + A_{sk11})} + M_{max} \frac{\bar{X}_{c11}}{I_{c11yy}} \\
&= \frac{1244}{31.96 + 18.45} + 1046 \times \frac{23.18}{6291} \\
&= 28.53 \text{ N/mm}^2
\end{aligned} \tag{446}$$

Hence the margin of safety,

$$MS = \frac{F_{allow}}{F_{uf}F_{total}} - 1 = \frac{88.63}{1.5 \times 28.53} - 1 = 1.0710 \tag{447}$$

B.10.5 Shear Failure

Spar cap configuration 11 is located in the top-rear corner of the tailplane box and experiences the most critical shear flow as a result of load case 1. The critical failure point is at BL316, where, according to the analysis of section 2.5, the top skin shear flow, $q_{sk} = 10.36 \text{ N/mm}$. For a shear ultimate strength, $F_{su} = 254.9 \text{ N/mm}^2$ and inter-rivet distance, $d_{ir} = 24 \text{ mm}$, the margin of safety was computed as,

$$\begin{aligned}
MS &= \frac{F_{su}(d_{ir} - d_r)(t_{sk} + t_{st2})}{F_{uf}q_{sk}d_{ir}} - 1 \\
&= \frac{254.9 \times (24 - 3.2)(0.41 + 0.41)}{1.5 \times 10.36 \times 24} - 1 \\
&= 10.66
\end{aligned} \tag{448}$$

Rivet Shear Failure

Spar cap configuration 11 is located in the top-rear corner of the tailplane box and experiences the most critical shear flow as a result of load case 1. The critical failure point is at BL316, where, according to the analysis of section 2.5, the bottom skin shear flow, $q_{sk} = 10.36 \text{ N/mm}$. For a pop rivet ultimate load, $P_{ru} = 600 \text{ N}$, taken from figure 3, the margin of safety was computed as,

$$MS = \frac{P_{ru}}{F_{uf}q_{sk}d_{ir}} - 1 = \frac{600}{1.5 \times 10.36 \times 24} - 1 = 0.6088 \tag{449}$$

C Fitting Stress Analysis Calculations

C.1 Lug A & Lug B Stress Analysis

C.1.1 Rivet Shear Failure

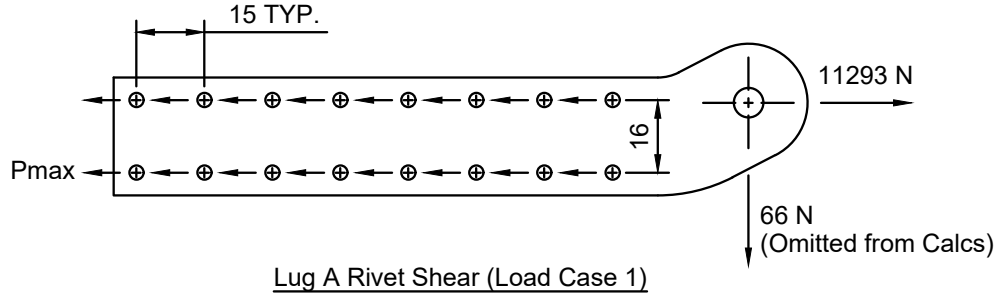


Figure 26: Free body diagram of lug A rivet shear subject to load case 1.

The critical load case for rivet shear failure in lugs A and B is load case 1, with reactions at both lugs as given in table 8, section 2.4; a free body diagram of the situation is given in figure 26. As the reaction force along the z axis is $< 1\%$ of the reaction force along the y axis, rivet shear resulting from the corresponding applied moment was neglected. Assuming that the applied load, $P_y = P_{load} = 11293$ N, and further neglecting the kink in the lug, as shown in figure 26, the maximum rivet shear load was computed as,

$$P_{max} = \frac{P_{load}}{N} = \frac{11293}{16} = 705.8 \text{ N} \quad (450)$$

where N is the total number of rivets. Hence for a CR3213-4 1/8" blind rivet ultimate load, $P_{ru} = 1246$ N, taken from figure 2, the margin of safety was computed as,

$$MS = \frac{P_{ru}}{F_{uf}F_{fit}P_{max}} - 1 = \frac{1246}{1.5 \times 1.15 \times 705.8} - 1 = 0.02340 \quad (451)$$

C.1.2 Tension Failure

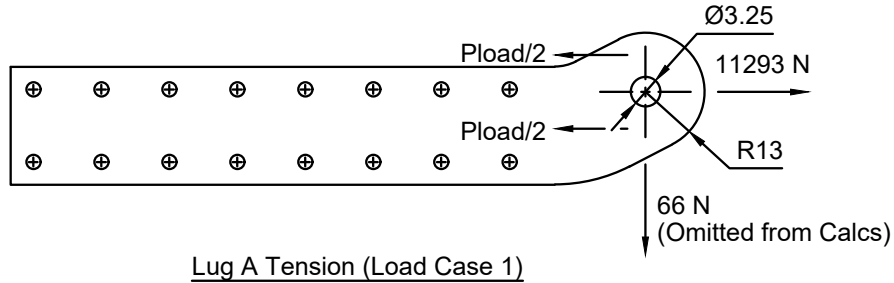


Figure 27: Free body diagram of lug A tension subject to load case 1.

The critical load case for tension failure in lug A is load case 1, with reaction forces as given in table 8, section 2.4; a free body diagram of the situation is given in figure 27. From the geometry given in figure 27, the ratio of the lug width to hole diameter, $w_{lug}/d_{lug} = 26/6.5 = 4$, hence the nett tension efficiency factor was found from figure 34 in appendix D to be $k_t \approx 0.74$. Hence the allowable load is identical to that given in (119), section 2.8.4.2, for lug P, $P_{allow} = 29775$ N. Assuming that the applied load, $P_y = P_{load} = 11293$ N, and further neglecting the kink in the lug, as shown in figure 27, the margin of safety,

$$MS = \frac{P_{allow}}{F_{uf}F_{fit}P_{load}} - 1 = \frac{29775}{1.5 \times 1.15 \times 11293} - 1 = 0.5285 \quad (452)$$

The critical load case for tension failure in lug B is load case 2, with reaction forces as given in table 8, section 2.4. As the reaction force along the y axis at lug B in load case 2 is $< 50\%$ of the reaction force along the y axis at lug A in load case 1, the margin of safety for lug B tension failure exceeds that of lug A.

C.1.3 Bearing Shear Out Failure

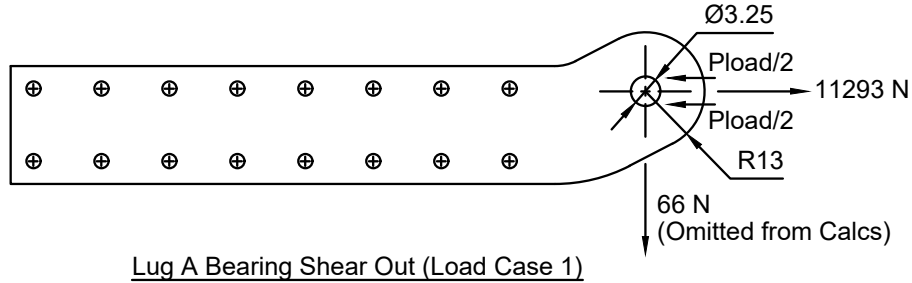


Figure 28: Free body diagram of lug A bearing shear out subject to load case 1.

The critical load case for bearing shear out failure in lug A is load case 1, with reaction forces as given in table 8, section 2.4; a free body diagram of the situation is given in figure

28. From the geometry given in figure 28, the ratio of the edge distance to hole diameter, $w_{lug}/(2 d_{lug}) = 13/6.5 = 2$, hence the shear-bearing efficiency factor was found from figure 34 in appendix D to be $k_{br} \approx 1.5$. Hence the allowable load is identical to that given in (121), section 2.8.4.2, for lug P, $P_{allow} = 20118$ N. Assuming that the applied load, $P_y = P_{load} = 11293$ N, and further neglecting the kink in the lug, as shown in figure 28, the margin of safety,

$$MS = \frac{P_{allow}}{F_{uf}F_{fit}P_{load}} - 1 = \frac{20118}{1.5 \times 1.15 \times 11293} - 1 = 0.03273 \quad (453)$$

The critical load case for bearing shear out failure in lug B is load case 2, with reaction forces as given in table 8, section 2.4. As the reaction force along the y axis at lug B in load case 2 is $< 50\%$ of the reaction force along the y axis at lug A in load case 1, the margin of safety for lug B bearing shear out failure exceeds that of lug A.

C.1.4 Transverse Shear Out Failure

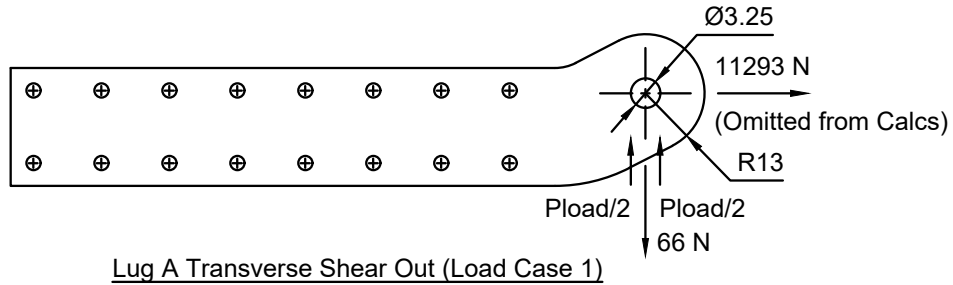


Figure 29: Free body diagram of lug A transverse shear out subject to load case 1.

The critical load case for transverse shear out failure in lugs A and B is load case 1, with reaction forces as given in table 8, section 2.4; a free body diagram of the situation is given in figure 29. From the geometry given in figure 29, the lug is symmetric about its longitudinal axis and the lug hole is concentric with the lug radius, hence the areas A_2 and A_3 denoted in figure 35, appendix D, are identical to those given in (123) and (124), section 2.8.4.2, for lug P. Hence the average bearing area is identical to that given in (125), section 2.8.4.2, for lug P and thus by extension the allowable load is identical to that given in (126), section 2.8.4.2, for lug P, $P_{allow} = 15021$ N. Assuming that the applied load, $P_z = -P_{load} = -66$ N, and further neglecting the kink in the lug, as shown in figure 29, the margin of safety,

$$MS = \frac{P_{allow}}{F_{uf}F_{fit}P_{load}} - 1 = \frac{15021}{1.5 \times 1.15 \times 66} - 1 = 130.9 \quad (454)$$

C.2 Lug C Stress Analysis

C.2.1 Rivet Shear Failure

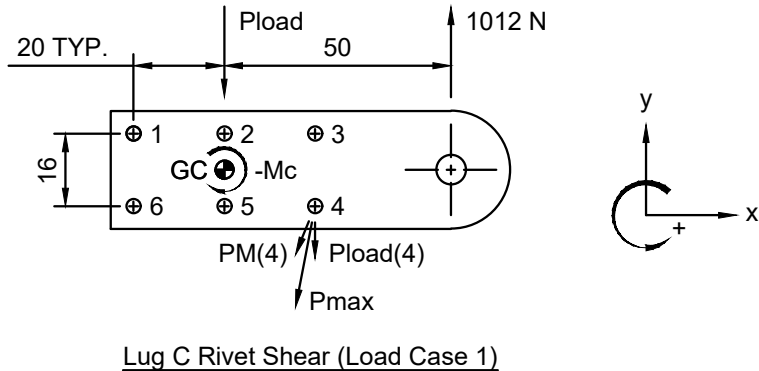


Figure 30: Free body diagram of lug C rivet shear subject to load case 1.

The critical load case for rivet shear failure in lug C is load case 1, with reaction forces as given in table 8, section 2.4; a free body diagram of the situation is given in figure 30. From the geometry given in figure 30, given that the applied load, $P_z = P_{load} = 1012 \text{ N}$, the moment at the centroid of the rivet pattern was computed as,

$$M_c = P_{load}L_c = 1012 \times 50 = 50600 \text{ N} \cdot \text{mm} \quad (455)$$

Hence derived data used to compute the maximum rivet shear load is given in table 31, where the moment and direct shear loads of the i th rivet were computed, respectively, as,

$$P_{M(i)} = \frac{|M_c| d_i}{\sum d_i^2} \quad P_{load(i)} = \frac{P_{load}}{N} \quad (456)$$

where N is the total number of rivets. Hence, accounting for the direction of the applied moment at the centroid, the total rivet shear load of the i th rivet was computed as,

$$P_{tot(i)} = \sqrt{(P_{M(i)x} + P_{load(i)x})^2 + (P_{M(i)y} + P_{load(i)y})^2} \quad (457)$$

Table 31: Derived data used to compute the maximum rivet shear load in lug C.

Rivet	d_i [mm]	d_i^2 [mm ²]	$P_{M(i)}$ [N]	$\cos \theta$	$\sin \theta$	$P_{M(i)x}$ [N]	$P_{M(i)y}$ [N]	$P_{load(i)}$ [N]	$P_{load(i)x}$ [N]	$P_{load(i)y}$ [N]	$P_{tot(i)}$ [N]
1	21.54	464.0	549.4	0.9285	0.3714	204.0	510.10	168.7	0	-168.7	397.7
2	8	64	204.0	0	1	204.0	0	168.7	0	-168.7	264.7
3	21.54	464.0	549.4	0.9285	0.3714	204.04	-510.10	168.7	0	-168.7	708.8
4	21.54	464.0	549.4	0.9285	0.3714	-204.04	-510.10	168.7	0	-168.7	708.8
5	8	64	204.0	0	1	-204.0	0	168.7	0	-168.7	264.7
6	21.54	464.0	549.4	0.9285	0.3714	-204.04	510.10	168.7	0	-168.7	397.7
Σ		1984									

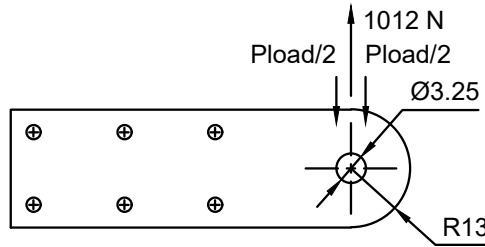
From table 31, the maximum rivet shear load is $P_{max} = 708.8$ N. Hence for a CR3213-4 1/8" blind rivet ultimate load, $P_{ru} = 1246$ N, taken from figure 2, the margin of safety was computed as,

$$MS = \frac{P_{ru}}{F_{uf}F_{fit}P_{max}} - 1 = \frac{1246}{1.5 \times 1.15 \times 708.8} - 1 = 0.01907 \quad (458)$$

C.2.2 Tension & Bearing Shear Out Failure

As there are no reaction forces acting on lug C along the y axis for load cases 1 and 2, and given that the reaction forces acting on lug C along the y axis for load cases 3 and 4 act in the direction of the rivet pattern centroid, away from the edge of the lug, tension and bearing shear out failure analyses are not applicable for lug C.

C.2.3 Transverse Shear Out Failure



Lug C Transverse Shear Out (Load Case 1)

Figure 31: Free body diagram of lug C transverse shear out subject to load case 1.

The critical load case for transverse shear out failure in lug C is load case 1, with reaction forces as given in table 8, section 2.4; a free body diagram of the situation is given in figure 31. From the geometry given in figure 31, the lug is symmetric about its longitudinal axis and the lug hole is concentric with the lug radius, hence the areas A_2 and A_3 denoted in figure 35, appendix D, are identical to those given in (123) and (124), section 2.8.4.2, for

lug P. Hence the average bearing area is identical to that given in (125), section 2.8.4.2, for lug P and thus by extension the allowable load is identical to that given in (126), section 2.8.4.2, for lug P, $P_{allow} = 15021$ N. Assuming that the applied load, $P_z = P_{load} = 1012$ N, the margin of safety,

$$MS = \frac{P_{allow}}{F_{uf}F_{fit}P_{load}} - 1 = \frac{15021}{1.5 \times 1.15 \times 1012} - 1 = 7.605 \quad (459)$$

D Figures

[SEE FIGURES OVERLEAF]

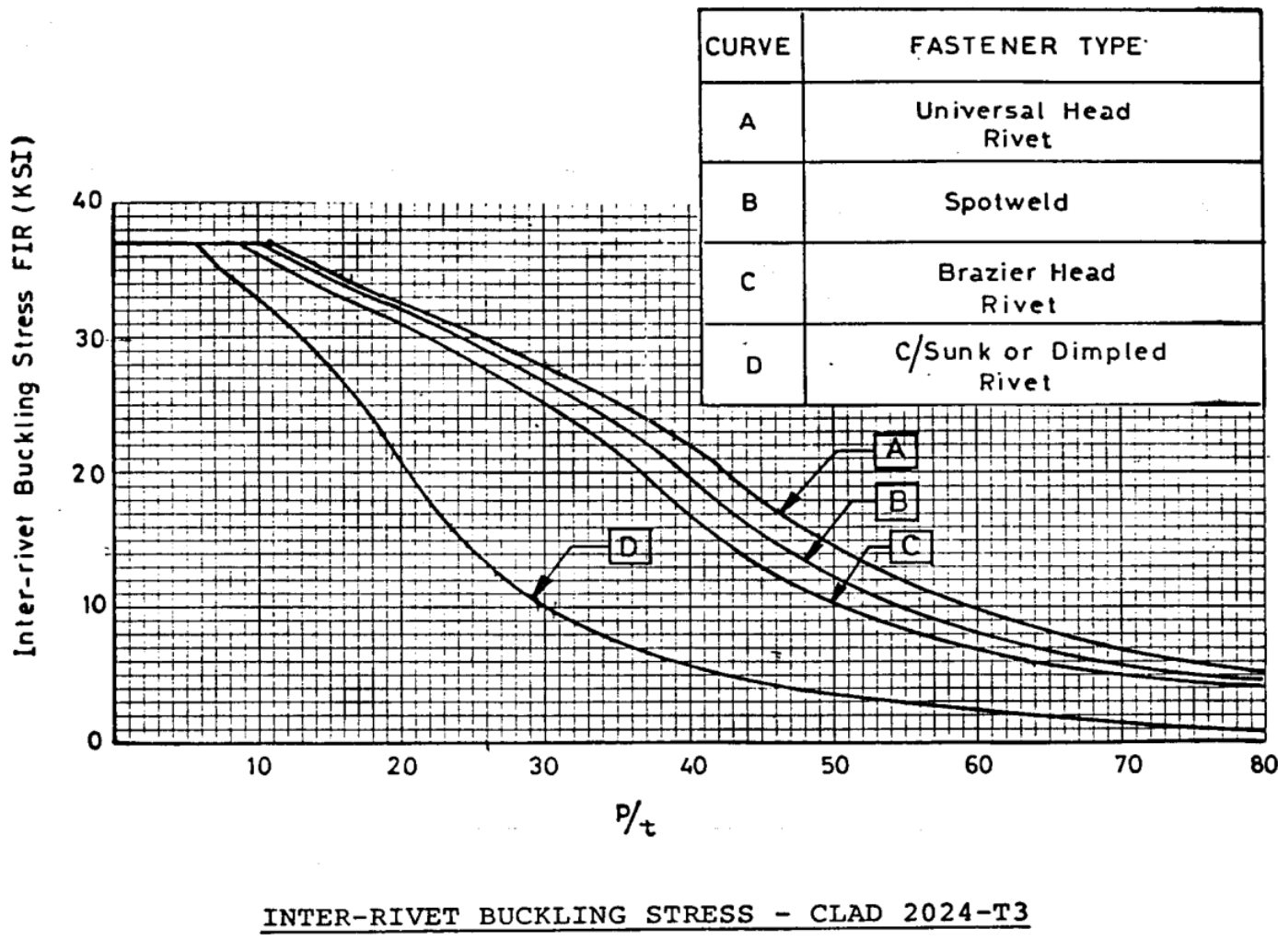


Figure 32: Inter-rivet buckling stress for riveted 2024-T3 clad plate; excerpt taken from Bruhn.

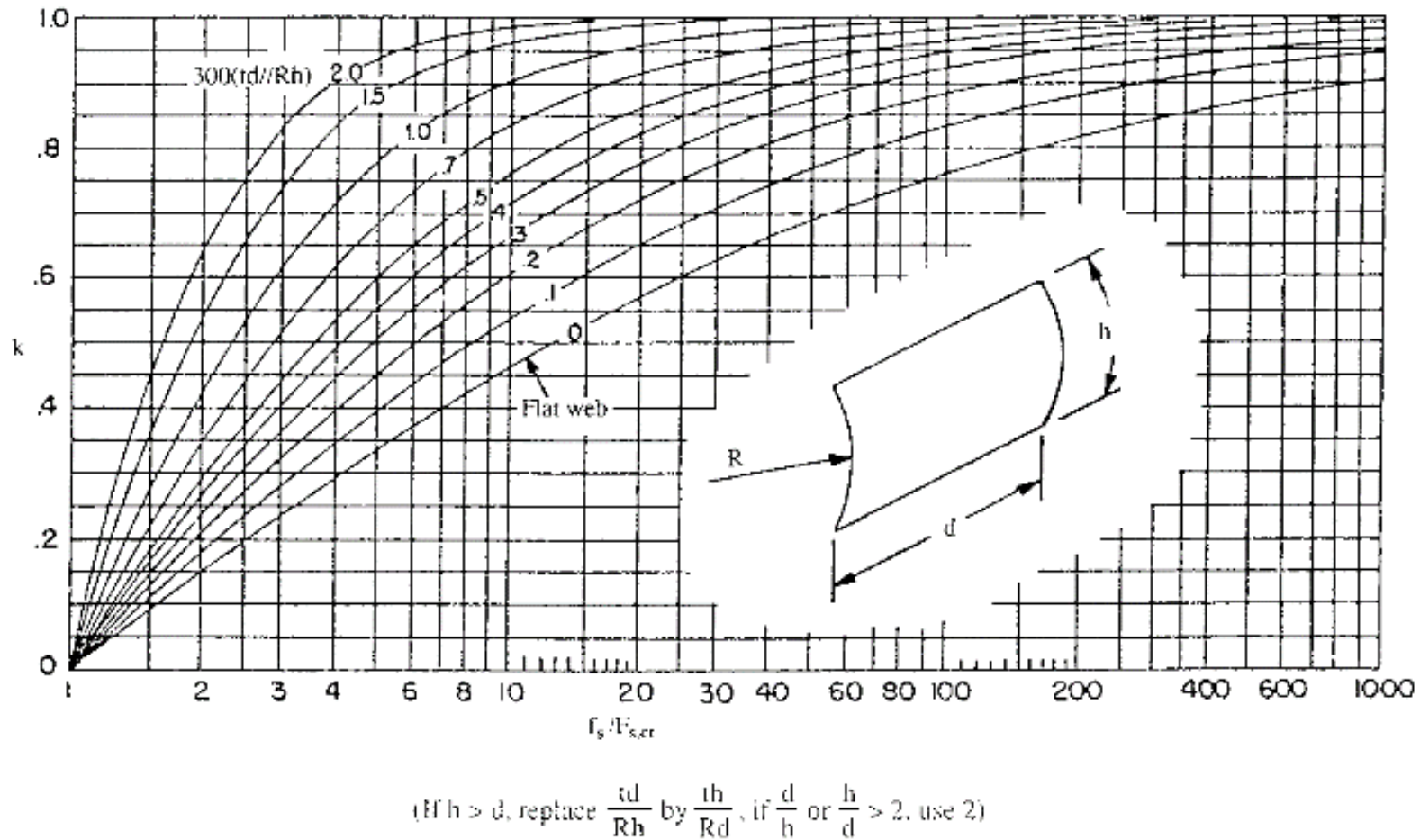


Figure 33: Diagonal tension factor for diagonal tension calculations; excerpt taken from Bruhn.

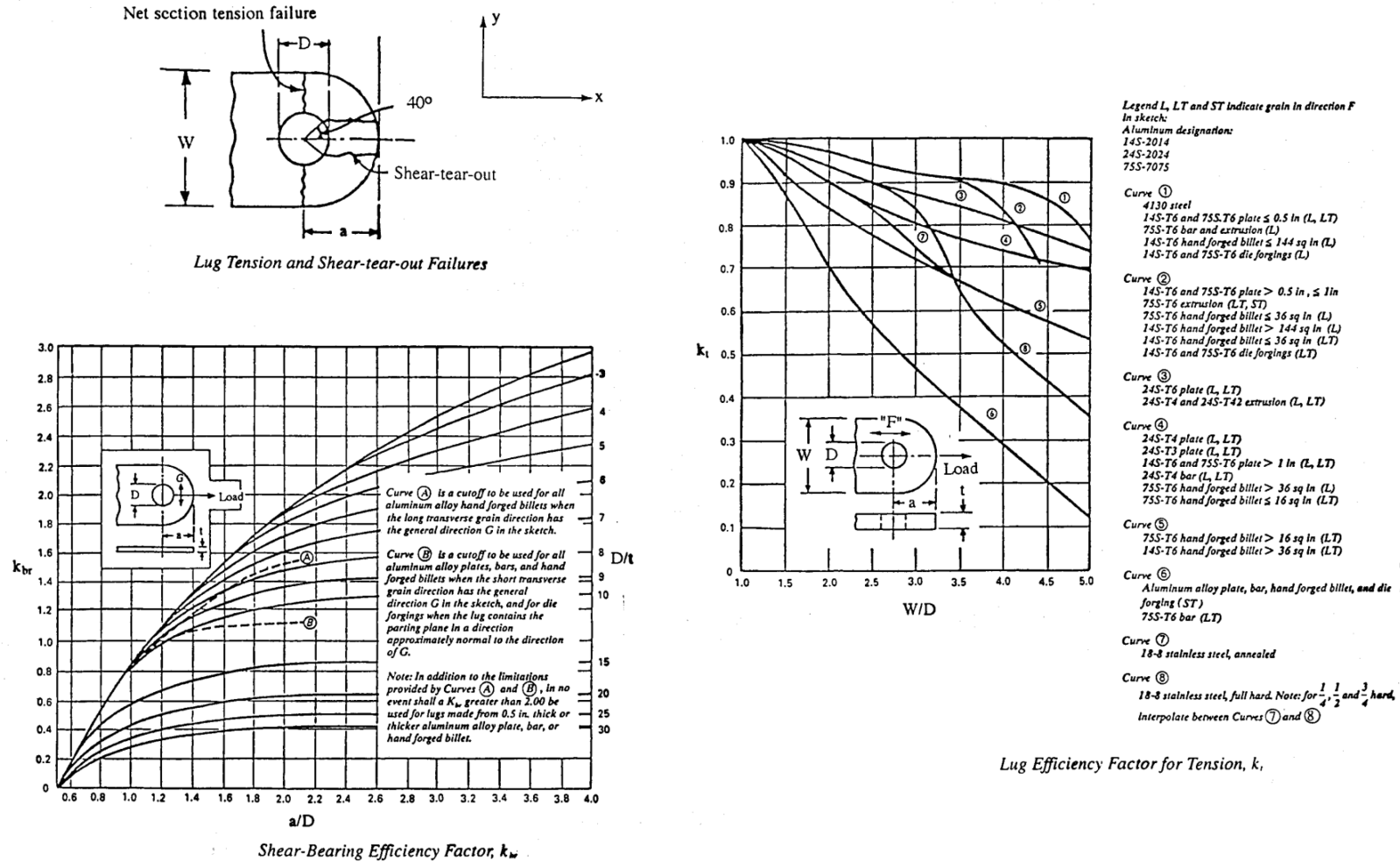


Figure 34: Tension and shear-bearing efficiency factors for aluminium and steel alloy lugs; excerpt taken from Bruhn.

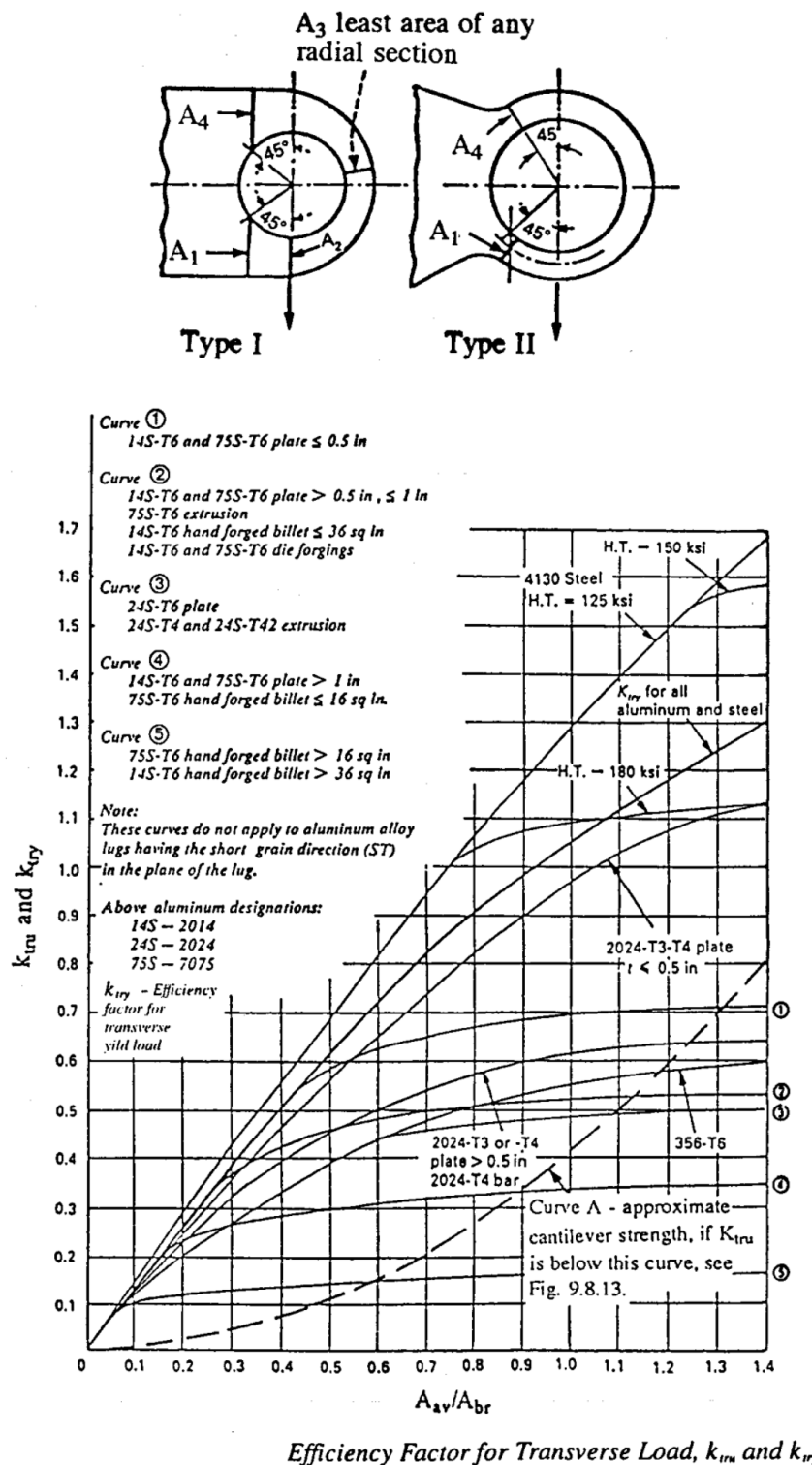


Figure 35: Transverse shear out efficiency factor for aluminium alloy lugs; excerpt taken from Bruhn.